# An In-Vitro and Finite Element Investigation on the Efficacy of Unloader Knee Braces on Meniscus Strain and Tibiofemoral Pressure

by

Mayank Kalra

A thesis

presented to the University of Waterloo

in fulfillment of the

thesis requirement for the degree of

Doctor of Philosophy

in

Mechanical and Mechatronics Engineering

Waterloo, Ontario, Canada, 2023

# Examining Committee Membership

The following served on the Examining Committee for this thesis. The decision of the Examining Committee is by majority vote.

| | |
|---|---|
| External Examiner | Ryan Willing<br>Associate Professor |
| Supervisor | Naveen Chandrashekar<br>Associate Professor |
| Supervisor | Duane Cronin<br>Professor |
| Internal Member | Stewart McLachlin<br>Assistant Professor |
| Internal Member | James Tung<br>Associate Professor |
| Internal-external Member | Thomas Willett<br>Associate Professor |

# Author's Declaration

This thesis consists of material all of which I authored or co-authored: see Statement of Contributions included in the thesis. This is a true copy of the thesis, including any required final revisions, as accepted by my examiners.

I understand that my thesis may be made electronically available to the public.

# Statement of Contributions

Mayank Kalra implemented and presented all methods in this dissertation including: i) cadaveric specimen preparation, ii) cadaveric specimen testing, iii) cadaveric strain and pressure data processing, iv) cadaveric data analysis including descriptive and inferential statistics, v) finite element right leg model extraction, vi) model modifications and enhancements, vii) uniaxial ligament tensile test simulations, viii) gait and squat activity simulations, ix) finite element data processing, and x) cadaveric vs. finite element data correlational analysis. Naveen Chandrashekar created a plan to implement the experimental and computational methods, reviewed experimental and computational data outcomes, and provided technical supervision and editorial feedback on the dissertation. Duane Cronin created a plan to implement the computational method, reviewed computational data outcomes, and provided technical supervision and editorial feedback on the dissertation.

Some of the thesis content has been previously published in the following journal articles or conference proceedings:

Kalra M, Bakker R, Tomescu SS, Polak AM, Nicholls M, Chandrashekar N. Unloader Braces Reduce Medial Meniscal Strain in ACL Intact Knee [abstract]. In: Proceedings of The 2018 Orthopaedic Research Society (ORS) Annual Meeting; 2018 March 10-13; New Orleans, LA, USA. Abstract #2243 Available at https://www.ors.org/Transactions/64/2243.pdf [Verified 2 Nov 2022]

Kalra, M., Bakker, R., Tomescu, S.S., Polak, A.M., Nicholls, M. and Chandrashekar, N., 2018. The effect of unloader knee braces on medial meniscal strain. *Prosthetics and Orthotics International*, 43(2), pp.132–139.

M.Kalra conducted all testing, data processing, statistical analysis, and drafted the articles. R.Bakker and A.Polak assisted with experimental specimen preparation and testing and reviewed the manuscript. N. Chandrashekar provided technical supervision, manuscript edits and review, and helped finalize the manuscript. S. Tomescu provided guidance during testing and reviewed the final manuscript. M. Nicholls reviewed the final manuscript.

Kalra M, Cronin D, Chandrashekar, N. Characterizing In-Situ Metatarsal Fracture Risk during Simulated Workplace Impact Loading [abstract]. In: Proceedings of The Canadian Society of Biomechanics The 21st Biennial Meeting, 2021 May 25-28; Virtual. Abstract #538. Available by request.

M. Kalra performed all simulations, processed and analysed all data, and drafted the manuscript. N. Chandrashekar and D. Cronin provided technical supervision and manuscript edits and review.

# Abstract

The medial and lateral menisci, situated in the knee joint, are most injured soft tissues in the human body. Meniscus injuries can be isolated or occur concurrently with an anterior cruciate ligament (ACL) injury. Certain tears are not amenable to surgical intervention and non-invasive treatment options such as unloader knee braces are theorized to benefit the knee joint during a medial meniscus injury. Unloader braces have shown favourable outcomes for medial osteoarthritis; however, there is a knowledge gap regarding the efficacy of these braces as an intervention for the meniscus.

This study investigated the efficacy of two medial unloader braces (i.e., Rebound Cartilage and Unloader Fit) on the medial meniscus and tibiofemoral joint compartment during simulated activities of daily living (ADL) in healthy and injured ACL states. Posteromedial and anteromedial meniscus strains and tibiofemoral cartilage pressures were measured on cadaveric specimens (n=10) while replicating gait, double leg squats (DLS), and single leg squats (SLS) using a dynamic knee simulator. In a complementary study, the experimental boundary conditions were applied to a pre-existing 50$^{th}$ percentile male right leg finite element (FE) model and the three ADLs were simulated in both ACL states with a simulated 10 Nm valgus moment (VM) unloader brace effect. The computational approach investigated additional outcomes that could not be measured experimentally such as posterolateral meniscus strains. Descriptive statistics were calculated for experimental strain and pressure outcomes and an analysis of variance (ANOVA) was conducted. Descriptive statistics were calculated for FE strain and pressures, and a cross-correlation analysis (CORA) was performed to compare between the FE model and experiment.

Both unloader braces resulted in significant reductions in mean and peak posteromedial meniscus strains during the ACL-intact state and significant differences in peak anteromedial meniscal strain ($p<.05$). Neither brace resulted in a significant difference in either strain outcome with an ACL deficiency ($p>.05$). There were no

significant differences in tibial cartilage pressures with the application of both braces during the ACL-intact state ($p>.05$). Both braces resulted in an intended valgus unload during DLS and gait, though not during SLS despite reductions in posteromedial meniscus strain during SLS. Strain and pressure outcomes revealed that the RC brace significantly outperformed the UF brace ($p<.05$), as intended by the manufacturer, moreover, this was more noticeable in the ACL-deficient state.

The FE simulations demonstrated strong kinematic validity (CORA=0.74–0.99) with the experiments and the simulated ADLs matched experimental behaviours with ACL-deficient and VM conditions. FE posteromedial meniscus strain outcomes were within the experimental corridors and strain and pressure outcomes were within 1–2 SD of the mean experimental outcomes. Posterolateral meniscus strains were 7-16% higher than posteromedial meniscus strains and helped demonstrate affirmative unloading mechanics when compared to the unbraced scenario. The VM approximated unloader brace mechanics as evidenced by strain and pressure increases in the lateral meniscus and cartilage, respectively, and demonstrated higher efficacy in the ACL-intact state over the -deficient state, similar to the experiment.

This study addressed a major literature gap in knee brace biomechanics by quantifying the efficacy of two commercially available unloader braces on the medial meniscus and demonstrated the viability of a FE approach to measure deep tissue strain. Future research can consider these braces for clinical research in patients with a healthy ACL and the FE model or framework can be used to investigate a variable brace moment BC, additional ADLs, or injury states such as meniscectomies/osteoarthritis.

# Acknowledgements

*I foremost acknowledge that the land on which I completed my doctoral degree is on traditional territory of the Neutral, Anishinaabeg and Haudenosaunee peoples. The University of Waterloo is situated on the Haldimand Tract, the land promised to the Six Nations that includes six miles on each side of the Grand River.*

I wish to acknowledge my supervisors Dr. Naveen Chandrashekar and Dr. Duane Cronin for their support throughout this multidisciplinary study that has helped us collaboratively address a major gap in knee biomechanics while strengthening my passion for injury biomechanics.

Additionally, I would like to acknowledge Dr. Sebastian Tomescu and Mr. Ryan Bakker for their guidance and assistance with experimental testing and Ms. Ania Polak for her assistance with experimental testing and computational simulations.

I am fortunate to have professional colleagues (Ania Polak, Daniel Loewen, Gajendra Hangalur, Harish Rao, Jin Zhu, Ryan Bakker, Sebastian Tomescu, Shamanth Hampali) who evolved into friends and helped me grow as a researcher and individual. Thank you!

To my friends who were always excited about the technicalities of my work, I thank you for the memorable after-hours story tales. To my brother and cousins who continuously helped me lose and regain my sanity, I thank you for the necessary distractions and frivolity. To my parents and family who passionately ~~supported~~ persisted for another doctor, I thank you for the drive.

Finally, to my love, I thank and cherish you the most for your unconditional love and support throughout this endeavor.

*Dedicated to*

*Shanti, Sunder, Shanti, Bogha, Meena, Chander, and the shoulders of giants!*

# Table of Contents

# List of Figures

# List of Tables

# List of Abbreviations

| | | |
|---|---|---|
| ACL | — | Anterior cruciate ligament |
| ADL | — | Activity of daily living |
| ANOVA | — | Analysis of variance |
| AP | — | Anterior-posterior |
| ART-C | — | Aligned ranked transform-contrast |
| ATT | — | Anterior tibial translation |
| BC | — | Boundary Condition |
| BMI | — | Body mass index |
| DKS | — | Dynamic knee simulator |
| DLS | — | Double leg squat |
| DVRT | — | Displacement variable linear transducer |
| FE | — | Finite element |
| GHBMC | — | Global human body models consortium |
| GRF | — | Ground reaction force |
| HEST | — | Hall effect strain transducer |
| KAM | — | Knee adduction moment |
| KOOS | — | Knee injury and osteoarthritis outcome score |
| LCL | — | Lateral collateral ligament |
| MCL | — | Medial collateral ligament |
| ML | — | Medial-lateral |
| MRI | — | Magnetic resonance imaging |
| NB | — | No brace/Unbraced |
| OA | — | Osteoarthritis |
| PCL | — | Posterior cruciate ligament |
| RC | — | Rebound Cartilage brace |
| SD | — | Standard deviation |
| SLS | — | Single leg squat |
| UF | — | Unloader Fit brace |
| VM | — | Valgus moment |

*The goal of research is to develop better mousetraps*
*The goal of nature is to develop better mice*

- *Unknown*

# I. Introduction

## 1.1 Literature Gap and Research Motivation

The medial and lateral menisci are crescent shaped tissues residing within the tibiofemoral joint that provide joint articulation, load distribution, and nutrition to the knee joint (Fox et al., 2012). Meniscus injuries are the most common soft tissue injuries amongst the general population, and medical experts previously recommended a total meniscectomy for injury treatment since the menisci were classified as vestigial tissues; however, recent studies have strongly shifted towards meniscal preservation (Boyd & Myers, 2003; Clayton & Court-Brown, 2008). The menisci have limited healing capacity and surgery is only recommended as the final option (Boyd & Myers, 2003; Lee, 2016). Furthermore, it is well established a meniscus injury increases the risk of future joint diseases such as osteoarthritis (OA) (Englund et al., 2009). Unloader knee braces have been suggested to reduce pain associated with meniscus tears; though, these suggestions appear deductive (Kovacs et al., 2002; Rao et al., 2015). Investigating meniscal tissue responses with unloader braces is necessary due to the emphasis on tissue preservation, limited healing capacity, and long-term injury consequences.

Research has predominantly focused on unloader braces as non-invasive interventions for OA and outcome measures such as pain scores, functional outcomes, quality of life improvements or patient confidence are all related to OA symptoms and disease progression (Briggs et al., 2012; Dessery et al., 2014; Fu et al., 2015; Hart et al., 2016; Kirkley et al., 1999; Laroche et al., 2014; Lindenfeld et al., 1997; Matsuno et al., 1997; Petersen et al., 2019; Pollo et al., 2002; Ramsey et al., 2007). Biomechanical studies have investigated outcomes such as knee adduction moment, ground reaction force, tibiofemoral contact force, or tibiofemoral joint space and these studies reported positive outcomes when using unloader braces as treatments or interventions for OA (Horlick & Loomer, 1993; Kirkley et al., 1999; Pollo & Jackson, 2006; Rannou et al., 2010).

Due to the complex geometry and deeply embedded nature of the menisci, direct tissue measurements are challenging and have only been investigated by few studies (Erbagci et al., 2004; Hollis et al., 2000; Seitz et al., 2012; Tomescu et al., 2018). Furthermore, the menisci are the knee joint's secondary stabilizers and meniscal injury risk greatly increases when the primary stabilizer (i.e., the ACL) becomes injured or remains untreated; thus, it is prudent to consider the state of the ACL when investigating the menisci (Granan et al., 2009; Lohmander et al., 2007; Maletis et al., 2011; Røtterud et al., 2013; Slauterbeck et al., 2009). Augmenting a functional knee brace while measuring meniscus responses has been previously done using a highly intricate in-vivo/in-silico/in-vitro approach on a dynamic knee simulator (DKS) (Tomescu et al., 2018). Recreating the in-vitro approach by Tomescu et al. (2018) offers a framework to investigate unloader braces on the meniscus tissues that is challenging to replicate by the general research community. Finite element (FE) modeling is a computational approach that allows biomechanists to simulate experimental boundary conditions (BCs) and measure responses within the human body on structures that cannot be ethically measured on live humans, or quantify responses that are challenging with in-vitro approaches. There have been FE investigations of unloader braces, though these have focused on brace outcomes related to OA similar to their experimental counterparts (Haris & Beng Chye Tan, 2021; Shriram et al., 2019; Stamenović et al., 2009).

The improvements in joint compartment space or forces due to unloader braces in OA patients leads experimental researchers to believe that unloader braces can have similar improvements on the meniscus tissue (Bhatia et al., 2014). FE investigations of unloader braces are still emerging, and computational studies have also focused on brace outcomes related to OA in static or quasistatic BCs. Moreover, FE studies on unloader braces are not focused on the meniscus tissue responses, and those that have modeled unloader braces are limited to BCs that do not reflect the conditions tested in many experiments. Therefore, the literature gap between unloader knee braces and the responses in the menisci in addition to the gap in FE studies prevents researchers and

clinicians from making substantive conclusions regarding unloader braces as an injury prevention/treatment strategy for the menisci.

## 1.2 Purpose of Research and Hypotheses

The overall aim of this study was to investigate the efficacy of unloader knee braces related to medial meniscus strain during activities of daily living (ADL) using an in-vitro and in-silico approach to address the literature gaps. The experimental and computational investigations focused on meniscus strain and tibiofemoral joint pressure as the primary and secondary outcome measures with four objectives and hypotheses:

Objective 1: Perform in-vitro tests on two distinct commercially available unloader braces and report the outcome measures during ADLs (i.e., double leg squat, gait, and single leg squat), while considering a healthy and injured ACL state. It is hypothesized the unloader braces will reduce medial meniscus strain and cause a shift in the joint pressure from the medial to lateral compartment compared to the unbraced scenario.

Objective 2: Extract the right leg from a pre-existing seated occupant $50^{th}$ percentile whole body male FE model, enhance the material properties and geometry, apply the in-vitro BCs to the model, and apply a valgus moment (VM) BC to simulate an unloading moment. It is hypothesized that an isolated VM results in greater lateral vs. medial tibiofemoral compartment pressure.

Objective 3: Calculate meniscus strain and tibiofemoral joint pressure from simulations of the three ADLs in the unbraced and VM scenarios while considering a healthy and inured ACL state. Similar to Objective 1, it is hypothesized that the VM in the FE model will reduce medial meniscus strain and cause a shift in the joint pressure from the medial to lateral compartment.

Objective 4: To compare and contrast meniscus strain and joint contact pressure between the experimental outcomes and the FE model for all activity-brace-ACL test combinations. For strain, it is hypothesized that FE meniscus strains will lie within their respective experimental corridors. For pressure, it is hypothesized that mean and peak joint contact pressures obtained from the FE simulations will be within two standard deviations of the experimental mean since mean outcomes do not necessarily reflect a singular model response.

## 1.3 Thesis Organization

This thesis is organized into eight chapters. Chapter 2 provides anatomical background on relevant lower extremity structures including the bones, joints, musculature, ligaments, menisci, and cartilage. Detailed information is provided on the muscle attachment sites, origins and insertions of the major ligaments and tissues within the knee, and the biochemical composition and biomechanical function of the menisci.

Chapter 3 presents a literature review relevant to ACL and meniscus injury epidemiology and treatment strategies. Subsequently, the 3-point leverage brace mechanism utilized by both braces in this study, a comprehensive overview of prior knee biomechanical literature discussing meniscus strain and tibiofemoral joint pressure measurement methods, as well as the findings and limitations of knee brace literature is presented. The University of Waterloo DKS, the previously developed combined in-vivo, in-silico, in-vitro approach used to experimentally simulate typical ADLs, and the extent of brace research conducted on this simulator is described. The latter portion of this chapter discusses background on the three components of FE modeling including BCs, geometry, and material properties, followed by model verification and validation. Previous models to investigate knee braces or knee biomechanics, including extensive details of the pre-existing 50$^{th}$ percentile male right leg model are detailed, and the chapter concludes with background on previous experimental material testing studies for relevant knee structures.

Chapter 4 provides details on the methods used to prepare cadaveric specimens for experimental testing, the unloader knee braces specific to this study, the process of utilizing prior in-vivo data to obtain the experimental kinematics and specimen specific muscle forces for the input conditions, the instrumentation used to measure meniscus strain and tibiofemoral joint pressure, and experimental data and statistical analysis for strain and pressure. Subsequently, a description of the right leg FE model extraction, modifications, enhancements, experimental BC implementation, and calculation of FE specific muscle forces is presented. The chapter concludes with strain and pressure assessments in the model and the comparison techniques between the model and experimental outcomes.

Chapter 5 presents all experimental results including descriptive and inferential statistics for meniscus strain measured in the posteromedial and anteromedial tissue regions. Statistics and overall intercondylar joint pressures are presented for the medial and lateral condyles. Moreover, all results include outcome measures in one unbraced and two braced scenarios, which were tested in an ACL-intact and ACL-deficient state.

Chapter 6 presents all computational results including uniaxial tensile test simulations on the major knee ligaments, calibrated ligament stress-strain input curves, mesh convergence outcomes for the menisci and articular cartilage, and the influence of model enhancements such as meniscus horns. These outcomes are all related to model extension simulations to replicate the initial position of ADLs in the experiment. A verification of the applied VM and simulation results for the ADLs in both VM and ACL states are presented.

Chapters 7 is a general discussion that establishes the accomplishments within the context of the study objectives and hypotheses. The computational outcomes are presented in relation to the experimental results. The overall study results are compared with relevant literature emphasizing this study's novelty and the feasibility of the methodology used to replicate high-rate dynamic experimental conditions in a computational model is assessed. This chapter concludes with the limitations of the study.

Finally, chapter 8 summarizes the strengths of the study and concludes with recommendations for future work.

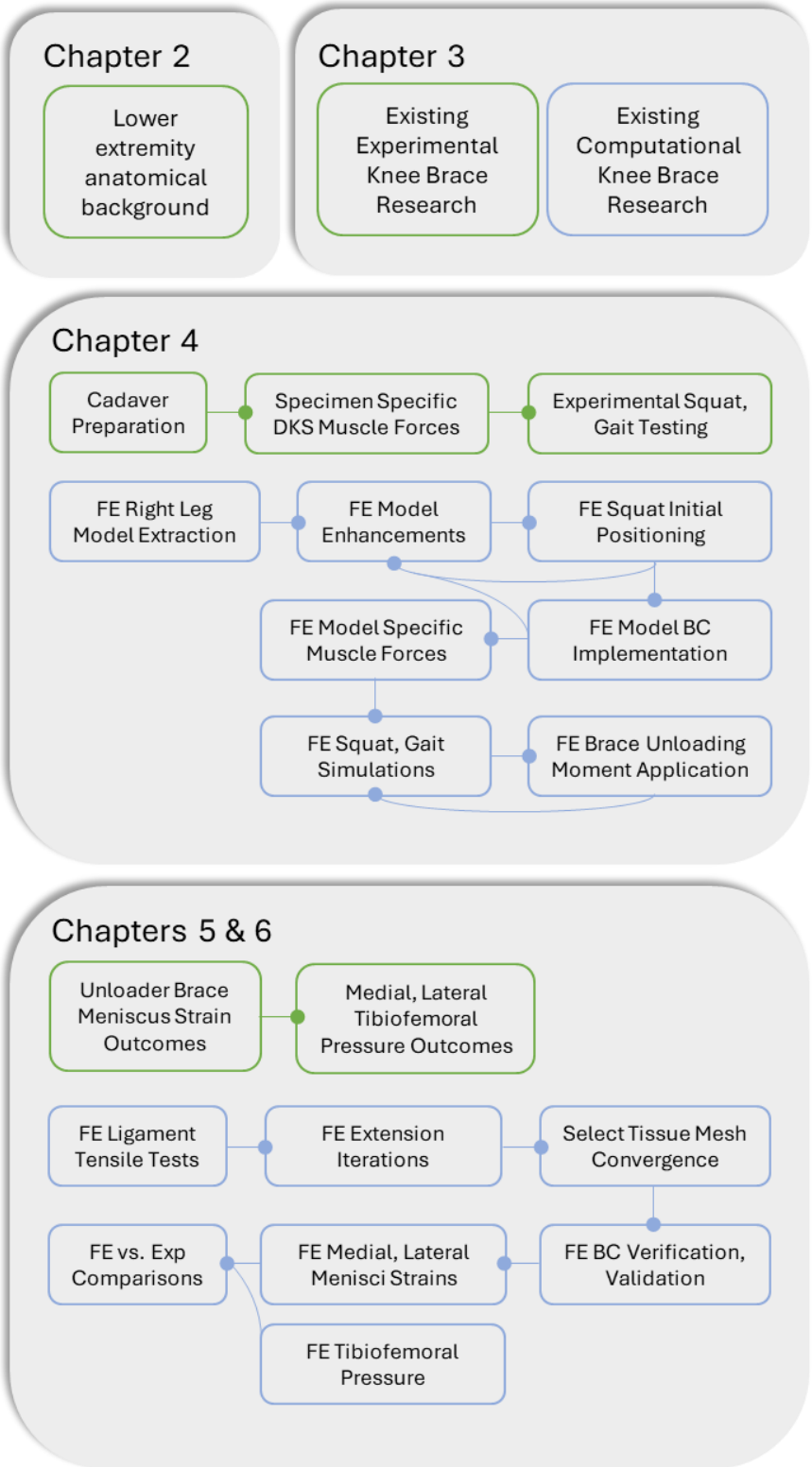


Figure 1.1: Organizational flow chart illustrating overall work flow for select chapters.

# II. Anatomical Background & Definitions

Anatomists use a standardized reference system when referring to the human body's relative and absolute positions, orientation, and motions. Applying mechanical concepts to the human body requires defining the terminology used by health care professionals and researchers. This chapter commences with the anatomical planes and directions related to the lower extremity and concludes with the anatomy of the knee joint and its structures relevant to the purpose of this study.

## 2.1 Anatomical Directions and Planes

The predominant anatomical pairs of directions used in this dissertation are anterior-posterior, medial-lateral, superior-inferior, proximal-distal, and superficial-deep (Fig. 2.1). In lay terms, anterior-posterior distinguish front-back positioning, superior-inferior refer to closer-further positioning from the cranium, and medial-lateral refer to closer-further positioning from the body's vertical centerline. Proximal-distal apply to extremities and refer to the relative position closer-further from the point of attachment between the extremity and trunk. Superficial-deep refer to the relative positioning closer-further from the surface of the body.

All human movement is defined by three pairs of rotation in the three anatomical planes (Fig. 2.2). Rotation in the sagittal plane includes flexion-extension in the anterior-posterior direction, the coronal plane includes abduction-adduction in the medial-lateral direction, and the transverse plane includes internal-external rotation (Fig. 2.3).

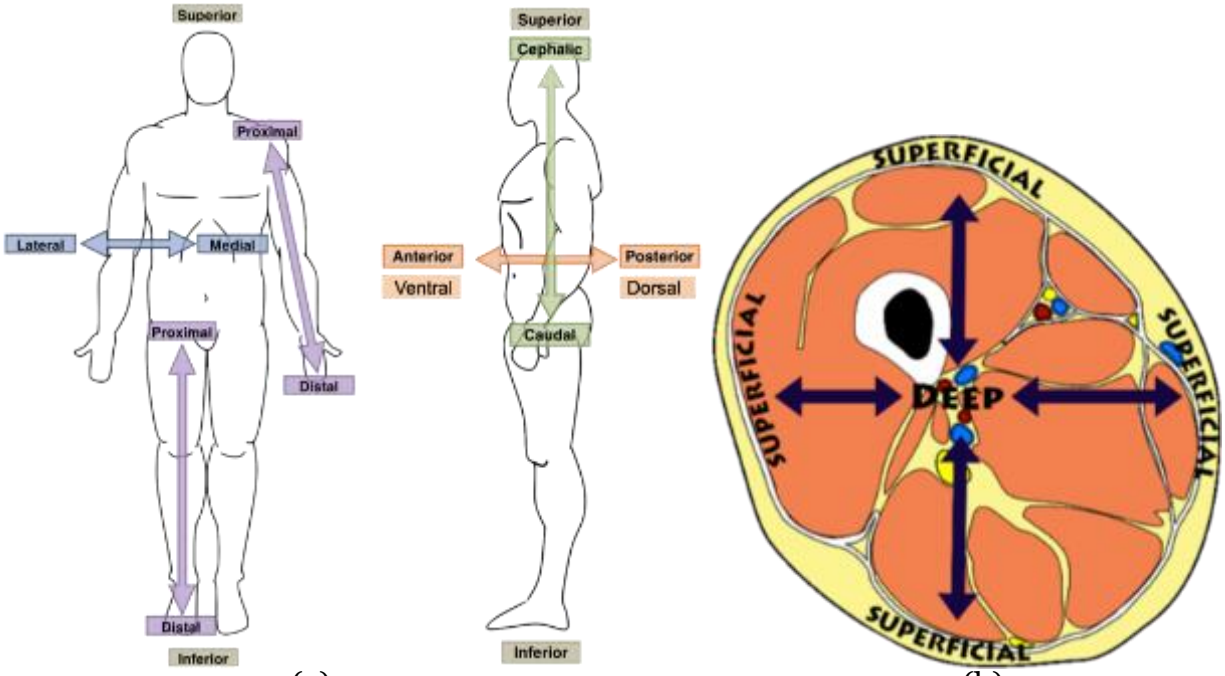


Figure 2.1: The pairs of anatomical pairs shown on the: (a) whole body; and (b) a cross-section of the thigh. Note: Ventral-dorsal and cephalic-caudal are identical to anterior-posterior and superior-inferior.[1]

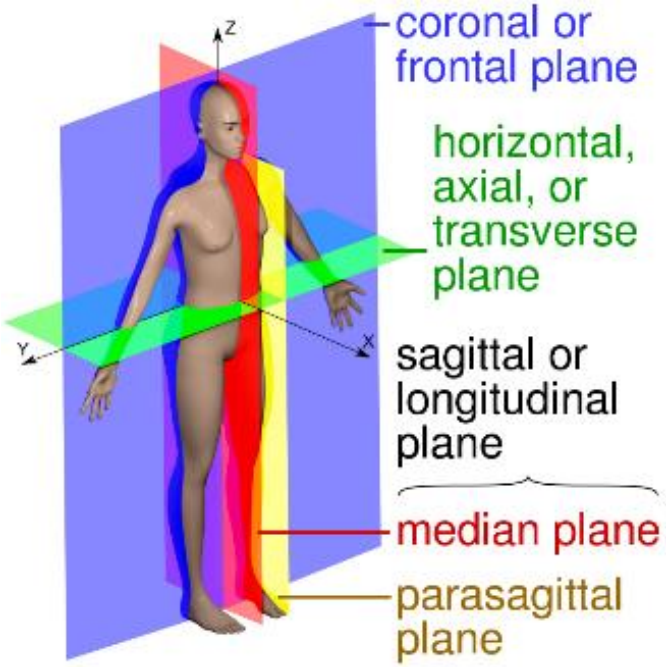


Figure 2.2: The three primary (coronal, transverse, sagittal) and the two secondary (median and parasagittal) anatomical planes of the human body.[2]

[1]Pairs of terms providing anatomical direction or orientation [Online image]. Authored by: Osteomyoamare. Located at: https://commons.wikimedia.org/wiki/File:Anatomical_Directions_2.png

[2] Cross-section of the thigh [Online image]. Authored by: Marshall Strother. Located at: https://commons.wikimedia.org/wiki/File:Thigh_cross_section.svg

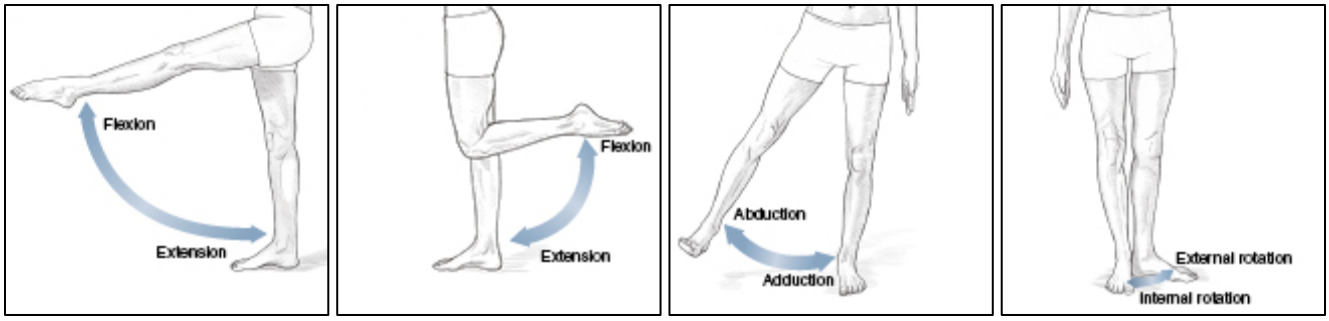

Figure 2.3: The three pairs of lower leg motion showing (hip and knee) flexion-extension, leg abduction-adduction, and leg internal-external rotation.[3]

## 2.2 Bones and Joints

### 2.2.1 *Bones*

The bones in the human body are classified into five categories, which include long bones, short bones, flat bones, irregular bones, and sesamoid bones. The lower extremity consists of 33 bones between the pelvis to the toes. However, this dissertation is focused on the upper and lower leg regions also known as the thigh and crus, respectively. The thigh and crus include three long bones, which are the femur, tibia, and fibula, and one sesamoid bone, which is the patella. Long bones have cross sectional geometries that resemble a cylinder or an ellipse and their nomenclature refers to the tubular shape of the bone. Typically, the length measured along the bone's proximal-distal axis greatly exceeds the length in any other anatomical axes. Their primary function throughout the human body is to provide leverage to muscles. Sesamoid bones are rounded bones embedded within tendons and are named due to their resemblance to sesame seeds. Sesamoid bones are present in joints that experience large amounts of pressure, and their functions are to absorb compressive forces during joint movement, aid in joint articulation, and improve the attached tendon's ability to transmit muscle forces.

The femur is the longest, heaviest, thickest, and strongest bone in the human body. It is the only bone within the thigh region and it accounts for approximately 25% of an adult's height (Betts et al., 2022). The spherical proximal femoral head articulates in the

[3] Major joint movement of the limbs [Online image]. Located at: https://doctorlib.info/yoga/pilates/4.html

acetabulum to form the hip joint, and the rounded bony protrusions on distal end are the femoral condyles, which articulate with the tibial condyles to form the two tibiofemoral joints (Fig. 2.4). Proximal to each condyle exist two irregular bony protrusions known as the medial and lateral epicondyles (Fig. 2.4). The epicondyles serve as attachment sites for many of the leg's muscles and ligaments. Additionally, the transepicondylar axis is a line connecting the prominences between the medial and lateral epicondyles (Fig. 2.5a-b); this axis has been shown to coincide with the functional flexion-extension axis, which has been further described as a fixed line around which the knee rotates during flexion and extension (Asano et al., 2005). The patellar trochlea (also known as the trochlear groove or patellar groove) is located on the antero-distal femur and it is the region which interacts with the patella (Fig. 2.4).

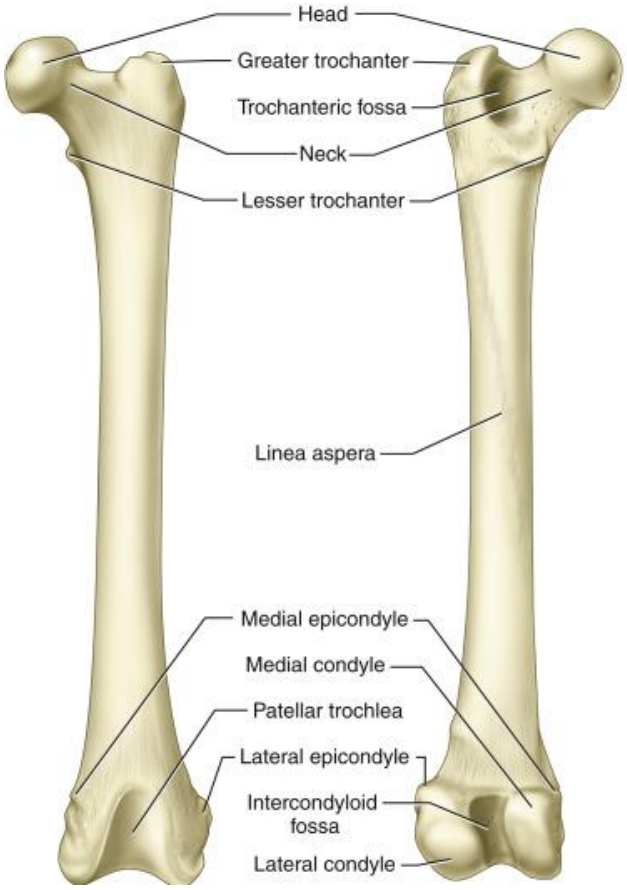


Figure 2.4: An anterior view (left) and posterior view (right) of a left leg femur bone.[4]

[4] Anatomy of the femur [Online image]. Located at https://www.sciencedirect.com/topics/agricultural-and-biological-sciences/femur

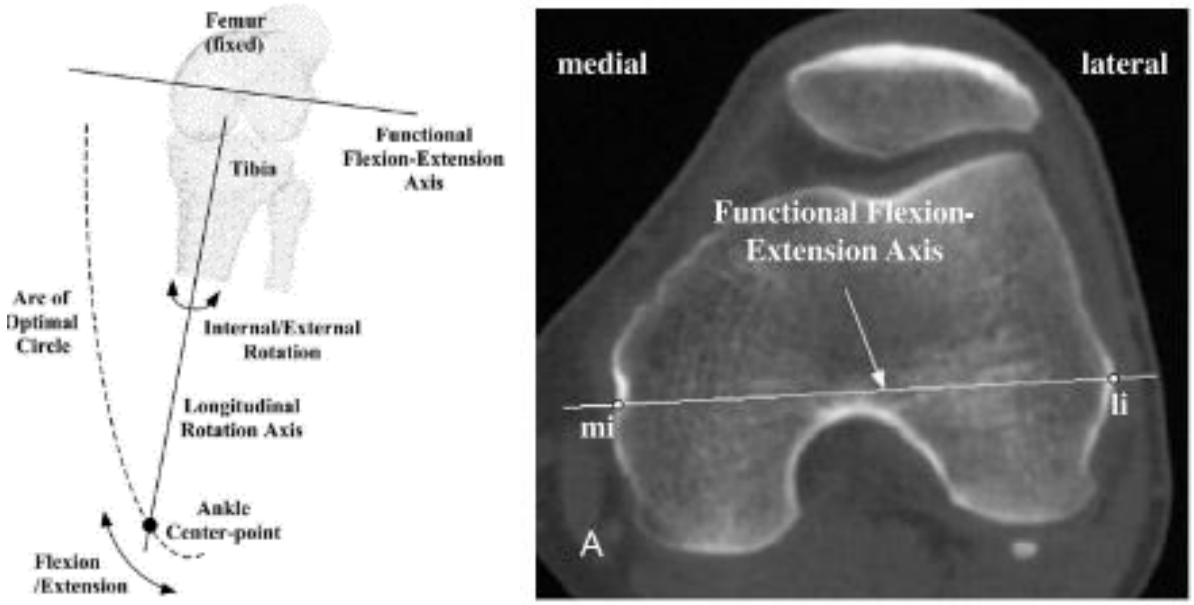


(a) (b)

Figure 2.5: (a) The functional flexion-extension axis shown (a) on an anterior view of a left leg during knee flexion; and (b) in a transverse plane CT-scan on a right leg. (Asano et al., 2005 – reprinted with permission from Elsevier)

The tibia is the largest bone in the crus, the second longest bone in the body, and the predominant weight bearing bone in the lower leg (Fig. 2.6). Unlike the femur the tibia does not have epicondyles and has planated medial and lateral condyles located at the proximal end of the bone. The superior surfaces on the condyles have smoothened articular surfaces which aid in tibiofemoral joint articulation with the femoral condyles. An important feature on the anterior tibia situated inferior to the condyles is the tibial tuberosity (also known as the tibial tubercle); this bony elevation is palpable without dissection and is the attachment site for the patellar tendon.

The fibula is a non-weightbearing bone located laterally in the crus, which predominantly serves as a stabilizer for the talocrural (or ankle) joint and as an attachment site for several muscles (Fig. 2.6). The fibula is a deep, slender long bone and the proximal fibular head and the distal lateral malleolus are the only regions that can be palpated. The fibula is supported between the proximal and distal tibia, and the fibular

shaft is attached to the tibular shaft via the interosseus membrane. The fibula does not directly provide stability to the knee joint since it does not have any attachments with the tibiofemoral or patellofemoral joints.

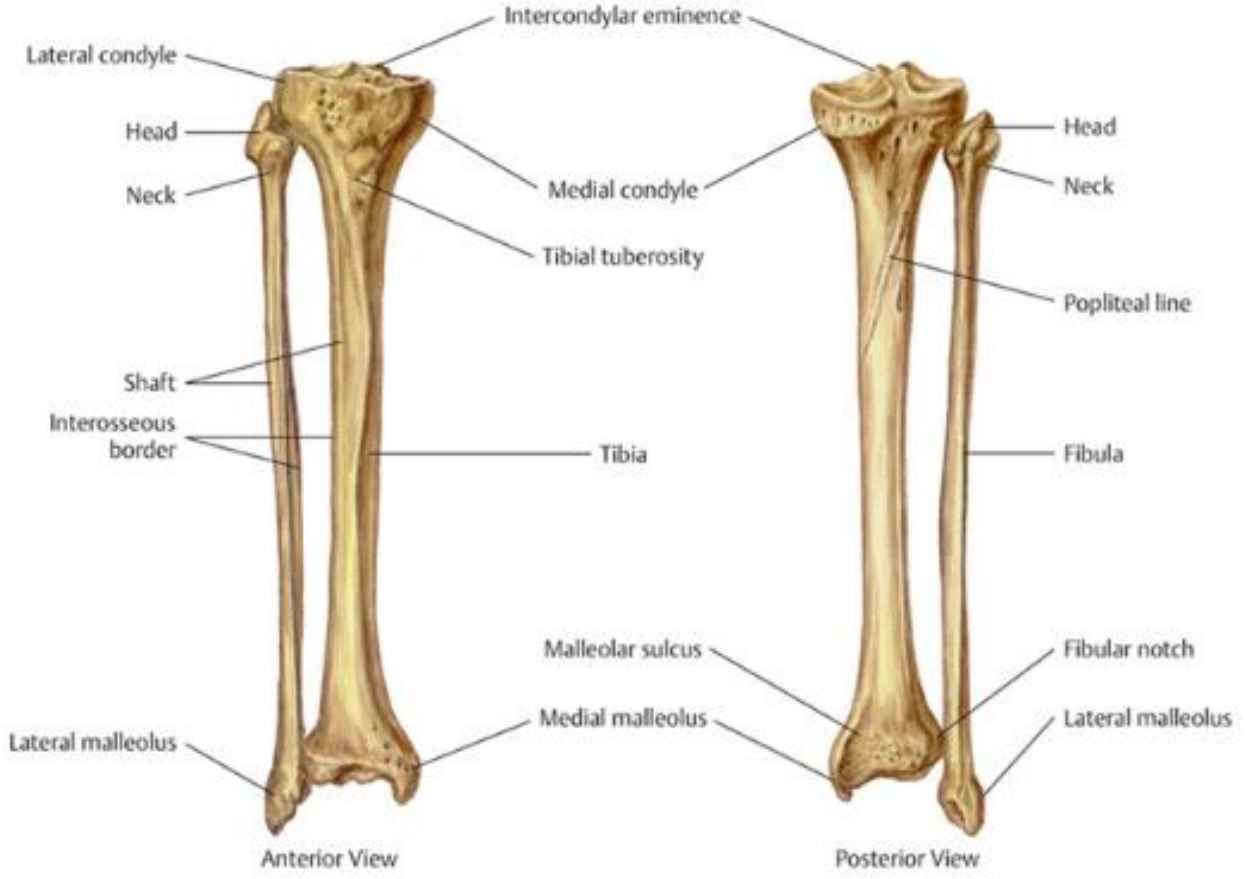


Figure 2.6: An anterior view (left) and posterior view (right) of the tibia and fibula bones in a left leg.[5]

The patella (referred to as the kneecap in lay terminology) is the largest sesamoid bone in the body, and it is embedded within the quadriceps femoris muscle tendon (Fig. 2.7) (Cox et al., 2021). It provides attachment sites for the quadriceps femoris tendon and the patellar ligament. Biomechanically, the patella functions as a fulcrum to improve efficiency of the quadriceps femoris and increase the moment arm of the patellar ligament during knee extension. The patella glides in the trochlea of the femur to form the articulating patellofemoral joint.

[5] Untitled [Online image]. (2016) Located at: https://musculoskeletalkey.com/fractures-of-the-tibiafibula/

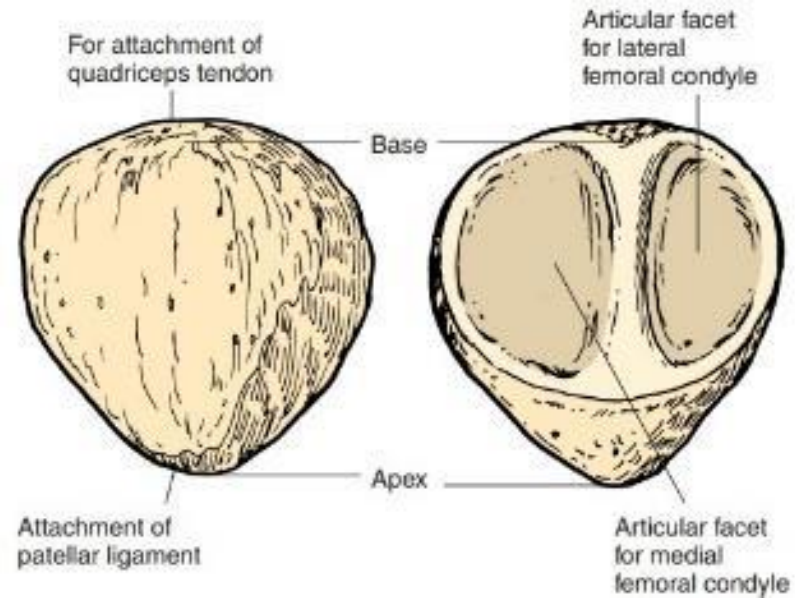

Figure 2.7: An anterior view (left) and posterior view (right) of a right leg patella bone.[6]

### 2.2.2 *Joints*

Joints are classified as fibrous, cartilaginous, or synovial based on their binding structure, and as synarthrosis, amphiarthrosis, or diarthrosis based on their functional mobility (Fig. 2.8) (Betts et al., 2022). This dissertation focuses on synovial diarthrotic joints. Diarthroses refer to freely mobile articulating joints and are further classified as uniaxial, biaxial, or multiaxial planar joints. Synovial joints are distinguished from other joint types by the presence of a joint cavity containing synovial fluid, which is encapsulated by articular cartilage and articular capsule. The bones articulating within synovial joints are not directly connected, they are connected through a series of ligaments. These distinct features reduce joint friction and increase joint mobility. All synovial joints are functionally classified as diarthrosis joints.

The knee joint is the largest and considered as the most complex joint in the human body. It can be classified as a multiaxial diarthrosis synovial joint consisting of three articulations (Betts et al., 2022). The medial and lateral articulating tibiofemoral joints are situated between the medial and lateral femoral and tibial condyles, respectively, and

[6] The Patella {Online image]. Located at: https://www.brainkart.com/article/The-Patella---Pelvic-Girdle_20928/

an articulating patellofemoral joint is contained between the femoral trochlea and the posterior patella. The knee joint has six degrees of freedom (Fig. 2.8) including three rotations which are flexion-extension, valgus-varus angulation, and internal-external (axial) rotation; in addition to three translations which are anterior-posterior translation, medial-lateral shift, and compression-distraction (superior-inferior translation).

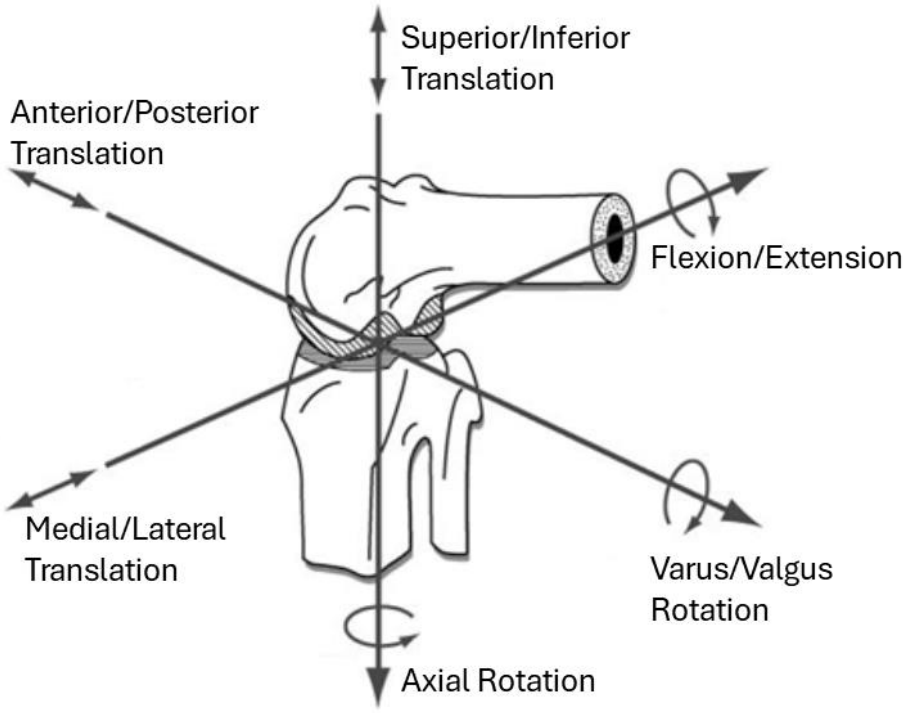


Figure 2.8: The three translational and three rotational degrees of freedom that articulate the knee joint (adapted from Komdeur et al., 2002 – reprinted with permission from Taylor & Francis).

Varus-valgus angulation of the knee joint is an important distinction when classifying OA and investigating unloader knee braces. Varus-valgus status is defined by the angulation of the distal joint segment, which refers to the distal tibia for the knee joint. Varus angulation (*genu varum*) refers to a medial angulation of the joint towards the body's midline, and valgus (*genu valgum*) refers to a lateral angulation. In lay terms a valgus knee configuration is often referred to as 'knock-kneed' while a varus configuration is known as 'bowlegged' (Fig. 2.9).

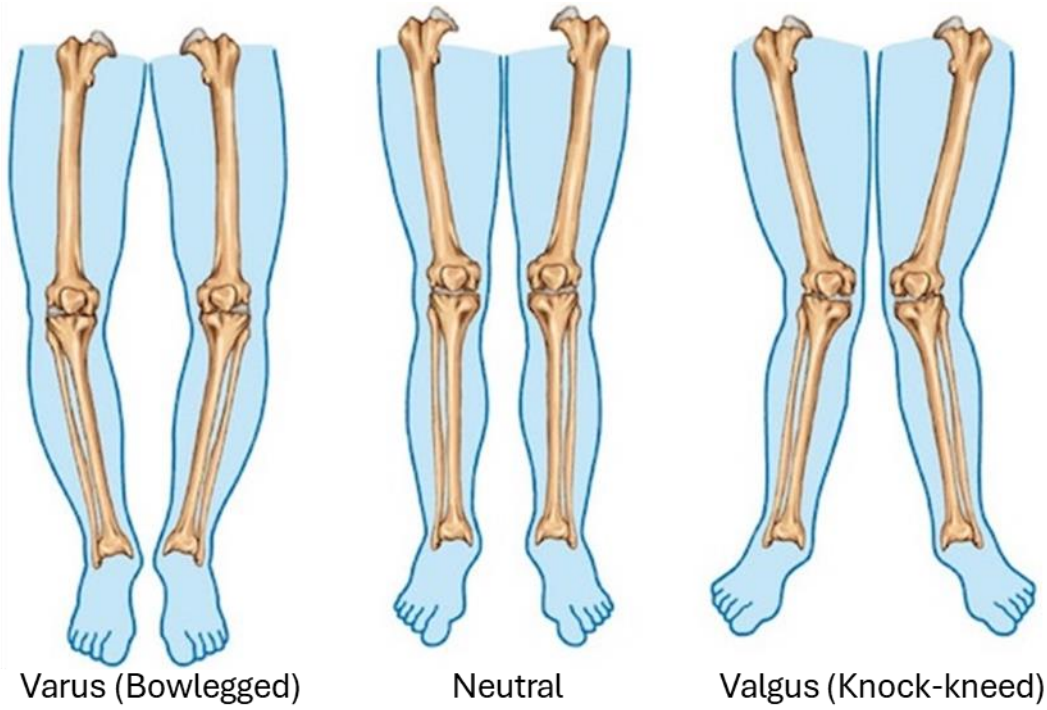


Figure 2.9: A normal (neutral), varus (bowlegged), and valgus (knock-kneed) representation of the knee joint.[7]

In addition to the knee joint, the tibiofibular joint is contained within the pelvis to toe region (Fig. 2.10). The proximal tibiofibular joint is a plane synovial joint, the distal tibiofibular joint is a fibrous joint, and the shafts of the tibia and fibula are a joined by an interosseus membrane which create a fibrous joint.

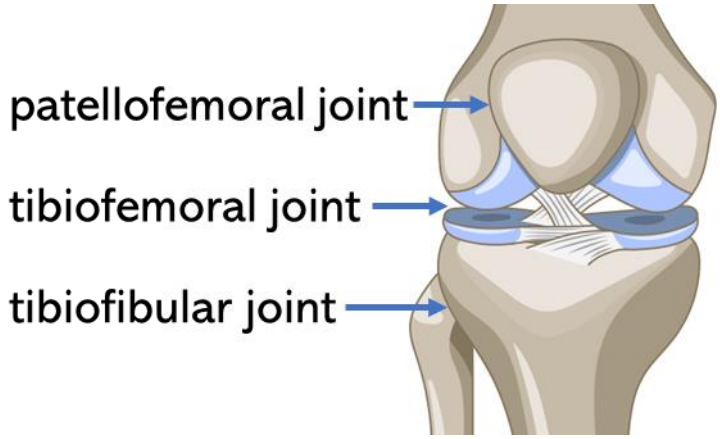


Figure 2.10: The knee joint (tibiofemoral and patellofemoral) and proximal tibiofibular joints.[8]

[7] Untitled [Online image]. Located at: https://kneereplacements.co.uk/realignment-osteotomy/
[8] Untitled [Online image]. Located at: https://www.resilienceorthopedics.com/knee/

## 2.3 Musculature

The major muscles of relevance to this dissertation are the quadriceps femoris (quadriceps), hamstrings, gastrocnemius, and popliteus muscles (Fig. 2.11). These muscles are responsible for hip and knee flexion-extension and leg internal-external rotation. The quadriceps are the largest muscles situated on the anterior thigh and they were previously considered as a group of four agonist muscles including the rectus femoris, vastus latereralis, vastus intermedius, and vastus medialis. Recently, a fifth quadriceps agonist muscle was discovered between the vastus lateralis and intermedius, which is named the tensor vastus intermedius (Grob et al., 2016). The hamstrings are a muscle group which form the bulk of the musculature on the posterior thigh, and they include the bicep femoris, semitendinosus, and semimembranosus muscles. Finally, the gastrocnemius and popliteus are single agonist muscles located on the posterior crus. Table 2.1 provides details on anatomical regions, actions, origins, and insertions for the aforementioned muscles and muscle groups.

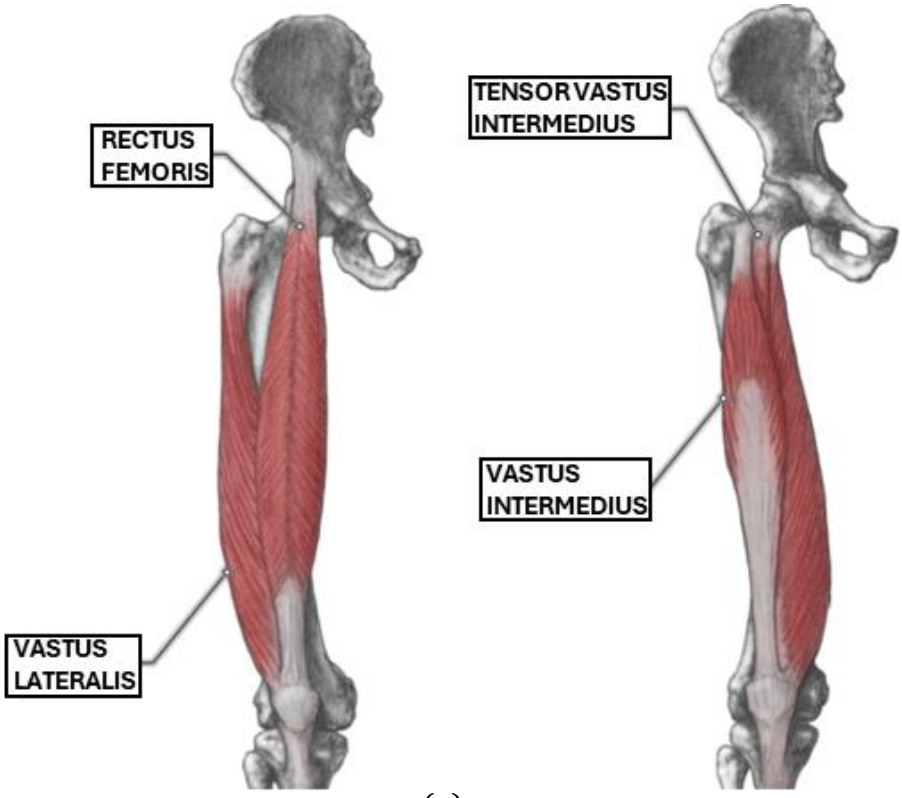


(a)

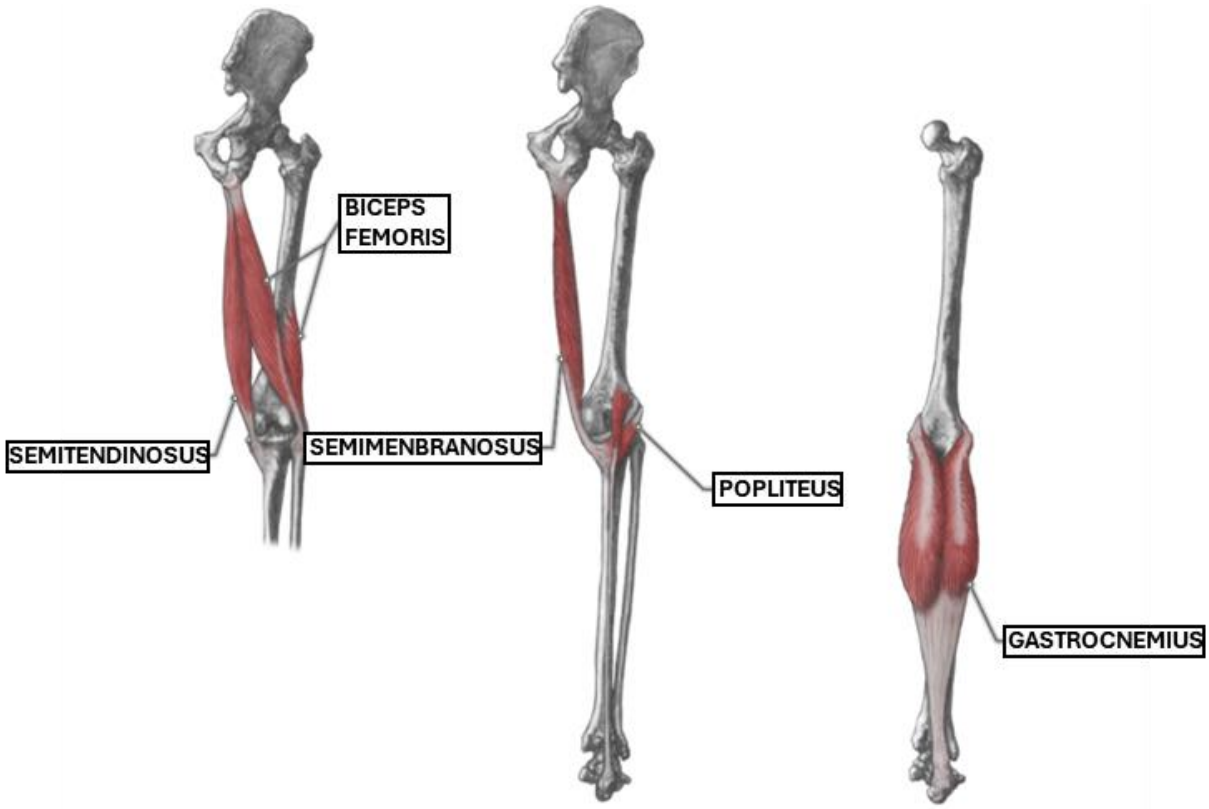


(b) (c)

Figure 2.11: Muscles shown on a right leg including (a) the anterior quadriceps femoris muscle[9]; (b) the posterior hamstrings and popliteus muscles; and (c) the posterior gastrocnemius muscle.[10]

[9] The anterior muscles of the knee [Online image]. (2020). Authored by: CrossFit. Located at: https://www.crossfit.com/essentials/knee-musculature-part-1-anterior-muscles

[10] The posterior muscle of the knee [Online image] (2020). Authored by CrossFit. Located at: https://www.crossfit.com/essentials/knee-musculature-part-2-posterior-muscles

Table 2.1: Anatomical details on major muscle and muscle groups of relevance in this study.

| Muscle Group | Agonist Muscle | Target Region | Target Bones | Action | Origin | Insertion |
|---|---|---|---|---|---|---|
| Quadriceps femoris | Rectus femoris | Anterior thigh | Femur, tibia, fibula | Tibial and fibular extension, thigh flexion | Anterior inferior iliac spine and superior margin of the acetabulum | Patella; tibial tuberosity |
| | Vastus lateralis | Anterior thigh | Tibia and fibula | Knee extension | Greater trochanter; intertrochanteric line; linea aspera | Patella; tibial tuberosity |
| | Vastus intermedius | Anterior thigh | Tibia and fibula | Knee extension | Proximal femur shaft | Patella; tibial tuberosity |
| | Vastus medialis | Anterior thigh | Femur, tibia, fibula | Knee extension | Anterior superior iliac spine | Patella; tibial tuberosity |
| | Tensor vastus intermedialis | Anterior thigh | Femur | Medialises the action and tenses on the aponeurosis of the vastus intermedius | Greater trochanter; intertrochanteric line; | Patella |
| Hamstrings | Biceps femoris | Posterior thigh | Femur, tibia, fibula | Tibial and fibular flexion, thigh extension and lateral rotation | Ischial tuberosity, linea aspera, distal femur | Fibular head, lateral tibial condyle |
| | Semitendinosus | Posterior thigh | Femur, tibia, fibula | Tibial and fibular flexion, thigh extension and lateral rotation | Ischial tuberosity | Superior tibial shaft |
| | Semimembranosus | Posterior thigh | Femur, tibia, fibula | Tibial and fibular flexion, thigh extension and lateral rotation | Ischial tuberosity | Medial tibial condyle, lateral femoral condyle |
| - | Gastrocnemius | Posterior crus | Tibia, fibula, calcaneus | Foot plantar flexion, tibia and fibular flexion | Medial and lateral femoral condyles | Posterior calcaneus |
| - | Popliteus | Posterior crus | Tibia, fibula | Tibial and fibular flexion, thigh and crus medial and lateral rotation | Lateral femoral condyle, lateral meniscus | Proximal tibia |

## 2.4 Cruciate and Collateral Ligaments

There are numerous ligaments which serve as stabilizing and supporting structures for the knee joint. The principal ones for this dissertation are the anterior cruciate ligament (ACL), posterior cruciate ligament (PCL), lateral collateral ligament (LCL), and medial collateral ligament (MCL).

### 2.4.1 *Cruciate Ligaments*

The ACL and PCL are intercapsular ligaments arranged in a criss-cross orientation that anchor the femur and tibia, and stabilize the knee joint in the anterior-posterior direction (Fig. 2.12). The ACL has attachment sites at the lateral intercondylar notch and the medial tibial plateau; while the PCL is reversed with attachments at the medial femoral condyle to the lateral tibial plateau. Both ligaments are composed of anteromedial and posterolateral bundles. The ACL is the knee's primary restraint against anterior translation of the tibia relative to the femur also known as anterior tibial translation as well as internal and external rotational loads (Duthon et al., 2006). Studies have reported the ACL has a mean length of 38 mm, a width ranging between 7-12 mm, and a cross-sectional area of 36 $mm^2$ and 44 $mm^2$ for females and males, respectively (Markatos, 2013; Zantop, 2005). Hashemi et al., (2011) reported similar values for the length (29.8 ± 2.5 mm for males and 26.8 ± 2.8 mm for females), though this study reported the minimum cross-sectional area as 78.3 ± 23.6 $mm^2$ for males and 56.7 ± 14.9 $mm^2$ for females. A previous study measured a mean ACL length and width of 38.3 ± 4.0 mm and 11.0 ± 1.8 mm, respectively (n=24) (Girgis et al., 1975). The PCL is the knee's primary restraint against posterior tibial translation and also acts as a secondary restraint to varus, valgus, and external rotation moments (Logterman et al., 2018). The PCL is nearly twice as thick as the ACL (Logterman et al., 2018) with a mean length and width of 38.2 ± 4.2 mm and 13.4 ± 1.7 mm, respectively (n=24) (Girgis et al., 1975).

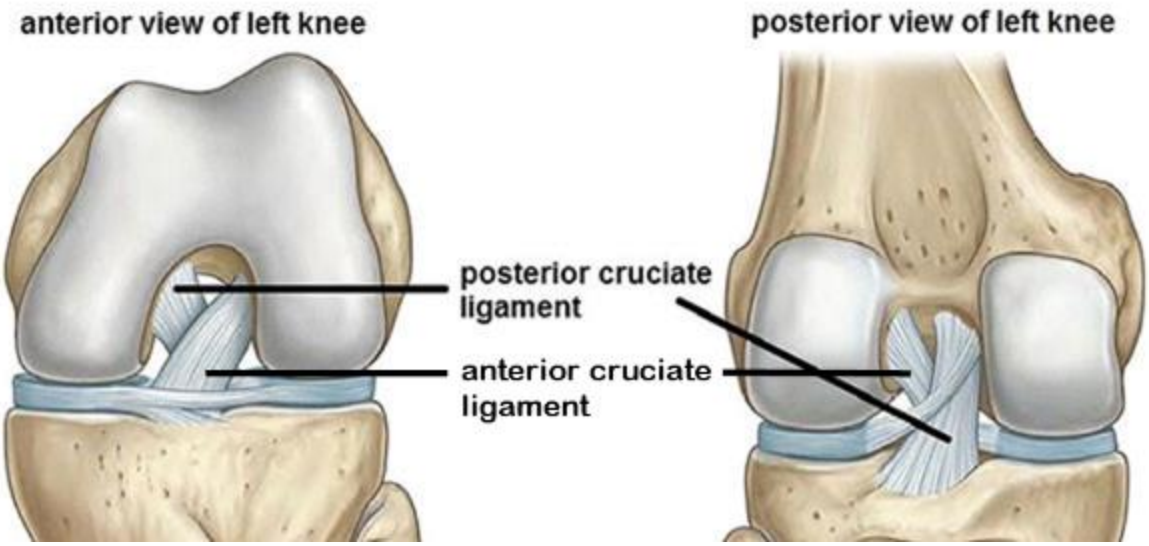

Figure 2.12:The criss-cross orientation of the ACL and PCL shown on a left leg.[11]

### 2.4.2 *Collateral Ligaments*

The LCL and MCL are extrinsic ligaments which serve to restrain varus-valgus rotation and to a lesser degree external knee rotation (Espregueira-Mendes & Silva, 2006; Schein, 2012). The LCL attaches from the distal lateral femur to the fibular head (Fig. 2.13), thus it is also referred to as the fibular collateral ligament. The mean length of the LCL is 63.1 ± 5.2 mm (Espregueira-Mendes & Silva, 2006). The primary function of the LCL is to stabilize the knee against varus stresses (Yaras et al., 2021). The MCL is the largest structure located on the medial knee joint region and it is comprised of a superficial and deep sections. The superficial MCL (also known as the tibial collateral ligament) attaches from the medial femoral epicondyle to two sites on the medial tibial (Fig. 2.13) (Andrews et al., 2017). The deep MCL is compromised of the meniscofemoral and meniscotibial ligaments, which attach from the medial femur to the medial meniscus and from the medial meniscus to the medial tibial plateau, respectively (Andrews et al., 2017). The superficial MCL is the knee's primary static stabilizer against valgus stress; while, the deep MCL is a secondary restraint against anterior tibial translation and a minor stabilizer against valgus stress (Andrews et al., 2017).

[11] Untitled [Online image]. (2020). Authored by: Kai Sigel. Located at: https://www.physiotutors.com/posterior-cruciate-ligament-tears/

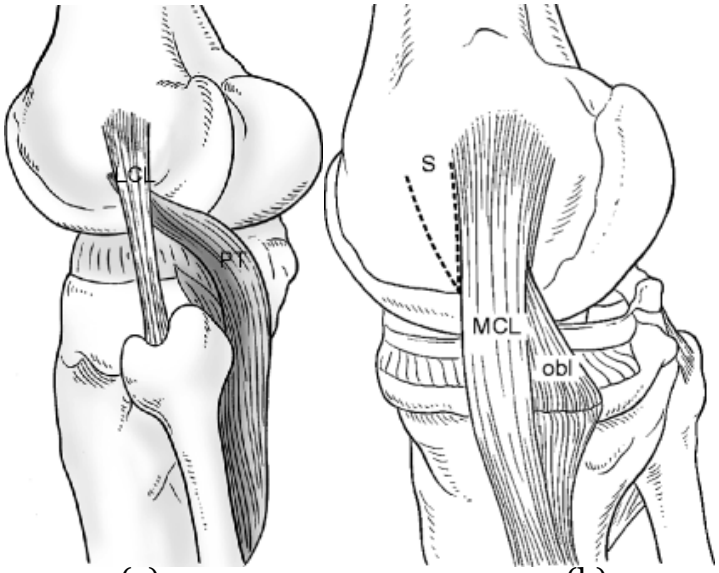

Figure 2.13: (a) Lateral view of left leg displaying the LCL and its attachment sites[12]; and (b) medial view of right leg displaying the MCL and its superficial attachment sites (note deep MCL attachments are concealed).[13]

## 2.5 Menisci

### 2.5.1 *Gross Anatomy*

The menisci (singular: meniscus) were historically described as vestigial structures; however, it has since been discovered that these fibrocartilaginous tissues are crucial to the knee joint and should be preserved (Boyd & Myers, 2003; Clayton & Court-Brown, 2008). The medial and lateral menisci (Fig. 2.14a) are crescent shaped tissues, which reside between the femoral and tibial articular cartilage in the medial and lateral knee joint compartments. The triangular cross-section and concavity in the superior menisci form a cradle for the convex femoral condyles, while the flat surface of the inferior menisci rests on the tibial plateaus. The medial meniscus is semilunar, 40-45 mm long, and covers 51-74% of the medial tibial articular surface. The lateral meniscus is close to semicircular, 32-35 mm long, and covers 75-93% of the lateral tibial articular surface. Both menisci have been formerly divided into three zones including the anterior horn, the

[12] Lateral collateral ligament [Online image]. Located at: https://radiologykey.com/lateral-supporting-structures-including-lateral-collateral-ligament-lcl/
[13] Superficial layer of medial collateral ligament [Online image]. Located at: https://radiologykey.com/medial-collateral-ligament-mcl/

body, and the posterior horn (Fig. 2.14b) (Fox et al., 2015). More recent studies show the medial meniscus has five inequal zones (Śmigielski et al., 2015). The prominent attachments for both menisci are via anterior and posterior meniscal roots located at their respective horn zones (Fig. 2.14c). Cadaveric analysis has shown that the medial meniscus horns are more superficial, larger in area, and further apart in the anterior-posterior direction than the lateral meniscus horns (Allen et al., 1995; Ferrer-Roca & Vilalta, 1980). The lateral meniscus is more compact than the medial meniscus and thicker than the medial meniscus in the anterior and medial sections (Table 2.2) (Ferrer-Roca & Vilalta, 1980).

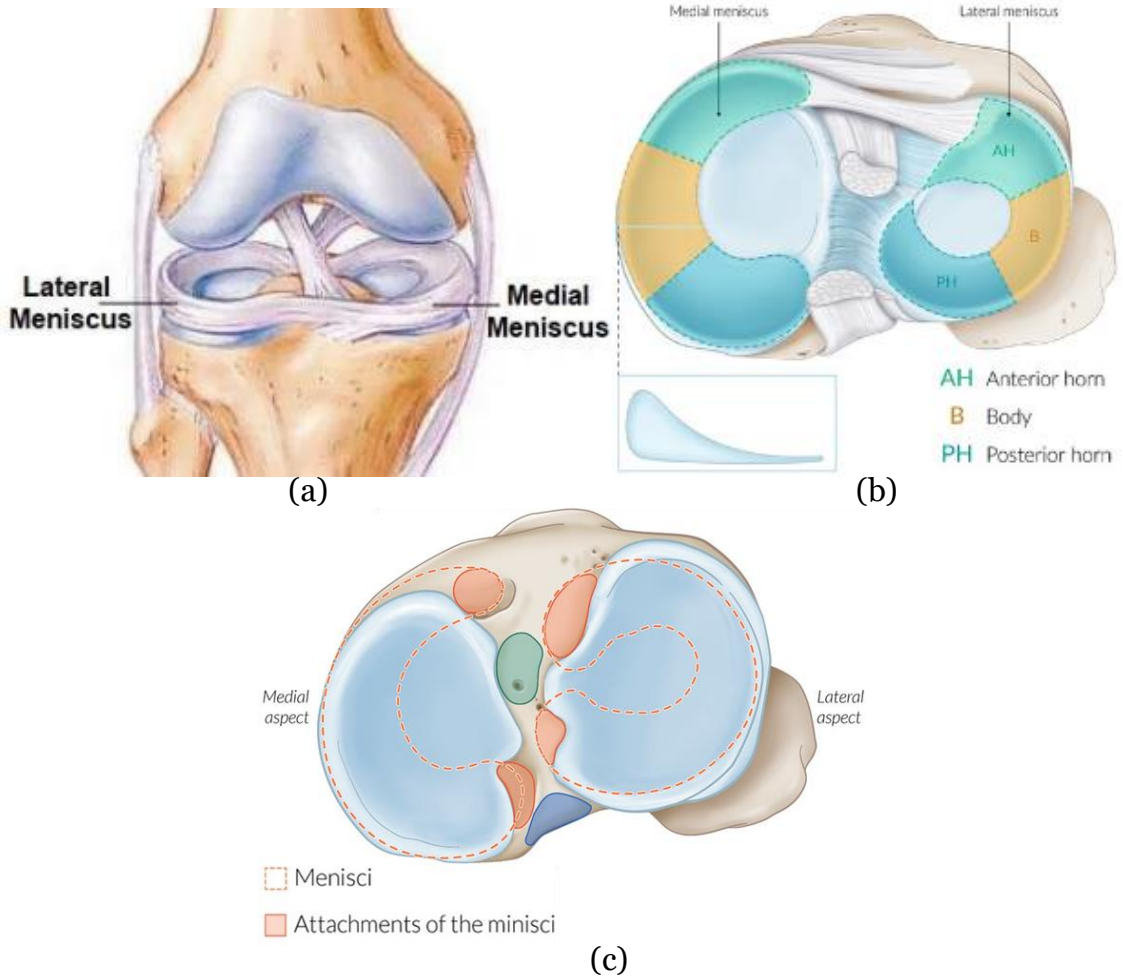


Figure 2.14: (a) anterior view of the menisci; (b) transverse view of the meniscal regions; and (c) transverse view of the meniscal root attachment sites.[14,15]

[14] Untitled [Online image]. Located at: https://www.gormackorthopaedics.co.nz/meniscal-tears
[15] Untitled [Online image]. Located at: https://www.amboss.com/us/knowledge/Thigh,_knee,_and_popliteal_fossa/

Table 2.2: Width and root attachment area measurements of "normal" meniscus tissues.

| | Mean (SD) widths along tissue circumference (mm)* | | | Area of Root Attachment ($cm^2$)‡ | |
|---|---|---|---|---|---|
| | Anterior | Midpoint | Posterior | Anterior | Posterior |
| Medial Meniscus | 7.7 (1.4) | 9.6 (0.5) | 10.6 (0.9) | 1.12 | 0.68 |
| Lateral Meniscus | 10.2 (0.4) | 11.6 (0.8) | 10.6 (0.5) | 0.76 | 0.94 |

*taken from Ferrer-Roca & Vilalta, 1980; ‡taken from Allen et al., (1995)

### 2.5.2 *Biochemistry and Biomechanics*

Water and collagen form 94% of the meniscal extracellular matrix by weight. In addition to zones in the transverse plane there are three zones along the tissue cross-section (Fig. 2.15a). These cross-sectional zones are named after the degree of vascularization and influence the type of collagen fiber contained within the zone. The most superficial region (the red-red zone) contains predominantly type I collagen fibers, and the deepest region (the white-white zone) contains 60% type II and 40% type I collagen. Furthermore, the orientation of these collagen fibers is based on surface layers within the cross-section (Fig. 2.15b). Circumferential fibers offer stability against hoop stresses and radial fibers provide stability against compressive and shear forces.

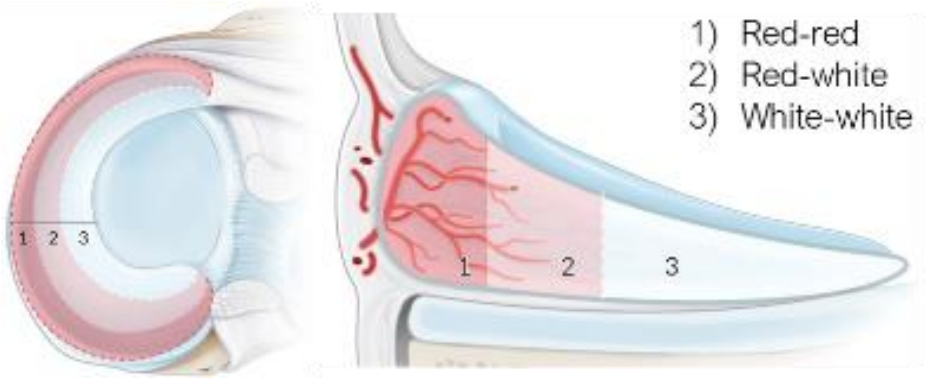


(a)

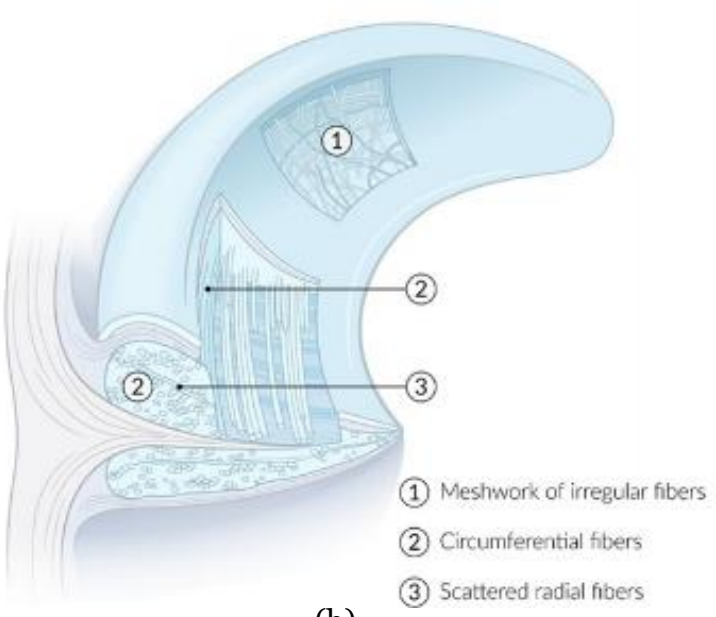


(b)

Figure 2.15: (a) Transverse and cross-sectional views of a meniscus illustrating vascularization zones; and (b) cross-sectional view of a meniscus illustrating collagen fiber orientation.[16]

The gross functions of the meniscus tissues are to protect the knee joint and help prevent early OA. Specific meniscus functions include shock absorption, compressive axial load distribution, joint lubrication, joint congruency, and proprioception (Fox et al., 2012). Studies report the menisci experience 40-60% of the total load acting on the knee joint in extension, and this amount increases to 90% in flexion (Dudphia, 2004; Walker & Erkman, 1975). The mechanism of load transfer during dynamic actions involves converting axial compressive forces into hoop stresses and tensile strain through the circumferential collagen fibers (Fig. 2.16a). Tensile strain causes both menisci to displace during flexion, the lateral meniscus experiences greater displacement due to excursion than the medial meniscus (Fig. 2.16b) (Allen et al., 1995). Dudphia et al., (2004) also reported the lateral meniscus experiences greater displacement on the tibia than the medial meniscus, yet their displacement values were reported as 10 mm for the lateral meniscus and 2 mm for the medial meniscus.

[16] Untitled [Online image]. Located at: https://www.amboss.com/us/knowledge/Thigh,_knee,_and_popliteal_fossa/

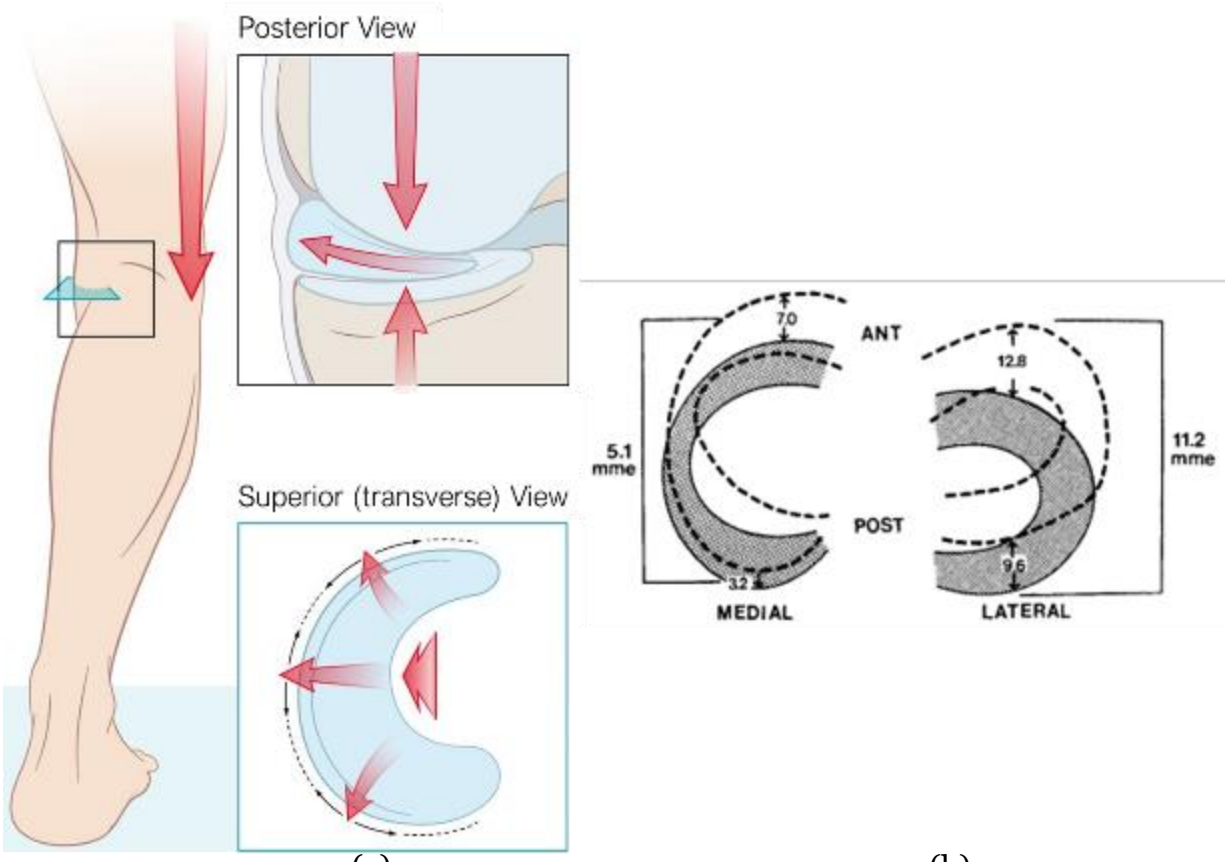


(a) (b)

Figure 2.16: (a) Biomechanical axial load distribution in the meniscus illustrated with posterior (black) and transverse (blue) cross-sectional slices[17]; and (b) Displacement of both menisci due to excursion (Allen et al., 1995).

## 2.6 Articular Cartilage

Hyaline (also known as articular) cartilage forms the articulating surfaces of diarthrodial joints (Huber et al., 2000). The knee joint has articular cartilage on the distal femur and proximal tibia between the tibiofemoral joints; and at the proximal femur and posterior patella between the patellofemoral joint (Fig. 2.17). Hyaline cartilage is the most common form of cartilage found within the human body, it is 65-80% water by weight, has a greater proportion of type II vs. type I collagen fibers, and functions as an elastic load-bearing material (Bhosale, 2008; Huber, 2000). Articular cartilage resists

[17] Untitled [Online image]. Located at: https://www.amboss.com/us/knowledge/Thigh,_knee,_and_popliteal_fossa/

joint compressive forces, aids with load distribution, and reduces friction force during joint motion.

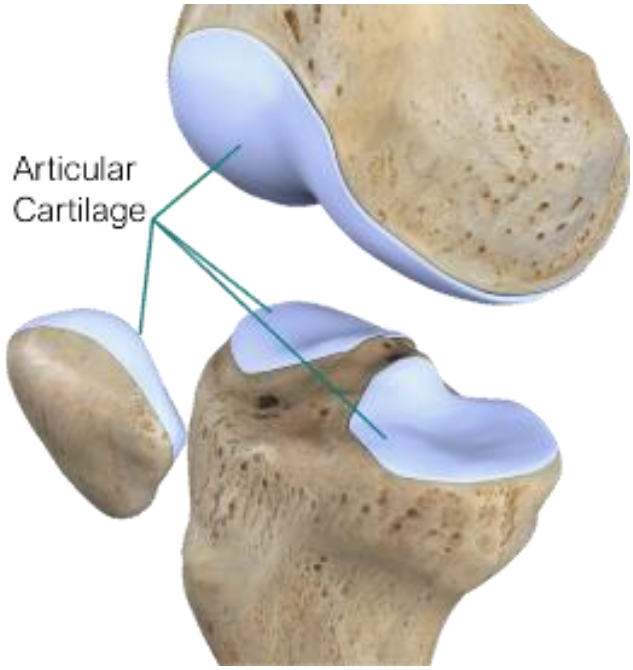


Figure 2.17: Femoral, tibial, and patellar hyaline (articular) cartilage surfaces.[18]

[18] Untitled [Online image]. Located at: https://pngio.com/images/png-a2602787/preview.html

# III. Literature Review

Meniscal injuries often occur in conjunction with or following ACL injuries (Lohmander et al., 2007) and are also linked to the progression of knee OA, thus it is essential to provide background on ACL injuries, meniscus injuries, OA, and treatment strategies including unloader knee braces. This chapter provides background regarding: (i) the two most commonly injured structures within the knee joint; (ii) experimental methods previously used to evaluate meniscus strain, as well as the function, usage, and effect of unloader braces; and (iii) computational knee biomechanical models.

## 3.1 Injury Epidemiology

### 3.1.1 *ACL Injuries*

The ACL is the predominant stabilizing structure within the knee joint, and it is the most commonly disrupted ligament from athletic injuries (Lohmander et al., 2007). There are over 200,000 incidences of ACL injuries annually in the United States resulting in an estimated cost of approximately $40,000–90,000/patient over the injury lifespan and an annual cost of $8–18 billion depending on the treatment method (Marshall et al., 2007; Mather et al., 2013; Prodromos et al., 2007). ACL sports injuries are predominantly non-contact injuries involving sudden decelerations due to changes in direction or landing motions seen in skiing, soccer, squash, handball, and basketball (Alentorn-Geli et al., 2009; Boden et al., 2010; Majewski et al., 2006).

ACL injuries typically affect young athletes aged 14–25 and require surgical correction or structured rehabilitation, with 90% of injuries in the United States requiring reconstruction (Paterno et al., 2014; Sanders et al., 2017) and numerous experts recommending a 60-week rehabilitation process (Paulos et al., 1981). Surgical interventions often take precedence since the majority of cases require a return to sport and a reconstruction is an attempt to prevent subsequent meniscal or cartilage injuries

(Mather et al., 2013). However, the majority of ACL reconstructions have a 5–6 times higher likelihood of sustaining a subsequent ACL injury compared to the injury risk for an uninjured individual (Paterno et al., 2014). Moreover, given the lengthy timelines for return to sport or rehabilitation treatment options without surgery, 70% of ACL-deficient individuals develop an injury to another part of the knee (Frobell et al., 2007). A longitudinal study reported that patients with an ACL tear have significantly higher risks of developing a meniscal tear, and cadaveric studies reported increased medial meniscal resultant forces as well as medial and lateral meniscal strains following ACL transection (Allen et al., 2000; Hollis et al., 2000; Sanders et al., 2015).

### 3.1.2 *Meniscal Injuries*

Meniscal injury epidemiology varies depending on the population studied, the geographic location, and the level of activity. Several studies have reported meniscus injuries are the second most common knee tissue injuries amongst athletes, indicating that they occur in tandem with ACL injuries and an untreated ACL can further exacerbate the incidence of injuries to the menisci (Allen et al., 2000; Lohmander et al., 2007; Majewski et al., 2006). While ACL injuries typically occur in the athletic population, meniscal injuries occur in the athletic and general population (Lohmander et al., 2007). When considering beyond the athletic population, meniscal injuries have been reported as the most commonly injured knee tissue with a mean annual incidence rate ranging between 23.8–90 per 100,000 inhabitants (Abrams et al., 2013; Clayton & Court-Brown, 2008; Fox et al., 2015; Hede et al., 1990; Lohmander et al., 2007; Nielsen & Yde, 1991). Clayton & Court-Brown (2008) reported meniscal tears as the most common soft tissue injury accounting for 22% of all soft tissue bodily injuries (n=2794) amongst 64,924 orthopaedic trauma patients between 12–90 years old. Moreover, the incidence rate for meniscal injuries was almost three times higher than ACL incidence rates amongst the general population (23.8 meniscal injuries vs. 8 ACL injuries per 100,000 patients).

Studies show meniscus injury incidences are higher in males compared to females. Meniscal injuries occur at later stages in life than ACL injuries, and while the mean ages of male and female meniscal injury patients are similar; the peak incidence ages differ greatly between sexes (Clayton & Court-Brown, 2008; Fox et al., 2015; Shea et al., 2004; Yu et al., 2005). Fox et al. (2015) stated meniscal tears occur 2.5–4 times more frequently in males vs. females and males account for 70–80% of all meniscal injuries (Drosos & Pozo, 2004; Greis et al., 1993; Hede et al., 1990). Clayton & Court-Brown (2008) reported the mean age of meniscal injury patients to be 33.8 years for males and 35.0 years for females. Comparatively, the same study found ACL injury patients had mean ages of 27.2 and 29.0 years for males and females, respectively. The peak incidences for meniscal injuries have been reported as 21–30 years for males and 11–20 years for females.

During an ACL deficient state, the medial meniscus becomes the primary stabilizer against ATT and it is thus more susceptible to injury (Granan et al., 2009; Lohmander et al., 2007, Maletis et al., 2011; Røtterud et al., 2013; Slauterbeck et al., 2009). Furthermore, an ACL deficiency coupled with a medial meniscus injury results in greater ATT than an ACL injury alone (Allen et al., 2000). The anatomy of the medial tibiofemoral compartment and geometry of the medial meniscus (Figs. 2.14a–c) are plausible causes of increased incidences of medial meniscus injuries. The medial meniscus sustains greater anterior-posterior translational loads, internal-external rotation loads and varus-valgus angular deviation in an ACL-deficient state (Greis et al., 2002; Hollis et al., 2000). It has been previously stated (§2.5.1) that the medial meniscus is smaller in width and cross-sectional area at the posterior root than the lateral meniscus. Studies reported that the medial meniscus represents the majority of meniscal injuries or repairs (Daniel et al., 1994; Englund, 2008; Frobell et al., 2007; Gee et al., 2020; Jones et al., 2012; Kilcoyne et al., 2012; Majewski et al., 2006; Sarraj et al., 2019); conversely some research concluded the lateral meniscus is more prominently injured (Fok & Yau, 2013; Yeh et al., 2012) (Fok & Yau, 2013; Yeh et al., 2012). Hollis et al. (2000) states that in an ACL-deficient knee lateral meniscus tears are associated with acute ACL injuries; whereas, medial meniscal

lesions are a result of more chronic ACL injuries, and Gee et al. (2020) states injury mechanism, acuity, and age are some factors which can dictate the injury location.

### 3.1.3 *Osteoarthritis*

Meniscus damage has been identified as a potent risk factor for the progression and development of OA (Englund et al., 2016). OA is a joint disease resulting in the degeneration of articular cartilage and is classified as primary (idiopathic) or secondary (Altman et al., 1986). In idiopathic OA, articular degeneration occurs with no prior history or obvious abnormality, whereas in secondary OA degeneration results from injury (trauma) or repetitive motion (Samson et al., 2007). In the US, OA symptoms become present after the age of 40, with the majority of 65-year old and 80% of 75-year old individuals displaying radiographic evidence of the disease (Hochberg et al., 1989). Moreover, tibiofemoral joint OA is the most common form of the disease affecting 11% of individuals older than 64 years of age (Felson et al., 1998; Naga et al., 2015). OA typically has a more profound effect on one side of the knee joint, with the medial compartment being more commonly affected (Halawi & Barsoum, 2017; Schmitt et al., 2008) and results in decreased joint-compartment space between the femur and tibia (Felson, 2006). OA symptoms include pain and discomfort ranging from mild inflammation to severe mechanical consequences such as grinding or degradation of the cartilage. Symptoms are typically accentuated with daily activities such as walking and (stair) climbing (Browner, 2003), and surgery is only recommended once all non-surgical treatment options have been attempted (Lee, 2012).

### 3.1.4 *Meniscus Injury Treatment Strategies*

Despite the recent success for non-operative treatment options, a third of meniscal injury patients will require surgical intervention (Mordecai et al., 2014). Meniscal surgeries are only feasible in certain conditions depending on factors such as the severity of the tear, location and nature of the tear, quality of the tissue, patient's age, and patient's

conditioning level (Frizziero et al., 2012; Laible et al., 2013). The most common surgical interventions for meniscal tears are meniscectomy, meniscal repair, and meniscal reconstruction (Doral et al., 2018). The state of the ACL is critical in the success of a meniscal procedure; a meniscal repair in conjunction with an ACL reconstruction has been reported with a 90% clinical success rate. However, if the ACL is left untreated this meniscal reparation success rate reduces to 50–67% (Fox et al., 2015). A meniscus allograft transplant is an alternative option; although, several contraindications and setbacks exist for the graft's limited success such as obesity, disease transmission and graft availability (Verdonk et al., 2013). Moreover, it is inconclusive if grafts prevent the progression of OA (Hergan et al., 2011). If a repair or graft is not plausible, a synthetic implant can be used. Artificial implants have been shown to alleviate pain; although, implant design, material properties, surface characteristics and fixation to the tibia and joint capsule are constraints the technology still needs to address (Fox et al., 2015).

Most meniscal surgeries require a four-month recovery period where the tissue needs to be protected from further damage (Fox et al., 2015), and during the rehabilitation period braces can be prescribed to protect the tissue (Heckmann et al., 2006; Mordecai et al., 2014). In many situations meniscal repair strategies are not feasible and arthroscopic meniscectomies remain the most common orthopaedic procedure; though recent evidence has shifted from meniscectomy to preserving the meniscus whenever it is possible (Beaufils & Pujol, 2017; Seil & Becker, 2016). Alternative non-operative treatment options for a degenerative meniscus injury include medications, exercise, activity modifications, physical therapy, weight loss, intra-articular injections, and bracing (Doral et al., 2018; Lee, 2016). Knee braces have been postulated to alleviate joint pain associated with a meniscal root tear (Bhatia et al., 2014).

## 3.2 The 3-Point Leverage Unloader Brace Mechanism

Knee braces are broadly classified as prophylactic, functional, rehabilitative, and unloader braces (Ramsey & Rusell, 2009). OA is not presently curable and unloader knee braces are designed to apply an external unloading (correction) moment to reduce stress on the affected arthritic joint compartment, with the intent to alleviate pain (Gravlee & Durme, 2007). The unloading moment is generated from a 3-point leverage mechanical design, which uses the strap tensions from three points of leverage. Two equal and opposite moments are created around the neutral hinge axis to produce an overall unloading moment (Fig. 3.1). Medial OA patients have a varus alignment (Fig. 3.2a) which can be corrected by a valgus unloading moment using a medial unloader brace (Fig. 3.2b), to return the joint to a (more) neutral position (Fig. 3.2c). In certain unloader brace designs the leverage point at or near the hinge axis may be represented by two points of contact due to a helical strap design (Fig. 3.2b).

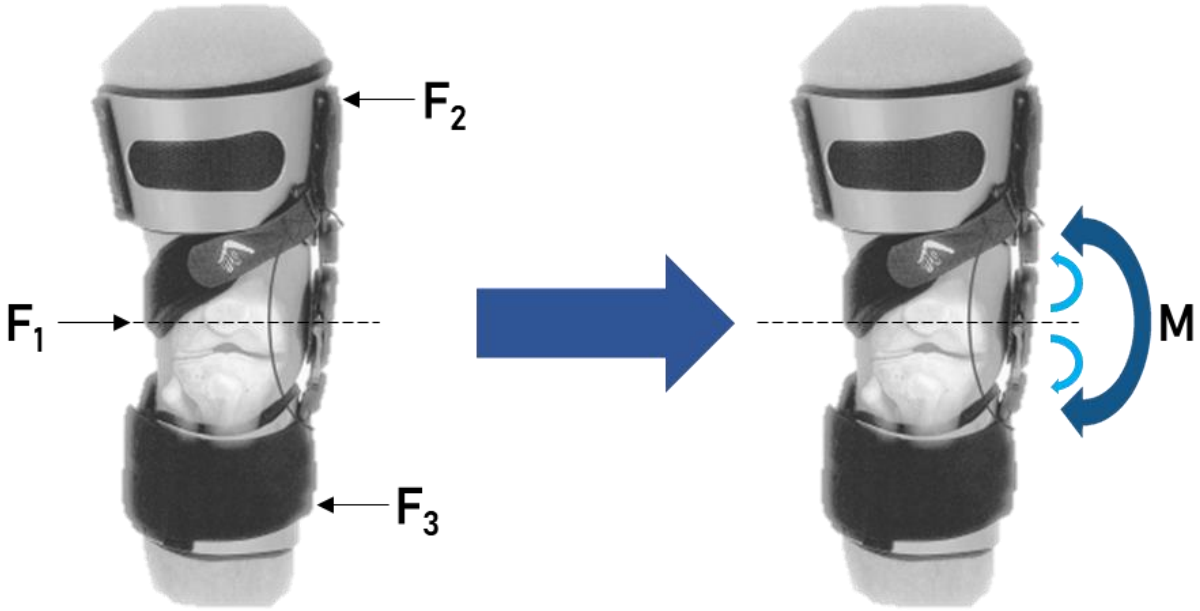


Figure 3.1: A right leg showing the 3-point leverage system illustrating the three points of force application ($F_1$, $F_2$, $F_3$), the medial hinge axis (at $F_1$), and the overall unloading correction moment (M) (adapted from Pollo et al. 2002).

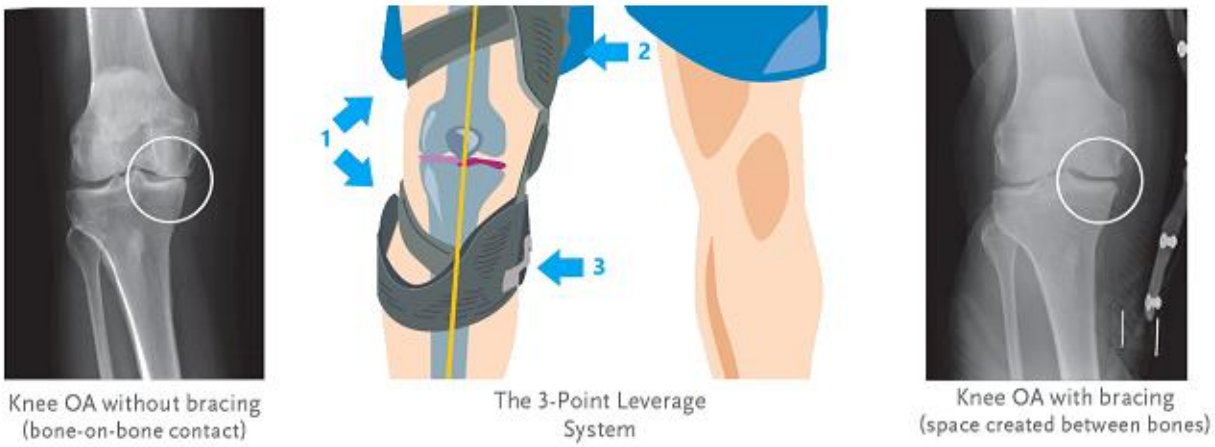


(a) (b) (c)

Figure 3.2: A right leg (a) unbraced X-ray scan illustrating medial knee compartment OA; (b) unloader knee brace illustrating a valgus unloading moment; and (c) braced X-ray scan illustrating a more neutral varus-valgus alignment.

Due to the deeply embedded nature of the menisci, few brace studies have investigated the effect of knee braces on meniscus tissues. Studies have prioritized numerous alternative outcomes to evaluate the effect or efficacy of knee braces through experimental and computational methodologies.

## 3.3 Experimental Knee Biomechanics

Experimental strain studies regarding the ACL involve in-vivo and in-vitro methodologies; whereas meniscus studies are predominantly in-vitro (Beynnon et al., 1992; Cerulli et al., 2003; Hollis et al., 2000; Jones et al., 1996; Taylor et al., 2011, Taylor et al., 2013). Strain gauges are a commonly used technique to measure tissue strain in specific directions and thin film resistive sensors are used to evaluate force or pressure (Anderson et al., 2003; Becker et al., 2005; Fukubayashi & Kurosawa, 1980, Schillhammer et al., 2012).

### 3.3.1 *Measuring Meniscal Tissue Strain*

Meniscal strain has been identified as an important outcome measure since a sustained increase in strain may be correlated with tissue damage (Pearsall & Hollis, 2004). Studies have used magnetic resonance imaging (MRI) or fluoroscopy to observe

the position and displacement of the menisci in different knee trauma states, weight bearing conditions, and flexion angles (Erbagci et al., 2004; Hajek et al., 1987; Lai & Levinson, 2010; Shefelbine et al., 2006; Vedi et al., 1999). It is highly advantageous to observe meniscus tissue in-situ; however, imaging modalities such as MRI or fluoroscopy cannot incorporate dynamic activities or knee braces.

Measuring biological tissue strains using an implantable strain sensor such as a displacement variable reluctance transducer (DVRT) (Figs. 3.3a-b) or a Hall Effect Strain Transducer (HEST) is common practice (Beynnon et al., 1992; Fleming et al., 1993; Johnson et al., 2006; Levin et al., 2013; Han et al., 2009; Tomescu et al., 2018, Zhang et al., 2021). These sensors measure changes in tissue length and strain is commonly computed using the engineering strain formulation. Both sensors provide direct strain measures that are highly representative of localized tissue environments, both are extremely sensitive and able to determine minute strain changes, and both have high sampling frequencies suitable for dynamic activities (Zhang et al., 2021). Similarly, both sensors are invasive, impinge the tissue, dependent on implantation alignment, and highly sensitive to sensor-body and cable interferences (Zhang et al., 2021). A major limitation of utilizing either of these sensors on biological tissues is determining the reference tissue length. Previous studies have alluded to the challenge and impracticality of determining the true reference length value and have used an arbitrary state or timepoint as the reference based on the desired outcome measures or loading conditions (Fleming & Beynnon, 2004; Levine et al., 2013; Taylor et al., 2013). The HEST has more limitations compared to the DVRT such as lower linear strain range, lower signal to noise ratio, lower sensitivity, and a sensitivity to temperature, which is perhaps why HEST sensors are less utilized (Zhang et al., 2021).

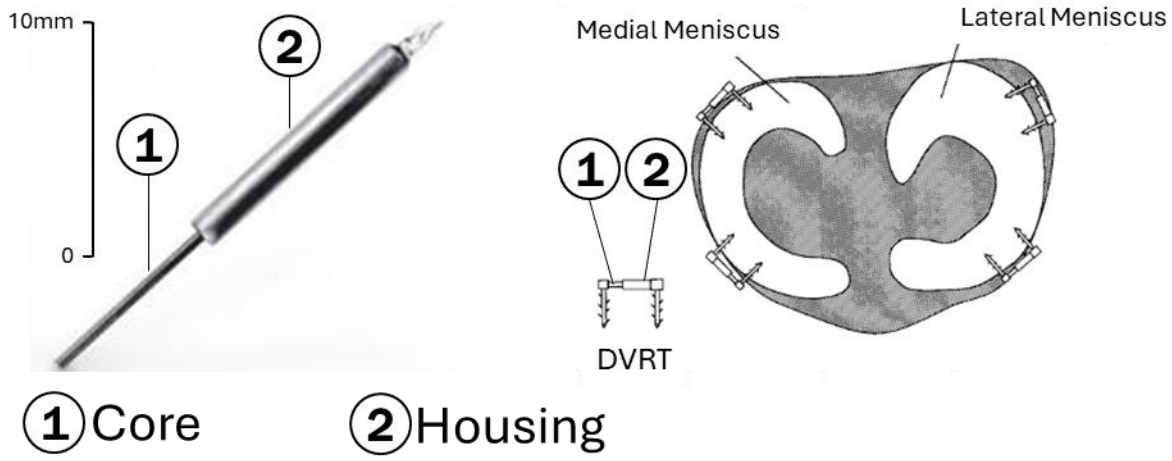


(a) (b)

Figure 3.3: (a) Enlarged view of displacement variable reluctance transducer (DVRT) showing housing and core components, and (b) DVRT inserted into meniscal tissues (adapted from Pearsall and Hollis, 2004).

Pearsall & Hollis (2004) used DVRTs to measure anterior and posterior medial and lateral meniscal circumferential strains at 0°, 30°, 60°, and 90° flexion angles given different injury states of the PCL, and the zero-strain reference length was the unloaded state at each flexion (Fig. 3.3b). Seitz et al. (2012) used a DVRT to measure anterior and posterior medial and lateral meniscal hoop strains under a partial meniscectomy condition on ten cadaver knees at various flexion angles, where the zero-strain reference was considered under an axial joint preload of 50 N. It is unclear whether Seitz et al. (2012) measured different zero-strain references for each loading condition. Similarly, Jones et al. (1996) measured anterior, central, and posterior in-vitro medial meniscus strain using a DVRT on intact and torn menisci by applying a compressive load to the knee joint at full extension and 30° flexion and showed an increase in meniscus strain with the presence of injury; there was no mention of how the zero-strain reference was considered. It is important to investigate meniscal outcomes as a function of the injury status of the ACL. Hollis et al. (2000) is a rare study that measured medial and lateral meniscus strains using DVRTs in an ACL-intact versus ACL-deficient condition with no mention of the zero-strain reference. Tomescu et al. (2018) investigated in-vitro medial meniscus strain with the influence of a functional ACL knee brace in an ACL-intact, -

reconstructed, -and deficient condition during gait and squats ADLs. The latter study considered an ADL specific zero-strain reference without the knee brace and reported decreases in peak meniscal tissue strain with the application of the brace and increases in peak strain with a deficient ACL. It remains to be seen whether unloader braces have similar effects on the meniscus tissue.

### 3.3.2 *Measuring Tibiofemoral Joint Pressure*

One of the earliest studies measuring tibiofemoral joint pressure and area used Prescale impression sheets (Fujifilm, Tokyo, Japan) (Fukubayashi & Kurosawa, 1980). Impression sheets record maximal momentary pressure upon contact, where the colour intensity of the impression corresponds to a pressure range. This method was not able to measure contact area and area was estimated from an additional silicon rubber cast of the tibiofemoral joint. Despite these limitations, this study was able to show pressure differences between normal and osteoarthritic knees (n=7). Further studies also relied on these impression sensors to measure contact pressures comparing normal vs. arthoplastic knees and indicated this method underestimated peak contact stresses and contact stress patterns differed between in-vitro and physiological conditions due to temperature differences (Szivek et al., 1995; Szivek et al., 1996). Future studies considered electronic resistive thin film pressure sensors capable of measuring pressure and area over a continuous duration (Harris et al., 1999; Matsuda et al., 1998). These studies validated the K-scan sensor (Tekscan Inc., Boston, MA, USA) by comparing them to the prior Fuji technology and showed comparable outcomes, with the exception that the K-scan sensors were able to measure contact areas more accurately under low loads. Numerous studies have since shown the feasibility of Tekscan sensors to measure inter-condylar joint pressure, with the model 4000 sensor (Fig. 3.3a) being commonly used (Anderson et al., 2003; Agneskirchner et al., 2004; Becker et al., 2005; Padalecki et al., 2014; Schillhammer et al., 2012; Seitz et al., 2012; Stuckenborg-Colsman et al., 2002; Thambyah et al., 2005; Van Thiel et al., 2011). The literature review in this dissertation as well as a systematic

review conducted by Moyer et al. (2015) found the only study to use Tekscan sensors to evaluate the effect of knee braces was Anderson et al. (2003). The in-vivo [Anderson] study surgically inserted model 6900 pressure mapping sensors (Fig. 3.3b) within the joint compartments of patients.

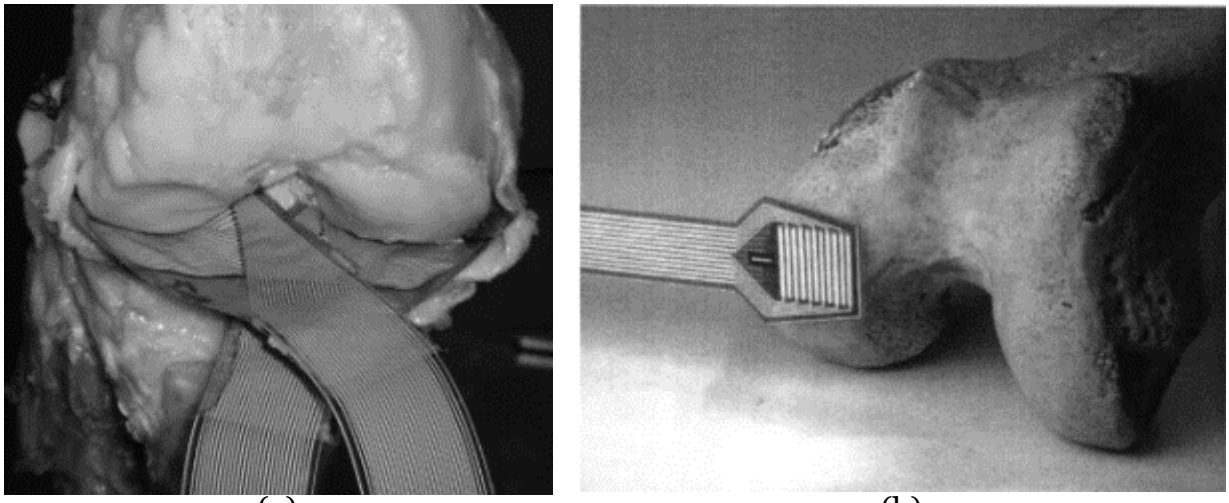

(a) (b)

Figure 3.4: Tibiofemoral insertion of the (a) Tekscan model 4000 sensor (Agneskirchner et al., 2007 – reprinted with permission from Elsevier); and Tekscan model 6900 sensor (Anderson et al., 2003 – reprinted with permission from Elsevier).

### 3.3.3 *Clinical and Biomechanical Unloader Brace Efficacy*

In-vivo clinical trials typically report brace efficacy on outcomes such as external knee adduction moment (KAM), joint separation, gait and posture performance, muscle activation, pain relief scores, quality of life scores, functional outcomes, electromyography, and/or pain medication dependence (Parween et al. 2019). There is an extensive breadth of literature stating a reduction in pain and/or improvements in pain scores while using unloader braces (Briggs et al., 2012; Dessery et al., 2014; Fu et al., 2015; Hart et al., 2016; Kirkley et al., 1999; Laroche et al., 2014; Lindenfeld et al., 1997; Matsuno et al., 1997; Petersen et al., 2019; Pollo et al., 2002; Ramsey et al., 2007). Additional clinical outcomes have shown brace usage has increased patient confidence in the willingness to perform daily activities and decreased the reliance on pain medications (Barnes et al., 2002; Finger & Paulos, 2002; Lindenfeld et al., 1997; Kirkley et al., 1999; Petersen et al., 2019). Moreover, patients prescribed knee braces have demonstrated

functional outcome improvements including a significant reduction in stair climbing time and a significant improvement in gait velocity (Divine & Hewitt, 2005; Fantini Pagani et al., 2010, Schmalz et al., 2010). The knee injury and osteoarthritis outcome score (KOOS) is a tool that assesses patient pain, symptoms, daily living function, sport and recreation function, and knee-related quality of life (Roos et al., 1998). Hjartarson & Toksvig-Larsen (2018) and Ostrander et al. (2016) have evaluated the efficacy of unloader braces and shown braces can improve KOOS outcomes in all five categories. A subset of clinical work for osteoarthritis management using unloader braces has reported biomechanical outcomes such as a reduction in KAM during gait analysis (Fu et al., 2015; Jones et al., 2013; Lamberg et al., 2016; Laroche et al., 2014; Orishimo et al., 2013; Fantini Pagani et al., 2010; Pollo et al., 2002), a reduction in the vertical and horizontal components of the ground reaction force (Schmalz et al., 2010), a reduction in tibiofemoral contact force (Kutzner et al., 2011; Pollo et al., 2002), an increase in the tibiofemoral compartment joint space (Dessinger et al., 2021; Nagai et al., 2019), and a reduction in muscle activity and co-contraction levels (Fantini Pagani et al., 2013). Despite the positive outcomes of unloader braces in clinical trials, the biomechanical effects are still being largely debated (Brouwer et al., 2006; Duivenvoorden et al., 2015; Richard Steadman et al., 2016).

The aggregate of unloader brace studies have focused on the existence/severity of osteoarthritic symptoms and outcome measures unrelated to the function of the menisci. Review studies such as Bhatia et al. (2014), Cavanaugh & Killian (2012), Kovacs et al. (2002), and Rao et al. (2015) suggest that unloader knee braces used for osteoarthritic prevention and treatment can be prescribed to patients dealing with meniscus injuries, these braces may alleviate joint pain associated with a root tear, and unloader braces can serve as a non-operative management strategy for partial or total meniscectomy patients. Additional research such as Shriram et al. (2019) and Thorning et al. (2016) are examples of computational and experimental methodologies, respectively, that have investigated the effects of valgus unloader braces on total and partial meniscectomized knee joints and patients. Amongst these studies the investigation of meniscal tissue response remains a

literature gap since their outcome measures include differences in peak KAM, KAM impulse, peak knee flexion moment, and tibiofemoral joint contact pressures in unbraced vs. braced scenarios.

### 3.3.4 *In-Vitro Knee Simulators*

Brace efficacy studies are typically done using in-vivo methodologies and are unable to investigate meniscal tissue outcomes. Dynamic testing is feasible using an in-vitro simulator capable of applying external kinematics, forces, and torques to a knee joint. Prior work simulating load on cadaveric knees has either focused on non-dynamic test conditions, considered dynamic conditions without considering accurate muscle force profiles, or did not focus on high speed knee motions. The University of California Los Angeles simulator is an example of a static simulator that requires weights to be hung from sutured muscle force cables. The three-degree of freedom (3-DOF) system can generate anterior-posterior tibial forces and interior-exterior tibial torque, while allowing sagittal plane flexion, tibial rotation, and valgus-varus angulation (Markolf et al., 2004). It is unable to replicate the mechanical effects due to time-varying muscle forces or kinematic accelerations. A more recent revision to static simulators is the test rig developed at Imperial College London (Stephen et al., 2016). The system permits loading scenarios in 6-DOF where each one can be statically varied using a hanging weight. The additional three degrees give deeper variability and understanding to biomechanical responses. Though, the effect of acceleration is still absent, and the simulator is limited to discrete measurements at 10-degree flexion angles.

There are several dynamic knee simulators that overcome the shortcomings of static simulators including the University of California Davis simulator, McGill University simulator, Purdue University Mark-II simulator, University of Michigan simulator, Texas Tech University simulator, University of Toledo simulator, and University of Waterloo simulator (Berns et al., 1990; McLean & Ahmed, 1993; Maletsky & Hillbury, 2005; Withrow et al., 2006; Hashemi et al., 2007; Levine et al., 2013 and Cassidy et al., 2013).

The McGill, TTU, Michigan, and Waterloo simulators are of particular interest to this study.

The McGill simulator developed by McLean et al. (1993) is very similar to a previous iteration developed by Szklar and Ahmed (1985). Both simulators lump flexor and extensor muscle groups into two cables connected to individual stepper motors to replicate muscle group displacements. The updated simulator replicates ground reaction force (GRF) with a foot-to-floor reaction force acting on the tibia (Fig. 3.4). The simulator performed a gait simulation, although the outcome was only validated against joint flexion angle and the system constrains the hip joint in all degrees. The displacement-time histories of the flexor and extensor muscle groups are also unclear.

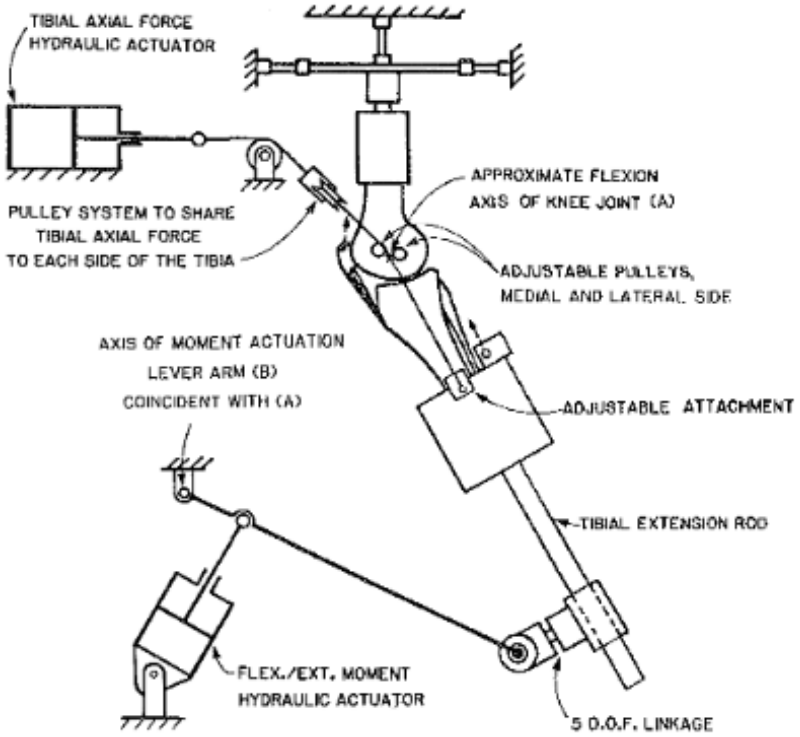


Figure 3.5: Pictorial representation of McGill University knee simulator featuring a flexion-extension and axial force actuators (McLean et al., 1993 – reprinted with permission from American Society of Mechanical Engineers).

The Michigan simulator (Fig. 3.5) includes gastrocnemius muscle cables for the medial and lateral heads, the combined quadriceps muscle via the quadriceps tendon and cables representing the medial and lateral hamstrings (Withrow et al., 2006). Despite the

extensive muscle force contributions, the simulator is limited to a single uniaxial impact load applied at the hip joint and does not permit control for the time varying muscle forces.

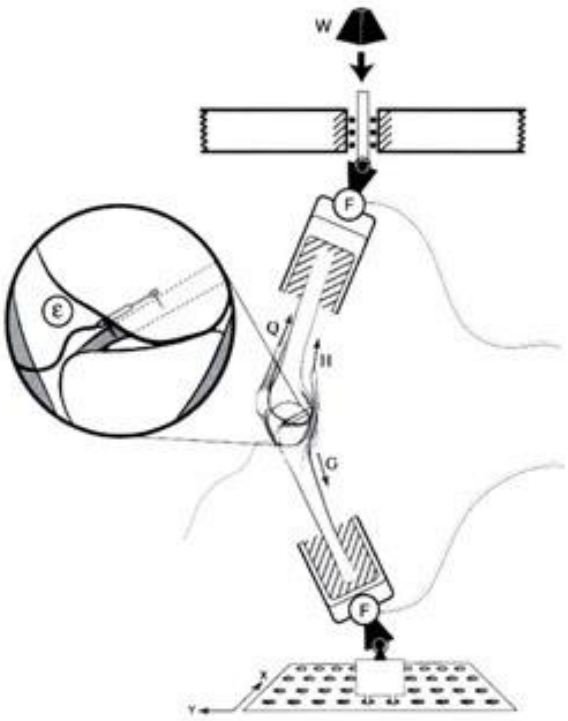


Figure 3.6: Illustration of the University of Michigan simulator displaying a DVRT sensor placed on the ACL, as well as flexor and extensor muscle force group cables (Withrow et al., 2006).

The Texas Tech University simulator (Hashemi et al., 2007) simulated jump landing motions (Fig. 3.6). Unlike the McGill simulator, the hip joint is permitted to translate in the anterior-posterior direction in addition to sagittal plane rotation. The system includes quadriceps and hamstrings muscle force group actuators capable of applying position or constant force controls. The study was able to successfully measure ACL strains in safe and injury-prone conditions, though it cites the absence of a gastrocnemius force cable as a limitation and does not account for time varying muscle forces.

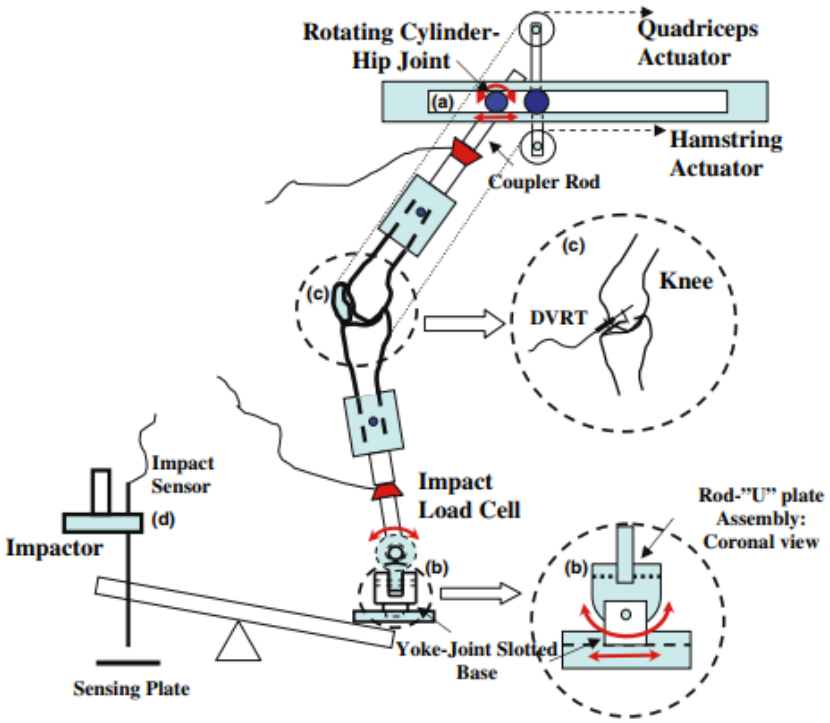


Figure 3.7: Illustration of the Texas Tech University simulator featuring quadriceps and hamstring muscle group actuated forces, as well as a DVRT implanted within the ACL (Hashemi et al., 2007 – reprinted with permission from Springer Nature).

The University of Waterloo DKS is considered a second generation update to the TTU version and integrates time varying joint kinematics and dynamics (Cassidy et al., 2013). The simulator has undergone numerous revisions and successfully simulated single leg jump landings, gait, and squatting motions in unbraced and braced scenarios (Cassidy et al., 2013; Bakker et al., 2016; Hangular et al., 2016; Tomescu et al., 2018). The DKS consists of two positional actuators for hip and ankle velocities and four additional actuators for quadriceps, hamstrings, gastrocnemius, and hip forces. This simulator permits sagittal plane flexion-extension of the hip and ankle joints, internal-external rotation of the femur and tibia, vertical hip, and antero-posterior ankle translation as well as varus-valgus knee movements. It is essential to note the ankle joint is constrained to single-axis rail and maintains physical contact throughout the gait simulation. While the simulator is limited to sagittal plane motion, the DKS addresses the issues other research laboratories have faced by incorporating high speed motion, large muscle force profiles typically seen in gait and squat activities, and accurate knee joint

kinematics. An extensive methodology based on a combined in-vivo, in-silico, in-vitro approach has been developed to perform single leg jump landing, gait, and squatting activities using this simulator (Cassidy et al., 2013; Hangalur et al., 2016; Tomescu et al., 2018).

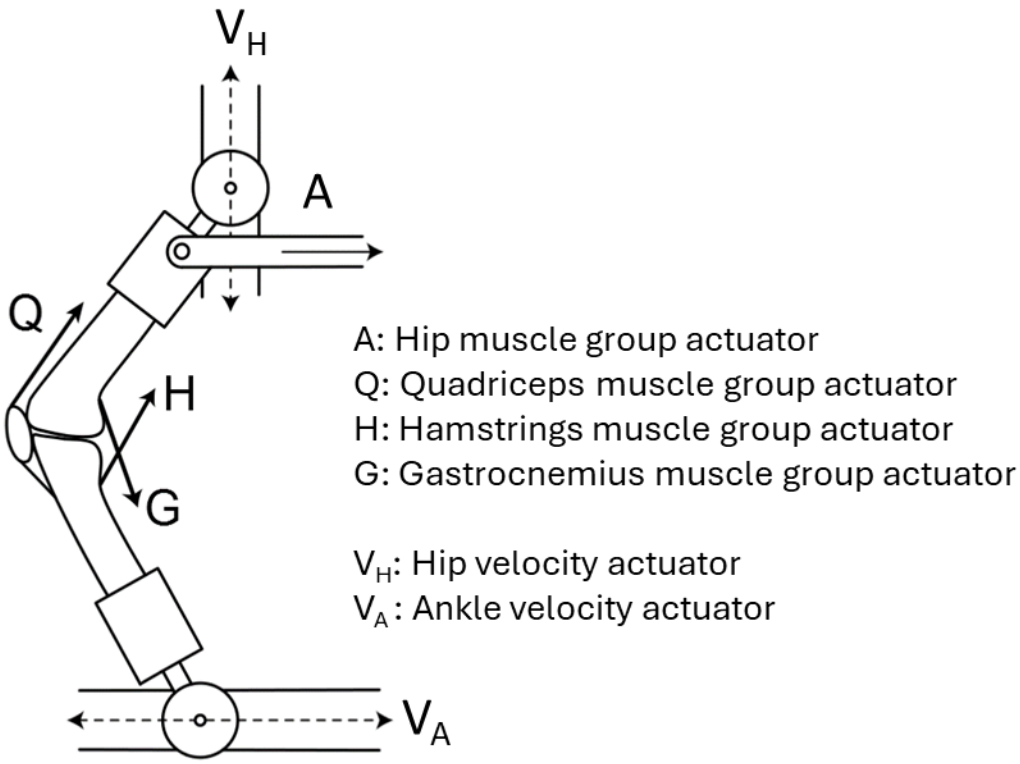


Figure 3.8: Illustration of the University of Waterloo dynamic knee simulator (adapted from Bakker 2014).

### 3.3.5 *The Waterloo DKS Combined In-Vivo, In-Silico, In-Vitro Approach*

Quantifying the effect of a knee brace on meniscus strain during ADLs has been done using the DKS. Tomescu et al. (2018) measured in-vivo lower extremity kinematics and ground reaction force on a healthy 28-year-old female participant performing gait, double leg squat (DLS), and single leg squat (SLS) ADLs. An in-silico phase was conducted by importing the in-vivo data to a biomechanical multibody model using the Gait2392 model ($23^o$ of freedom, 92 muscles, Fig. 3.7) in OpenSim (Delp et al., 1990). This former study computed flexion angle, time-varying hip and ankle joint kinematics, and net moments for the quadriceps, hamstrings, gastrocnemius, and hip muscle groups (Fig.

3.8). The Gait2392 model resulted in kinematics that were within 1 SD of previous in-vivo work for all ADLs, and gait muscle activation patterns that were in general agreement with a previous study (Tomescu 2017). The individual muscle contributions in the quadriceps muscle group included the rectus femoris, vastus medialis, vastus lateralis, and vastus intermedius; the hamstrings group included the semimembranosus, semitendinosus, biceps femoris long-head, and biceps femoris short-head; and the gastrocnemius group included the medial and lateral heads. The four muscle force, hip velocity, and ankle joint velocity time histories formulated the six input conditions to recreate the in-vivo activity on the DKS, and a unique kinematic and kinetic dataset has been reported for each of the three ADLs (Tomescu et al., 2018). The experimental gait and squat kinematics were reported within one standard deviation of the in-vivo measurements and the ACL and meniscal tissues response strain patterns showed similar results compared to previous literature, indicating the DKS was not solely limited to simulating jump landing motion. Using the in-vivo results from Tomescu et al. (2018), gait and squatting simulations can theoretically be performed to measure the effect of an unloader brace on meniscus strain.

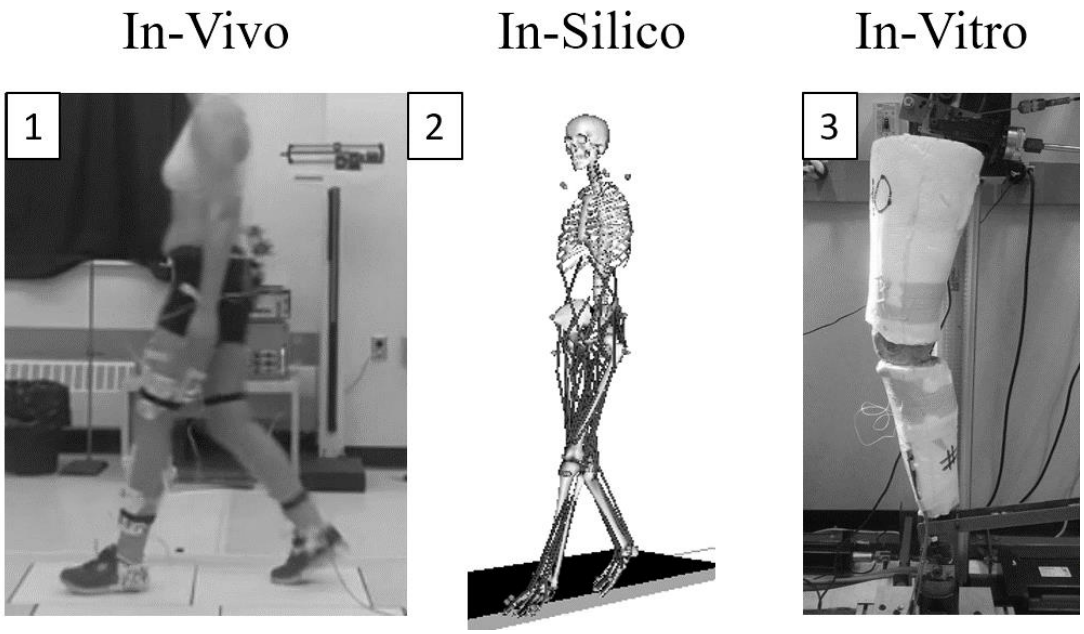


Figure 3.9: Illustration of the in-vivo, in-silico and in-vitro processes (Tomescu et al., 2018 – reprinted with permission from Springer Nature).

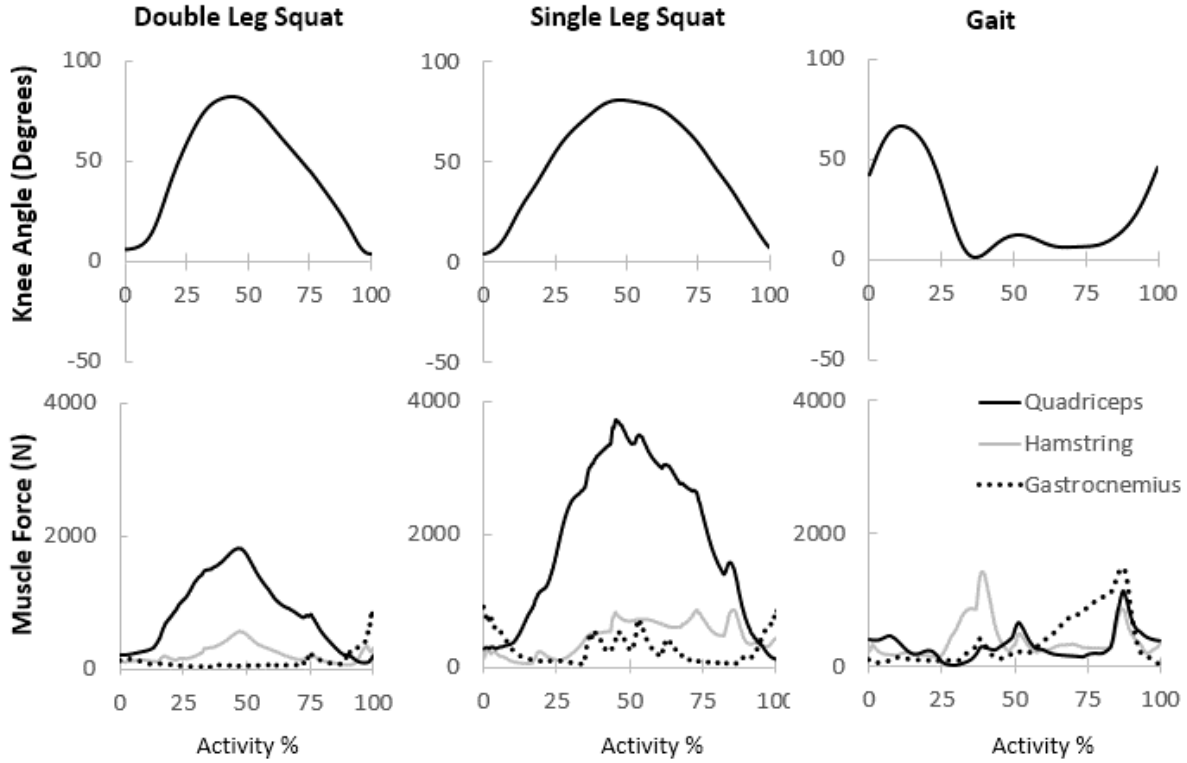


Figure 3.10: Flexion (knee) angle and Muscle Force outputs from OpenSim for double leg squat (left), single leg squat (center), and gait (right) simulations (Tomescu et al., 2018 – reprinted with permission from Springer Nature).

## 3.4 Human Body Finite Element Modelling

Computational research is a valuable complementary methodology to experimental research. The finite element (FE) method is the most commonly used approach in orthopaedic biomechanics since these models: are widely adjustable and customizable, avoid experimental challenges (e.g., ethical constraints, participant recruitment, specimen availability), can predict location specific injury responses anywhere within the body, and can more accurately predict injury intensity (Augat et al., 2021; King, 2017). The FE method is an approximation to solve problems in a continuous system that requires geometrical, material, and boundary condition (BC) inputs in order to generate an output or response (Fig. 3.9) (Schmitt et al., 2019).

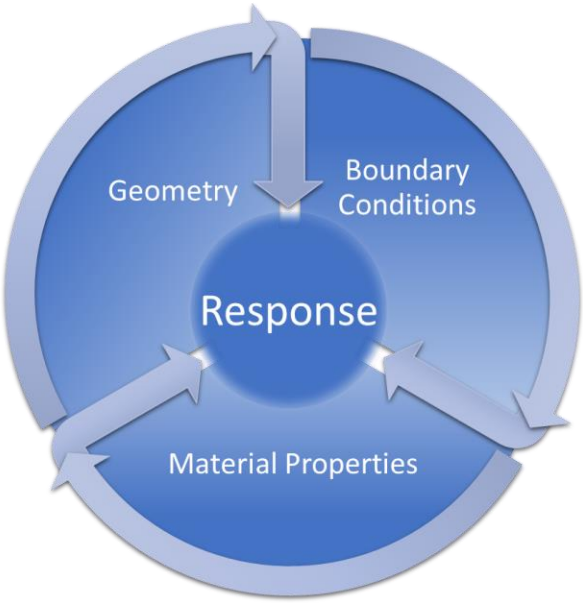


Figure 3.11: Iterative representation of the inputs required in the FE method.

A FE geometry is often created from detailed MRI and computed topography scans of live participants or post-mortem specimens and consists of parts discretized into small volumetric entities known elements (Augat et al., 2021, Schmitt et al., 2019). Inter-element connectivity and intra-element boundaries are defined by nodes and an accumulation of elements constitutes a mesh. Geometric detail, mesh resolution, and the assessment of mesh convergence should be governed by the model intent or impact scenario (Schmitt et al., 2019). Boundary conditions are applied to specific geometries based on the intent or constraints of the simulation and should be applied in ascending order of complexity to ascertain BC validity and model fidelity (Schmitt et al., 2019)

Material property formulations and their implementation are considered the most challenging facets of human body FE modeling (Schmitt, 2019). Material properties are based on experimental human tissue testing studies, which are often limited and highly conditional due to biological variability and limitations with the chosen experimental procedure (Schmitt et al., 2019). Ideally, material properties are measured in terms of stress-strain and implemented in FE models relating stress to strain; however, properties are pragmatically measured with force-displacement and converted to stress-strain assuming uniform deformation (Schmitt et al., 2019). Additionally, material properties

are strain rate dependant and in a FE model the element strain rate, strain, and stress may be dependant on the element size (Schmitt et al., 2019). Therefore, it is recommended to consider material properties that reflect the strain rates in model and to conduct a mesh convergence to quantify the response sensitivity to mesh size (Schmitt et al., 2019).

Verification and validation are key concepts defined by FE literature to quantify model performance and explain or reduce model prediction uncertainty, where verification is often an accuracy check within the model and validation involves assessing model performance against an independent set of data (Schmitt et al., 2019). Validation is traditionally conducted by comparing a model response to a previous model or experimental response, or by assessing the model response within a certain range or 'corridor' of responses. Moreover, cross-correlation methods have been used to quantify the degree of agreement between reference and model responses (Schmitt et al., 2019).

## 3.5 Finite Element Knee Biomechanics

Although FE models can be expensive and time consuming to develop, the cost of applying an existing validated model is modest (Augat et al., 2021). The FE method has been extensively utilized in lower extremity biomechanical research to complement experimental research; however, pre-existing lower body models commonly do not include anatomically accurate parts of the four major structural knee ligaments, cartilage, patella, or menisci. FE models can reduce their computational costs by reducing the number of elements, focusing on a subset of parts, or reducing part complexity such as modelling ligaments as 1D non-linear spring elements (Ali et al., 2016; Aspden, 1985; Baldwin et al., 2012; Bendjaballah et al., 1995; Halonen et al., 2013; Harris et al., 2016; Haris et al., 2021; Haut Donahue et al., 2003; Kang et al., 2017; Li et al., 2001; Mononen et al., 2013; Park et al., 2019; Spilker et al., 1992; Yao et al., 2006; Yao et al., 2012; Zielinska et al., 2006). Certain studies have lower body FE models with the major ligaments and tissues represented by 3D structures (Fig. 3.10) with various types of BCs,

element formulations, and material models (Table 3.1) (Beillas et al., 2001; Guo et al., 2009, Kiapour et al., 2014; Kwon et al., 2014; Peña et al., 2005, Ramaniraka et al., 2005, Shriram et al., 2019; Untaroiu et al., 2013; Vairis et al., 2013, Wan et al., 2011, and Westermann et al., 2013).

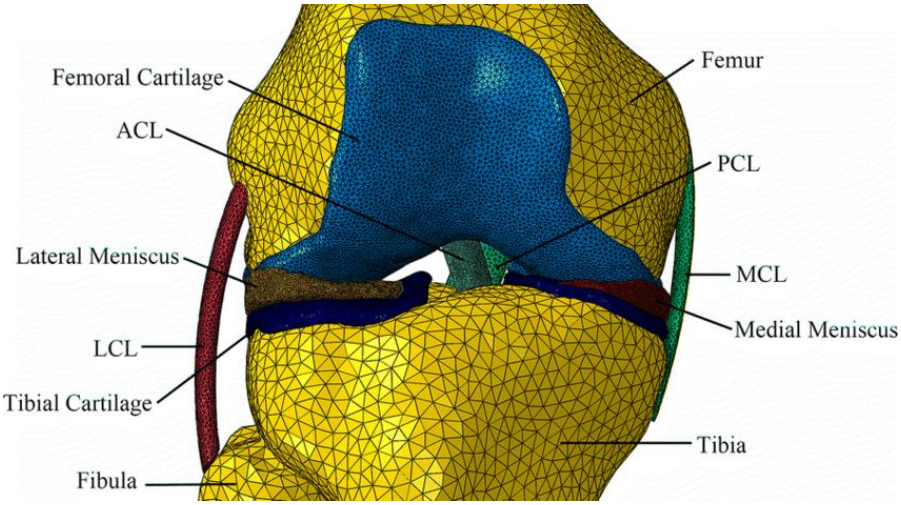

Figure 3.12: Example of an anatomically representative FE model (Zhu et al., 2019).

Table 3.1: Simulation, validation, and ligament and menisci formulation in select lower body finite element models.

| | Simulation | Ligament Element Formulation | Ligament Material Model | Menisci Element Formulation | Menisci Material Model | Validation Method |
|---|---|---|---|---|---|---|
| Beillas (2001) | Tibial axial loading, patellar impact, anterior-posterior tibial loading, lateral loading, sled test | Shell and brick elements | Viscoelastic | Solid elements | Linear elastic | In-vitro tibial impact and prev. in-vitro literature |
| Guo (2009) | Instantaneous femoral axial load during gait | Hexahedral | Hyperelastic transverse isotropic | Hexahedral | Linear elastic isotropic | Prev. FE literature |
| Kiapour (2014) | Quasistatic testing including 0–50Nm abduction, 0–50Nm abduction+20Nm internal tibial rotation, 0–90° unloaded flexion, 15Nm internal tibial rotation; 134N anterior tibial shear + 15Nm internal tibial rotation all under 400N quadriceps and 200N hamstrings force<br><br>Dynamic testing including jump landing with 1200N quadriceps and 800N hamstrings force | Hexahedral | HGO | Hexahedral | Linear elastic transverse isotropic | In-vitro testing from prev. Kiapour (2011, 2012) studies |
| Kwon (2014) | 2600N peak femoral axial loading with 0–58° extension–flexion and ± 5° tibial rotation profile | Hexahedral | Hyperelastic | Hexahedral | Linear elastic isotropic | Prev. in-vitro literature |
| Peña (2006) | 1150 compression +134N horizontal load; 1150N compression+10Nm valgus torque; all 3 loads combined | Hexahedral | Hyperelastic transverse isotropic | Hexahedral | Linear elastic isotropic | Prev. in-vitro and FE literature |
| Ramaniraka (2005) | Flexion-extension | Hexahedral | Hyperelastic | Hexahedral | Unspecified | Prev. clinical literature |

| | | | | | | |
|---|---|---|---|---|---|---|
| Shriram (2019) | Gait | Tetrahedral | Hyperelastic transverse isotropic | Tetrahedral | Hyperelastic transverse isotropic | Prev. in-vivo/in-vitro/in-silico literature |
| Untaroiu (2005) | Quasi-static three-point bending on femur, tibia, fibula, dynamic flesh compression, dynamic femur three-point bending, dynamic full leg three-point bending, dynamic full leg four-point bending. | Hexahedral | Quasi-linear viscoelastic | Hexahedral | Linear elastic transverse isotropic | Prev. experimental literature data |
| Vairis (2013) | 1150 compression +134N horizontal load; 1150N compression+10Nm valgus torque; all 3 loads combined | Tetrahedral | Linear elastic & Hyperelastic | Tetrahedral | Linear elastic | FE outcomes from Pena et al. 2006 |
| Wan (2011) | 134N posterior femoral force | Tetrahedral | Hyperelastic | Tetrahedral | Linear elastic transverse isotropic | Prev. in-vitro and FE literature |
| Westermann (2013) | Lachman test | Hexahedral | HGO | Hexahedral | HGO | Prev. in-vivo/in-vitro literature |

HGO: Holzapfel-Gasser-Ogden; prev.: previous

Two of these studies performed in-vitro experiments to validate their respective models using similar loading conditions (Beillas et al., 2001; Kiapour et al., 2014). The Guo et al. (2009) and Wang et al. (2014) models performed gait or squatting simulations; however, they did so with limited dynamic, kinematic, and kinetic boundary conditions. Guo et al. (2009) simulated a gait cycle by applying a posterior perturbation to the femur while retaining the tibia and fibula fixed, along with a vertical load to the full leg to simulate body weight. Wang et al. (2014) simulated a squat with 400 N of quadriceps force and a 300 N body weight load. The Kiapour et al. (2014) model is a thoroughly developed lower extremity model that validated various quasi-static and dynamic loading conditions such as knee abduction, internal tibia rotation, anterior shear, and jump landing under the influence of quadriceps and hamstring forces (Table 3.1). The model has limitations with gait since it does not include time-varying gait BCs and associates the quasi-static loading scenarios to equivalent gait situations. The Global Human Body Models Consortium (GHBMC) developed a 50$^{th}$ percentile male full human body model (M50) that has been used to simulate lower extremity vehicular occupant impacts (Untaroiu et al., 2005). Moreover, the M50 has been utilized to simulate a jump landing using the Waterloo DKS kinematic and kinetic BCs (Polak, 2019), and can potentially be adapted to simulate squat and gait ADLs.

### 3.5.1 *GHBMC 50$^{th}$ Percentile Male Human Body Model*

The M50 was developed as a seated occupant for injury prediction and prevention in automotive impact scenarios (Fig. 3.11) (Gayzik et al., 2011). The model geometry was developed from supine MRI, x-ray, and external surface scans of a live participant (age: 26 years; height: 175.3 ± 2.54 cm; mass: 77.1 ± 3.9 kg; BMI: 25.1 ± 2.0 kg/m$^2$). At the time of development, the whole body model comprised 847 parts, 557 material definitions, 1.95 million elements, and 1.30 million nodes (Gayzik et al., 2011). A limitation of the M50 is that validation studies have focused on automotive impact scenarios with lower extremity validation studies focusing on femur, tibia, fibula, and full

leg three- and four-point bend tests, skin surface compression tests, various knee and full leg directional impactor tests, and bending/compressive/combined loads on the femur and tibia (Table 3.2) (Untaroiu et al., 2005; Untaroiu et al., 2013; Khor et al., 2018; M50 manual v4-5).

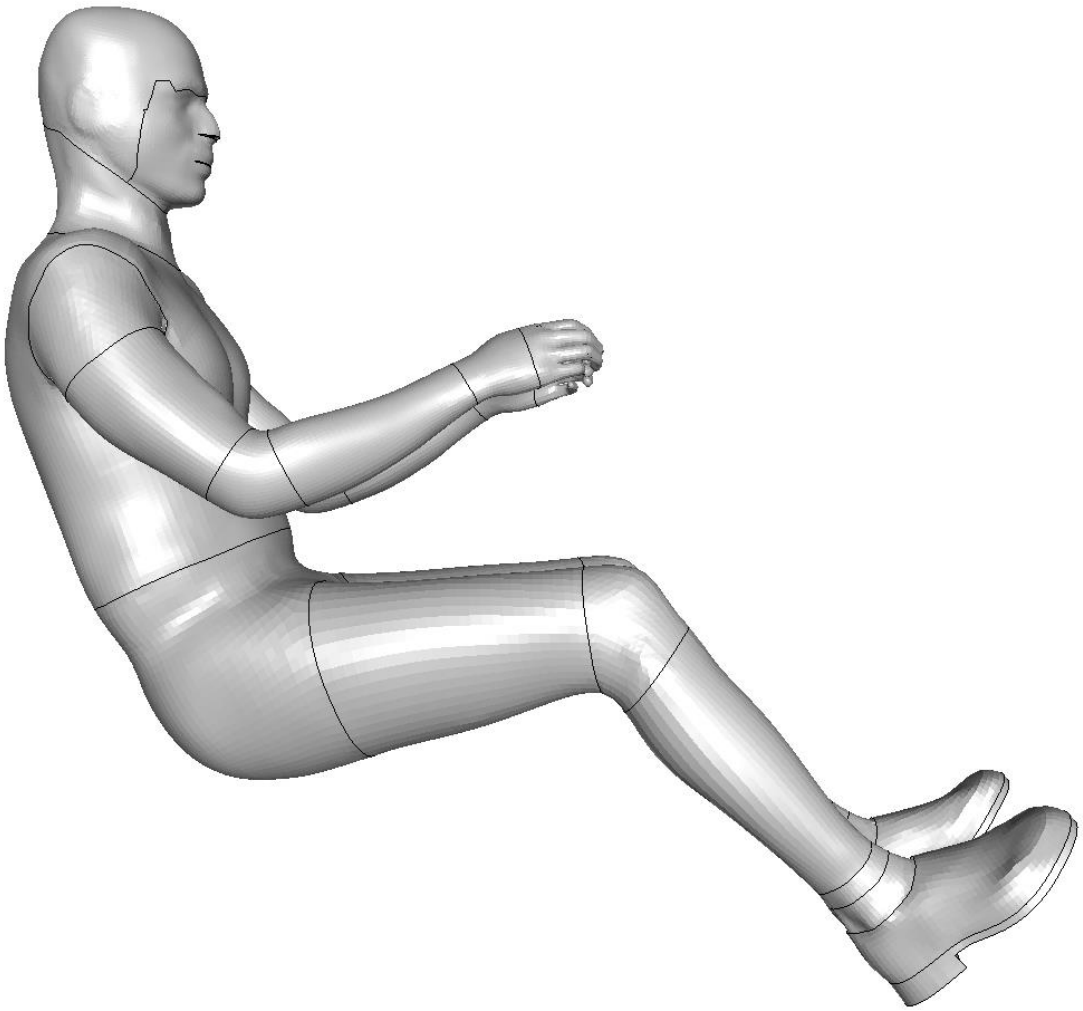

Figure 3.13: GHBMC M50 seated occupant human body model.

Table 3.2: Lower extremity validation tests for M50 v4-4, adapted from M50 manual v4-4.

| Structure/Region – Simulation | Evaluation Criteria | Reference |
|---|---|---|
| Thigh model – medial side impact | Impact force vs. Deflection | Kerrigan et al. (2004)<br>Untaroiu et al. (2005) |
| Femoral shaft – bending | Impact force vs. Deflection | Funk et al. (2004)<br>Untaroiu et al. (2005)<br>Irwin et al. (2002) |
| Femoral shaft – 3-point bending, combined bending and compression | Impact force vs. Deflection | Untaroiu et al. (2013) |
| Femoral shaft – 3-point bending, axial rotation | Impact force vs. Deflection | Khor et al. (2018) |
| Femoral shaft – impact in anterior-posterior and posterior-anterior bending and compression | Impact force vs. Axial force | Ivarsson et al. (2009) |
| Femoral head – compression loading to fracture | Force | Keyak et al. (1997) |
| Femoral head – compression loading to fracture | Force | Untaroiu et al. (2013) |
| Lower leg – combined compression and bending | Force vs. Moment | Untaroiu et al. (2008)<br>Ivarsson et al. (2009)<br>Taylor et al. (1996) |
| Tibial shaft – lateral and medial bending | Force vs. Deflection | Kerrigan et al. (2003) |
| Lower limb (knee-thigh model) – impact | Force vs. Time | Rupp et al. (2003) |
| Lower limb (knee-thigh-hip model) – knee impact | Force vs. Time | Rupp et al. (2002)<br>Rupp et al. (2003) |

Few studies have analyzed knee ligament or soft tissue mechanics using the M50 model. Lin et al. (2018) reported peak failure loads in the collateral and cruciate ligaments during a belted occupant impact and Polak (2019) reported ACL-strain during single leg jump landing simulations. These two former studies demonstrated that the M50 is capable of simulating knee tissue responses, and Polak (2019) replicated an activity based on kinematic and kinetic BCs from the Waterloo DKS. These previous outcomes lead to the presumption that this model would be suitable to simulate gait and squat ADLs. However, neither of these studies reported meniscal tissue responses, thus, it remains to be explored whether the M50 can address this literature gap. Polak (2019) reported

modifying the meniscus material model to linear elastic since the original material formulation reported zero strain during a jump landing, though there was no mention of strain following the modification. Moreover, the M50 defines an identical material model for all four cruciate and collateral ligaments as a quasi-linear transversely isotropic viscoelastic model based on quasistatic MCL tensile tests taken from literature (Untaroiu et al., 2005). Polak (2019) modified the ACL material model based on an ACL tensile test taken from literature, replicated a uniaxial ACL tensile test in the M50, and reported that the modified material resulted in more comparable force-elongation outcomes when compared with the original experimental studies. Based on the findings in Polak (2019) it is evident the M50 requires a material enhancement to the ACL and menisci, and it is possible that the LCL, MCL, and PCL responses may also improve with enhancements to their respective material models, as the ACL did. As previously stated material properties and formulations are the most challenging aspects of human body FE modelling and require a thorough investigation of prior experimental literature.

### 3.5.2 *Material Properties for Select Knee Soft Tissues*

In the M50 the modeled soft tissue knee structures include the ACL, LCL, MCL, PCL, lateral meniscus, medial meniscus, and tibiofemoral cartilage (Fig. 3.12). Experimental studies have investigated the material properties of these biological structures under a variety of loading conditions. Butler et al. (1986) conducted tensile tests on ACL, LCL, MCL, and PCL specimens, although the findings are highly conditional since the study tested a small collection of individual ligament fibers and did not consider the anatomical orientation or complete geometry of the structures.

Grood & Noyes (1976) and Woo et al. (1991) investigated the effect of specimen age on the material response of the ACL. Both studies demonstrated similar material stiffnesses between younger and older age groups and higher ultimate loads from younger donors. Chandrashekar et al. (2006) correlated the ACL tensile response to donor anthropometry. This study reported similar ACL structural properties comparatively to

Woo et al. (1991) and similar structural and modulus of elasticity compared with Grood & Noyes (1976). The strain, stress, and strain energy density at failure reported by Chandrashekar et al. (2006) disagree with Grood & Noyes (1976), since it was reported by Chandrashekar et al. (2006) that Grood & Noyes (1976) underestimated cross-sectional area measurements by using a micrometer. Chandrashekar et al. (2006) determined the minimum ACL cross-sectional area using a non-contact imaging technique.

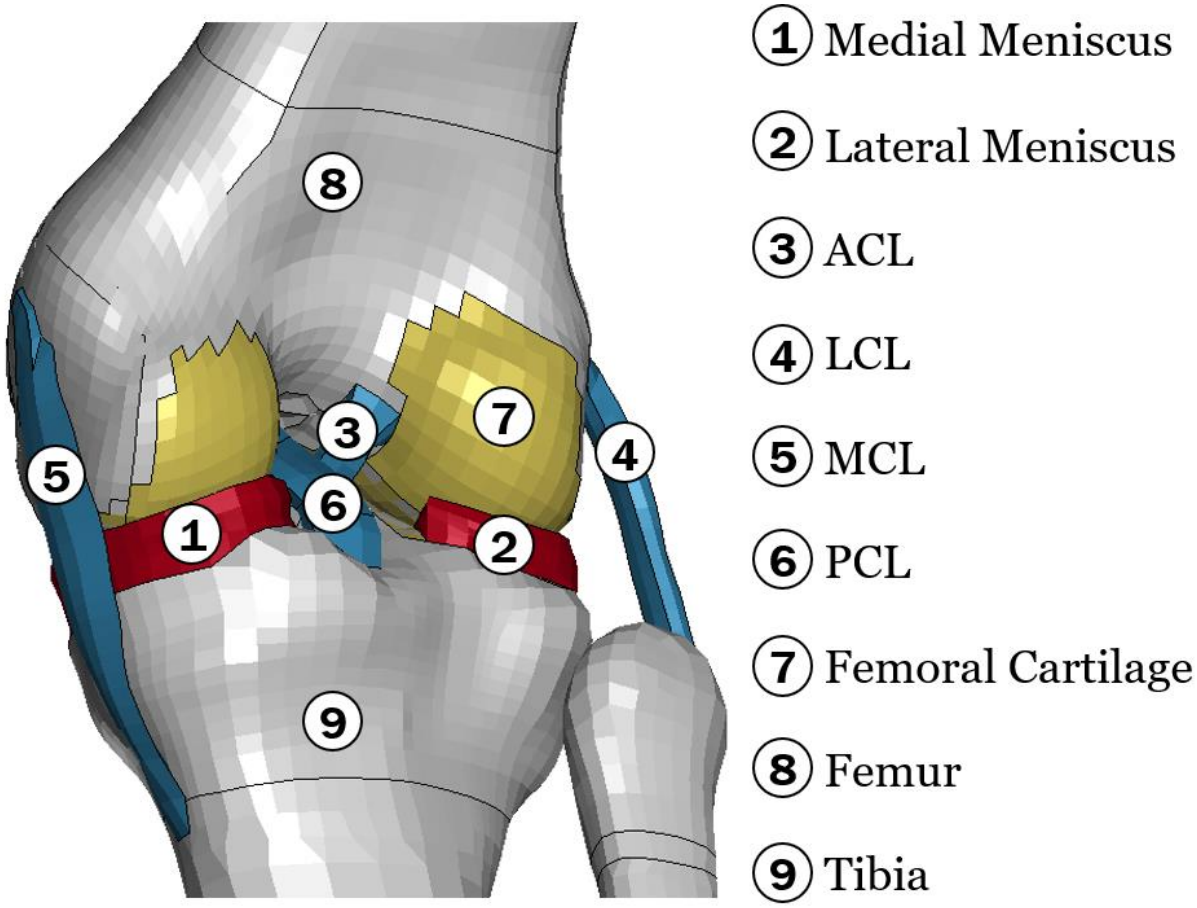


Figure 3.14: Tissue structures within the M50 knee joint, tibial cartilage is not shown.

Numerous studies have reported material properties for the collateral ligaments and three of these reported force-elongation outcomes (Ciccone et al., 2006; Kennedy et al., 1976; Maynard et al., 1996; Robinson et al., 2005; Sugita et al., 2001; Wijdicks et al., 2010; Wilson et al., 2012). Wilson et al. (2012) conducted bone-ligament-bone tensile tests for the LCL and MCL, while Robinson et al. (2005) and Wijdicks et al. (2010)

conducted similar tensile tests for the different layers of the MCL. Harner et al. (1995) and Race et al. (1994) prepared the femur, PCL, and tibia in a similar manner and documented the in-situ load-elongation behaviour by performing passive flexion-extension tests and tensile tests, respectively.

Human articular cartilage material properties have been reported from experimental indentation testing with mean elastic moduli within 1–11 MPa and Poisson's ratios within 0.45–0.49 depending on the loading rate, tissue site, anatomical location, tissue health, and donor age (Burgin et al., 2014; Butz et al., 2011; Franz et al., 2001; Hori & Mockros, 1976; Lu & Mow, 2008; Ly Richard et al., 2013, Shepherd & Seedhom, 1999). Select FE studies with a linear elastic material model have utilized a wider range of these values (elastic moduli: 4–25 MPa and Poisson's ratios: 0.3-0.45) (Kiapour et al., 2014; Łuczkiewicz et al., 2016; Ramaniraka et al., 2005; Shriram et al., 2017).

The material behaviour of the medial meniscus has been studied by Lechner et al. (2000) and Chia et al. (2008), whereas the behaviour of both menisci has been studied by Tissakht & Ahmed (1995). LeRoux & Setton (2002) conducted experimental and FE validated meniscus material properties in the circumferential and radial direction. The study reported radial and circumferential Young's moduli in the range of 3-40 MPa and 63-316 MPa, respectively. FE studies have referenced material properties based on the aforementioned studies and implemented a linear elastic isotropic menisci material model with a Young's modulus between 20–250 MPa and a Poisson's ratio between 0.45–0.49 (Beillas et al., 2004; Peña et al., 2007). Hauch et al. (2010) performed axial tensile tests of the four meniscus horn attachments and reported mean linear stiffnesses of the anterior and posterior medial meniscus horns as 169.4(24.2) and 207.2(52.8) N/mm, respectively. Moreover, the stiffness coefficients for the anterior and posterior lateral meniscus horns were reported as 215.8(78.8) and 129.5(36.9) N/mm, respectively.

Utilizing a pre-existing FE model to better understand unloader brace mechanics on meniscus strain and tibiofemoral pressure would negate many of the experimental

challenges; however, due to the limited unloader brace studies investigating meniscus strain responses during ADLs it would be challenging to validate the tissue response with an isolated numerical approach. Therefore, conducting this study using a dual in-vitro/in-silico approach would overcome this challenge and address the gap related to meniscal tissue response with unloader braces.

# IV. Methods

The present study replicated three ADLs on a DKS using an experimental approach with cadaveric knees from post-mortem human specimens to measure meniscus strain and tibiofemoral joint pressure with the effect of unloader knee braces. The ADLs were simulated in-silico using the experimental BCs on a detailed FE right leg model that was extracted from the GHBMC 50$^{th}$ percentile male human body model. A valgus moment was applied to the FE knee joint to create an unloading moment and meniscus strain and tibiofemoral pressure outcomes were processed and compared with the experimental outcomes.

## 4.1 Experimental In-Vitro Knee Testing

A double leg squat, single leg squat, and gait were experimentally tested in ACL-intact and -deficient states in an unbraced scenario and with the application of two unloader braces. The 3 ADL × 3 brace scenarios × 2 ACL states formulated 18 unique test conditions (Table 4.1). A detailed methodology based on former studies was employed to dissect and apply cables to each specimen for the DKS, and intermediary steps were done to create a specimen mould and a foam thigh and crus to support each brace.

### 4.1.1 *Cadaver Specimen Preparation*

This study was approved by the office of research ethics at the University of Waterloo. Ten fresh-frozen cadaver knee specimens were procured for experimental testing (Innoved Institute, Rosemont, IL, USA). The specimens were selected from donors less than or equal to 60 years in age at the time of death, specified to include at least 20 cm of the thigh and crus measured from the mid-patella, and chosen from unique donors to investigate the braces on a wider sample size (Table 4.2). The specimens were selected presuming no existence of OA, and the bone quality and joint integrity were verified by a registered orthopaedic surgeon.

Table 4.1: Experimental testing order and conditions for 18 unique test cases.

| Test ID# | Activity (D/W/S)[1] | Brace (N/R/U)[2] | ACL (1/0)[3] |
|---|---|---|---|
| 01 | D | N | 1 |
| 02 | D | R | 1 |
| 03 | D | U | 1 |
| 04 | W | N | 1 |
| 05 | W | R | 1 |
| 06 | W | U | 1 |
| 07 | S | N | 1 |
| 08 | S | R | 1 |
| 09 | S | U | 1 |
| 10 | D | N | 0 |
| 11 | D | R | 0 |
| 12 | D | U | 0 |
| 13 | W | N | 0 |
| 14 | W | R | 0 |
| 15 | W | U | 0 |
| 16 | S | N | 0 |
| 17 | S | R | 0 |
| 18 | S | U | 0 |

1: Denotes Activity with D: double leg squat; W: walk; S: single leg squat
2: Denotes Brace scenario with N: unbraced; R: rebound cartilage brace; U: unloader fit brace
3: Denotes ACL state with 1: ACL-intact; 0: ACL-deficient

Table 4.2: Donor information with descriptive statistics for ten cadaver specimens

| ID (#) | Sex (F/M) | Foot (L/R) | Age (years) | Height (cm) | Mass (kg) | BMI (kg/m2) |
|---|---|---|---|---|---|---|
| 1 | F | L | 30 | 178 | 107 | 34 |
| 2 | M | R | 50 | 188 | 61 | 17 |
| 3 | F | R | 50 | 165 | 50 | 18 |
| 4 | M | R | 44 | 180 | 73 | 22 |
| 5 | M | R | 54 | 165 | 54 | 20 |
| 6 | F | R | 47 | 157 | 34 | 14 |
| 7 | M | L | 60 | 165 | 50 | 18 |
| 8 | F | R | 55 | 173 | 59 | 20 |
| 9 | M | R | 57 | 183 | 98 | 29 |
| 10 | F | L | 50 | 173 | 68 | 23 |
| Mean (SD) | | | 49.7 (8.4) | 173 (9.6) | 65.3 (22.3) | 21.5 (5.9) |

F: Female, M: Male, L: Left, R: Right, BMI: body mass index, SD: standard deviation

Prior to dissection, the femoral and tibial canals were tapped with a 15.875 mm (⅝”) and 12.7 mm (½”) NC tap, respectively, and a threaded Grade 8 high-strength steel rod was inserted into each canal. The experiment required all specimens to have limb lengths measuring 424 mm and 401 mm for the femur and tibia, respectively (Tomescu et al., 2018). The limb lengths were measured by palpating the approximate location of the mid-intercondylar joint space to the hip and ankle pin joints on the DKS. The steel rods would eventually attach to the DKS hip and ankle components and were sized according to the limb lengths. Two acetate end plates and four guide rods were placed at the proximal and distal boundaries of the leg (Fig. 4.1a). A guide drill bit was inserted in the distal diaphyseal region of the tibia (Fig. 4.1a). The specimen was encased using 127 mm (5”) medical casting tape (3M, Saint Paul, MN, USA) to create the outer shell of a custom negative mould for each specimen, which retained the guide rods and guide drill positions (Fig. 4.1b). The end plates, threaded rods, guide rods, and guide drill ensured the dissected femur and tibia had the same anterior-posterior (AP) and medial-lateral (ML) spatial positioning as the un-dissected specimen, while the guide drill ensured the same transverse plane spatial rotation. Finally, the thigh and crus circumferences were measured to select appropriate knee brace sizes.

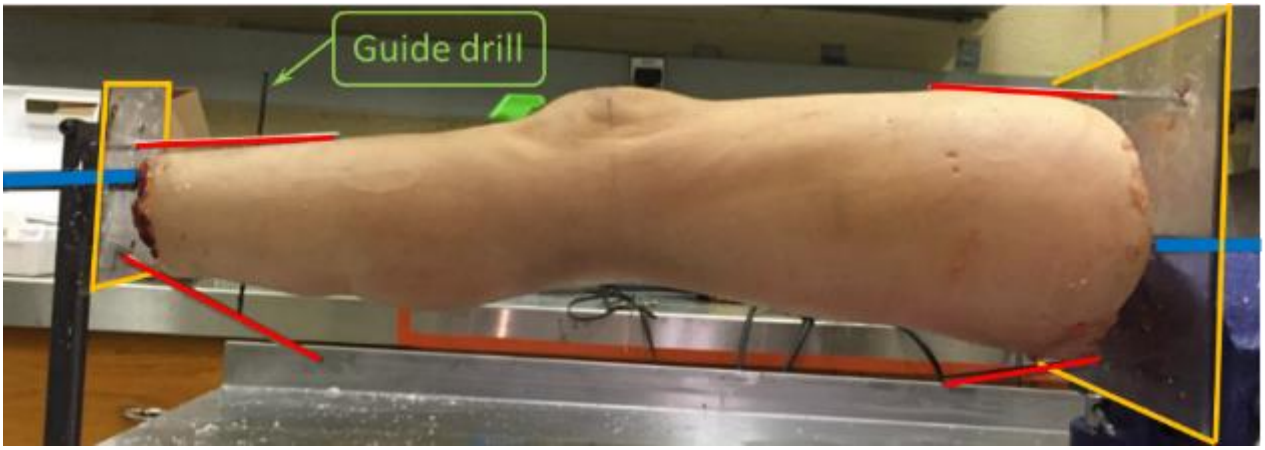


(a)

(b)

Figure 4.1: (a) A pre-dissected cadaver specimen with threaded rods (blue), guide rods (red), end plates (yellow), and a guide drill; and (b) the outer shell of the mould encased around the same specimen.

To dissect each specimen gentle incisions were made along the long axis of the specimen on the anterior and posterior surfaces (anterior incision shown in Fig. 4.2A until exposing a thin transparent fascia, which separates the superficial layers from the knee joint capsule and the musculature. Upon identifying the fascia, circumferential incisions were made to separate the superficial layers from musculature (Fig. 4.2B) until all cutaneous and subcutaneous layers were removed (Fig. 4.2C). All major muscles were individually separated by hand and each muscle body was traced to its attachment site to expose the muscle tendons (Fig. 4.2D). The majority of muscle tendons are attached to the knee joint; thus, to maintain joint integrity the tendons were left intact and the muscle bodies were dissected. The crus muscles were separated from the tibia and removed (Fig. 4.2E-F) prior to the thigh muscles (Fig. 4.2G-I). The popliteus muscle was not dissected since it has been shown to help stabilize the knee joint and does not interfere with specimen preparation or experimental testing (Harner et al., 1998). The surfaces of the bones were lightly scraped to remove any remnants of muscle tissue and to create smooth surfaces (Fig. 4.2J). The quadriceps tendon was removed, and incisions were made in the patellar tendon and joint capsule to prepare the specimen for cable attachment and sensor placement (Fig. 4.2K-L).

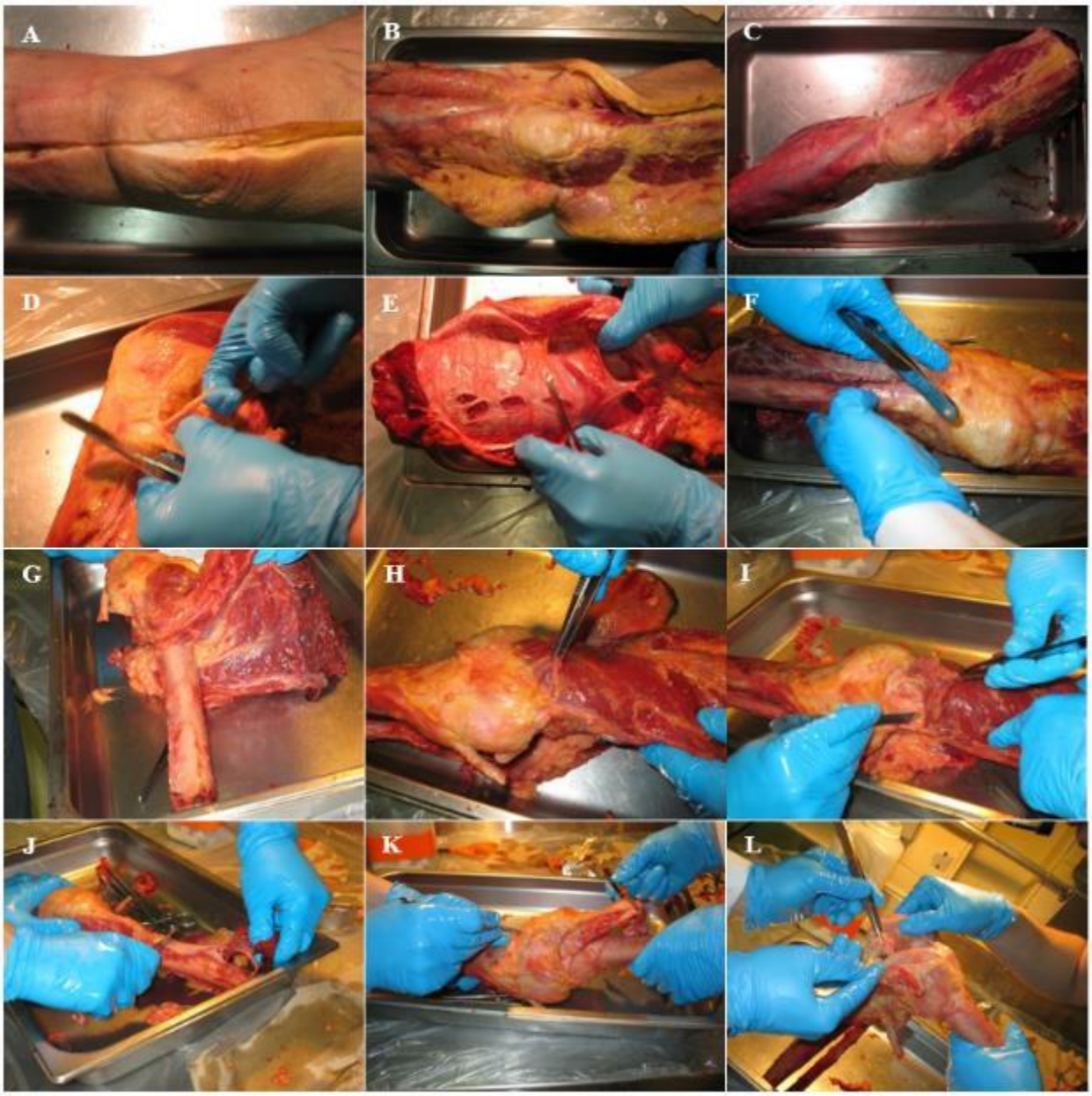


Figure 4.2: Various steps of cadaver knee dissection with A-C showing skin, subcutaneous tissue removal, D-F showing removal of lower leg musculature surrounding the tibia, G-J showing removal of upper leg musculature surrounding the femur and K-L showing preparation of the knee joint for cabling (reprinted from Bakker 2014).

Three steel cables were anchored around the knee joint to emulate the function of the quadriceps, hamstring, and gastrocnemius muscle groups. Each muscle force cable represented the combined force contributions from a group of muscles (explained in §3.3.5) and assumed a unanimous muscle force attachment site, which was selected to approximate the anatomical muscle tendon attachment sites. The quadriceps cable was

the most complex to install and initially required drilling a through hole along the superior-inferior axis of the patella, which served as a channel for the cable. The tibial tuberosity was chosen as the cable attachment site since it is also the muscle group insertion site (Fig. 4.3). The cable was secured using an M2.5 (7/64") cable crimp sleeve to replicate the patellar tendon. The basic quadriceps extensor mechanism consists of three interlinked structures including the quadriceps muscle and tendon, patella, and patellar tendon (Astur et al., 2011). The quadriceps muscle force cable (superior to the patella) formed the combined link between the quadriceps muscle group and tendon. The patella and patellar tendon link were left intact, and two washers were placed superior and inferior to the patellar through hole to retain its original position. By retaining the patella's original position, the flexion and extension mechanism manipulated the patella similar to the interlinked anatomical structure. Finally, the quadriceps muscle force cable (inferior to the patella) recreated the patellar tendon since it was secured to the tibia in the same anatomical location as the patellar tendon, and the crimp was secured such that the tension in the cable matched the anatomical patellar tendon.

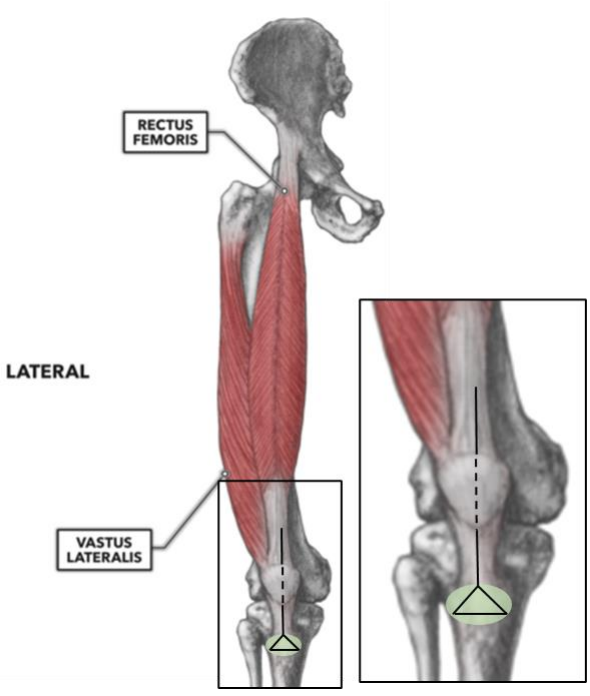


Figure 4.3: The quadriceps muscles anatomical insertion site highlighted in green and an approximate representation of the muscle force cable attachment site.

The hamstring insertions points are on the medial tibia and on the fibular head (Fig. 4.4). The hamstring cable was looped around the upper-mid diaphysis of the tibia, secured using an M2.0 (3/32”) cable crimp sleeve, and inserted in a hollow metal guide tube oriented in the direction of the femur. The looped architecture of the hamstring cable attachment allowed the cable to manipulate the tibia similar to the natural muscle (Fig. 4.4).

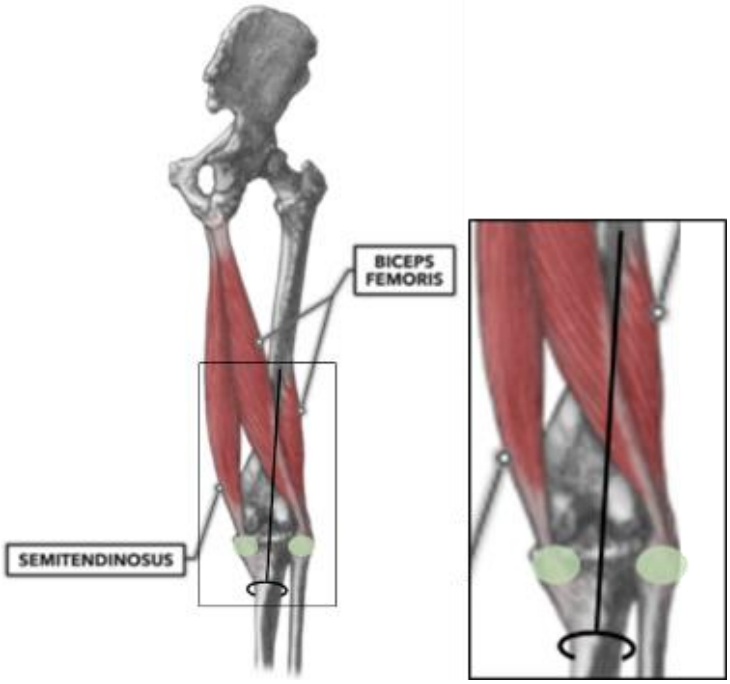


Figure 4.4: The hamstring muscles anatomical insertion sites highlighted in green and an approximate representation of the muscle force cable attachment site.

The two gastrocnemius muscle heads insert on the medial and lateral condyles (Fig. 4.5). Two holes were drilled approximately 1 cm superior to the femoral condyles, the cable was inserted in these holes, looped around the anterior femur, and secured to itself with an M2.0 (3/32”) cable crimp sleeve near the femoral intercondylar notch. This attachment technique closely replicated the function of the natural gastrocnemius muscle and its attachment sites (Fig. 4.5). The final step in the ‘cabling’ process was to wrap the femur and tibial surfaces with 50.8 mm (2”) casting tape (3M, Saint Paul, MN, USA) to safeguard against cracks or fractures (Fig. 4.6).

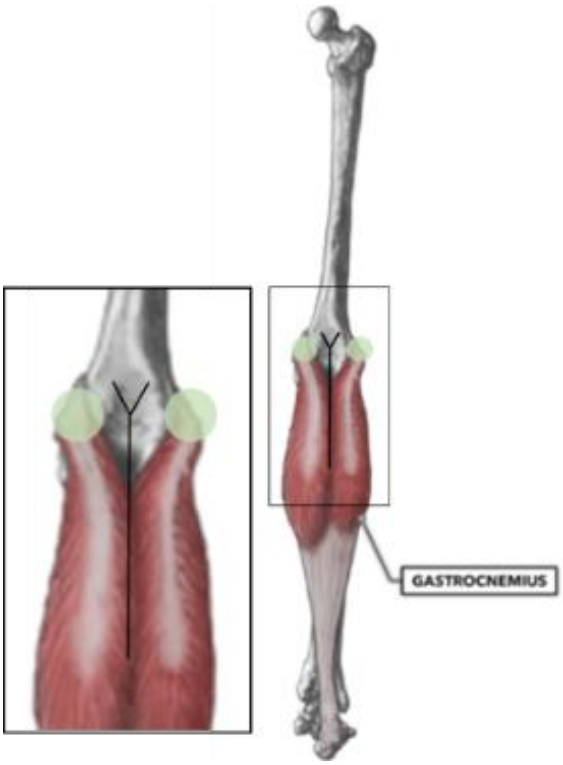


Figure 4.5: The gastrocnemius muscle anatomical origin sites highlighted in green and an approximate representation of the muscle force cable attachment site.

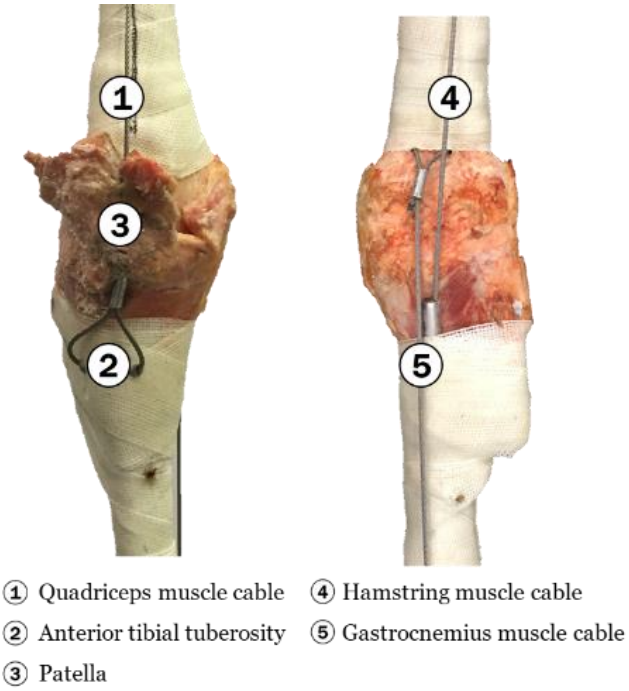


Figure 4.6: Anterior (left) and posterior (right) views of a right knee with the muscle force cables. Posterior view adapted from Polak (2019).

The ‘cabled’ specimen was aligned using the guide rods and guide drill in the negative mould (Fig. 4.1b). The acetate plates helped align the mould and created a seal at the superior and inferior ends. A liquid foam solution (Sunmate; Dynamic Systems Inc., Leicester, NC, USA) with a compressive stiffness of 17.6 N/mm, which is similar to the average stiffness of contracted muscle, was poured into the cast to create a replica of the un-dissected specimen (Hangalur et al., 2016). The foam solution was left to cure for at least two hours at room temperature and humidity and then placed in the freezer for storage until testing (Fig. 4.7a). The final steps to prepare the specimen for testing were to remove the mould (Fig. 4.7b), cautiously cut the foam surrounding knee joint, remove any foam within the joint or muscle force cable channels, ensure the joint range of motion was not impeded during the foaming process, and apply the knee brace to the specimen to observe the fit.

(a) (b)

Figure 4.7: (a) Sample specimen contained within its sealed negative mould; and (b) the ‘foamed’ specimen with hip, ankle attachment rods and three muscle force cables.

### 4.1.2 *Unloader Knee Brace Placement*

The current study investigated two OA Unloader braces (*Ossur Inc.*, Richmond, BC, Canada). The Rebound Cartilage (RC) and Unloader Fit (UF) are typical 3-point leverage designs, which apply a valgus moment to relieve joint pain (Fig. 4.8). The RC brace consists of two pairs of helical and horizontal straps that are buckled above and below the medial hinge to secure around the thigh and crus. The tension in each pair of straps is controlled with a rotational knob located on the anterior surface of the brace. The UF brace consists of two helical straps that attach on the anterior and posterior brace surface above the patella. The tension in both straps is controlled by a single knob. The UF brace has one horizontal strap inferior to the patella to tighten around the crus. Both braces are non-custom, off the shelf models ranging in size from XS-XL for the UF and S-XL for the RC. According to the manufacturer's instructions the appropriate size is determined by measuring the circumference of the thigh and crus approximately 152 mm (or 6") superior and inferior to the mid-patella. Both braces are available in a medial or lateral OA configuration. All braces used in this study were configured for medial OA to measure the efficacy related to outcomes in the medial compartment, which has the hinge located on the medial side (Fig. 4.8).

Prior to experimental trials, each prepared specimen was equipped with an appropriately sized RC and UF brace according to the manufacturer's instructions to ensure a secure fit. For the RC brace the center of the medial hinge was aligned with the mid patella and AP midline[19], and for the UF brace the top edge of the medial hinge was approximately 1 cm higher than the top edge of the patella[20]. A passive flexion-extension was done to ensure the brace remained firmly secure and did not hinder or modify the natural movement of the knee. The placement of both braces is shown in §4.1.9 when the specimen is mounted on the DKS.

[19] Rebound Cartilage Instructions for Use [Online resource]. Authored by: Ossur, Inc. Located at: https://media.ossur.com/ossur-dam/image/upload/pi-documents-global/Rebound_Cartilage_1029_001_4.pdf

[20] Unloader Fit Instruction for Use [Online resource]. Authored by Ossur, Inc. Located at: https://assets.ossur.com/library/36179/Unloader


Figure 4.8: Images of the braces used in the current study with (a) Rebound Cartilage (RC) brace shown on a right leg[21] and (b) Unloader Fit (UF) brace shown on a left leg[22].

### 4.1.3 *Measuring Specimen Specific Muscle Moment Arms*

Time-varying net moments for the quadriceps, hamstrings, gastrocnemius, and hip muscle groups during squat and gait ADLs were taken from Tomescu et al. (2018). The experiment required that every specimen had consistent muscle moments to guarantee consistent muscle force rotations about the knee joint, and ensure all specimens performed the same activity as the in-vivo participant.

Since each specimen has different quadriceps, hamstrings, and gastrocnemius muscle cable moment arms due to unique knee geometries, using one set of muscle force profiles would result in varying inter-specimen muscle moments. The experimental hip muscle moment arm had a constant value of 6 cm irrespective of the cadaveric specimen and did not require specimen specific modifications. The quadriceps, hamstring, and gastrocnemius muscle moment arms were measured for all 10 specimens by securing the distal or proximal end of the knee to a custom-built apparatus (Fig. 4.9). A static weight was secured to one of the three muscle cables and three passive flexion-extension trials

[21] Untitled [Online image]. Located at: https://www.orthomed.ca/ossur-rebound-cartilage-custom
[22] Untitled [Online image]. Located at: https://www.synergyortho.com/product/unloader-fit/

were performed while recording the changes in knee flexion angle and cable length, which were measured with a goniometer (model SG150, Biometrics Ltd., Newport, UK) and linear variable displacement transducer (Omega Engineering, Norwalk, CT, USA) (Fig. 4.9), respectively. Data was collected using a custom-built data acquisition module and LabVIEW (National Instruments, Austin, TX, USA) program. The moment arm was calculated using the rate of change between the cable length and flexion angle (Eq. 4.1) (An et al., 1984; Sherman et al., 2013), and the mean of three trials was calculated. This process was repeated for the remaining two muscle cables.

$$r = \frac{dl}{d\theta} \tag{4.1}$$

where:
r is the moment arm
dl is the rate of change in cable length
dθ is the rate of change in flexion angle

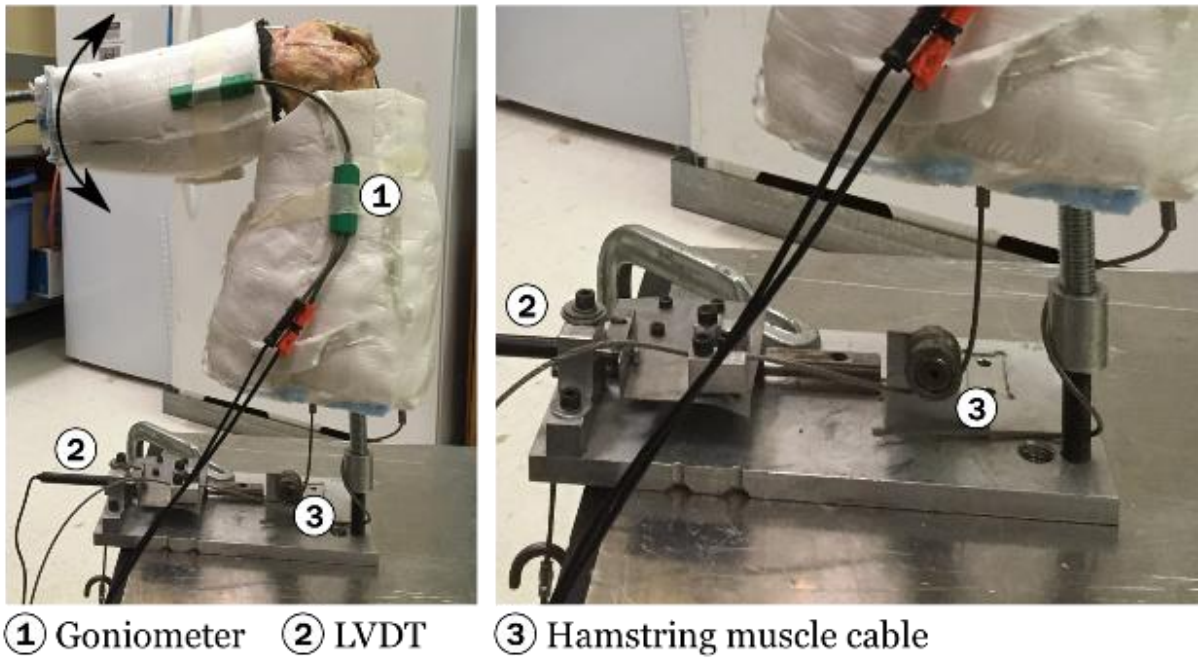


Figure 4.9: Moment arm set up instrumented with a goniometer and a linear variable reluctance transducer performing an extrusion of the hamstring muscle cable by passive flexion (black arrow).

### 4.1.4 *Implementing Kinetic Muscle Force Boundary Conditions*

The muscle moment-time history data for the quadriceps, hamstrings, gastrocnemius, and hip muscle groups was based on in-vivo/in-silico DLS, gait, and SLS outcomes from Tomescu et al. (2018) and a previously validated method was used to convert the muscle group moments to specimen specific resultant force-time histories based on specimen-specific muscle moment arms using Eq. 4.2 (Cassidy et al., 2013).

$$F_{mc} = \frac{\sum F_m \cdot d_m}{d_{mc}} \tag{4.2}$$

where:
$F_{mc}$ is the resultant cadaveric muscle group cable force
$d_{mc}$ is the cadaveric muscle group cable moment arm
$F_m$ is the resultant in-silico muscle group force
$d_m$ is the in-silico muscle group moment arm

A custom MATLAB script (Mathworks, Natick, MA, USA) was used to compute the muscle force time histories for all four muscle groups, based on the three measured moment arms and the constant hip moment arm (Hangalur et al., 2016). The present study generated 10 triads of specimen specific muscle force-time history curves based on the 3 ADLs. The muscle force actuator for the quadriceps cable had a force limit of 10 kN (RSA32, Tolomatic Inc., Hamel, MN, USA), while the remaining actuators were rated for up to 5 kN (14 H, Macron Dynamics Inc., Croydon, PA, USA). Muscle force data were collected during all trials using 1-dimensional single DOF load cells rated for ~9 kN (2000 lbs) (Omega Engineering, Norwalk, Connecticut, USA). The quadriceps and hamstring muscle cables were oriented in the direction of the femoral diaphysis (Fig. 4.6), and gastrocnemius muscle cable were oriented in the direction of the tibial diaphysis (Fig. 4.6). These orientations were selected to reflect the anatomical muscle lines of action, thus each muscle cable had one degree of freedom. The hip force was actuated through a bracket attachment with the mechanical hip joint oriented in the posterior direction.

### 4.1.5 *Implementing Kinematic Hip and Ankle Boundary Conditions*

The hip and ankle velocity input data for each activity were obtained from prior in-vivo/in-silico research conducted by Tomescu et al. (2018), and every specimen used identical velocity-time histories (Fig. 4.10). Double and single leg squat tests consisted of peak flexion angles of 83° and 81°, respectively, in 1.9 s, and gait testing replicated an in-vivo gait performed at 1.9 steps/s for 1.05 s. Hip and ankle kinematics were generated from their respective positional actuators (Macron Dynamics Inc., Croyden, PA, USA). Each actuator can achieve velocities up to 5 m/s$^2$ and accelerations up to 200 m/s$^2$. According to the experimental coordinate system (Fig. 4.11), the hip was free to translate in the y-direction (superior-inferior direction) and rotate about the z-axis (sagittal plane). The ankle was free to translate in the x-direction (AP direction), z-direction (ML direction), free to rotate about the y-axis (transverse plane), and free to rotate about the z-axis (sagittal plane).

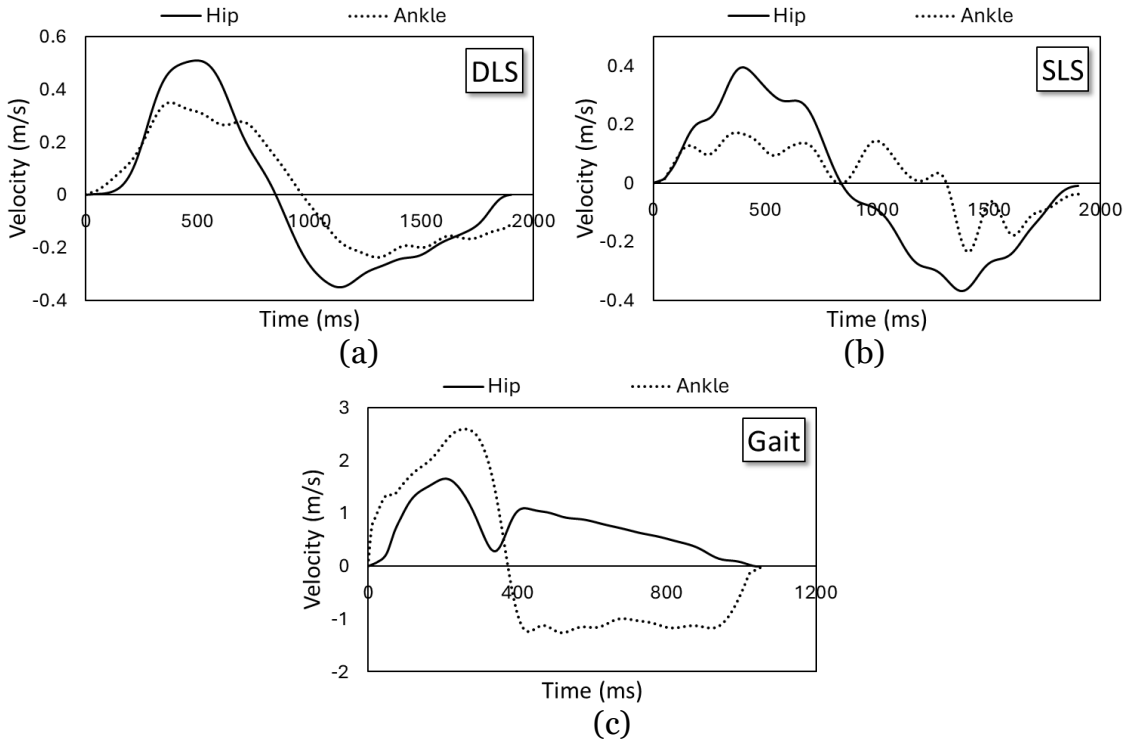


Figure 4.10: Hip and ankle velocity time history input curves for (a) double leg squat, (b) single leg squat, and (c) gait.

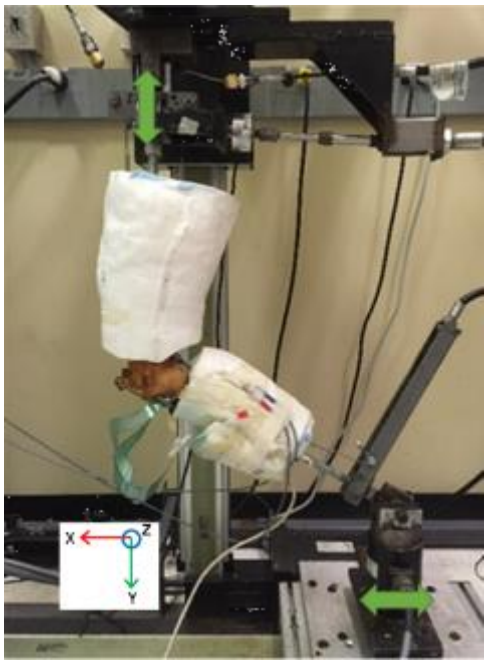

Figure 4.11: Experimental coordinate reference system with hip and ankle velocity directions indicated by green arrows.

### 4.1.6 *Meniscus Strain Instrumentation*

The strain measurements on the posteromedial and anteromedial meniscal tissues were done using microminiature DVRT (MicroStrain Inc., Burlington, VT, USA) (Fig. 4.12a-b). Each sensor has a linear stroke length of ±4.5 mm, a linear voltage range of ±5 V, an accuracy of ±1.5%, a resolution of 4.5 μm, and is pre-calibrated by the manufacturer.

The DVRTs were connected to a dual-channel signal conditioner that relayed the voltage outputs every 0.01 s to a custom LabVIEW program. Strain was calculated using the engineering strain formulation, with the lengths determined from Eq. (4.3).

$$L = O + S(V - V_o) \tag{4.3}$$

where
O is the initial stroke length in mm
S is the sensitivity factor in mm/V
V is the measured voltage at any time (t) in V
$V_o$ is the voltage measurement measured at the initial stroke length (O) in V
L is the calculated gauge length at any time (t) in mm

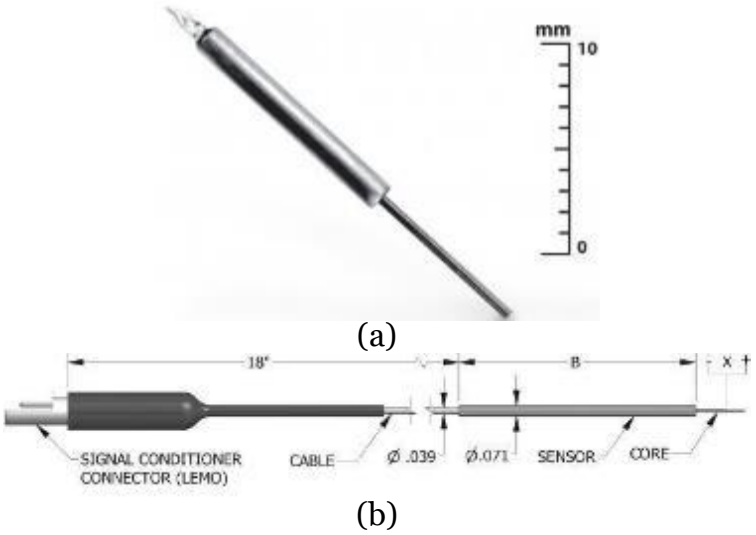


Figure 4.12: (a) Microminiature displacement variable reluctance transducer (DVRT); and (b) General DVRT assembly and dimensions, where the sensor length (B) is 26.8 mm and the stroke length (x) is ±4.5 mm.[23]

### 4.1.7 *Tibiofemoral Joint Pressure Instrumentation*

The tibiofemoral joint contact forces and areas were measured using resistive pressure mapping sensors (Tekscan Inc. Model 4000, South Boston, MA, USA). The sensor has two sensing surfaces designed for medial and lateral intercondylar joint surfaces (Fig. 4.13) with a maximum pressure limit of 68 948 kPa. Each sensing surface contains 26 rows and 22 columns of sensels in a sensing area of 33 by 27.9 mm, which equates to 62.0 sensels/cm$^2$ (Table 4.3). Each sensel measured the applied force in sensel units (su) (force limit: 255 su, resolution: 1 su), and the outputs were recorded using the I-Scan pressure mapping system, which included the data acquisition handle (model: Evolution Handle) capable of achieving scanning speeds up to 100 Hz, and the I-Scan v5.90 pressure mapping software. A different sensor was used for each specimen and every sensor was equilibrated, calibrated, and coated in duct tape to improve sensor durability and repeatability and avoid rupturing sensor layers due to shear forces (Wilharm et al., 2013). While increasing the baseline thickness of pressure sensors may increase measurement errors, applying a protective coating is common to mitigate shear

[23] Untitled [Online images]. Located at: https://www.microstrain.com/sites/default/files/m-lvdt_series_datasheet.pdf

forces and sensor failure for repeated measurements (Ostermeier et al., 2007; Stuckenborg-Colsman et al., 2002; von Lewinski et al., 2005; Wu et al., 1998).

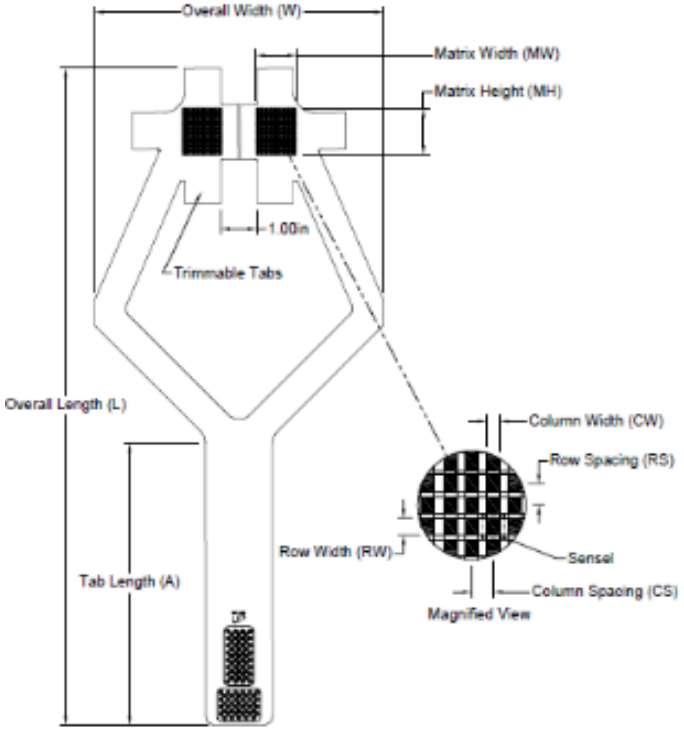


Figure 4.13: Representation and dimensions of Tekscan Pressure Sensor (model 4000)[24]

Table 4.3: Manufacturer provided values for sensor dimensions in Fig. 4.10a.

| Description | Value (mm) |
|---|---|
| Overall length (L) | 462.0 |
| Overall width (W) | 203.2 |
| Tab length (A) | 198.1 |
| Matrix height (MH) | 27.9 |
| Matrix width (MW) | 33.0 |
| Row Width (RW) | 1.0 |
| Column Width (CW) | 0.8 |
| Row Spacing (RS) | 1.3 |
| Column Spacing (CS) | 1.3 |

Sensor equilibration is recommended prior to testing to ensure consistent output values between adjacent sensels and trials. According to the manufacturer's documentation, "The equilibration process allows the software to compensate for any

[24] Untitled [Online image]. Located at: https://www.tekscan.com/products-solutions/pressure-mapping-sensors/4000

variation or uneven output across individual sensing elements, caused by manufacturing [processes] or repeated use of the sensor" (I-Scan Product Selection Guide)[25]. Each sensor was equilibrated by applying a constant pressure over the sensor surface using an air bladder contained within a metal housing (similar to Fig. 4.14a) and recording an equilibration curve using the I-Scan pressure mapping system. Sensor calibration was done following equilibration using a compression tester (force limit: 5000 N, resolution: 0.2 N) (Mark-10, Copiague, NY, USA). A cylindrical indenter was used to apply compressive forces in 10 approximately equal intervals ranging from 0-5000 N (Fig. 4.14b). The applied compressive force in N and sum of the measured force across all sensels in su, were recorded. A sensitivity value was calculated based on the linear slope between applied and measured forces. To prepare the sensor for insertion the lateral tabs were trimmed and four holes were made in the upper and lower tabs (Fig. 4.15). Medial and lateral incisions were made on the anterior and posterior coronary ligaments from the meniscal horn attachments until the collateral ligaments similar to previous in-vitro work (LaPrade et al., 2014; Padalecki et al., 2014 von Lewinski et al., 2006). It has been reported that this method of inserting pressure-sensitive films is nondestructive and reliable since an osteotomy to the coronary ligaments did not significantly affect mean pressure, maximum pressure, contact area, anterior-posterior force, and internal-external rotation during compressive loads (Martens et al., 1997). Carefully expanding these incisions revealed the menisci and a thin suture was passed through the opening to separate the menisci from the tibial surface. The pressure sensor was passed through this narrow opening to measure lateral and medial inter-condylar pressure between the meniscal-tibial interface. The upper and lower tabs were bent and fastened to the tibia using screws (Fig. 4.16).

[25] I-Scan Product Selection Guide [Online resource]. Located at: https://www.tekscan.com/resources/product-guide/i-scan-product-selection-guide

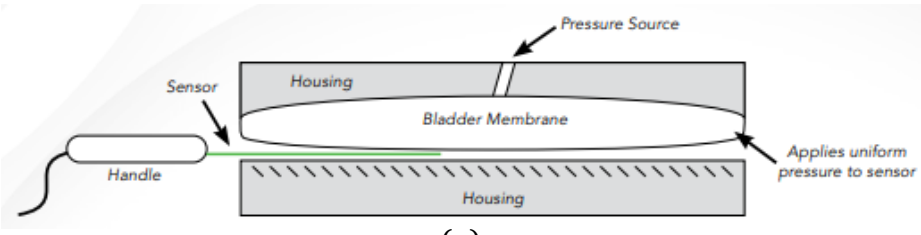


(a)

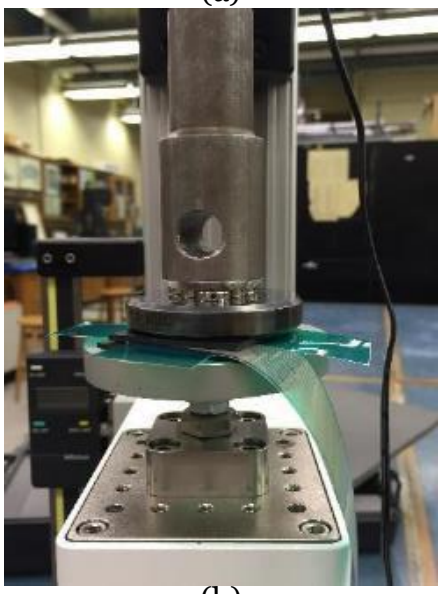

(b)

Figure 4.14: Representation of (a) sensor equilibration similar to the set up used in the current study and (b) sensor calibration setup using Mark-10 compression tester.

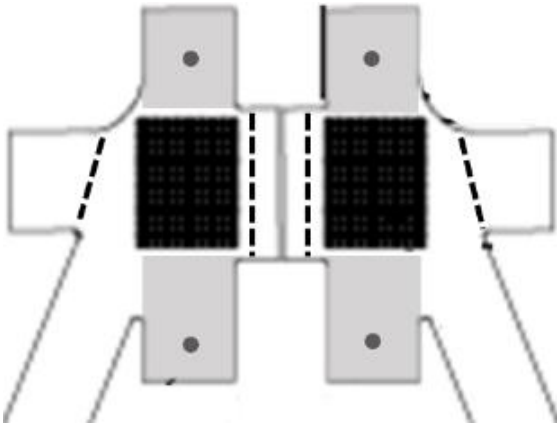

Figure 4.15: Modifications made to Tekscan Model 4000 sensor with dashed lines depicting trimmed edges, black circles depicting mounting holes, and shaded regions representing duct tape protective layer.

### 4.1.8 *Mounting the Specimen to the DKS*

Final steps for experimental preparation involved securing the femoral and tibial threaded rods to the hip and ankle DKS attachments, verifying the limb length

measurements, fastening each muscle force cable to the respective actuator, adjusting the Q-angle on the hip attachment, manually verifying that flexion/extension was predominantly in the sagittal plane, and setting the knee flexion angle to approximately 5–15$^{o}$ to avoid hyperextension, since a cadaver knee has greater range of motion than a live participant due to the absence of the joint capsule and supporting structures. With the specimen securely mounted a DVRT was pinned to the anteromedial meniscus (Fig. 4.16a) and the posteromedial meniscus (Fig. 4.16b).

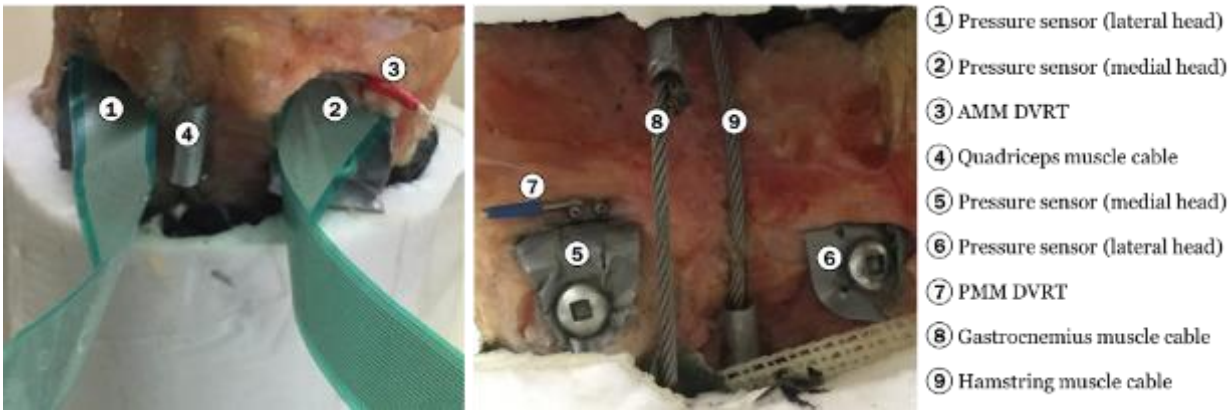


(a) (b)

Figure 4.16: Close up view of the DVRT and pressure sensor implementation shown on a sample specimen in the (a) anterior view and (b) posterior view.

### 4.1.9 *Experimental Test Matrix*

The behaviour of biological tissues depends on their strain history and relaxation function and repetitive stretching affects stiffness. Preconditioning a tissue with loading/unloading cycles eliminates uncertainty caused by repeated loading and one study preconditioned meniscal tissue samples for 10 cycles prior to compressive testing (Chia et al., 2008; Elson & Genin, 2016). The present study preconditioned the meniscal tissue with a minimum of 10 passive flexion-extension cycles while mounting the specimen to the simulator followed by one preconditioning flexion-extension cycle using only the hip and ankle kinematic actuators. Each specimen was tested in one unbraced (NB) and two braced scenarios (RC & UF) in DLS, SLS, and gait ADLs (Fig. 4.17-4.18). The testing order was unanimously set to DLS, gait, and SLS for all specimens and the NB

trials were conducted prior to the RC and UF trials. Trial order was not varied because: i) it was precautionary to place SLS after DLS and gait since SLS had the highest likelihood of specimen failure, and ii) the RC brace had an easier application and was less disruptive to the joint position and instrumentation, thus it was tested first to show closer comparisons to the unbraced scenario. Moreover, every activity-brace combination was initially tested in a healthy, uninjured ACL (ACL-intact) state followed by a dissected ACL (ACL-deficient) state. The 18 unique experimental conditions (3 ADL × 3 brace scenarios × 2 ACL states) were tested twice for a total of 36 trials/specimen.

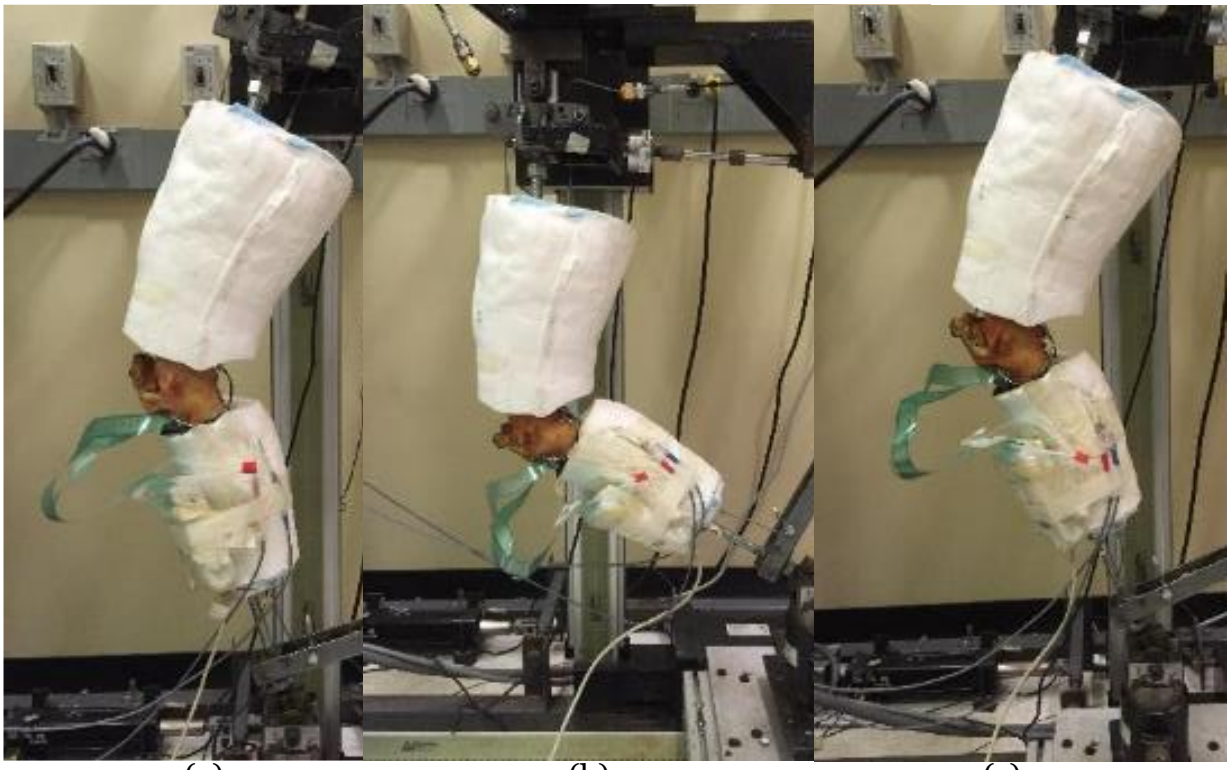

(a) (b) (c)

Figure 4.17: Experimental setup of an unbraced right leg specimen in a start position for (a) DLS, (b) gait and (c) SLS.

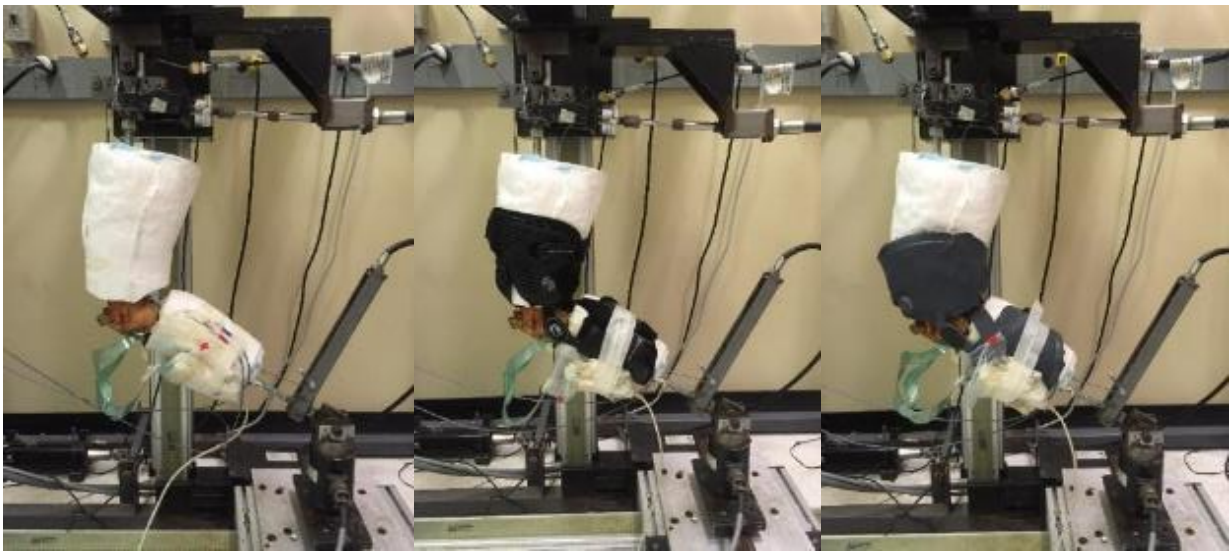

(a) (b) (c)

Figure 4.18: Experimental setup of a right leg in the walk position for (a) an unbraced cadaver, (b) a cadaver mounted with RC brace and (c) a cadaver mounted with UF brace.

## 4.2 Experimental Data Analysis

### 4.2.1 *Meniscus Strain*

Strain was computed using the engineering strain formulation and the length of the DVRT at the initial time state (i.e., t=0) in the NB scenario was used as the reference length (Eq. 4.4) for each brace scenario in every activity-ACL combination based on a similar brace study (Tomescu et al., 2018). This study reports relative strain where negative strain values can indicate a decrease in tensile strain or an increase in compressive strain; although, due to the nature of hoop stresses and circumferential tensile strain in the menisci (Fig. 2.16) it is foreseen that the measured strains are tensile in nature. The mean posterolateral meniscus strain and anterolateral strain time histories for every test condition were obtained by computing the mean of both trials at each time state. Descriptive statistics were computed on mean time histories for all 18 test conditions per specimen and the overall mean and peak strains were obtained for all successful testing conditions. Mean and peak strain residuals were checked for normality and outliers (Kim, 2013; Kozak & Piepho, 2018). A repeated measures analysis of variance (ANOVA) and a post-hoc t-test with a Bonferroni family wise correction factor ($\alpha$=.05)

were performed to determine the efficacy of each brace and their interactions with ACL status (brace*ACL) and activity (brace*Activity). An additional ANOVA analysis was conducted without the NB case to compare strain outcomes between the two braces.

$$\varepsilon = \frac{L - L_o}{L_o} \times 100\% \tag{4.4}$$

where:
L is the gauge length in mm determined from Eq. 4.3
$L_o$ is the gauge length in mm determined from Eq. 4.3 for the NB scenario at time t=0
ε is engineering strain in mm/mm × 100%

### 4.2.2 *Tibiofemoral Joint Pressure*

Mean medial and lateral tibiofemoral joint pressure distributions were calculated for each experimental condition using the measured force and area from the pressure sensors. The area was considered as the sum of all sensels that experienced a force exceeding 1 N. The means of two trials in each test condition were computed in an identical manner as the strain outcomes. Descriptive statistics were obtained from the mean time history for each experimental condition. Similar to strain, the pressure residuals underwent tests for normality and outliers. Pressure data was not normally distributed and required a rank transform to conduct non-parametric statistic tests and a modified aligned ranked transform contrast (ART-C) was conducted prior to multifactorial non-parametric interaction testing (Elkin et al., 2021). The ANOVA conducted on the strain data was conducted on the aligned and ranked pressure data.

## 4.3 50th Percentile Male Lower Extremity Finite Element Modelling

The GHBMC 50th percentile male was considered since it has been developed with the geometrical and anatomical components relevant to this study and since a jump landing has been formerly simulated using this model (Polak, 2019). The extensive methodology required to simulate squat and gait ADLs on this model included extracting the right leg, enhancing aspects within the model, extending the leg, applying the

experimental initial and boundary conditions, and assessing the model. An unloader brace was replicated by applying a valgus moment (VM) and simulations included three ADLs in two brace scenarios (i.e., NB and VM) and two ACL states (i.e., intact and deficient) similar to the experimental tests (Table 4.4). To simulate the effect of the ACL-deficient state the ACL part was removed.

Table 4.4: Computation simulation matrix for 12 unique conditions (in no particular order).

| Simulation ID# | Activity (D/W/S)[1] | VM (1/0)[2] | ACL (1/0)[3] |
|---|---|---|---|
| 01 | D | 0 | 1 |
| 02 | W | 0 | 1 |
| 03 | S | 0 | 1 |
| 04 | D | 1 | 1 |
| 05 | W | 1 | 1 |
| 06 | S | 1 | 1 |
| 07 | D | 0 | 0 |
| 08 | W | 0 | 0 |
| 09 | S | 0 | 0 |
| 10 | D | 1 | 0 |
| 11 | W | 1 | 0 |
| 12 | S | 1 | 0 |

1: Denotes Activity with D: double leg squat; W: walk; S: single leg squat
2: Denotes Valgus Moment effect with 0: disabled; 1: enabled
3: Denotes ACL state with 1: ACL-intact; 0: ACL-deficient

## 4.4 Lower Extremity Finite Element Model Modifications and Enhancements

### 4.4.1 *Right Leg FE Model Extraction*

The right leg was extracted from the seated occupant 50$^{th}$ percentile male human body model (GHBMC M50 version 4.4) (Fig. 4.19). The model extraction initially included all unmodified parts inferior to the hip joint and superior to the ankle joint. Anatomical tissues and muscles that were dissected from the specimens such as the cutaneous and subcutaneous layers and muscles were excluded from the model (Table 4.5). Additional hip and foot bones that were part of the lower extremity were removed. Ultimately, the bones in the model included the femur, patella, tibia, and fibula similar to

the experiment and all soft tissue structures surrounding the knee joint were retained (Table 4.6).

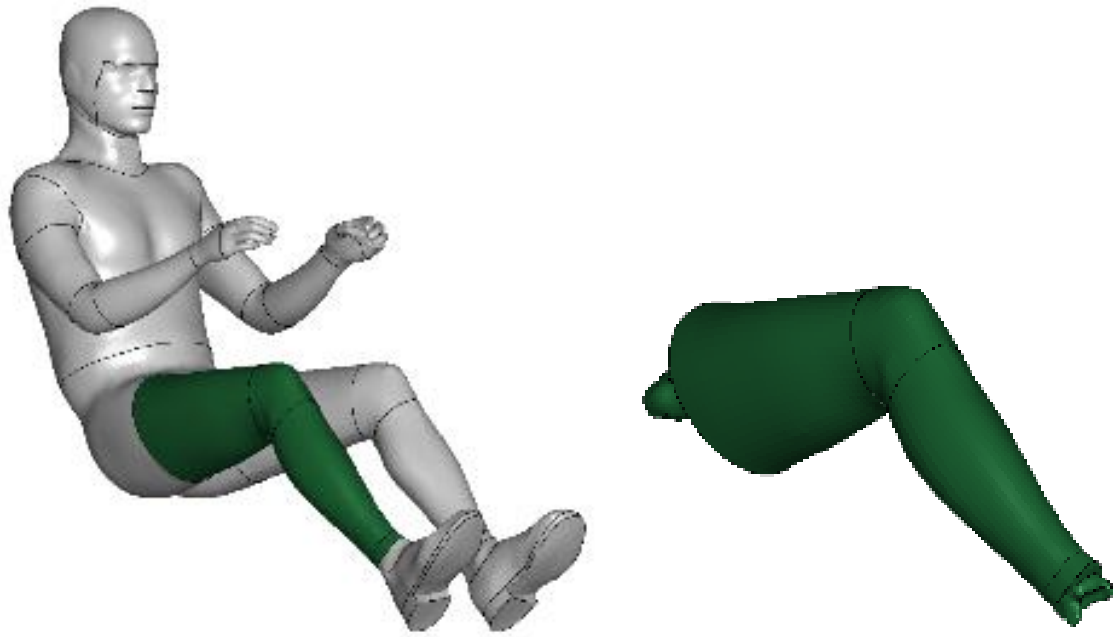

(a) (b)

Figure 4.19: (a) Whole body M50 model (v4-4) and (b) the unmodified extracted right leg FE model.

Table 4.5: Excluded parts list in FE model.

| Part Description | Number of Elements | Element Type |
|---|---|---|
| Achilles tendon | 78 | Shell |
| Deep thigh tissue | 600 | Solid |
| Distal tibia (cortical) | 568 | Shell |
| Femur fascia | 1594 | Shell |
| Gastrocnemius muscle (lateral) | 1 | Beam |
| Gastrocnemius muscle (medial) | 1 | Beam |
| Femur head (cortical) | 616 | Shell |
| Hip capsule | 1733 | Shell |
| Joint capsule | 1687 | Shell |
| Knee, Ankle subcutaneous tissue | 9077 | Solid |
| Plantaris muscle | 1 | Beam |
| Quadriceps muscle | 4 | Beam |
| Shank subcutaneous tissue | 10920 | Solid |
| Skin | 5130 | Shell |
| Soleus muscle (lateral) | 1 | Beam |
| Soleus muscle (medial) | 1 | Beam |
| Thigh subcutaneous tissue | 8325 | Solid |
| Tibia fascia | 2790 | Shell |

Table 4.6: Complete list of included parts in extracted FE model.

| Part Description | Number of Elements | Element Type | Material Model Description |
|---|---|---|---|
| Anterior cruciate ligament | 44 | Solid | Transversely isotropic hyper viscoelastic soft tissue model |
| Distal femur (trabecular) | 10539 | Solid | Elastic plastic metals model with kinematic hardening |
| Distal femur (cortical) | 1350 | Shell | Viscoplastic strain rate dependant |
| Distal/Proximal tibia (trabecular) | 5669 | Solid | Elastic plastic metals model with kinematic hardening |

| | | | |
|---|---|---|---|
| Distal/Proximal fibula (cortical) | 459 | Shell | Viscoplastic strain rate dependant |
| Distal/Proximal fibula (trabecular) | 944 | Solid | Elastic plastic metals model with kinematic hardening |
| Femur cartilage | 663 | Shell | Linear isotropic hypoelastic |
| Femur condyle (cortical) | 1991 | Shell | Viscoplastic strain rate dependant |
| Femur diaphysis | 9407 | Solid | Viscoplastic strain rate dependant |
| Femur head (trabecular) | 1067 | Solid | Elastic plastic metals model with kinematic hardening |
| Femur head (trabecular) | 1058 | Solid | Elastic plastic metals model with kinematic hardening |
| Femur neck (cortical) | 871 | Shell | Viscoplastic strain rate dependant |
| Femur neck (trabecular) | 5415 | Solid | Elastic plastic metals model with kinematic hardening |
| Fibula diaphysis | 4980 | Solid | Viscoplastic strain rate dependant |
| Interosseus membrane | 181 | Shell | Elastic plastic metals model with kinematic hardening |
| Lateral collateral ligament | 79 | Solid | Transversely isotropic hyper viscoelastic soft tissue model |
| Lateral meniscus | 109 | Solid | Elastic plastic metals model with kinematic hardening |
| Medial collateral ligament | 118 | Solid | Transversely isotropic hyper viscoelastic soft tissue model |
| Medial meniscus | 102 | Solid | Elastic plastic metals model with kinematic hardening |
| Patella (cortical) | 654 | Shell | Viscoplastic strain rate dependant |
| Patella (trabecular) | 961 | Solid | Elastic plastic metals model with kinematic hardening |
| Patellar cartilage | 184 | Shell | Linear isotropic hypoelastic |
| Posterior cruciate ligament* | 36 | Solid | Transversely isotropic hyper viscoelastic soft tissue model |
| Posterior cruciate ligament* | 32 | Solid | Transversely isotropic hyper viscoelastic soft tissue model |
| Proximal femur | 1103 | Shell | Viscoplastic strain rate dependant |
| Proximal Tibia (cortical) | 990 | Shell | Viscoplastic strain rate dependant |
| Quadriceps-patellar tendon | 456 | Shell | Piecewise linear elastic plastic |
| Tibia cartilage (medial) | 83 | Shell | Linear isotropic hypoelastic |
| Tibia cartilage (lateral) | 105 | Shell | Linear isotropic hypoelastic |
| Tibia diaphysis | 4399 | Solid | Viscoplastic strain rate dependant |

*PCL was composed of 2 parts

### 4.4.2 *Femoral and Tibial Bone Modifications*

Similar to the experimental limb length measurement procedure (see §4.1.1), the femoral and tibial limb lengths in the model were measured and resulted in values of 470 mm and 386 mm, respectively. The diaphyses for both bones were linearly scaled along the direction of the diaphyseal axis using the built in scaling function, with the model's femoral diaphysis scaled (from 470 mm) to 424 mm and the model's tibial diaphysis scaled (from 386 mm) to 401 mm. Scaling ensured that the initial limb lengths matched the experimental setup such that hip and ankle kinematics would have a similar effect in the model. This scaling modification was not applied to the epiphyses or metaphyses in either bone since it was not necessary to scale these parts to achieve the experimental limb length values. Scaling decreased femoral diaphyseal elements by approximately 0.27 mm and increased tibial element dimensions by 0.17 mm along the axial directions, element dimensions along the radial directions were unmodified. An alternative method could have been to add or remove elements, though this would distort the original shape and circumferences leading to element discontinuities and contact issues.

The combined superior and inferior tibial epiphyses part was separated into two parts to apply the experimental ankle BC to the inferior tibia. The femoral head and neck trabecular bone parts were combined into a single part for ease of hip BC application. It is noteworthy that the anatomical femoral head and inferior tibia were removed from the cadaveric specimens, though they were retained in the model since their presence did not impact computational simulations. A linear elastic material model was applied to the modified hip and ankle parts using a density of 1.1 g/cm$^3$, a Poisson's ratio of 0.3, and a stiffened Young's modulus of 200 GPa, since the DKS attachments are hardened steel.

### 4.4.3 *Enhancing the Cruciate and Collateral Ligaments*

The constitutive model for each ligament was updated to a phenomenological hyperelastic material model (Hirokawa & Tsuruno, 1997; Peña et al., 2006) with material properties taken from previous experimental studies (see §3.5.2) (Chandrashekar et al.,

2006; Harner et al., 1995; Wilson et al., 2012) (Table 4.7). These studies were selected on the basis that they provided geometrical properties and force-elongation outcomes such that their uniaxial tensile tests could be replicated and compared with the model. While the ACL stress-strain responses reported by Grood & Noyes (1976) is very similar to Chandrashekar et al. (2006), the present study considered the outcome from Chandrashekar et al. (2006); since the greater accuracy in geometric properties may strongly influence the ACL behaviour in the model. For the LCL and MCL, a singular study met the inclusion criteria (Table 4.7). There were two studies that met the criteria for the PCL and amongst these Harmer et al. (1995) was selected since it provided a typical force-elongation curve for both bundles of the PCL (Table 4.7).

Table 4.7: FE model material properties for major tissues within the knee.

| Tissue | Material Model | E (MPa) | ρ ($g/cm^3$) | ν | K (MPa) | Experimental Reference |
|---|---|---|---|---|---|---|
| ACL | Hyperelastic | LC | 1.0 | - | 2000 | Chandrashekar, 2006 |
| LCL | Hyperelastic | LC | 1.0 | - | 2000 | Wilson, 2012 |
| MCL | Hyperelastic | LC | 1.0 | - | 2000 | Wilson, 2012 |
| PCL | Hyperelastic | LC | 1.0 | - | 2000 | Harner, 1995 |

LC: load curve; E: elastic modulus; ρ: density; ν: Poisson's ratio; K: bulk modulus

Isolated bone-ligament-bone models were extracted for each ligament in the model similar to the experimental studies to simulate uniaxial tensile tests (Fig. 4.20). The inferior plug was kept fixed and the superior plug had an imposed velocity boundary condition directed along the ligament axis. The material curves were calibrated based on the resulting cross-sectional force and tissue elongation, with results presented in §6.1.1. The initial ACL, LCL, MCL, and PCL strains were assumed to be approximately 5% at full extension in FE studies (Gantoi et al., 2013; Shriram et al., 2017), which do not coincide with experimental work. Experimental studies reported that the LCL and MCL are near a zero strain state between 0–30$^o$ and 0–45$^o$, respectively (Jeffcote et al., 2007) and the ACL achieves zero strain around 35$^o$ during an open-kinetic-chain active flexion-extension, and this varies due to the activity and posture (Beynnon & Fleming, 1998). Ligament strains were not an objective of this study since unloader braces mechanics are not

intended to reduce ligament relief, thus assigning initial ligament strains were not deemed necessary for this study.

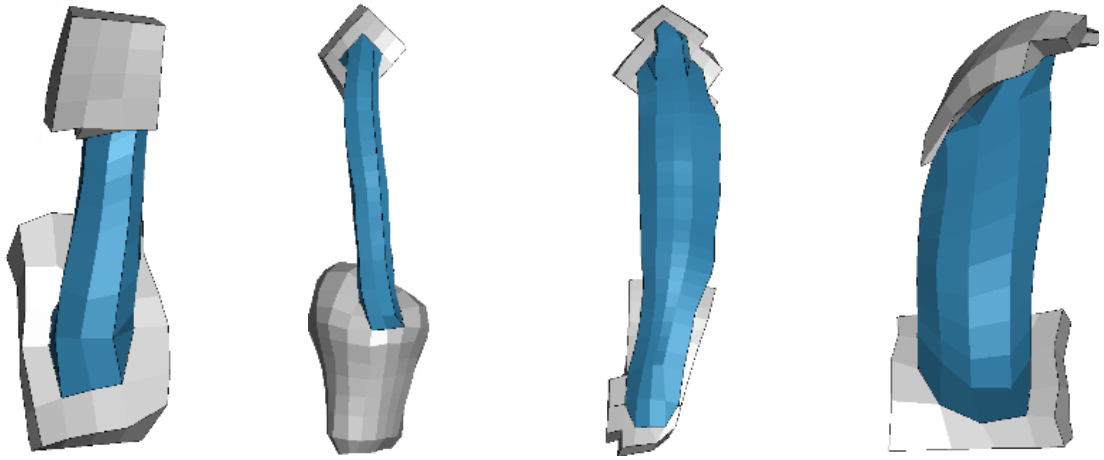

(a) (b) (c) (d)

Figure 4.20: FE isolated ligament uniaxial tensile tests for the (a) ACL, (b) LCL, (c) MCL, and (d) PCL.

### 4.4.4 *Enhancing the Menisci*

The majority of the FE enhancements were done on the menisci. The material model was updated to an elastic isotropic material for both menisci with an elastic modulus of 20 MPa, a density of 2.0 g/cm$^3$ and Poisson's Ratio of 0.49 (Pena et al., 2007). Both menisci shared nodes with their respective tibial cartilage parts. Node sharing between the tibial cartilages and menisci is not anatomically representative since each meniscus can translate and deform independently of the tibial cartilage. The inferior meniscal surfaces were assigned an independent set of nodes and the medial and lateral contact definitions were redefined by establishing contacts between the inferior meniscal and superior tibial cartilage surfaces.

Separating the menisci and cartilage nodes introduced an unconstrained translational degree of freedom between the parts since the original model did not have meniscal horns, coronary ligaments, a transverse ligament, or meniscofemoral ligaments. Meniscal horns are the predominant constraint that bind the menisci to the tibia, thus each meniscus was augmented with anterior and posterior horns using 1D linear spring elements (Dong et al., 2012; Guess et al., 2010; Shriram et al., 2017). Originally, four

linear springs were attached between meniscal and tibial nodes at each of the four horn sites, with the combined spring stiffness is 180 N/mm at each site (Hauch et al., 2010).

The meniscal elements in the model have a circumferential element length of approximately 4-6 mm. Each tissue contains three layers of elements in the superior-inferior direction and two layers in the AP direction. Since meniscal strain is the primary measured metric, it was perceived a meniscal mesh refinement would be necessary for more accurate comparisons with the experimental data. Each meniscus mesh was refined by splitting the elements in all three dimensions, thereby splitting each cubic element into eight smaller elements (Fig. 4.21). A refined mesh increased the number of nodes at each horn site and provided additional locations to attach spring elements. The number of spring elements were doubled to provide more uniform nodal distributions at the horn sites, the individual spring stiffnesses were reduced, and the overall stiffness at each horn remained unchanged (Fig. 4.21).

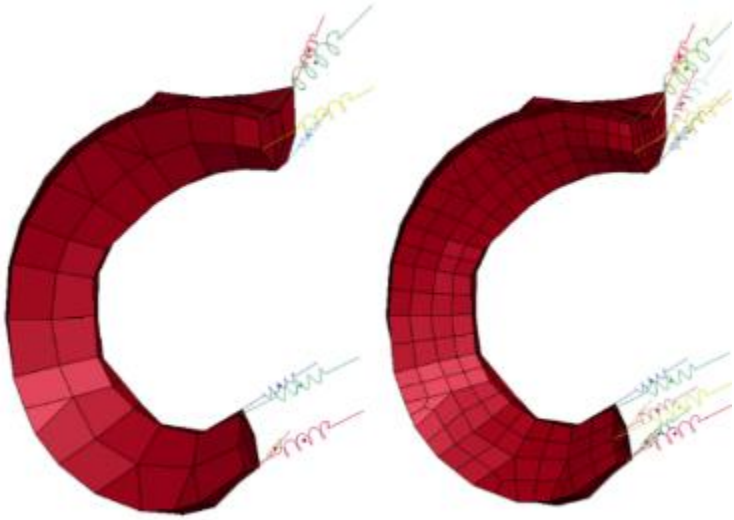

Figure 4.21: Superior view of original, coarse mesh (left) and refined, fine mesh (right) medial menisci with corresponding linear spring horn elements.

### 4.4.5 *Enhancing the Articular Cartilage*

The original patellar, femoral, and tibial cartilage parts used an elastic material formulation with E=20 MPa, ν=0.20, and ρ=2.0 g/cm$^3$. The elastic modulus was modified to 10 MPa since this is an approximate midpoint within the 9.2 – 10.9 MPa mean moduli

range from prior experimental indentation studies (Richard et al., 2013; Shepherd & Seedhom, 1999). The Poisson's ratio was modified to 0.45 to reflect an isotropic single phase linear elastic material formulation used in FE studies investigating tibiofemoral pressures with similar elastic moduli (Łuczkiewicz et al., 2016; Shriram et al., 2017).

Similar to the menisci, the tibial cartilage mesh was refined based on the presumption it would yield more accurate pressure outcomes. The original mesh for the medial cartilage contained element lengths between 2.4-8.4 mm, while the lateral cartilage had elements ranging between 2.6-7.5 mm. Following mesh refinement element dimensions were reduced by a factor of two (Fig. 4.22)

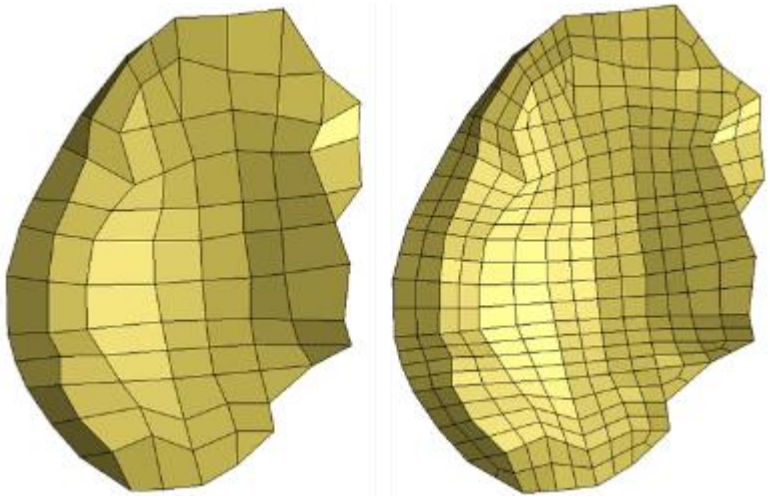

Figure 4.22: Superior view of original, coarse mesh (left) and refined, fine mesh (right) medial tibial cartilage.

## 4.5 Applying Experimental Boundary Conditions to the FE Model

Each experimentally tested activity had initial hip and ankle positions in the experimental coordinate system. To match the modelling initial conditions with the experiment, a local coordinate system was defined for each activity and local origins were based on the initial experimental positions. The coordinate directions were established using the transepicondylar axis as the functional flexion-extension axis, which represented the z-axes on the DKS and model (Fig. 4.23) (Asano et al., 2005). The FE AP and superior-inferior directions were defined as the x-axis and y-axis, respectively (Fig. 4.24).

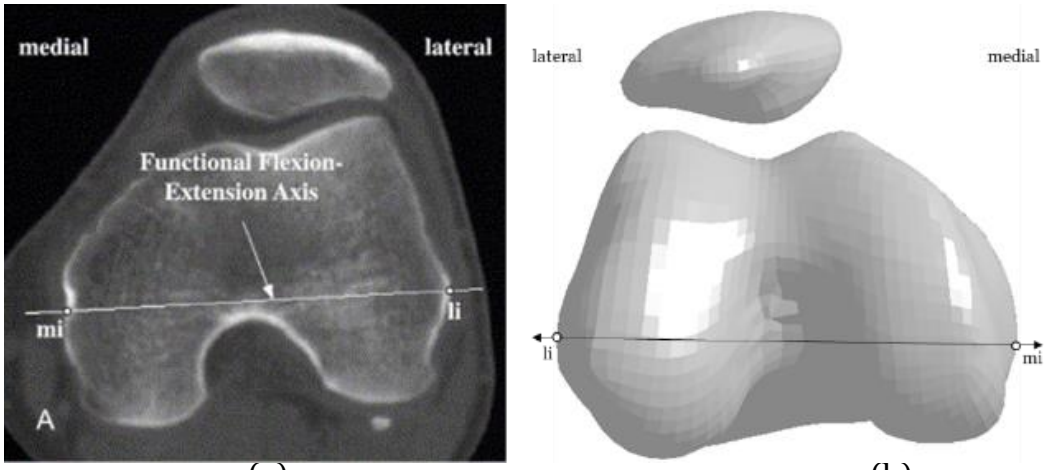


(a) (b)

Figure 4.23: The functional flexion-extension axis: (a) for a participant's left knee (Asano et al., 2005 – reprinted with permission from Elsevier); and (b) implemented in the FE model as the z-axis.

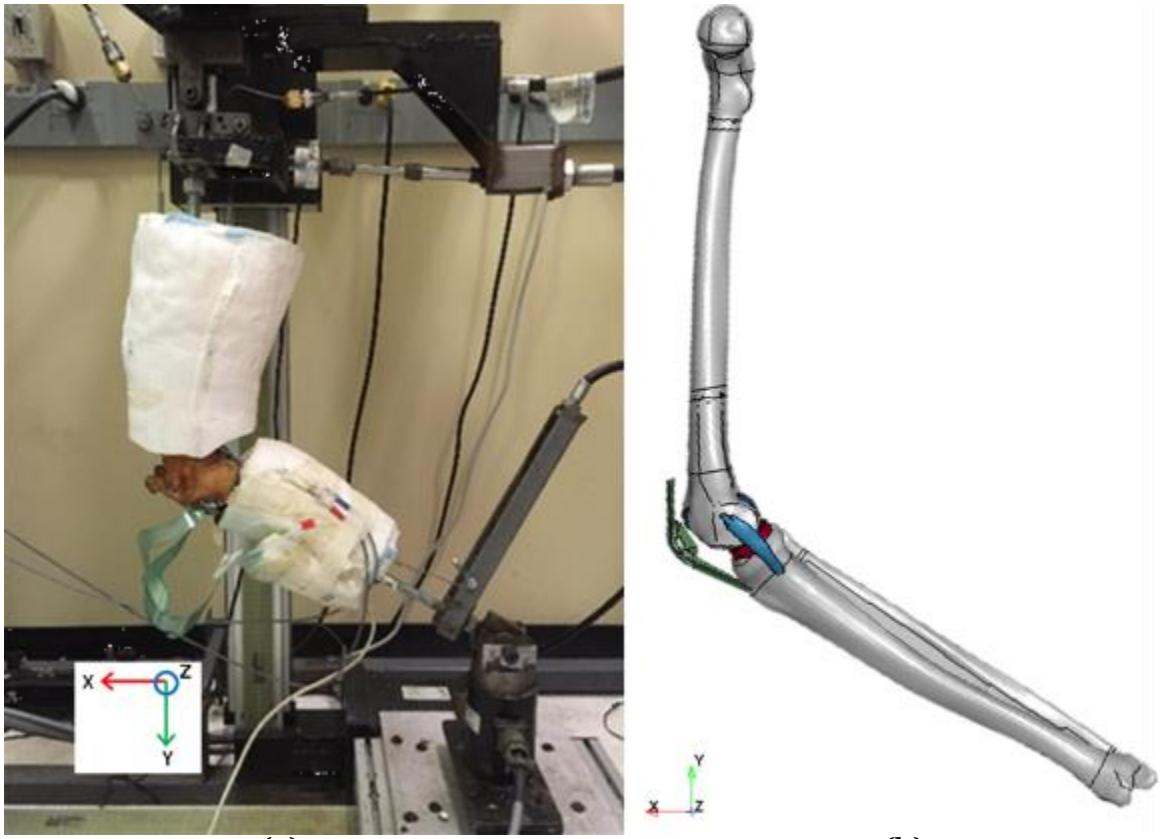


(a) (b)

Figure 4.24: Local coordinate systems and joint directions indicating positive vector orientation for: (a) the experimental; and (b) computational gait setup.

Quadriceps, hamstrings, gastrocnemius, and hip muscle force BCs were applied to the model over nodal sets corresponding to the experimental muscle force cable action sites, and each muscle force direction vector was parallel to the diaphysis. The FE quadriceps tendon was removed to reflect the experimental test condition (Fig. 4.25). The quadriceps and hamstring FE muscle force vectors were directed parallel to the femur and originated at the superior patella and superoposterior tibial epiphysis, respectively (Fig. 4.26). Since the muscle force cable in the experiment replicated a patellar tendon and the patella tendon was retained in the model, the extensor mechanism functioned similarly between the experiment and model. The FE gastrocnemius muscle force was directed parallel to the tibia and originated at the inferoposterior femoral epiphysis (Fig. 4.26). The FE hip force was assigned to a set of nodes located 6 cm from to the superior femoral head and directed in the (posterior) x-direction (Fig. 4.26). Model specific muscle force-time histories were obtained identically as the experimental procedure and required simulating the FE muscle moment arm values (described in §4.6.2).

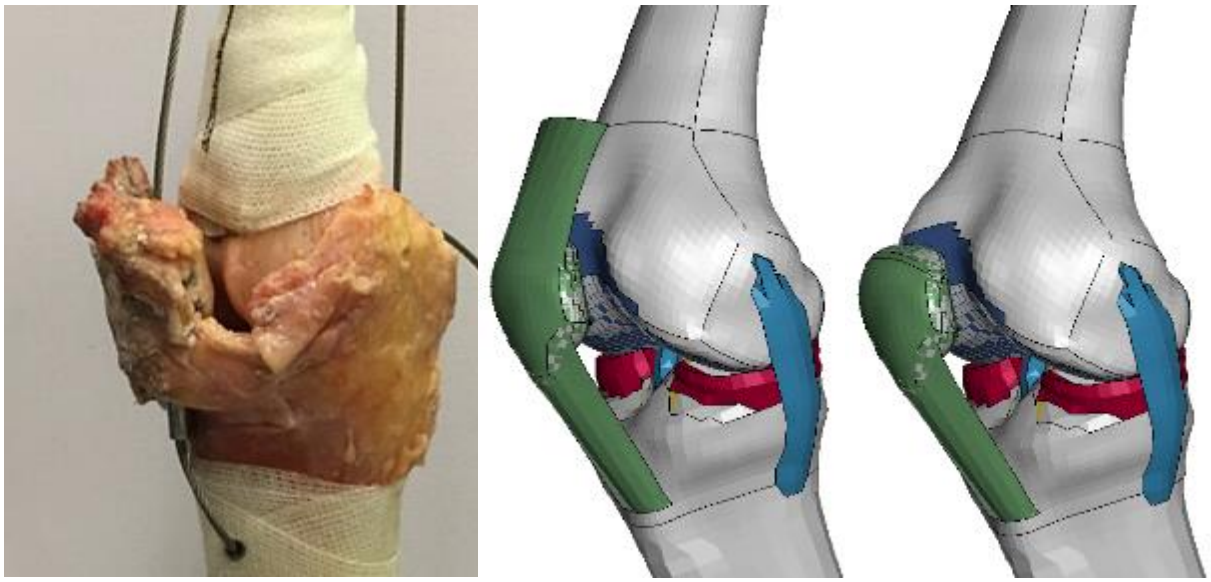

(a) (b) (c)

Figure 4.25: The experimental quadriceps tendon (a), the original FE quadriceps tendon (b), and modified FE excluding quadriceps tendon (c).

Hip and ankle kinematic (velocity) BCs were implemented at nodes on the FE femoral head and inferior tibia. The hip velocity was oriented in the y-direction and the ankle velocity was oriented in the x-direction (Fig. 4.26). The time histories for each activity were identical to the experiment since they were the same for each cadaver (Fig. 4.10). The FE hip joint at the superior femur was free to translate in the x- and y-directions and free to rotate about the z-axis. The FE ankle joint was free to translate in the x- and z-directions and free to rotate about the y- and z-axes.

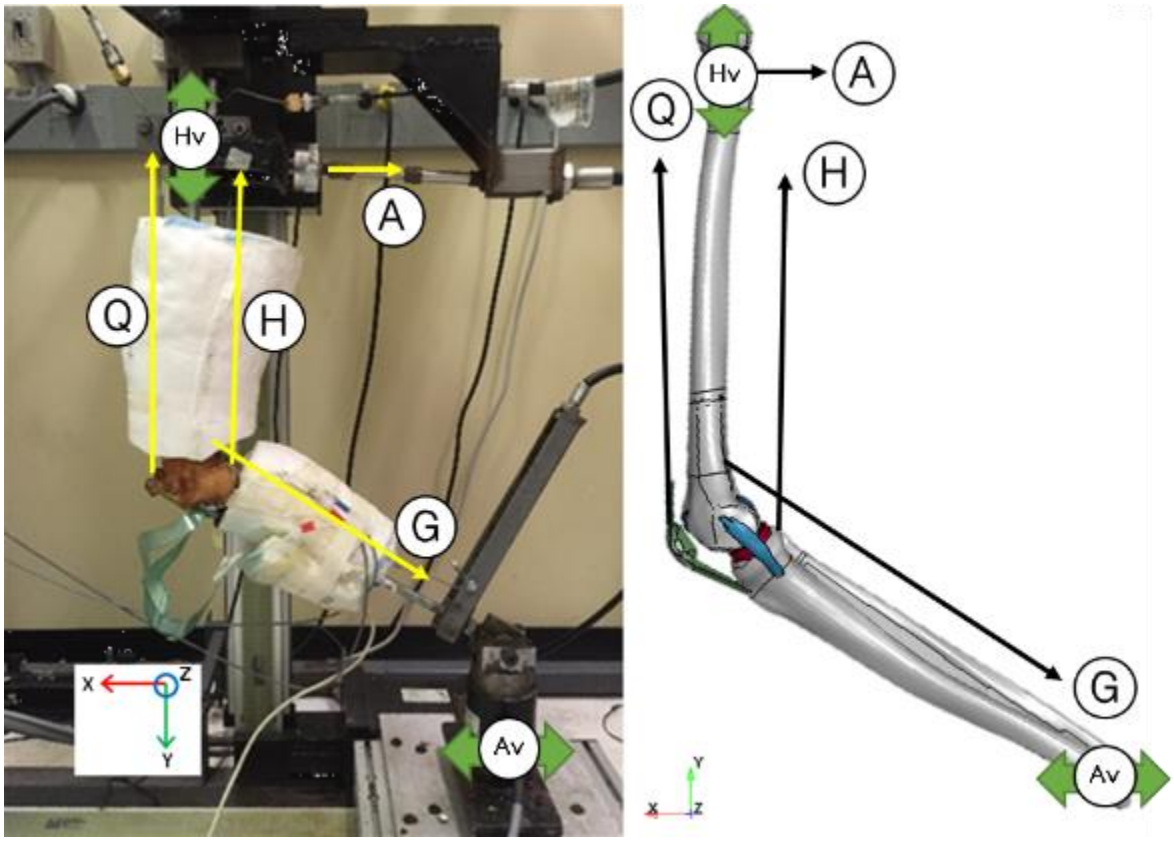


Figure 4.26: The directions for the hip velocity (Hv), ankle velocity (Av), hip muscle force (A), quadriceps muscle force (Q), hamstring muscle force (H), and gastrocnemius muscle force (G) shown for: (a) the experimental gait; and (b) the FE gait setups.

## 4.6 Lower Extremity Finite Element Model Simulations

Prior to simulating the DLS, gait, and SLS ADLs, a series of simulations were conducted to position the model to a similar initial position as the experiment, determine FE muscle moment arms, and apply a valgus moment.

### 4.6.1 *FE Model Initial Position Simulation*

The extracted FE joint angle measured 49°, while the initial flexion angles of the in-vivo participant were 6° for the DLS, 5° for the SLS, and 42° for gait. The initial experimental angles on the DKS were approximately 5–15° greater than the in-vivo values to avoid specimen hyperextension. For the DLS and SLS the model was extended to an initial flexion angle of 10°, while the gait retained the default position because it approximated the initial experimental gait flexion angle. An iterative hip velocity and quadriceps, hamstring, and gastrocnemius muscle force BC approach was used to decrease the flexion angle to 10°.

Table 4.8: Comparison of experimental range and FE initial positions during each ADL.

| ADL | Experiment | Model |
|---|---|---|
| Double leg squat | 11° – 21° | 10° |
| Gait | 47° – 57° | 49° |
| Single leg squat | 10° – 20° | 10° |

### 4.6.2 *FE Model Moment Arm Simulations and Muscle Force Input Curves*

Moment arm simulations were performed to determine the FE quadriceps, hamstring, and gastrocnemius muscle moment arms and three model specific muscle force time histories for each activity. For the quadriceps and hamstrings muscle moment arms, the superior femur parts were constrained in all directions (Fig. 4.27) and the appropriate muscle force was applied to displace the crus. For the gastrocnemius muscle moment arm, the inferior tibial parts were constrained in all directions and a gastrocnemius muscle force was applied to displace the thigh. Moment arms were calculated based on nodal displacements and flexion angle using Eq. (4.1), similar to the experimental procedure (§4.1.3). The three model specific moment arms and the 6 cm hip moment arm (used on all experimental specimens) were used to scale the in-vivo/in-silico DLS, gait, and SLS muscle moment data obtained from Tomescu et al. (2018). This process resulted in model specific quadriceps, hamstrings, and gastrocnemius, and a

generic hip muscle force time history curves in an identical manner as the experiment (§4.1.4).

### 4.6.3 *FE Model Static Valgus Moment Simulation*

A VM was applied to the model to simulate the effect of a medial unloader brace. Two opposite 10 Nm moments were applied to a series of nine nodes on the femoral and tibial diaphyses about the AP axis, which created a net 10 Nm valgus moment (Neville et al., 2018). To verify the application and effect of the VM, a 300 ms simulation was conducted with only the VM BC active while the proximal hip and distal ankle were constrained in the ML direction.

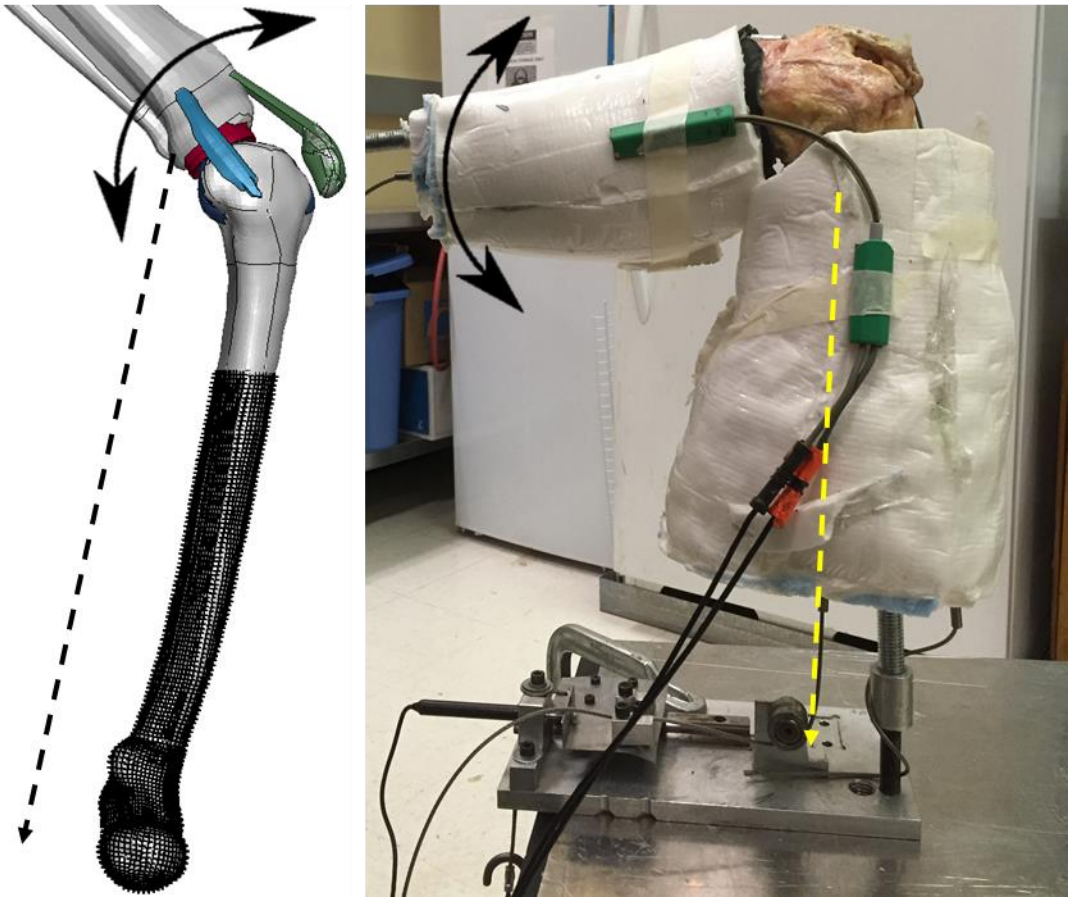

Figure 4.27: FE model hamstring moment arm simulation showing the fixed femur BC, the hamstring force BC (dashed arrow), and the crus motion similar to experimental setup.

## 4.7 Assessing the Computational Knee Model

Joint flexion angle and minimum tibiofemoral joint separation were used to assess model outcomes during initial positioning simulations. The main outcomes during the ADL simulations were meniscus tissue deformation in the circumferential direction, applied force on the tibial cartilage, and the loaded area on the cartilage. Posteromedial meniscus strain and medial and lateral tibial compartment pressures were compared to the experimental outcomes.

### 4.7.1 *Meniscus Strain*

Posteromedial meniscus strain was the predominant metric used to evaluate experimental brace efficacy and posterolateral meniscus strain was an additional outcome retrieved from the FE simulations. Engineering strain was calculated by measuring the nodal distance at the posteromedial meniscus and posterolateral meniscus using nodes that had an initial separation of approximately 5 mm (Fig. 4.28). Anteromedial meniscus strain was computed since anteromedial meniscus was measured during the experimental trials, while anterolateral meniscus strains were an additional outcome measure in the model. The FE strain measurements were based on similar anatomical locations compared with the experiment. Similar to the experiment, the FE VM strains were computed using the length at the initial time state during the unbraced simulation; however, the initial nodal distances between the NB and VM scenarios were identical since each simulation initiated in a stress and strain free state. Modeling the effect of the VM on the initial stresses and strains in the meniscal tissue would require an entirely different experimental methodology to first measure the unbraced resting loads on the meniscal tissue, and second to simulate how an isolated VM affects these resting loads.

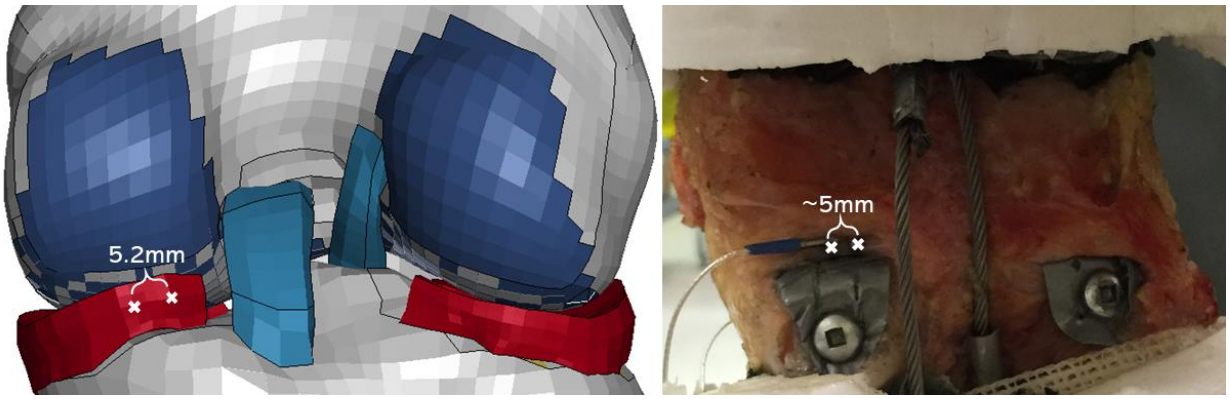


Figure 4.28: Nodal location of posteromedial meniscus strain measurement similar to the experimental measure.

### 4.7.2 *Intercondylar Joint Pressure*

Tibiofemoral joint pressure was calculated from the applied forces and areas measured on the cartilage parts, similar to the experimental pressure sensor data analysis. The sum of all nodal forces on the medial and lateral cartilages were obtained for each simulation condition. Mean cartilage pressure was calculated by dividing the mean force measured during all simulation states by the total area in all elements that had a von Mises stress exceeding 0.01 MPa. Peak cartilage pressure was calculated by dividing the peak force during the trial measured on the cartilage by the calculated area at the time state of the peak force.

### 4.7.3 *Comparison with Experimental Outcomes*

Objective evaluation methods are utilised to compare test and simulation signals such as experimental and computational responses (Vavalle et al., 2013). Vavalle et al. (2013) used three objective evaluation methods to compare finite element simulation responses against in-vitro test responses in a frontal sled crash impact. The investigated evaluation methods were magnitude and phase error factors, cumulative standard deviation, and the CORrelation and Analysis (CORA) method; and the study reported that CORA was the most comprehensive amongst the three because unlike CORA, the error

factors method does not account for experimental variance and cumulative standard deviation is a point-by-point comparison that does not consider phase shifts (Vavalle et al., 2013). The CORA method compares two responses based on three factors, which are size, phase, and progression (Fig. 4.29), and calculates a CORA rating between 0 (i.e., no correlation) and 1 (i.e., perfect correlation) based on the weighted average of the three factors (Eq. 4.5) (Gehre et al., 2009).

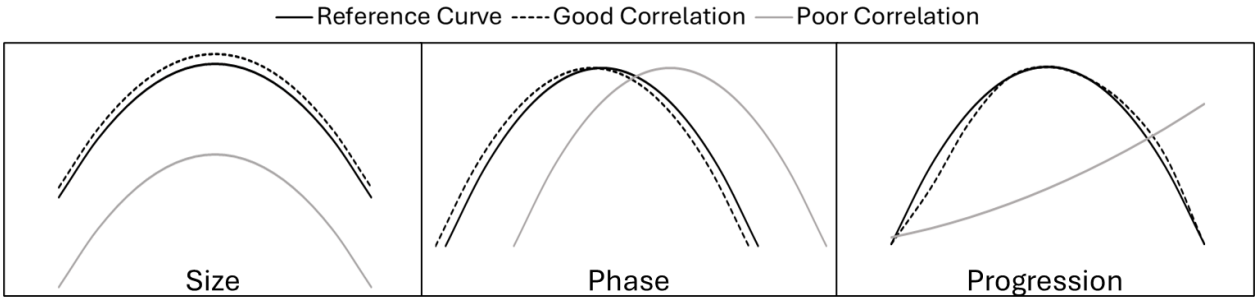


Figure 4.29: Illustration of good and poor correlations for size, phase, and progression ratings.

$$\text{CORA} = W_Z \times Z + W_P \times P + W_R \times R \tag{4.5}$$

where:
CORA is the cross correlation rating such that $0 \leq \text{CORA} \leq 1$
Z is the size rating such that $0 \leq Z \leq 1$
P is the phase rating such that $0 \leq P \leq 1$
R is the progression rating such that $0 \leq R \leq 1$
$W_Z$ is the size weight factor such that $0 \leq W_Z \leq 1$
$W_P$ is the phase weight factor such that $0 \leq W_P \leq 1$
$W_R$ is the progression weight factor such that $0 \leq W_R \leq 1$
and $W_Z + W_P + W_R = 1$

Model performance was evaluated and compared with experimental data using the cross-correlation approach (CORA v4.0.4) for flexion angle and posteromedial and anteromedial meniscal strains. This study considered size, phase, and progression between the experimental and model outcomes to be equally important, thus $W_Z = W_P = W_R = 1/3$. Initially FE model postero- and anteromedial strains were cross-correlated to a specimen that most closely resembled the model for each activity-brace-ACL combination. Subsequently, this process was repeated for the remaining specimens and a mean correlation rating with standard deviation was calculated. Furthermore, CORA

analyses were conducted between the model input and output kinematic and kinetic BC to verify BC implementation accuracy. Finally, FE mean and peak tibiofemoral pressures were compared to the experimental means and standard deviations.

# V. Experimental In-Vitro Results

Specimens were tested using the 18 unique testing conditions (Table 4.1) and eight specimens were successfully tested in every condition. Specimen #6 had a very low body mass index (BMI) and resulted in patellar failure during the first SLS trial; thus, an artificial patella was fabricated out of resin and DLS and gait activities were completed without SLS trials. Specimen #10 hyperextended during the first gait trial, which could have been due to knee laxity. Upon examination by a registered orthopaedic surgeon there were no signs of damage to the knee ligaments and tissues or to the muscle cable attachment sites, and the remainder of DLS and SLS trials were completed, though gait trials were disregarded for this specimen. Thus, double leg squats were tested on all ten specimens, gait was tested on specimens #1–9, and single leg squats were tested on specimens #1–5 and 7–10. Furthermore, posteromedial meniscus strain was measured in every tested specimen and anteromedial meniscal strain was measured not measured in specimens #2–5 due to modifications in experimental methodology and sensor malfunction (Table 5.1). The measured specimen specific moment arm values were used to convert in-vivo/in-silico muscle moments to muscle force time histories (Table 5.2).

Table 5.1: Specimens (Spec.) included for posteromedial and anterolateral strain analyses in each ADL.

| | Posteromedial meniscus strain | Anteromedial meniscal strain |
|---|---|---|
| Double leg squat | Spec. #1–10 | Spec. #1, 6–10 |
| Gait | Spec. #1–9 | Spec. #1, 6–9 |
| Single leg squat | Spec. #1–5, 7–10 | Spec. #1, 7–10 |

Table 5.2: Specimen specific muscle moment arm measurements (n=10).

| Specimen ID# | Quadriceps MA (mm) | Hamstrings MA (mm) | Gastrocnemius MA (mm) |
|---|---|---|---|
| 1 | 42 | 25 | 22 |
| 2 | 37 | 46 | 22 |
| 3 | 64 | 43 | 17 |
| 4 | 33 | 25 | 16 |
| 5 | 37 | 15 | 11 |
| 6 | 31 | 24 | 21 |
| 7 | 38 | 18 | 20 |
| 8 | 40 | 28 | 18 |
| 9 | 35 | 29 | 17 |
| 10 | 44 | 23 | 24 |
| Exp. Mean (SD) (n=10) | 40.1 (9.3) | 27.6 (9.9) | 18.8 (3.8) |

MA: Moment Arm, Exp.: Experimental, SD: Standard Deviation

## 5.1 Posteromedial Meniscus Relative Strain

It is crucial to reiterate that this study measured relative strain with the zero reference considered as the start of each unbraced test, and negative strain did not imply compressive strain, rather relatively less tensile strain due to the nature of loading on the meniscus and the orientation of the DVRT. Posteromedial meniscus strain was collected for every specimen and the mean and peak strains were processed for each successful activity-brace-ACL combination. The mean and peak posteromedial meniscus strains for all ten specimens did not produce statistical outliers based on the mean, median, Grubbs, and generalized extreme student deviate tests. Moreover, all mean and peak strains (n=10) were within 3 standard deviations of the mean values.

Mean sample posteromedial meniscus strains (n=10) were generally lower for both braces in the ACL-intact state and higher in the deficient state (Fig 5.1). The brace, brace*activity, and brace*ACL*activity interactions were not significant on posteromedial meniscus mean and peak strains ($p>.05$); however, the brace*ACL interaction was statistically significant for mean posteromedial meniscus strains between the NB-RC ($p=.048$) and NB-UF ($p<.001$) brace scenarios and for peak posteromedial meniscus strain between the NB-UF ($p<.001$) scenario. Post-hoc analysis revealed a significant

effect of the brace only in the ACL-intact state for mean posteromedial meniscus strains between the NB-RC (p=.006) and NB-UF (p=.001) scenarios, as well as peak posteromedial meniscus strain between the NB-UF (p=.001) scenario. Mean strains were lower for the braced trials while the ACL was intact for every test condition except for the RC brace during DLS (Fig. 5.1). The means of the posteromedial meniscus strains indicated both braces reduced the overall mean (Table 5.3) and peak (Table 5.4) strains by approximately 2-4% for the ACL-intact state; with the exception of the RC brace during DLS, which had higher mean (2.6%) and peak (1.1%) strain values compared to the NB scenario.

There was a nonsignificant effect of the brace in the ACL-deficient state (p≥.065). The RC brace during SLS was the only instance which resulted in a lower mean posteromedial meniscus strain compared the NB scenario (Fig. 5.1). The overall sample mean strains were higher with a deficient ACL, with the exception of the RC brace during SLS (Table 5.3). Similarly, the overall sample peak strain values were higher in the ACL-deficient state, except for the RC brace during DLS (Table 5.4).

When comparing posteromedial meniscus strain outcomes between the RC-UF brace scenarios, the peak and mean strains were not significant for the effect of the brace or the brace*activity and brace*ACL*activity interactions (p≥0.073). The mean (p=.016) and peak (p=.003) strains were significantly different for the brace*ACL interaction; further pairwise comparisons revealed a significant effect of the brace in the ACL-deficient state for mean (p=.036) and peak (p=.016) strain. During the ACL-intact state the strain plots (Fig. 5.1) and means (Tables 5.3-5.4) for both braces revealed comparable results, with the exception of the RC brace during DLS, which was higher than the UF brace by approximately 3%. During the ACL-deficient state the overall sample mean (Table 5.3) and peak (Table 5.4) strains indicated the UF brace was approximately 1-3% higher than the RC brace.

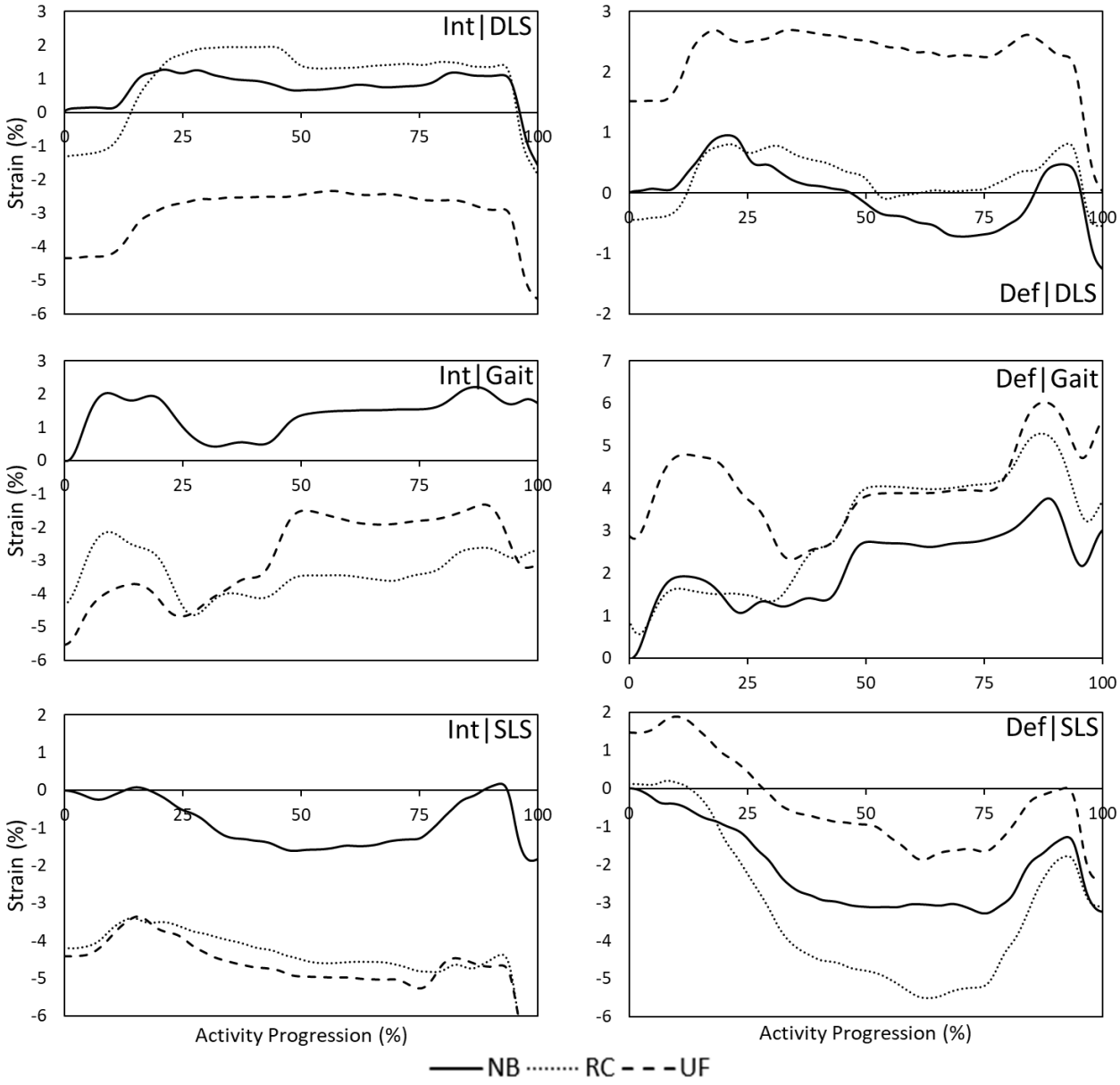


Figure 5.1: Mean posteromedial meniscus relative strain for specimens #1-10 for ACL-intact and -deficient states (Int, Def) for double leg squat (DLS) (n=10), Gait (n=9), and single leg squat (SLS) (n=9) trials with unbraced (NB), rebound cartilage (RC), and Unloader Fit (UF) bracing scenarios.

Table 5.3: Mean (SD) of the mean posteromedial (n=10) and anteromedial (n=6) meniscus relative strains.

| | Posterior Medial Meniscus Relative Strain (%) | | | Anterior Medial Meniscus Relative Strain (%) | | |
|---|---|---|---|---|---|---|
| ACL, Activity | NB | RC | UF | NB | RC | UF |
| Int, DLS | 0.79 (2.7) | 1.1 (8.2) | -2.9 (8.2) | -0.18 (1.1) | -2.5 (2.5) | -4.5 (4.4) |
| Int, Gait | 1.4 (2.2) | -3.3 (5.5) | -2.8 (5.0) | 0.67 (1.4) | -1.3 (3.7) | -4.0 (4.7) |
| Int, SLS | -0.83 (2.2) | -4.3 (5.8) | -4.6 (3.6) | -0.16 (0.8) | 0.39 (5.0) | -1.8 (5.4) |
| Def, DLS | 0.00 (3.1) | 0.26 (4.9) | 2.3 (6.6) | -0.68 (2.4) | -0.87 (6.4) | -1.3 (5.8) |
| Def, Gait | 2.2 (2.5) | 3.0 (4.8) | 4.0 (7.4) | -0.30 (1.4) | 0.30 (8.9) | -0.29 (10.1) |
| Def, SLS | -2.1 (1.9) | -3.2 (4.4) | -0.37 (4.9) | 0.16 (3.0) | 0.97 (4.9) | 1.7 (5.9) |

NB: Unbraced, RC: Rebound Cartilage, UF: Unloader Fit, Int: Intact, Def: Deficient, DLS: Double leg squat, SLS: Single leg squat

Table 5.4: Mean (SD) of the peak posteromedial (n=10) and anteromedial (n=6) meniscus relative strains.

| | Posterior Medial Meniscus Relative Strain (%) | | | Anterior Medial Meniscus Relative Strain (%) | | |
|---|---|---|---|---|---|---|
| ACL, Activity | NB | RC | UF | NB | RC | UF |
| Int, DLS | 2.5 (2.5) | 2.6 (8.0) | -1.7 (8.2) | 0.76 (0.8) | -1.6 (2.7) | -3.5 (4.5) |
| Int, Gait | 3.6 (3.0) | -0.39 (5.6) | -0.17 (5.5) | 1.6 (1.6) | -0.10 (3.8) | -2.7 (5.0) |
| Int, SLS | 0.83 (0.9) | -2.6 (4.5) | -3.0 (3.4) | 0.85 (0.8) | 1.5 (4.9) | -0.8 (5.8) |
| Def, DLS | 2.3 (2.4) | 1.7 (4.5) | 4.0 (7.6) | 1.2 (0.9) | 0.27 (6.5) | -0.32 (6.3) |
| Def, Gait | 4.9 (3.4) | 5.5 (6.2) | 7.4 (8.3) | 2.5 (1.9) | 2.8 (10) | 2.3 (11.2) |
| Def, SLS | 0.37 (0.7) | 0.38 (3.1) | 2.2 (5.5) | 2.8 (2.7) | 3.7 (6.6) | 4.1 (7.9) |

NB: Unbraced, RC: Rebound Cartilage, UF: Unloader Fit, Int: Intact, Def: Deficient, DLS: Double leg squat, SLS: Single leg squat

## 5.2 Anteromedial Meniscus Relative Strain

Anteromedial meniscus strain was not collected for specimens #2–4 due to adaptations in the experimental procedure, and it was not reported for specimen #5 due to sensor malfunction (Table 5.2). Mean strain plots (Fig. 5.2) and the overall means of the mean and peak strain values (Tables 5.3–5.4) were computed similarly to posteromedial meniscus strain for every successful test combination. The effect of the brace was significantly different for anteromedial meniscus mean strain in the NB-UF (p=.004) scenario, as well as for anteromedial meniscus peak strain in the NB-RC (p=.037) and NB-UF (p=.004) scenarios. Mean anteromedial meniscus strain was not significantly different (p=.061) in the NB-RC scenario. Moreover, there were no

significant differences between RC-UF scenarios for mean (p=.095) and peak anteromedial meniscus strain (p=.078). Finally, the mean and peak anteromedial meniscus strains for the interactions (brace*ACL, brace*activity, and brace*ACL*activity) were not significant (p≥.182) for either of the braces or between the two braces.

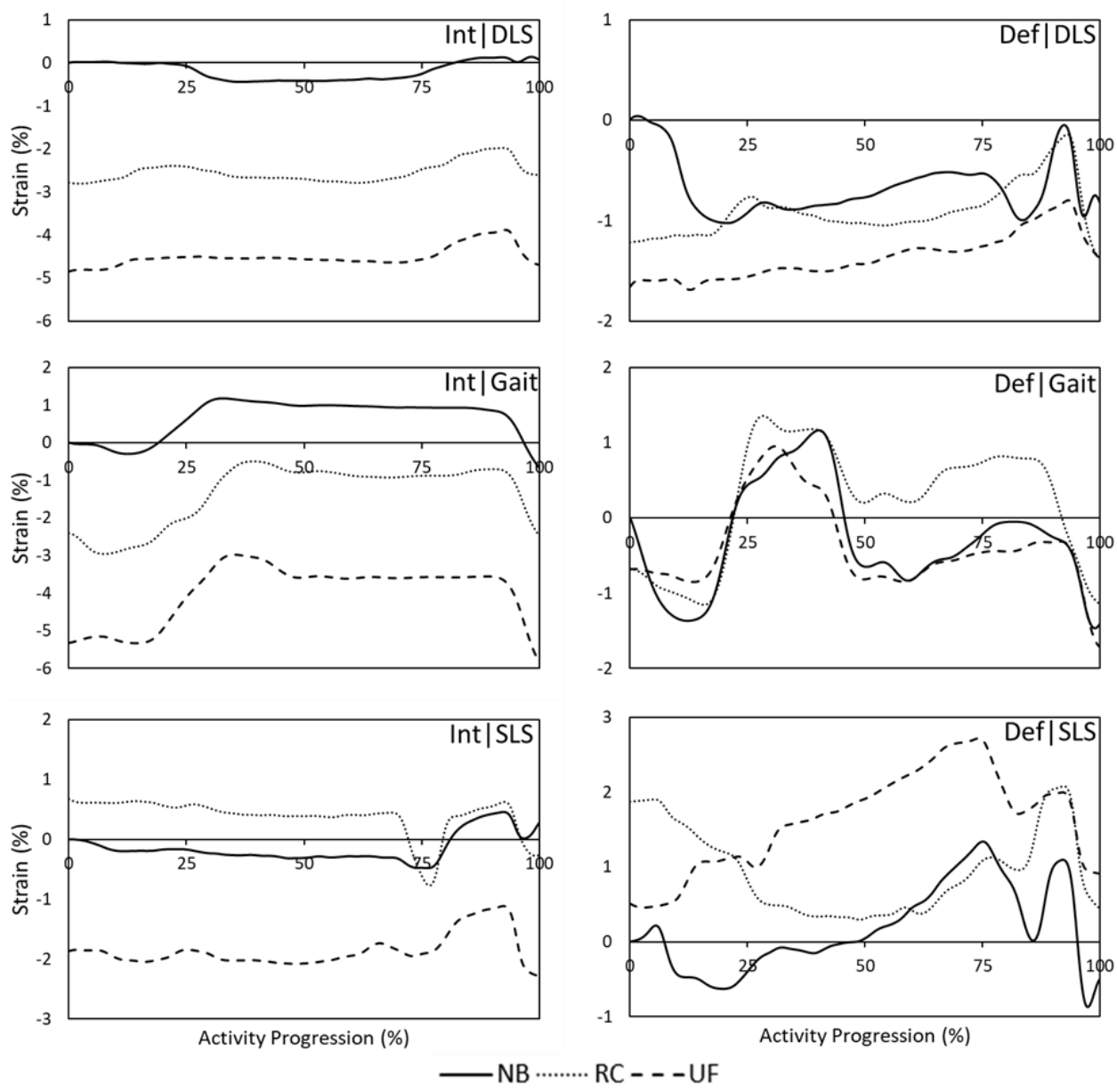


Figure 5.2: Mean anteromedial meniscus strain for specimen #1, 6-10 for ACL-intact and -deficient conditions (Int, Def) in double leg squat (DLS) (n=6), Gait (n=5), and single leg squat (SLS) trials (n=5) with unbraced (NB), rebound cartilage (RC), and Unloader Fit (UF) bracing scenarios.

## 5.3 Tibiofemoral Joint Pressure

Tibiofemoral joint pressure was measured on every specimen except for specimen #4 due to an extremely narrow intercondylar joint space. Moreover, due to damaged sensels during the experiment specimen #3 resulted in erroneous pressure data. An 11-point calibration was conducted on each sensor similar to previous literature (Wilharm et al. 2013), with a sample calibration result depicting a linear trend between sensor output and applied force (r=0.99) (Fig. 5.3). Calibration factors were similar for the other specimens with correlation coefficients ≥ 0.98 (Table 5.5). Sample medial and lateral pressure recordings during ACL-intact DLS in all three brace scenarios reveal decreased peak pressures during the knee brace trials as evidenced by the colder colour palette (Fig. 5.4). In some situations sensels initially had missing values that eventually became fully operational (Fig. 5.4). Missing sensel values were interpolated from adjacent sensels.

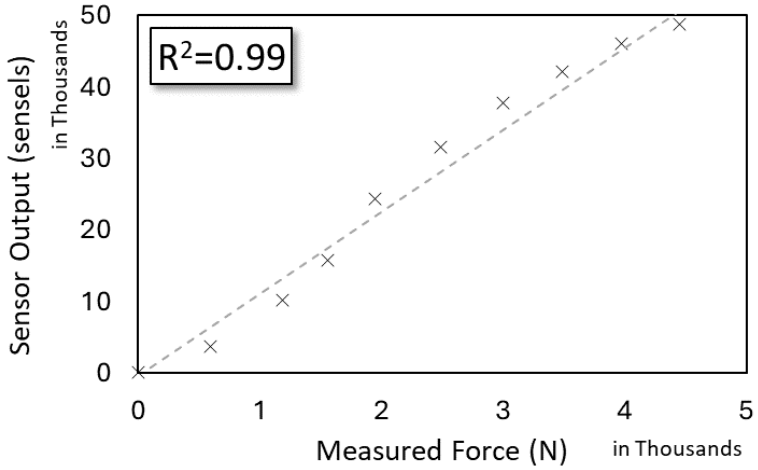


Figure 5.3: Typical sensor output shown for the sensor used on specimen #1.

Table 5.5: Calibration factors for sensors used to measure tibiofemoral joint pressure (n=8).

| | Specimen ID (#) | | | | | | | |
|---|---|---|---|---|---|---|---|---|
| | 1 | 2 | 5 | 6 | 7 | 8 | 9 | 10 |
| Calibration Factor (sensels/N) | 11.3 | 13.4 | 9.7 | 8.6 | 14.5 | 16.7 | 14.6 | 18.3 |

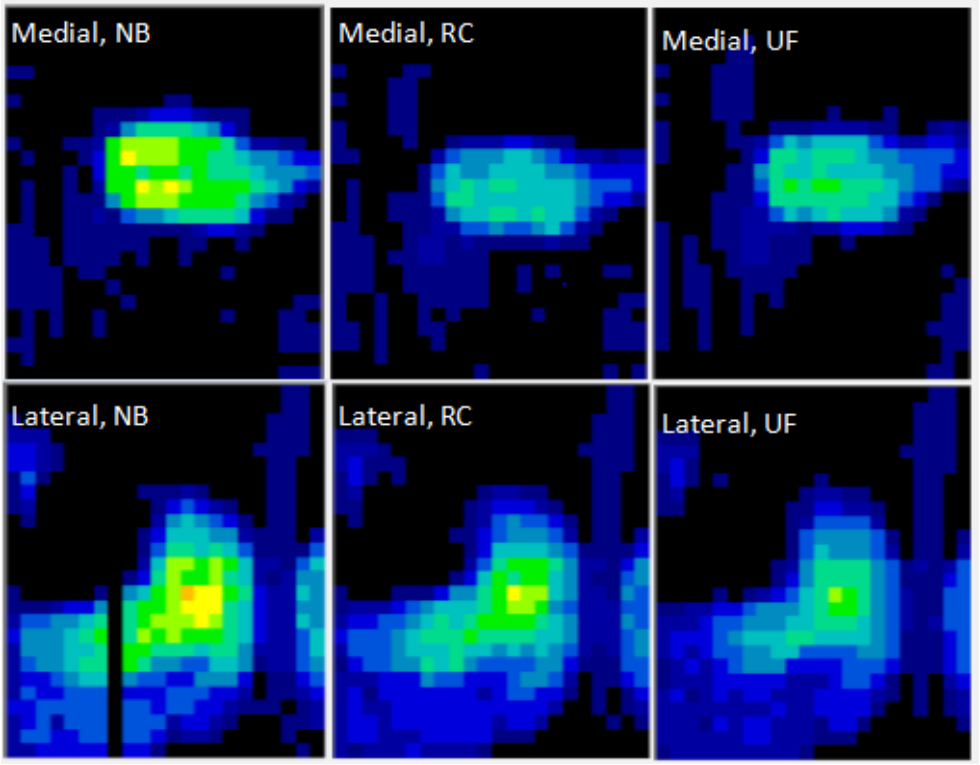

Figure 5.4: An unbraced and braced Tekscan pressure recording for specimen #8 performing a DLS in an ACL-intact condition, where NB: unbraced, RC: rebound cartilage brace, UF: unloader fit brace.

There was no significant effect of the brace or any of the brace interactions (brace*ACL, brace*activity) for either brace (compared to the NB) in the mean or peak medial tibiofemoral pressures ($p>.05$); although, there was a significant difference between the two braces on the peak medial pressure ($p=.032$). For the lateral condyle, the UF brace demonstrated significantly different brace*ACL interactions for the mean pressure when compared against the NB ($p=.032$) and RC brace ($p=.015$) scenarios and for the peak pressure in the NB ($p=.035$) scenario; a post hoc analysis depicted a significant difference in the mean pressures between the UF brace and the NB ($p=.020$) and RF brace ($p=.020$) scenarios in the ACL-deficient state, the ACL-intact state was not significantly different ($p>.05$).

Overall, the braces had a nonsignificant ($p>.05$) effect on the tibiofemoral joint pressures during the ACL-intact state, with the mean medial and lateral tibiofemoral pressures depicting similar trends (Fig. 5.5) and values (Table 5.6) between the NB and braced (RC, UF) scenarios. The peak pressures on the medial compartment were higher

than the lateral compartment during the DLS and SLS (Table 5.6). Moreover, the inclusion of the braces had decreases of 0.2 MPa in the peak medial and 0.1 MPa in the peak lateral compartment pressures during DLS (Table 5.6). During SLS, the braces increased the peak medial pressure and decreased the peak lateral pressures (Table 5.6). Gait trials demonstrated a decrease (by 0.1-0.2 MPa) in the mean medial and lateral compartment pressures, though the lateral compartment pressures had a lower decrease than medial pressures (Table 5.6).

The braces produced greater differences in the ACL-deficient state than in the ACL-intact state. Both braces produced lower medial joint pressure trends during DLS and gait, and higher trends during SLS (Fig. 5.6). Similar to the ACL-intact state, the mean and peak pressures during DLS and SLS were higher in the medial compartment (Table 5.7); however, unlike the ACL-intact state, the peak lateral compartment pressures showed more substantial increases of 0.1-0.3 MPa during the braced trials with a deficient ACL for all three activities (Table 5.7). While there were significant differences ($p<.05$) in the mean pressure with the UF brace in the ACL-deficient state, the majority of brace comparisons were nonsignificant ($p>.05$) like the ACL-intact state.

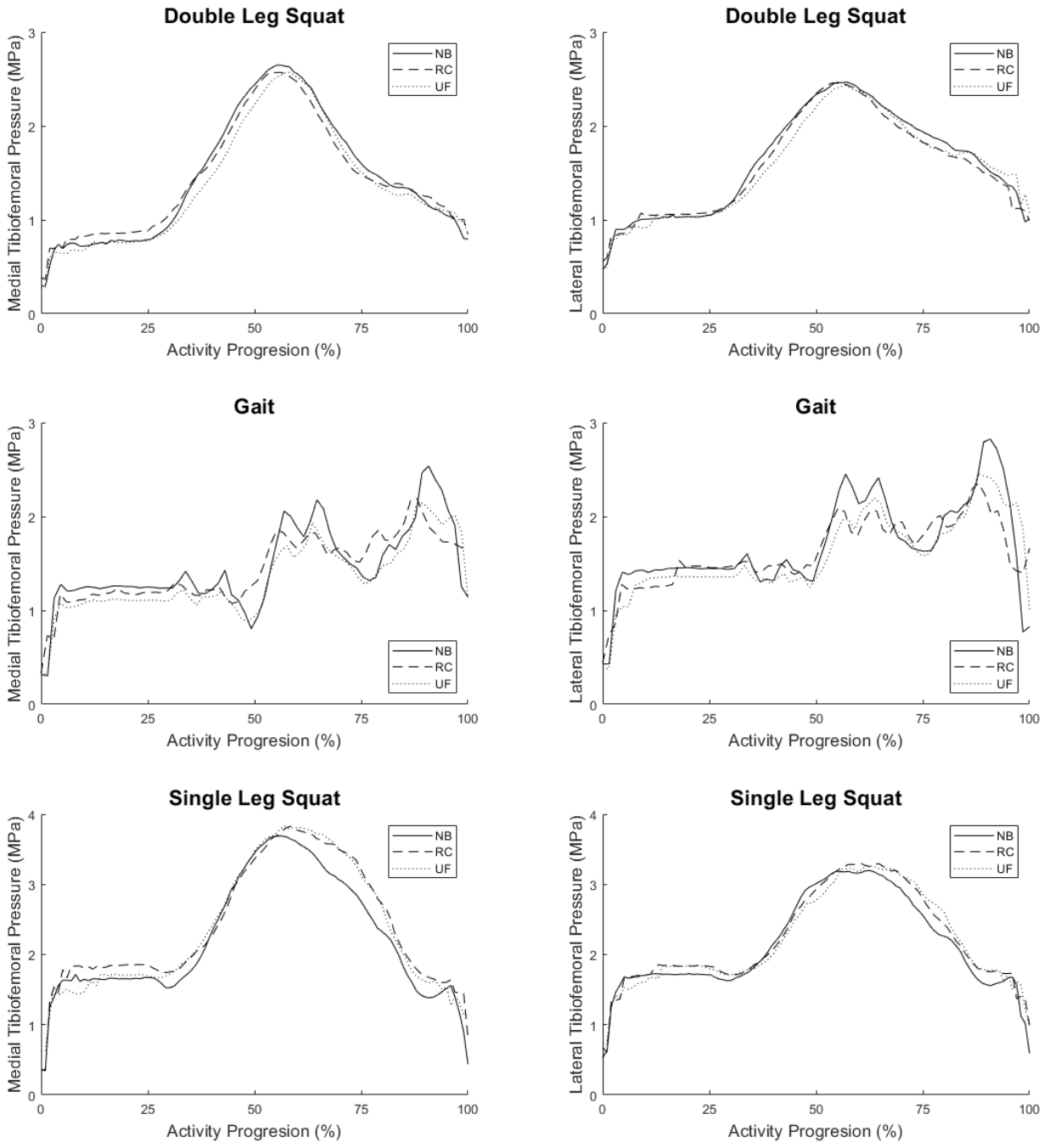


Figure 5.5: Mean medial (left) and lateral (right) tibiofemoral joint pressures for all three activities with the ACL-intact (n=6) where NB: no brace; RC: rebound cartilage brace; UF: unloader fit brace.

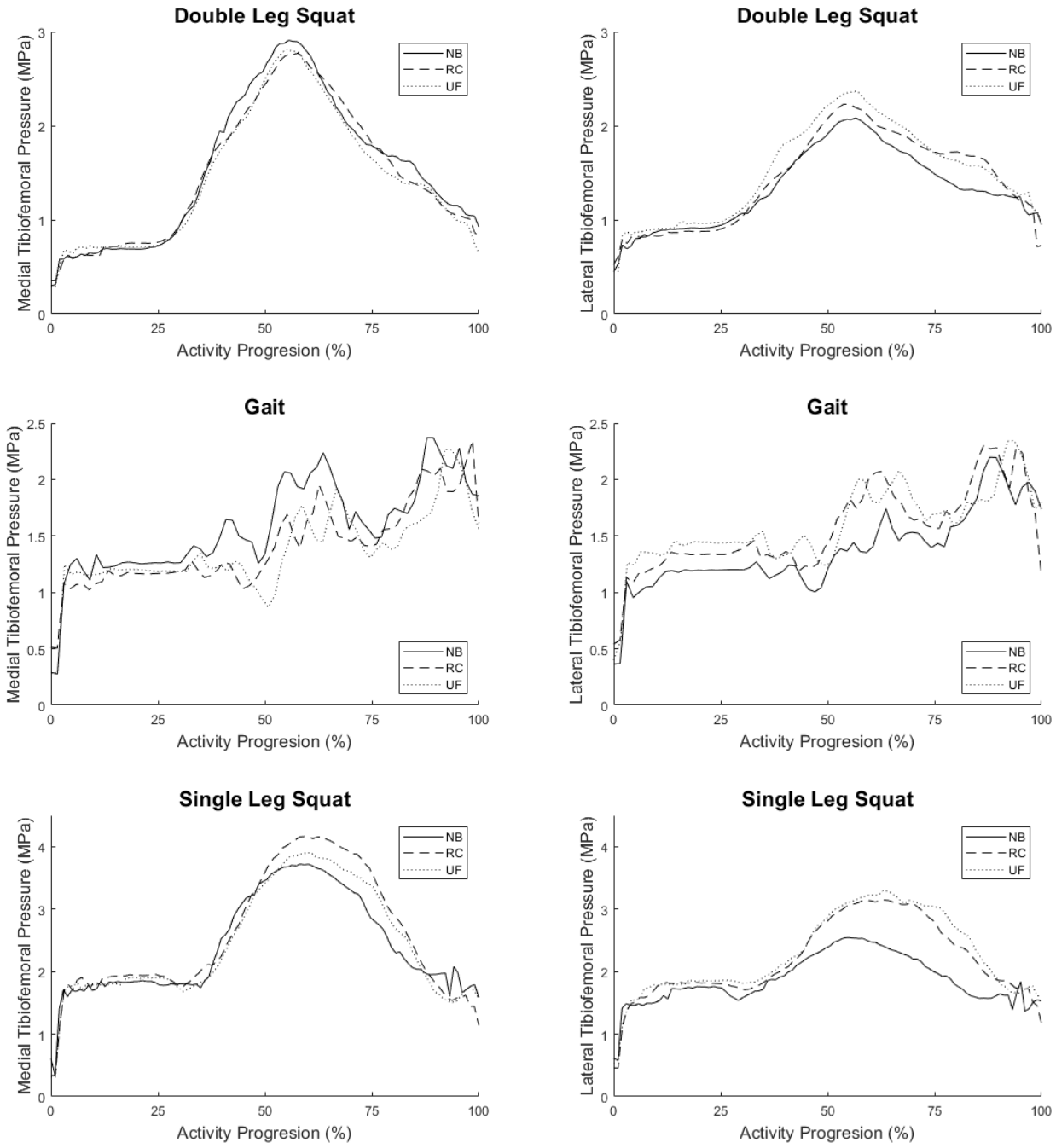


Figure 5.6: Mean medial (left) and lateral (right) tibiofemoral joint pressures for all three activities with the ACL-deficient (n=6) where NB: no brace; RC: rebound cartilage brace; UF: unloader fit brace.

Table 5.6: Mean (SD) of the mean and peak medial and lateral tibiofemoral joint pressures during 3 activities and 3 brace scenarios with the ACL intact (n=8).

| | DLS | | | Gait | | | SLS | | |
|---|---|---|---|---|---|---|---|---|---|
| | NB | RC | UF | NB | RC | UF | NB | RC | UF |
| Med. Mean P (MPa) | 1.5 (0.3) | 1.5 (0.4) | 1.3 (0.3) | 1.5 (0.2) | 1.4 (0.3) | 1.3 (0.3) | 1.8 (1.0) | 2.0 (0.9) | 1.8 (0.9) |
| Lat. Mean P (MPa) | 1.5 (0.4) | 1.5 (0.5) | 1.4 (0.4) | 1.6 (0.5) | 1.5 (0.6) | 1.5 (0.6) | 1.7 (0.9) | 1.8 (0.9) | 1.7 (0.9) |
| Med. Peak P (MPa) | 2.8 (0.5) | 2.6 (0.6) | 2.6 (0.8) | 2.7 (0.3) | 2.8 (0.3) | 2.5 (0.5) | 3.2 (1.8) | 3.3 (1.6) | 3.3 (1.7) |
| Lat. Peak P (MPa) | 2.5 (0.5) | 2.4 (0.8) | 2.4 (0.5) | 2.8 (1.0) | 2.5 (1.0) | 2.5 (0.8) | 3.0 (1.5) | 2.8 (1.4) | 2.8 (1.3) |

Med: medial; Lat: lateral; P: pressure; DLS: double leg squat; SLS: single leg squat; NB: no brace; RC: rebound cartilage brace; UF: unloader fit brace; SD: standard deviation

Table 5.7: Mean (SD) of the mean and peak medial and lateral tibiofemoral joint pressures during 3 activities and 3 brace scenarios with the ACL deficient (n=8).

| | DLS | | | Gait | | | SLS | | |
|---|---|---|---|---|---|---|---|---|---|
| | NB | RC | UF | NB | RC | UF | NB | RC | UF |
| Med. Mean P (MPa) | 1.4 (0.4) | 1.4 (0.4) | 1.5 (0.3) | 1.5 (0.4) | 1.5 (0.4) | 1.4 (0.2) | 1.9 (0.9) | 2.1 (1.0) | 1.9 (0.9) |
| Lat. Mean P (MPa) | 1.4 (0.3) | 1.3 (0.5) | 1.5 (0.4) | 1.4 (0.4) | 1.5 (0.6) | 1.5 (0.4) | 1.6 (0.7) | 1.8 (0.9) | 1.8 (0.9) |
| Med. Peak P (MPa) | 2.8 (1.1) | 2.8 (1.0) | 2.7 (0.7) | 2.6 (0.8) | 2.6 (0.5) | 2.5 (0.4) | 3.2 (1.6) | 3.3 (2.0) | 3.2 (1.8) |
| Lat. Peak P (MPa) | 2.3 (0.5) | 2.2 (0.7) | 2.4 (0.5) | 2.5 (0.6) | 2.5 (0.9) | 2.5 (0.7) | 2.7 (1.3) | 2.7 (1.5) | 2.9 (1.4) |

Med: medial; Lat: lateral; P: pressure; DLS: double leg squat; SLS: single leg squat; NB: no brace; RC: rebound cartilage brace; UF: unloader fit brace; SD: standard deviation

The brace outcomes are more evident when comparing pressure changes in the medial compartment and the relative lateral to medial pressure differences with the application of the braces. The percent differences in medial compartment pressures demonstrated that the mean and peak medial pressures decreased with both braces in DLS and gait test conditions as evidenced by the reductions (i.e., negative values) in tibial pressure, while both braces resulted in an increase in medial pressure during SLS (Fig. 5.7). The difference between lateral and medial pressures (ΔP) demonstrated that both braces caused increases in the lateral tibial pressure compared to the medial as evidenced by increases in ΔP (i.e., positive values), thus the braces effectively shifted the load from the medial to lateral compartment for all ADLs (Fig. 5.8). In every braced DLS or gait test

condition with a mean or peak medial pressure decrease there was a positive lateral-medial pressure difference indicating that a valgus moment unloading decreased pressure in the medial compartment and increased pressure in the lateral compartment as intended. In the SLS braced test conditions there was also a positive lateral-medial pressure difference indicating a valgus shift despite an overall increase in the medial compartment pressure indicating that the medial compartment was not unloaded, rather the lateral compartment experienced a relatively larger pressure increase.

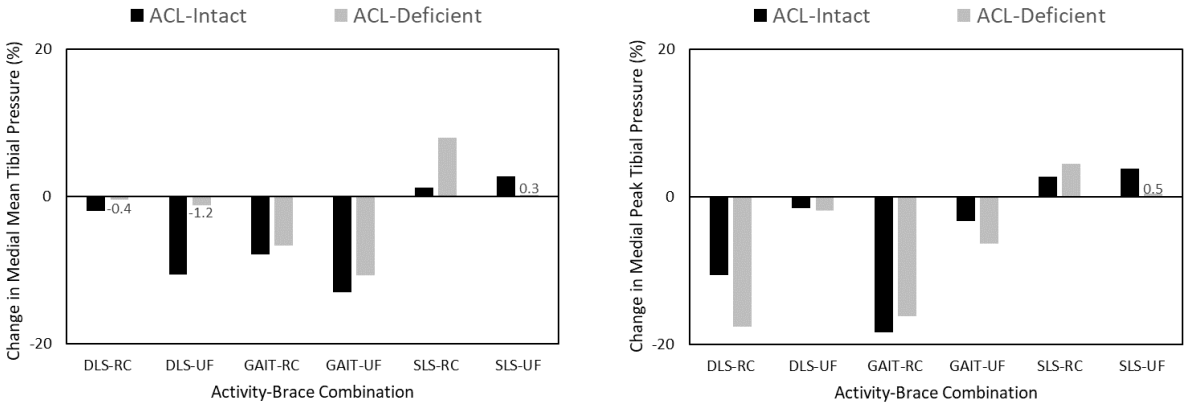


Figure 5.7: Percent differences in (a) mean and (b) peak medial tibial cartilage pressure in braced scenarios.

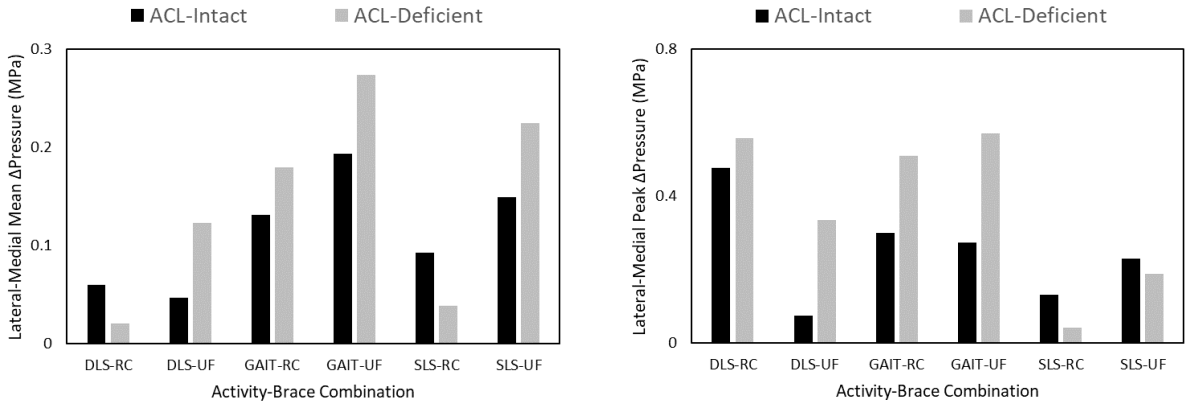


Figure 5.8: Lateral and medial tibial cartilage (a) mean and (b) peak pressure differences for each activity-brace combination relative to unbraced-activity combinations.

# VI. Computational Results

This chapter reports outcomes from the geometric and materials enhancements required to mimic the initial experimental position for each activity, verifies the application of the experimental input BCs to the FE simulations, and concludes with strain and pressure outcome measures similar to the experimental study.

## 6.1 FE Model Extension

Adapting the FE leg model to match the initial experimental boundary conditions proved to be the most challenging task, and the majority of the model improvements were consequences of unsuccessful knee extension attempts. Gait simulations did not require modifications from the initial seated position; squat simulations required a decrease in seated flexion angle from 49° to approximately 10°. Initial attempts constrained the femur and applied increasing magnitudes of quadriceps force to extend the tibia, with minor modifications to the femoral and tibial parts and no changes to the tissues and ligaments surrounding the knee. The model demonstrated overly stiff and resistant joint kinematics with a maximum applied quadriceps force of 1800 N, which resulted in a minimum flexion angle of 25.6°. Attempting a tibial displacement BC produced a full extension (~5° flexion angle), however, the outcome was extremely aggressive and resulted in an unnatural joint geometry with excessive tibiofemoral joint separation (Fig. 6.1). It became evident that the minimum part separation distance between the tibial and femoral condyles needed to be augmented as an outcome measure during extension simulations. The targets for joint separation were the minimum distances between femoral and tibial cartilages in the medial and lateral compartments, which were 2.5+0.5 and 3.5+0.5 mm, respectively. Moreover, the target for minimum flexion angle was approximately 5° to ensure full range of motion during the gait simulations. The tibial displacement BC was removed and the majority of extension simulations were conducted

using a quadriceps force condition; however, the final few leg model extension iterations used a combination of boundary and muscle force BCs to minimize joint separation (presented in §6.1.3).

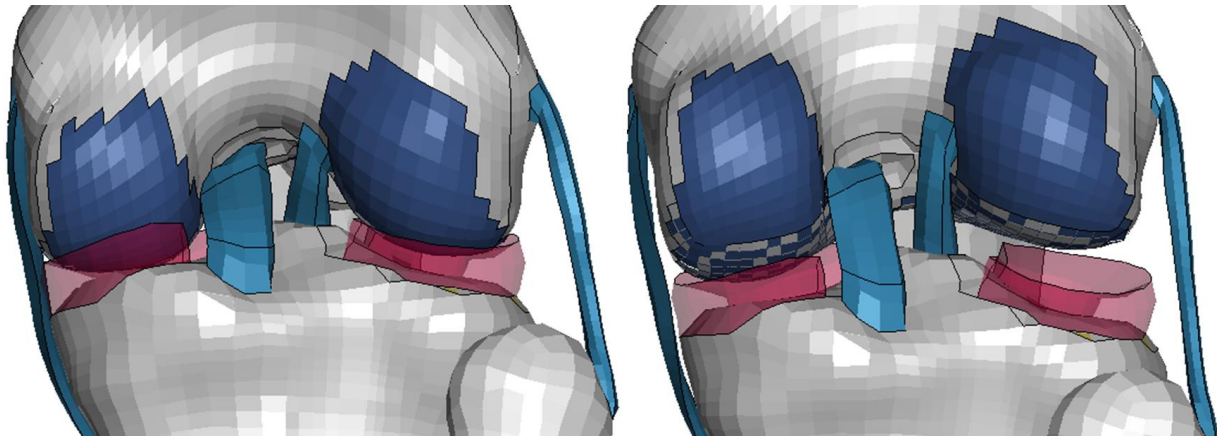

(a) (b)

Figure 6.1: Posterior view depicting tibiofemoral joint separation in the (a) 49° seated; and (b) fully extended states.

### 6.1.1 *Select Ligament Uniaxial Tensile Tests*

It was hypothesized that inaccurate ligament material models in the ACL, LCL, MCL, and PCL were causing the excessive joint separation and/or hindering the joint's ability to extend. Ligament specific stress-strain or force-displacement curves from literature were used to update the material properties for each ligament (Chandrashekar et al., 2005; Harner et al., 1995; Wilson et al., 2012). Force-elongation outcomes from isolated uniaxial tension simulations of the knee ligaments with the updated stress-strain input curves (grey curves in Fig. 6.2) were compared with experimental studies (dashed black curves in Fig. 6.2) and demonstrated vast discrepancies, due to cross-sectional area differences between the experimental studies and the model (Table 6.1). A scale factor (S, Table 6.1) was calculated between the experimental and FE cross-sectional areas, and each FE force-elongation result was scaled such that the model's ligaments would reflect the experimental outcomes. Each scale factor was further calibrated ($S_c$, Table 6.1) until the scaled FE result (red curves in Fig. 6.2) were calibrated to the experimentally measured properties. These four scaled force-elongation results were converted to stress-

strain curves using the measured FE cross-sectional area and axial length of each ligament part. Updating these four ligament material models resulted in a minimum flexion angle of 24.2° with a reduction in the applied quadriceps force to 1400 N and joint separation distances of 6.7 and 10.1 mm for the medial and lateral compartments, respectively. It was foreseen that meniscal enhancements were necessary to improve model performance and outcomes during extension.

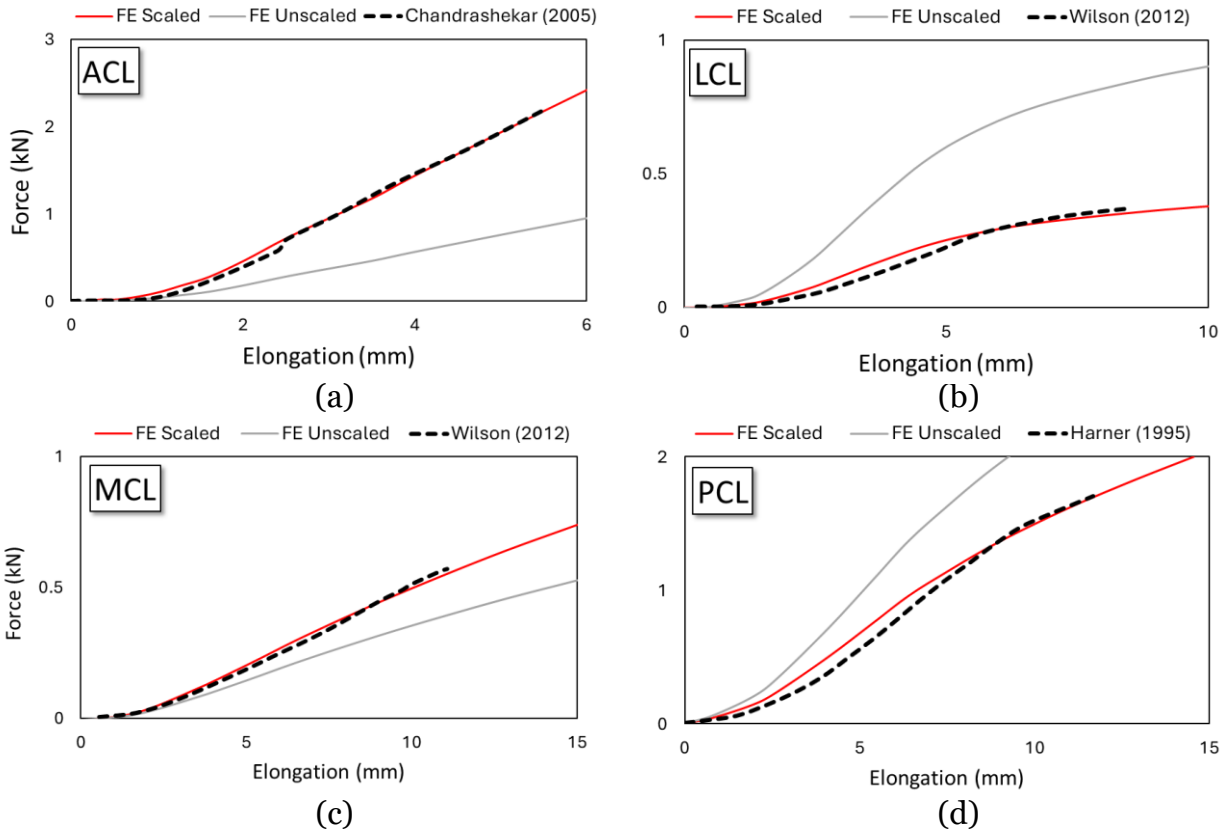


Figure 6.2: Uniaxial FE tensile test simulations comparing force-elongation with experimental literature for the (a) ACL; (c) LCL; (c) MCL; and (d) PCL.

Table 6.1: FE and reference literature (Ref.) ligament cross-sectional areas with scale factor (S) and calibrated scale factor ($S_c$).

| Part | FE Area ($mm^2$) | Ref. Area ($mm^2$) | S | $S_c$ |
|---|---|---|---|---|
| ACL | 34 | 87 | 2.6 | 2.5 |
| LCL | 18 | 10 | 0.6 | 0.4 |
| MCL | 31 | 53 | 1.7 | 1.4 |
| PCL | 52 | 41 | 0.8 | 0.7 |

### 6.1.2 *Meniscal Tissue and Horn Enhancements*

The linear plastic kinematic material model and/or geometric configuration of the meniscal parts were suspected to affect knee joint extension. Updating the menisci material model to an elastic material (Table 4.6) alongside the ACL, PCL, LCL, MCL material enhancements resulted in a knee flexion angle of 13.2° with an extension force of 1400 N and yielded medial and lateral joint separations of 6.6 and 6.1 mm, respectively. However, this modification did not demonstrate typical sagittal plane rotation, rather joint extension caused the anterior regions of both menisci to penetrate the tibial cartilage and resulted in the joint 'locking' and 'pivoting' around the menisci rather than rotating. The anterior portions of the menisci also experienced excessive compression (Fig. 6.3). It was determined the menisci did not translate in the anterior-posterior direction since the menisci and tibial cartilage parts shared common nodes with an absence of contact definitions between the cartilage and menisci.

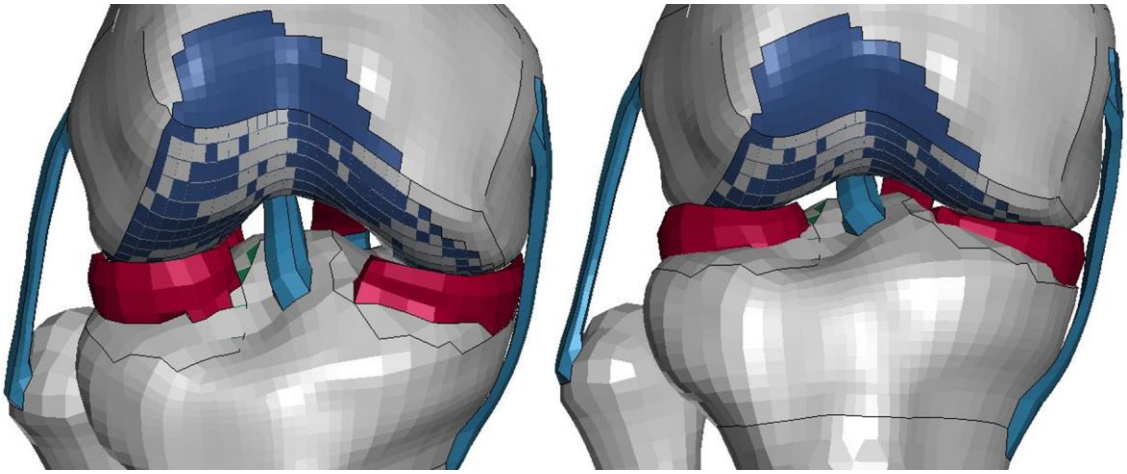

(a) (b)

Figure 6.3: Anterior view depicting the (a) original menisci; and (b) the compressed menisci following knee extension.

The menisci were assigned a new set of nodes to permit a sliding degree of freedom between the cartilage parts. To stabilize the menisci, four 1-dimensional spring elements were added to replicate the meniscal horns at each of the horn sites with a combined material stiffness of 180 N/mm per site (Guess et al., 2015; Hauch et al., 2010). These

modifications resulted in improved sagittal plane joint mechanics during extension and a minimum flexion angle of 10.6°, though further adaptations were made to the extension BCs to attain a slightly lower flexion angle and the target joint separation distances.

### 6.1.3 *Combined Kinematic, Kinetic Extension Boundary Conditions*

The application of a single quadriceps force resulted in a force imbalance around the knee joint; thus, the extension BCs were improved to include a hip velocity with three muscle forces (quadriceps, hamstrings, gastrocnemius). The hip velocity-time history magnitude was taken from the experimental input hip velocity condition during DLS. Simplified muscle force-time histories were created based on a ramp-step function with the values taken from previous in-vivo/in-silico results (Tomescu et al., 2018). Knee extension was simulated using various iterations of peak muscle forces and the final iteration was selected since it achieved the desired flexion angle and the targeted medial and lateral joint separation distances (Table 6.2). The nodal positions at the 10° flexion state from this extension iteration were extracted and used as the initial state for the DLS and SLS models to replicate the respective initial experimental start positions.

Table 6.2: Flexion angle and intercondylar joint separation values (parentheses represent difference compared to the initial value) during FE extension.

| Quadriceps Force (N) | Hamstrings Force (N) | Gastrocnemius Force (N) | Minimum Flexion Angle (°) | Medial Separation (mm) | Lateral Separation (mm) |
|---|---|---|---|---|---|
| 223 | 103 | 232 | 1.4 | 3.7(+1.2) | 5.8(+2.3) |
| 565 | 87 | 73 | 3.1 | 4.2(+1.7) | 5.4(+1.9) |
| 1115 | 515 | 1160 | 2.7 | 1.8(-0.7) | 2.4(-1.1) |
| 446 | 155 | 232 | 2.6 | 2.6(+0.1) | 5.0(+1.5) |
| 446 | 155 | 464 | 2.6 | 2.6(+0.1) | 3.8(+0.3) |

## 6.2 FE Model Preparatory Simulations

### 6.2.1 *Static Valgus Moment Assessment*

The applied VM was effective in its ability to unload the medial joint compartment in a static simulation (explained in §4.6.3). It was uncertain if the VM could be applied instantaneously, therefore a ramp-step VM BC was simulated prior to an instantaneous one. In either BC condition there was higher mean effective von-Mises stress in lateral meniscus elements (n=109) compared to the medial meniscus (n=102) indicating the VM produced the intended unloading effect (Fig. 6.4).

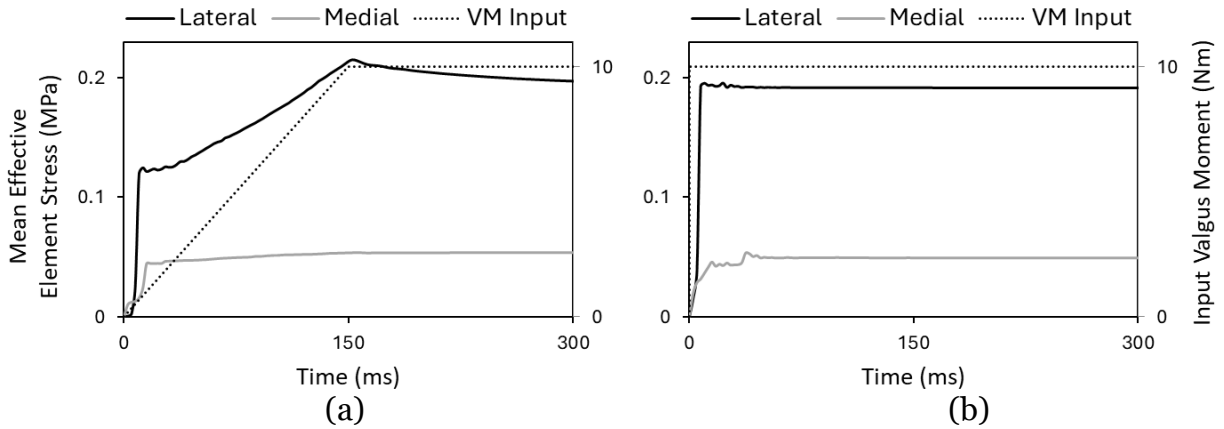


Figure 6.4: Mean medial and lateral menisci effective (von-Mises) stresses for (a) a ramp-step VM loading condition; and (b) an instantaneous VM (valgus moment) input loading condition.

### 6.2.2 *FE Model Moment Arms & Muscle Forces*

Muscle moment arm simulations revealed quadriceps, hamstrings, and gastrocnemius values were in descending order, respectively, similar to the experimental means (n=10) (Table 6.3). Muscle moment arms were used as a selection criteria for the closest matching specimen to the model over other factors such as age, mass, height, or BMI because moment arms are proportional to joint geometry (Sherman et al., 2013). The FE quadriceps moment arms were at least 1 SD greater than every other specimen and the two closest specimens to the model were specimens #3 and specimen #10. Specimen #3 was chosen as the closest matching specimen because unlike specimen #1 it had an identical gastrocnemius moment arm and a hamstring moment arm that

differed by 3 mm compared to the model. The three FE specific moment arms and the 6 cm hip moment arm (identical to all experimental specimens) were used to scale the in-vivo/in-silico DLS, gait, and SLS muscle forces obtained from Tomescu et al. (2018). This process resulted in model specific quadriceps, hamstrings, gastrocnemius, and hip muscle force-time history curves for each activity, similar to the process done for each cadaveric specimen (Fig. 6.5). Moreover, the 500 ms cable pre-tension load generated for the experiment was removed and modified with a 100 ms ramp to the initial value in the model. The total duration of the squat and gait simulations were 2080 ms and 1180 ms, respectively.

Table 6.3: Muscle moment arms for the FE model and experimental specimens (n=10).

| Specimen ID# | Quadriceps MA (mm) | Hamstrings MA (mm) | Gastrocnemius MA (mm) |
|---|---|---|---|
| FE Model | 53 | 40 | 17 |
| 1 | 42 | 25 | 22 |
| 2 | 37 | 46 | 22 |
| 3 | 64 | 43 | 17 |
| 4 | 33 | 25 | 16 |
| 5 | 37 | 15 | 11 |
| 6 | 31 | 24 | 21 |
| 7 | 38 | 18 | 20 |
| 8 | 40 | 28 | 18 |
| 9 | 35 | 29 | 17 |
| 10 | 44 | 23 | 24 |
| Exp. Mean(SD) | 40.1(9.3) | 27.6(9.9) | 18.8(3.8) |

MA: Moment Arm, Exp.: Experimental, SD: Standard Deviation

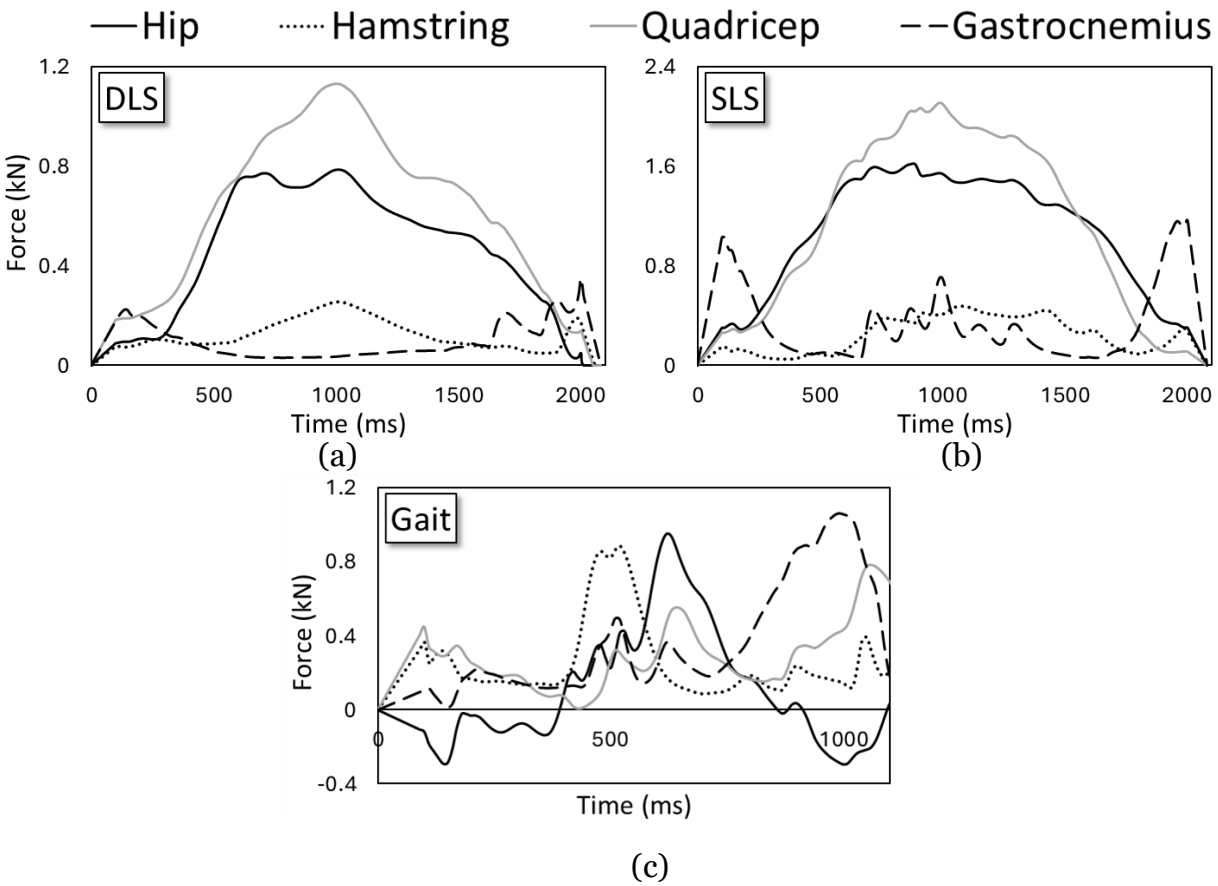


Figure 6.5: Hip, hamstring, gastrocnemius, and quadriceps muscle force time history input curves for (a) double leg squat, (b) gait, and (c) single leg squat.

## 6.3 Meniscal and Articular Cartilage Mesh Convergence

Simulations of an ACL-intact NB DLS and gait revealed the menisci and tibiofemoral cartilage had differing strain and pressure outcomes with a mesh refinement. The effect of the mesh was more pronounced on the DLS than gait. The DLS mean and peak posteromedial meniscus strains decreased by 2.4% and 6.3%, respectively, when the approximate element size was reduced from 5 mm to 2.5 mm, whereas the gait outcomes had decreases of 0.4% and 1.4% in the mean and peak strains, respectively (Table 6.4). A subsequent mesh refinement resulted in identical DLS mean and peak strains and minimal strain disparities for the gait simulation. Therefore, a meniscal mesh with an approximate element length of 2.5 mm was selected.

ACL-int NB DLS simulations with modified tibial cartilage mesh sizes resulted in mean and peak cartilage force differences of 0.1–3.6% with each refinement (Table 6.5). Based on the negligible differences associated with a smaller mesh size, the original mesh was retained for the cartilage.

Table 6.4: Mean and peak relative meniscal strain based on approximate meniscal part element size.

| | 5 mm | 2.5 mm | 1.25 mm |
|---|---|---|---|
| DLS Mean Strain (%) | 4.6 | 2.2 | 2.2 |
| DLS Peak Strain (%) | 12.0 | 5.7 | 5.7 |
| Gait Mean Strain (%) | 1.2 | 0.8 | 0.7 |
| Gait Peak Strain (%) | 3.7 | 2.3 | 2.1 |

DLS: Double Leg Squat

Table 6.5: Mean and peak cartilage force based on approximate cartilage part element size.

| | Medial Tibial Condyle | | | Lateral Tibial Condyle | | |
|---|---|---|---|---|---|---|
| | 5mm | 2.5 mm | 1.25 mm | 5 mm | 2.5 mm | 1.25 mm |
| Mean Force (N) | 505 | 514 | 533 | 683 | 701 | 720 |
| % Difference | - | 1.8 | 3.6 | - | 2.6 | 2.7 |
| Peak Force (N) | 766 | 783 | 786 | 1240 | 1273 | 1272 |
| % Difference | - | 2.2 | 0.4 | - | 2.6 | -0.1 |

## 6.4 Gait and Squat Simulations

The summary of model enhancements prior to simulating squats and gait includes a model geometry specific update to the ACL, LCL, MCL, and PCL material models and properties, changes to the meniscal and cartilage material models and properties, an extension of the model from a seated to a 10° flexion angle standing position, refinements to the meniscal mesh, and the implementation of a VM to simulate a braced scenario.

### 6.4.1 *Boundary Condition Verification and Kinematic Validation*

The kinematic and kinetic BC outcomes were confirmed against the experimental inputs in all three ADL simulations to assert the accuracy of the BC implementation. The BC outcomes mirrored the experimental input conditions indicating strong verification results. Hip velocity was greater than the ankle for both squat simulations, whereas this

was the opposite during gait (Fig. 6.6). The FE quadriceps muscle force outcomes were nearly identical to the input conditions apart from an initial and final load ramp (Fig. 6.7). The remaining three muscle force comparisons are not shown since they displayed identical trends compared to their input values (Fig. 6.5).

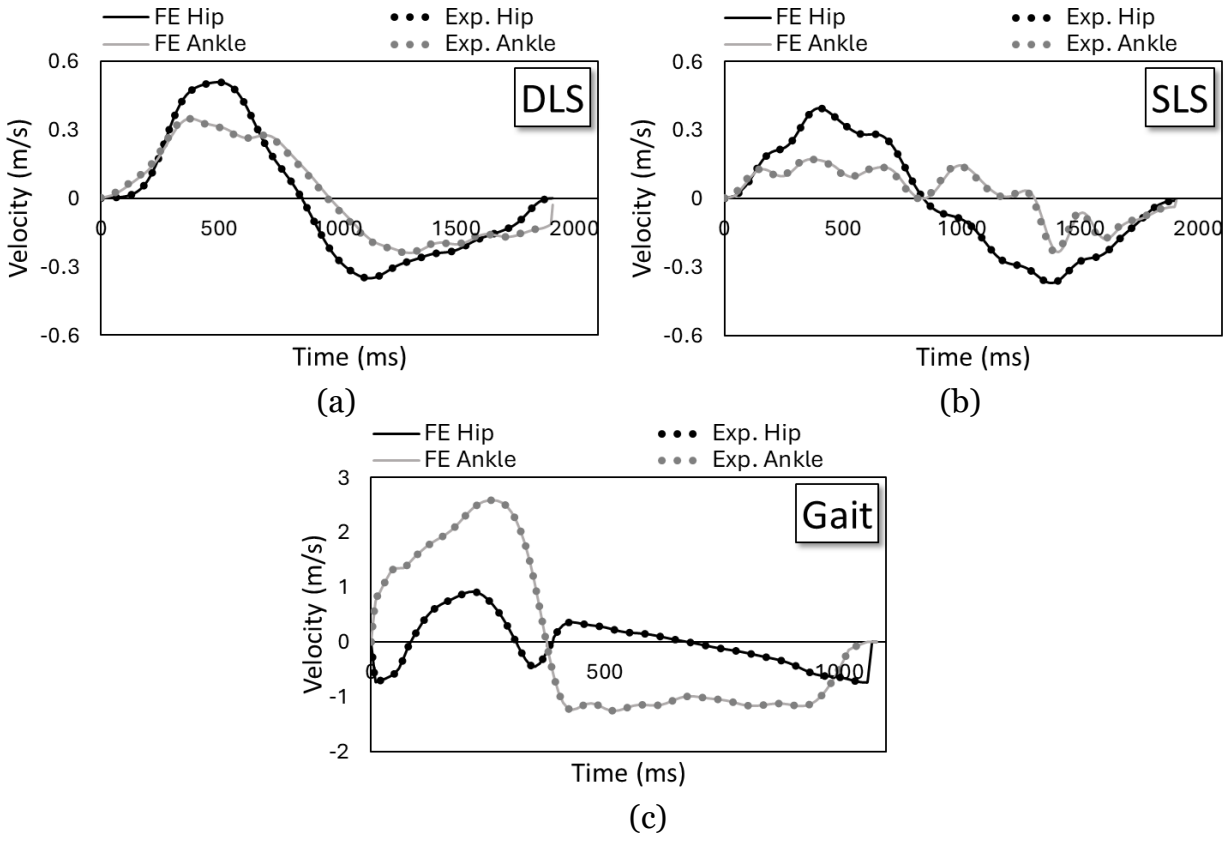


Figure 6.6: Kinematic verification of FE outputs vs. experimental (Exp.) inputs for (a) DLS; (b) SLS; and (c) Gait.

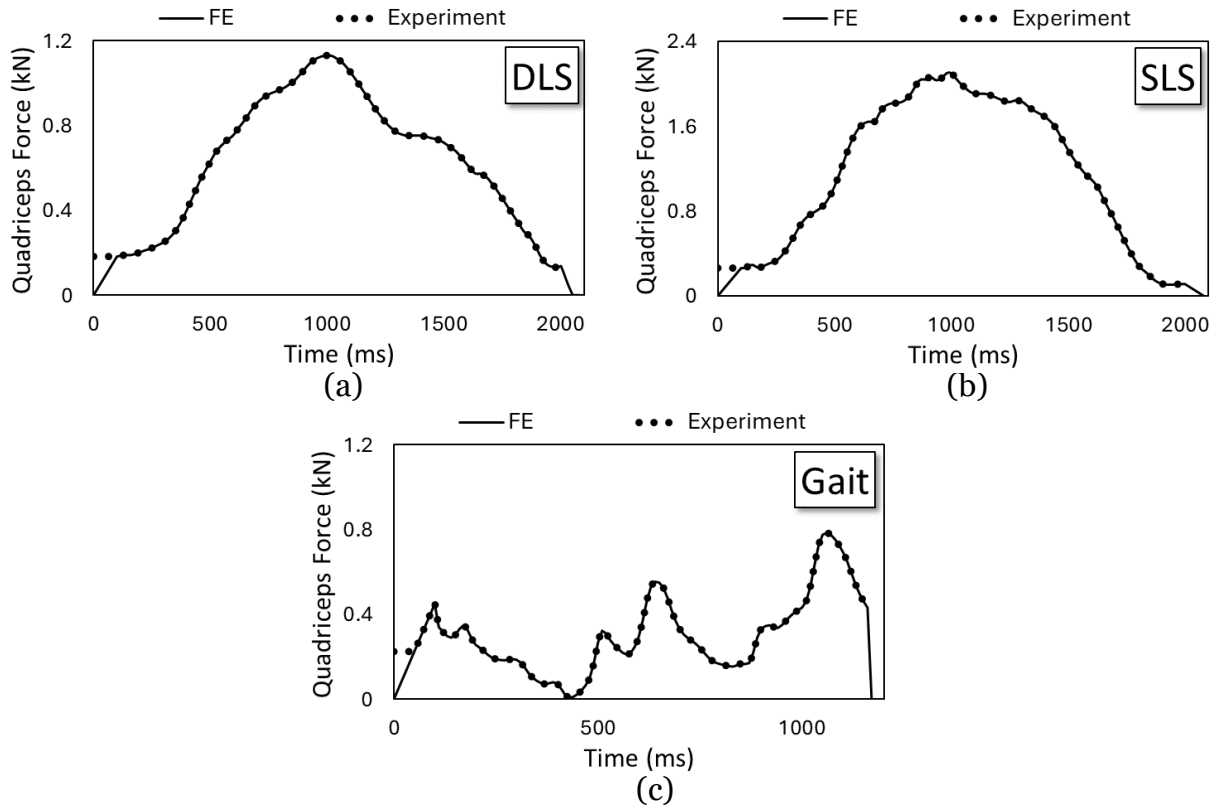

Figure 6.7: A sample kinetic verification of FE quadriceps force outputs vs. experimental inputs for (a) DLS; (b) SLS; and (c) Gait.

Knee flexion angle was not available from the experiment; however, it was available from Tomescu et al. (2018) since the kinematics were based on that study. Joint flexion angle closely resembled the previously reported OpenSim results for the DLS and SLS. The mean reference value was 47.5° (range: 3.9–82.8°) for DLS, while the model had a mean angle of 46.2° (range: 9.3–85.9°) with a CORA rating of 0.99 (Fig. 6.8a). For SLS, the reference mean was 49.8° (range: 4.6–81.3°) and the model had a mean of 51.1° (range: 4.1–86.8°) with a CORA rating of 0.97 (Fig. 6.8b). The gait simulation did not reach full extension like the OpenSim result following the toe-off stance at approximately 350 ms. The reference gait had a mean angle of 23.2° (range: 0.54–66.5°), whereas the model had a mean of 39.3° (range: 20.7–71.8°) with a CORA rating of 0.74 (Fig. 6.8c).

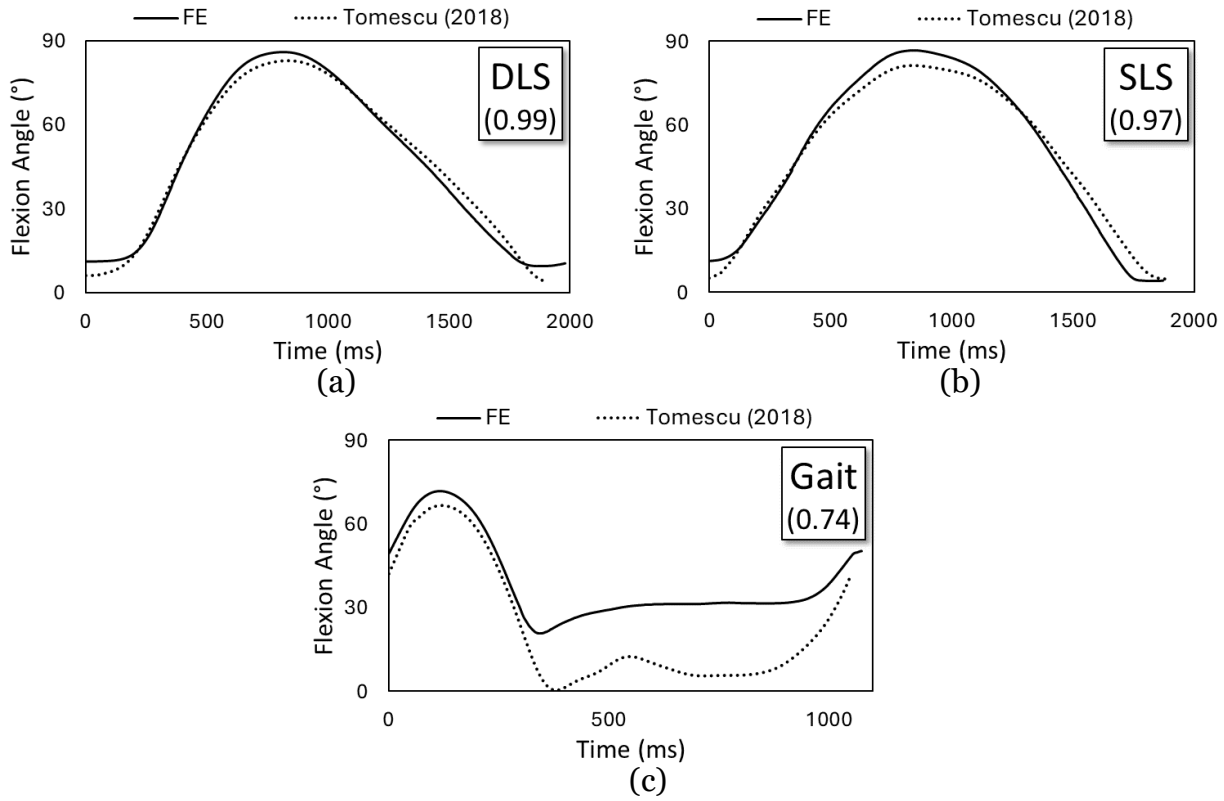


Figure 6.8: FE kinematics compared with Tomescu et al. (2018) when evaluating flexion angle for (a) DLS; (b) SLS; and (c) Gait.

### 6.4.2 *Posteromedial and Posterolateral Meniscus Strain*

Posteromedial and posterolateral meniscus strains were computed for each activity and ACL-state combination for the NB and VM simulation conditions (Fig. 6.9). The mean posteromedial meniscus strains between the NB and VM scenarios were nearly identical for gait and SLS in the ACL-intact and ACL-deficient states (Table 6.6). DLS saw a 0.2% reduction with the VM applied for both ACL states. Peak strain was higher during the DLS and SLS simulations with the VM in either ACL state and for the ACL-intact state during gait by 0.1-1.2% (Table 6.7). The ACL-deficient gait simulation had a peak strain reduction of 0.5% with the application of the VM.

Posterolateral meniscus strains were higher than posteromedial meniscus strains by approximately 7-16% (Tables 6.6–6.7). During the DLS simulations the posterolateral meniscus mean and peak strains between the NB and VM scenarios were nearly identical with differences of 0.1-0.3% (Tables 6.6–6.7). SLS strains showed similar trends,

although there was a momentary rise in the ACL-intact peak strain with the VM causing a strain difference of 1.8% compared with the NB scenario (Fig. 6.9). The ACL-intact and -deficient gait simulations demonstrated more prolonged periods of higher strain with the VM as shown by a 0.7-0.9% increase in the mean strains (Table 6.6). This increase likely reflects the intended medial unloading outcome of the VM leading to an increase in lateral compartment loads.

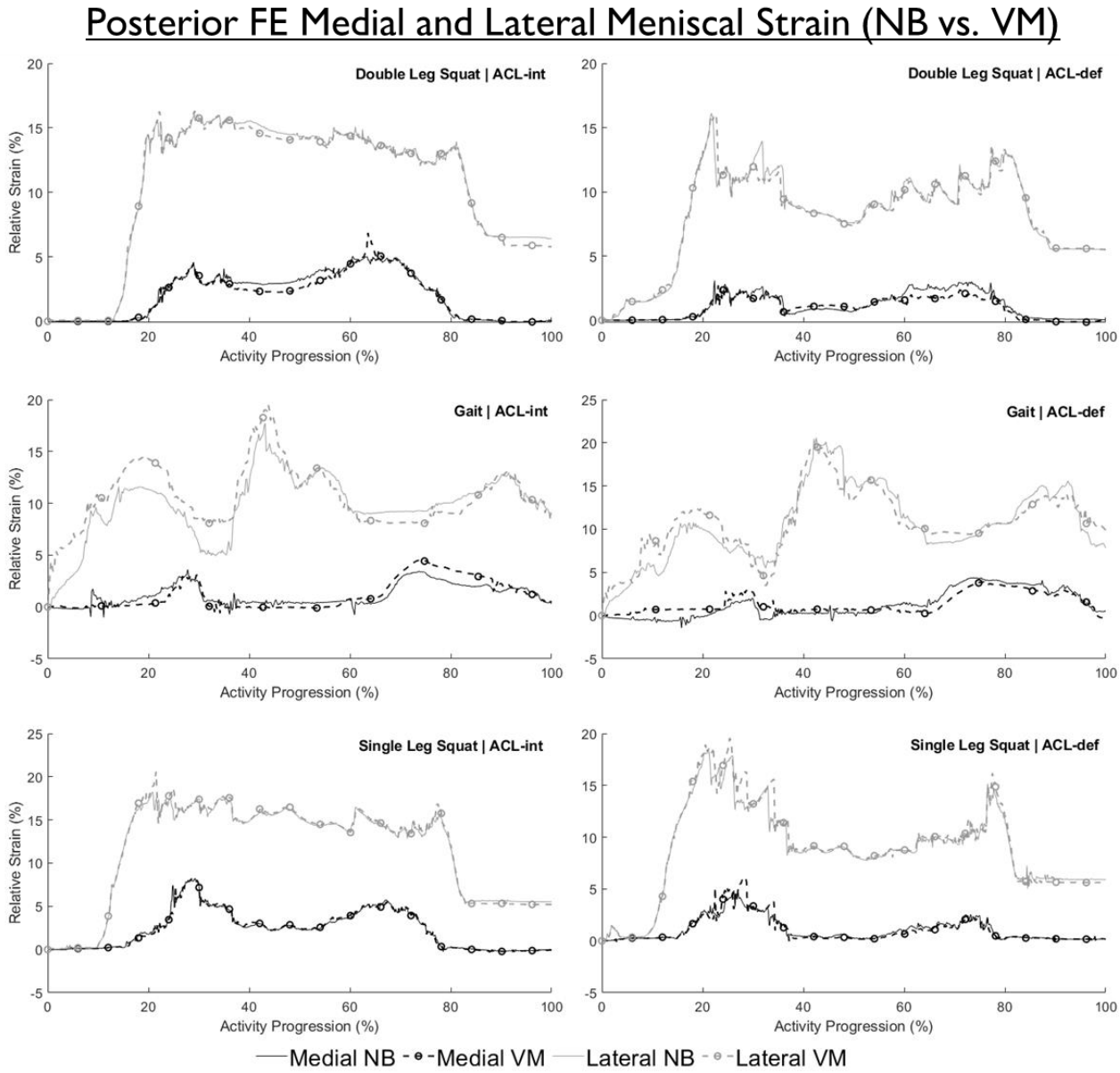


Figure 6.9: Posteromedial and posterolateral meniscus strains for the unbraced (NB) and valgus moment (VM) simulations in ACL-intact (ACL-int) and -deficient (ACL-def) states.

Table 6.6: Mean posteromedial and posterolateral meniscus strains for the unbraced (NB) and valgus moment (VM) simulations.

| | Posteromedial Meniscus Strain | | | | | | Posterolateral Meniscus Strain | | | | | |
|---|---|---|---|---|---|---|---|---|---|---|---|---|
| | Double Leg Squat | | Gait | | Single Leg Squat | | Double Leg Squat | | Gait | | Single Leg Squat | |
| | NB | VM | NB | VM | NB | VM | NB | VM | NB | VM | NB | VM |
| ACL-intact | 2.0 | 1.9 | 1.1 | 1.2 | 2.3 | 2.3 | 10.6 | 10.4 | 9.8 | 10.7 | 11.4 | 11.5 |
| ACL-deficient | 1.1 | 0.9 | 1.3 | 1.4 | 1.0 | 1.0 | 8.2 | 8.1 | 10.5 | 10.8 | 8.8 | 9.0 |

NB: Unbraced, VM: Valgus moment

Table 6.7: Peak posteromedial and posterolateral meniscus strains for the unbraced (NB) and valgus moment (VM) simulations.

| | Posteromedial Meniscus Strain | | | | | | Posterolateral Meniscus Strain | | | | | |
|---|---|---|---|---|---|---|---|---|---|---|---|---|
| | Double Leg Squat | | Gait | | Single Leg Squat | | Double Leg Squat | | Gait | | Single Leg Squat | |
| | NB | VM | NB | VM | NB | VM | NB | VM | NB | VM | NB | VM |
| ACL-intact | 5.0 | 6.9 | 3.6 | 4.6 | 8.2 | 8.3 | 16.1 | 16.3 | 17.7 | 19.5 | 18.2 | 20.6 |
| ACL-deficient | 3.1 | 2.7 | 4.4 | 3.9 | 4.9 | 6.1 | 16.1 | 16.0 | 20.6 | 20.2 | 18.3 | 19.6 |

NB: Unbraced, VM: Valgus moment

### 6.4.3 *FE and Experimental Posteromedial Meniscus Strain Comparisons*

Posterolateral meniscus strain was not measured in the experimental tests and when compared to unbraced experimental strain outcomes the FE posteromedial meniscus strains showed mixed results. Posteromedial meniscus strain-time histories (Fig. 6.10) and descriptive statistics (Table 6.8) were compared between specimen #3 and the model for all unbraced activity-ACL conditions, and a cross correlation analysis was performed to assess the similarities between the specimen and model responses. CORA ratings ranged between 0.48–0.67 for the ACL-intact comparisons and 0.51–0.60 for the ACL-deficient states (Table 6.9). The ACL-intact and -deficient FE strain outcomes had similar phase and progression trends as well as comparable peak strains during double leg squats and gait simulations compared with the experiment (Fig. 6.10). Peak strain in the model during single leg squats was greater than specimen #3 due to the absence of a

valgus-varus BC coupled with the increase in muscle forces during single leg squats. In the model there was no change in joint position when transitioning from a double to single leg stance and the increased muscle forces during single leg squats had a more profound effect in the model on the medial compartment, thus resulting in greater posteromedial meniscus strains.

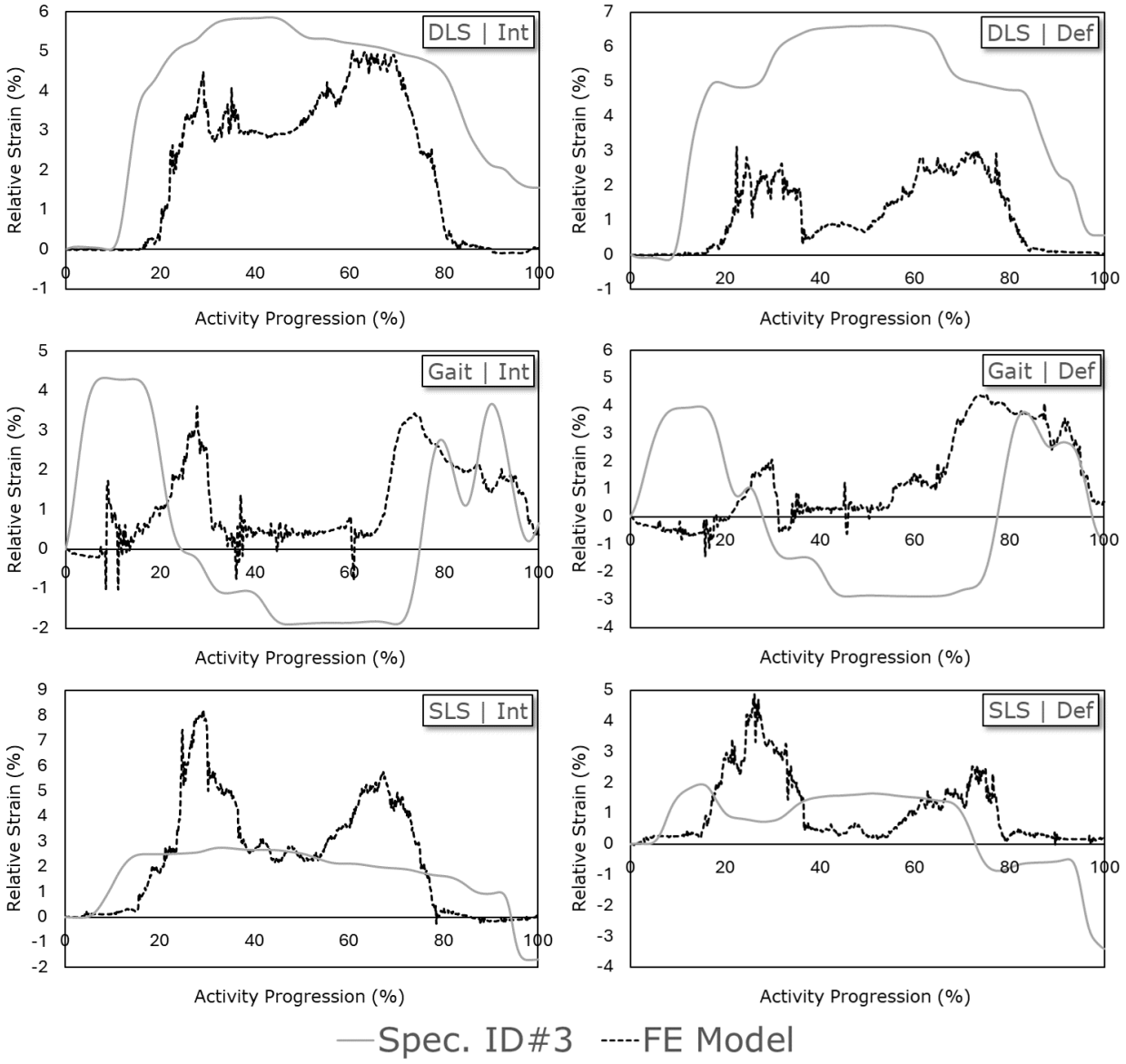


Figure 6.10: Posteromedial meniscus relative strains for the FE model and specimen #3.

Table 6.8: Mean posteromedial meniscus strains for specimen #3 and the FE model.

| | ACL-intact | | ACL-deficient | |
|---|---|---|---|---|
| ADL | Spec. #3 | Model | Spec. #3 | Model |
| Double leg squat | 4.0 | 2.0 | 4.4 | 1.1 |
| Gait | 0.50 | 1.1 | 0.01 | 1.3 |
| Single leg squat | 1.7 | 2.3 | 0.60 | 1.1 |

Table 6.9: Posteromedial meniscus strain cross correlation comparison ratings between the FE model and specimen #3.

| ADL | ACL-intact | ACL-deficient |
|---|---|---|
| Double leg squat | 0.67 | 0.51 |
| Gait | 0.48 | 0.54 |
| Single leg squat | 0.62 | 0.60 |

The experimental sample mean and peak double and single leg squat strains were higher in the model; though the FE DLS was contained within the experimental corridors, while the FE SLS strain was mostly elevated above all cadaveric trials (Fig. 6.11). For the ACL-intact state mean and peak FE DLS strains were 1.2–2.5% higher than the experimental means, whereas the FE SLS mean and peak strain results were 3.1–7.5% higher. The ACL-deficient simulations had smaller mean and peak strain differences of 0.7–1.1% during DLS and 3.1–5.7% during SLS compared to the respective experimental outcomes. Gait simulations more closely resembled the experimental outcomes with differences ranging between 0–0.4% for the mean and peak strains (Fig. 6.11). The mean (SD) of the CORA ratings were between 0.33 (0.17) to 0.44 (0.14) for each activity-ACL combination (Fig. 6.11).

The FE VM simulations were compared with both experimental braces (Figs. 6.12–6.13) and demonstrated mean differences of 0.1–0.8% and peak differences of 3.4–4.7% during DLS in the two ACL states. The FE gait simulation mean strains were 0.7–2.3% higher compared to both experimental brace outcomes with either ACL state, while the peak FE strains were 2.7–4.3% higher. SLS FE strains had the highest differences compared to the experimental strains. Mean ACL-intact and -deficient SLS strains were

3–3.7% higher and peak strains were 9.3–10.1% higher than the corresponding experimental outcomes. Finally, CORA ratings were between 0.24 (0.18) to 0.56 (0.13) when compared to the RC brace and 0.25 (0.15) to 0.41 (0.17) for the UF brace.

Overall, FE strains during gait most closely resembled the experimental gait strains followed by DLS and SLS. In addition to being highly elevated above the experimental values, the FE SLS strains were the opposite sense. Moreover, the NB mean and peak strains in the ACL-deficient state were lower for both squat simulations and higher for the gait simulation than the ACL-intact strain, which were identical trends seen in the experimental results.

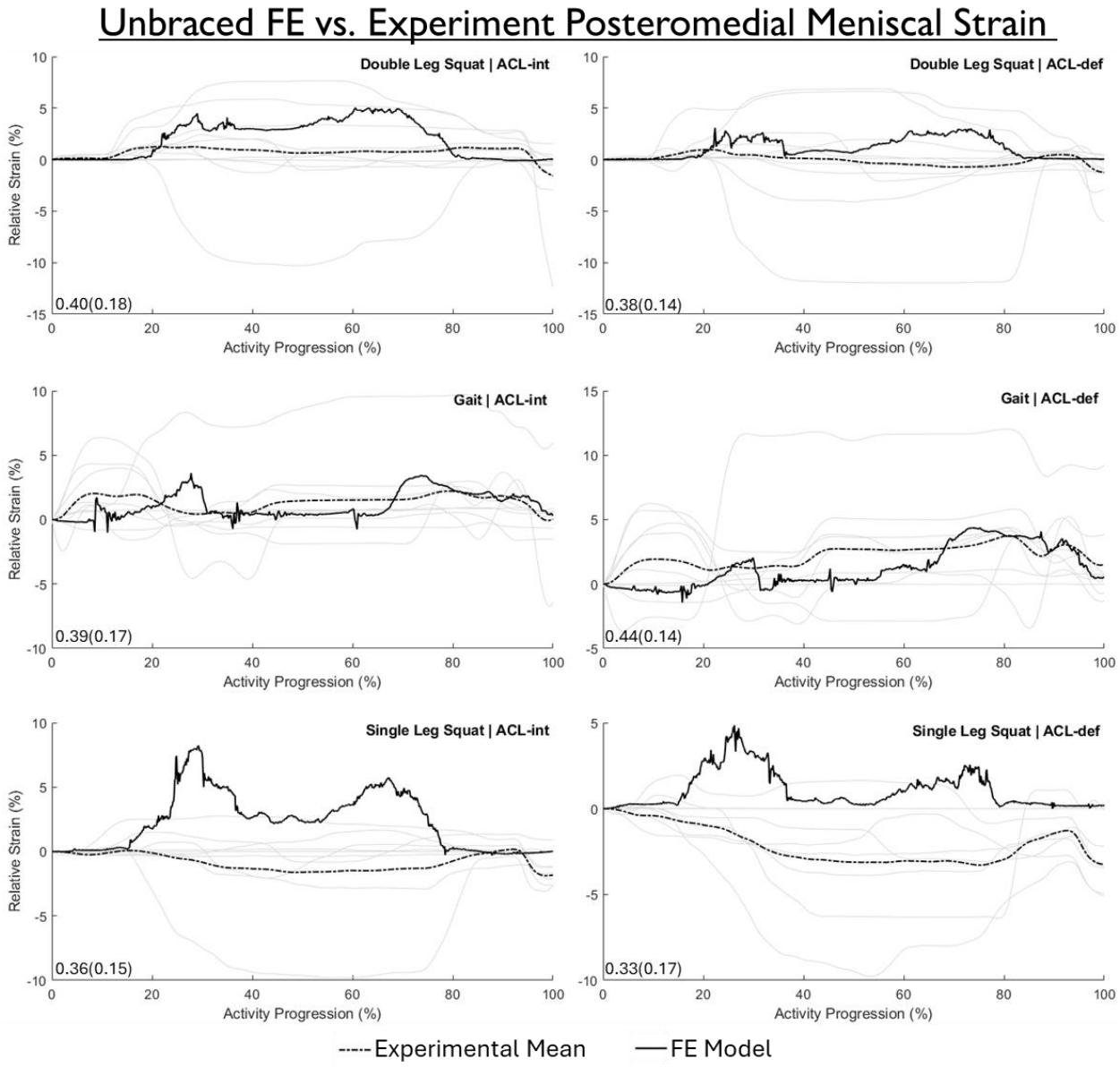


Figure 6.11: Unbraced FE posteromedial meniscus strain compared with unbraced experimental strain mean and corridors.

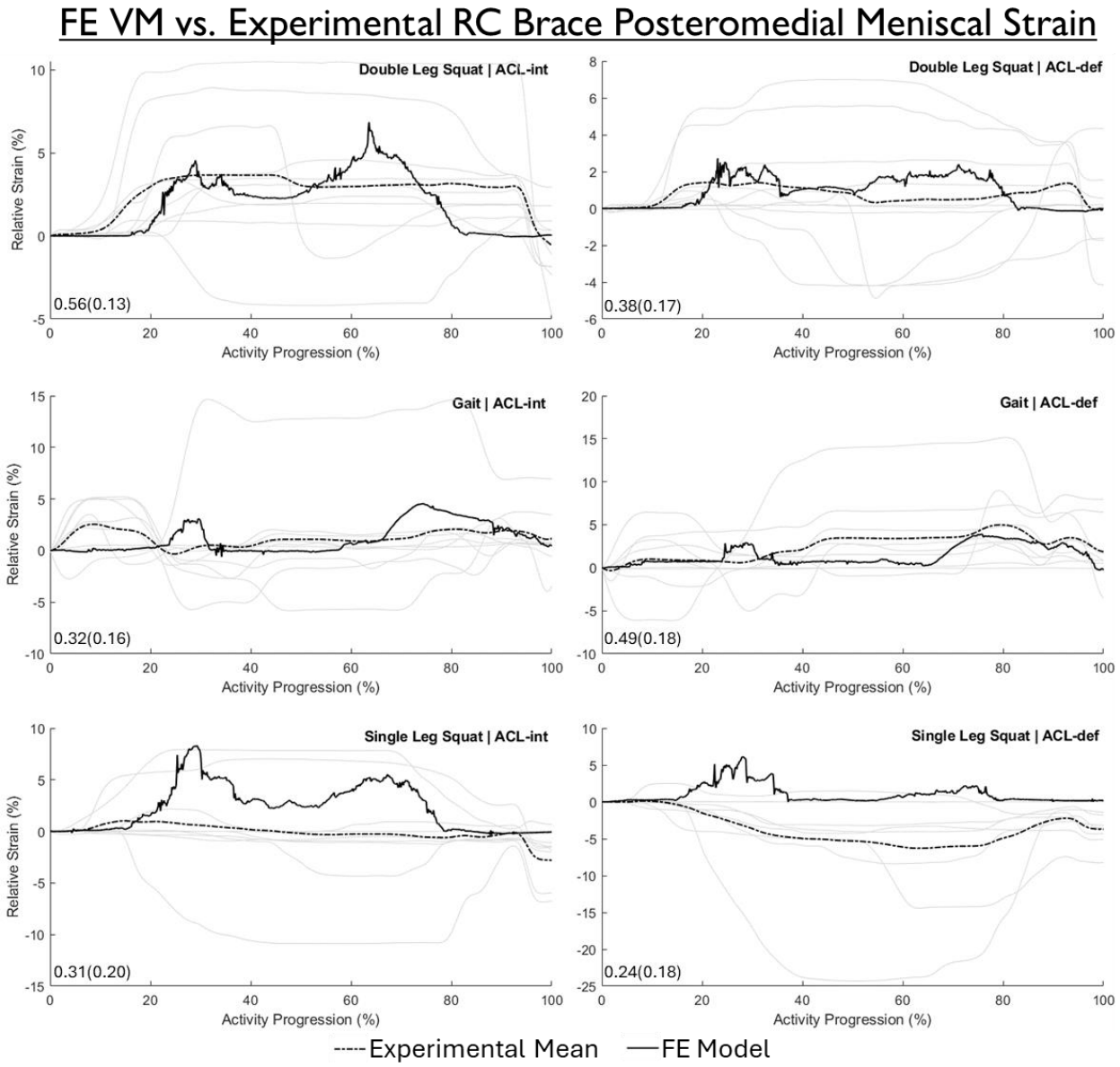


Figure 6.12: FE valgus moment (VM) posteromedial meniscus strain compared with Rebound Cartilage (RC) braced experimental strain mean and corridors.

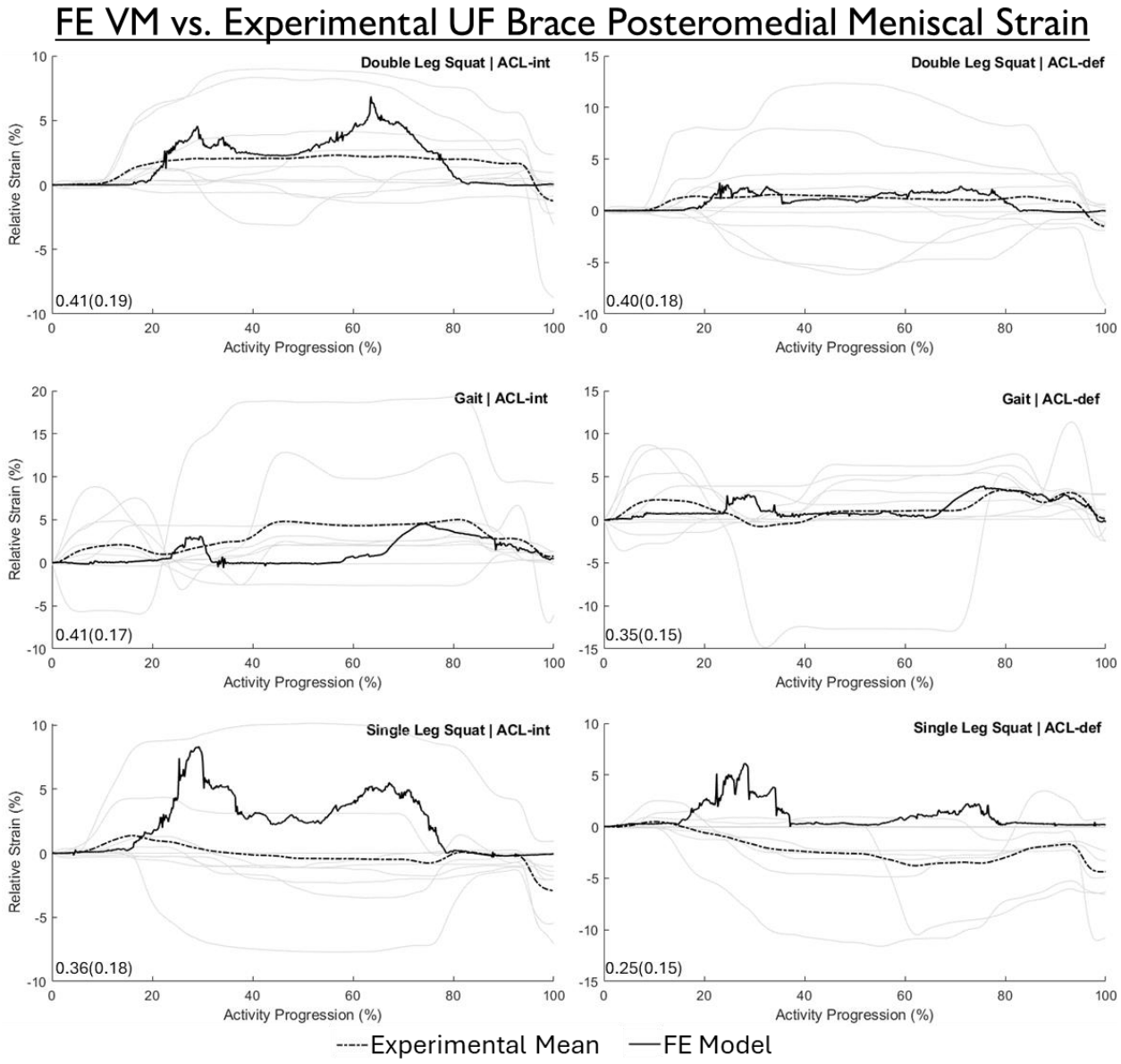


Figure 6.13: FE valgus moment (VM) posteromedial meniscus strain compared with Unloader Fit (UF) braced experimental strain mean and corridors.

### 6.4.4 *Anteromedial and Anterolateral Meniscal Strain*

Anteromedial and anterolateral meniscus strains were computed for each activity-ACL combination for the NB and VM simulation conditions (Fig. 6.14). Mean and peak anteromedial and anterolateral meniscus strains were almost equal in ACL-intact DLS simulations between the NB and VM scenarios (Tables 6.10–6.11). During SLS, mean anteromedial meniscus strain was higher in the ACL-intact VM scenario (Table 6.10),

while the remainder of the ACL-intact anteromedial and anterolateral meniscus SLS strain values were nearly identical (Table 6.11). Gait simulations demonstrated an increase in mean (Table 6.10) and peak (Table 6.11) anteromedial meniscus and anterolateral meniscus strains with the VM for the ACL-intact state; however, the anterolateral meniscus sustained a greater increase (of 1.2%) with the VM than the anteromedial meniscus (0.7%) indicating the VM had a greater relative effect on the lateral meniscus.

The ACL-deficient state resulted in more pronounced anteromedial meniscus and anterolateral meniscus mean strain differences in most of the squat simulations and all of the gait simulations (Fig. 6.14). Gait simulations resulted in an increase in mean anteromedial meniscus and anterolateral meniscus strains with the VM (Table 6.10), though the anterolateral meniscus strain increase (of 1.3%) was greater than the anteromedial meniscus strain increase (of 0.4%) (Table 6.10). The peak strain saw a decrease of 2.0% in anteromedial meniscus strain and an increase of 1.0% in anterolateral meniscus strain (Table 6.11). Gait simulations with both ACL states indicated a medial unloading effect from the VM.

Table 6.10: Mean anteromedial and anterolateral unbraced (NB) and valgus moment (VM) FE strains.

| | Anteromedial Meniscus Strain | | | | | | Anterolateral Meniscus Strain | | | | | |
|---|---|---|---|---|---|---|---|---|---|---|---|---|
| | Double Leg Squat | | Gait | | Single Leg Squat | | Double Leg Squat | | Gait | | Single Leg Squat | |
| | NB | VM | NB | VM | NB | VM | NB | VM | NB | VM | NB | VM |
| ACL-intact | 1.0 | 1.0 | 0.35 | 0.42 | 0.72 | 0.80 | 0.79 | 0.79 | 5.6 | 6.8 | 1.3 | 1.4 |
| ACL-deficient | 0.70 | 0.73 | -1.5 | -1.1 | 0.31 | 0.31 | 0.51 | 0.40 | 3.9 | 5.2 | 0.31 | 0.29 |

Table 6.11: Peak anteromedial and anterolateral unbraced (NB) and valgus moment (VM) FE strains.

| | Anteromedial Meniscus Strain | | | | | | Anterolateral Meniscus Strain | | | | | |
|---|---|---|---|---|---|---|---|---|---|---|---|---|
| | Double Leg Squat | | Gait | | Single Leg Squat | | Double Leg Squat | | Gait | | Single Leg Squat | |
| | NB | VM | NB | VM | NB | VM | NB | VM | NB | VM | NB | VM |
| ACL-intact | 2.4 | 2.5 | 8.2 | 9.7 | 1.9 | 2.0 | 4.7 | 4.7 | 11.8 | 14.7 | 10.6 | 10.6 |
| ACL-deficient | 2.4 | 2.5 | 4.5 | 2.5 | 1.8 | 1.9 | 3.2 | 2.7 | 9.3 | 10.3 | 4.1 | 3.5 |

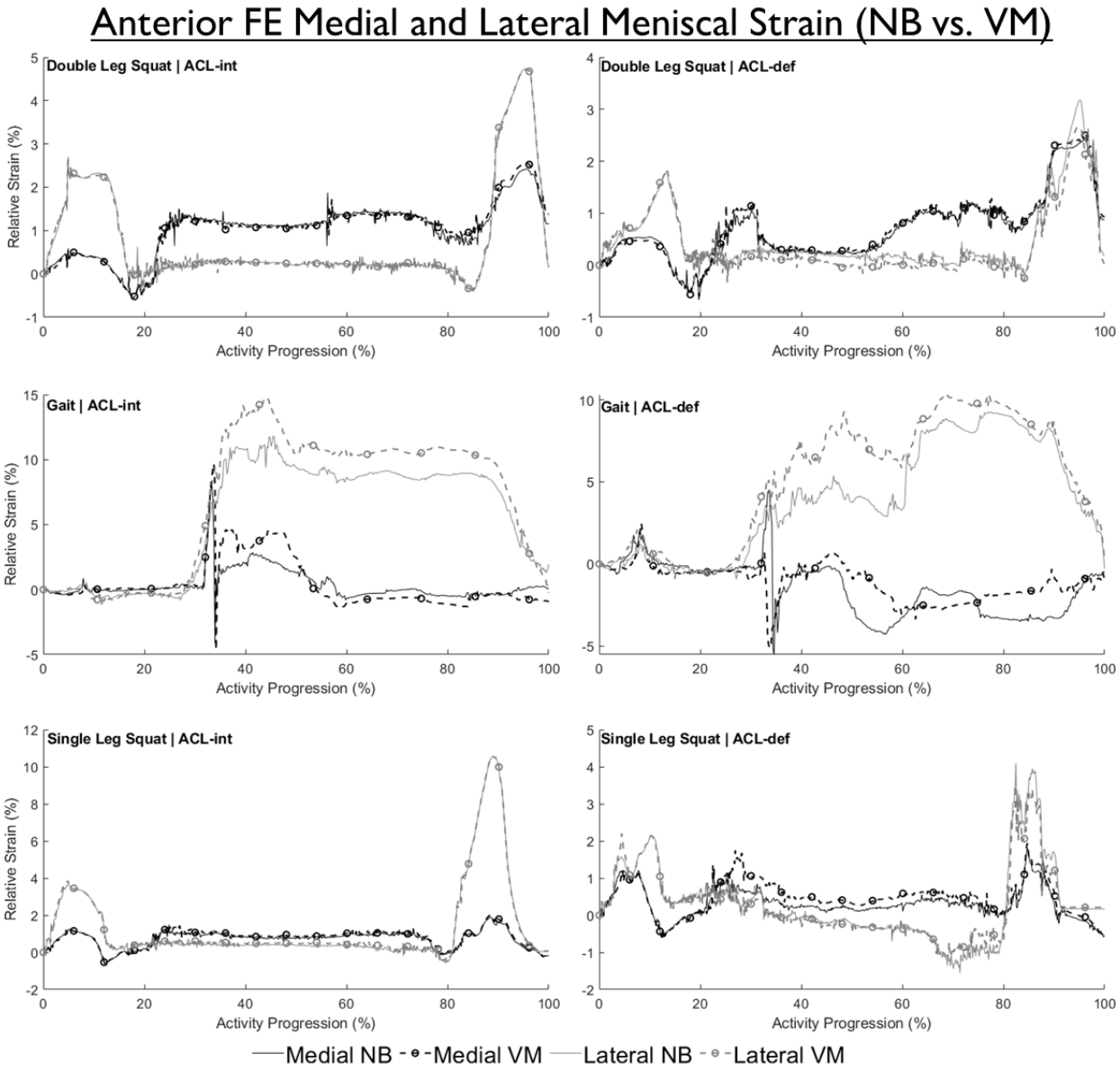


Figure 6.14: Anteromedial and anterolateral meniscal strains for the unbraced (NB) and valgus moment (VM) simulations.

### 6.4.5 *FE and Experimental Anteromedial Meniscus Strain Comparisons*

The FE anteromedial strain outcomes resembled specimen #3 during the ACL-intact state more than the ACL-deficient state (Fig. 6.15). The ACL-intact FE anteromedial meniscal strains had mean strains that were at most 0.3% different compared to specimen #3 (Table 6.12) with CORA ratings approximating 0.46–0.58 (Table 6.13), whereas the ACL-deficient simulations had mean strains that were 1.5–12%

different compared to the reference specimen with lower CORA ratings ranging from 0.36–0.43. It has been well established that an ACL deficiency results in increased anterior tibial translation, which could have been a contributing factor to the increased strains experienced by specimen #3 during both squats ADLs. The model did not have prescribed BCs that caused anterior tibial translation nor did it have kinematic BCs that reflect a participant with an ACL deficiency.

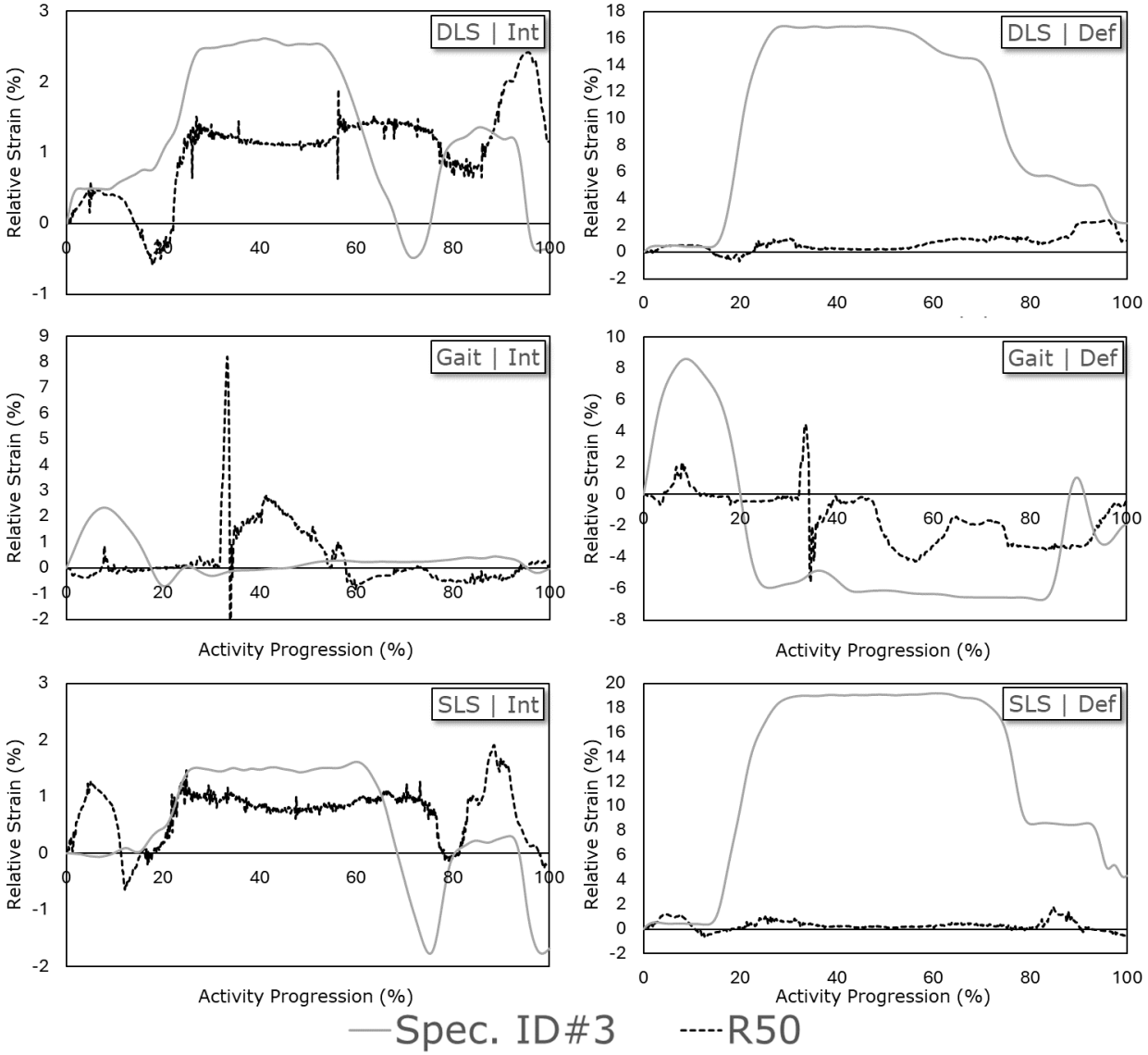


Figure 6.15: Anterolateral meniscal relative strains for the FE model and specimen #3.

Table 6.12: Mean anteromedial meniscal strains for specimen #3 and the FE model.

| | ACL-intact | | ACL-deficient | |
|---|---|---|---|---|
| ADL | Spec. #3 | Model | Spec. #3 | Model |
| Double leg squat | 1.3 | 1.0 | 10.1 | 0.70 |
| Gait | 0.3 | 0.35 | -3.0 | -1.5 |
| Single leg squat | 0.50 | 0.72 | 12.5 | 0.3 |

Table 6.13: Anteromedial meniscal strain cross correlation comparison ratings between the FE model and specimen #3.

| ADL | ACL-intact | ACL-deficient |
|---|---|---|
| Double leg squat | 0.58 | 0.36 |
| Gait | 0.46 | 0.43 |
| Single leg squat | 0.56 | 0.36 |

Anteromedial meniscal strain was collected for a subset of the experimental sample for DLS (n=6), gait (n=5), and SLS (n=5). Mean and peak anteromedial meniscus strains were higher for both squats in the model than the experiment during the ACL-intact state in the NB scenario with mean (SD) CORA ratings of 0.30 (0.17) and 0.40 (0.20) for DLS and SLS, respectively (Fig. 6.16). The FE strain during gait was closer to the experimental mean outcome and experimental corridors, with the exception of a peak in model at approximately 35% during the gait progression (Fig. 6.16). The ACL-deficient results showed lower FE strains for gait and SLS with mean(SD) CORA ratings of 0.45 (0.01) and 0.29 (0.14), respectively. FE strain during the ACL-deficient DLS demonstrated the highest correlation (CORA = 0.47) with the experimental outcomes (Fig. 6.16).

Both experimental braces exhibited similar comparisons with the FE strain outcomes (Figs. 6.17–6.18). DLS and SLS FE VM strains were higher than the experimental RC and UF brace mean outcomes in the ACL-intact state, while the remainder of FE strains were similar to experimental mean outcomes. Both knee braces also displayed similar mean correlation ratings with the model depending on the activity-ACL state combination with values between 0.29-0.47 for the RC brace and values ranging from 0.30-0.46 for the UF brace.

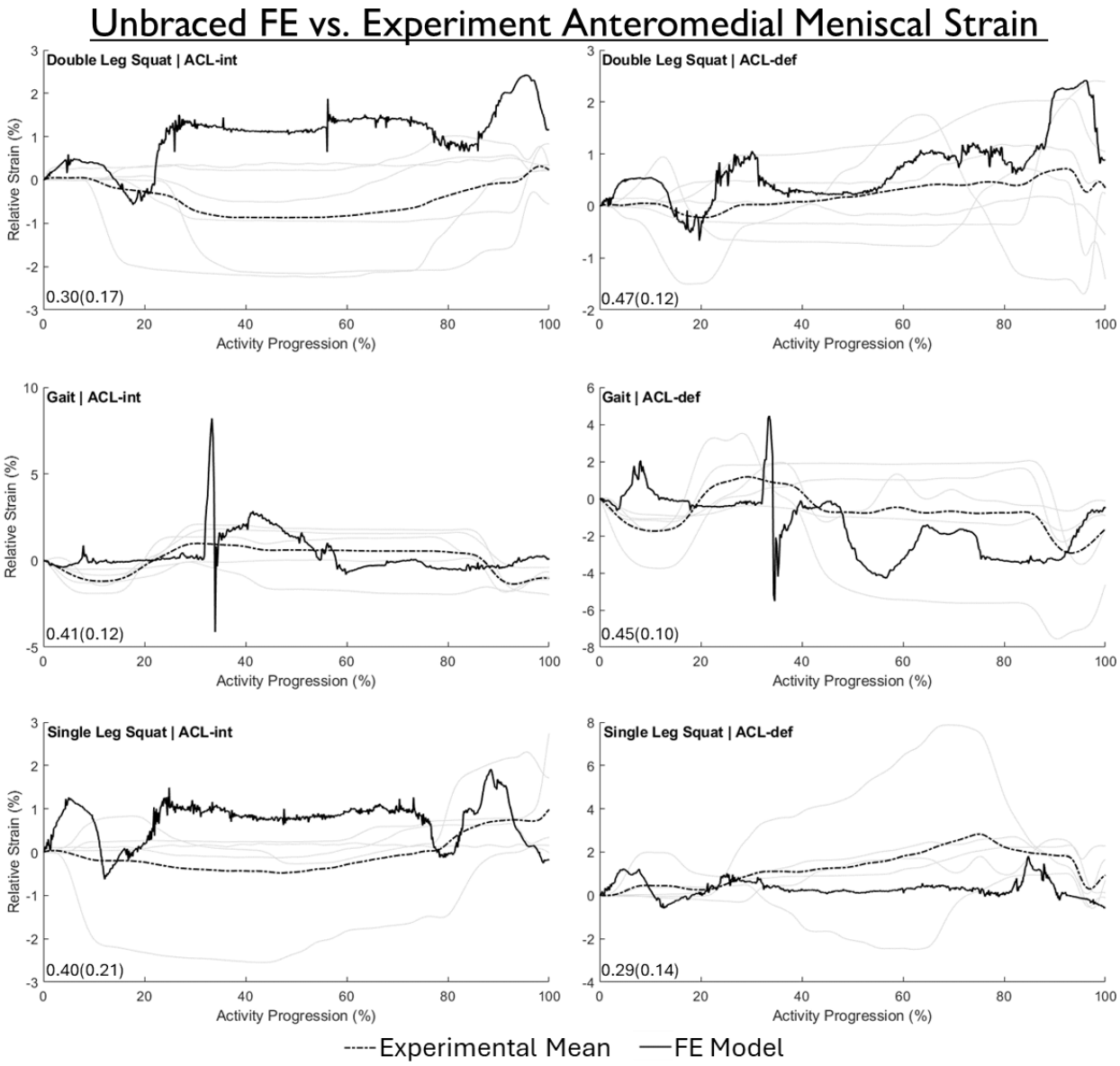


Figure 6.16: Unbraced FE anterolateral meniscus strain compared with unbraced experimental strain mean and corridors.

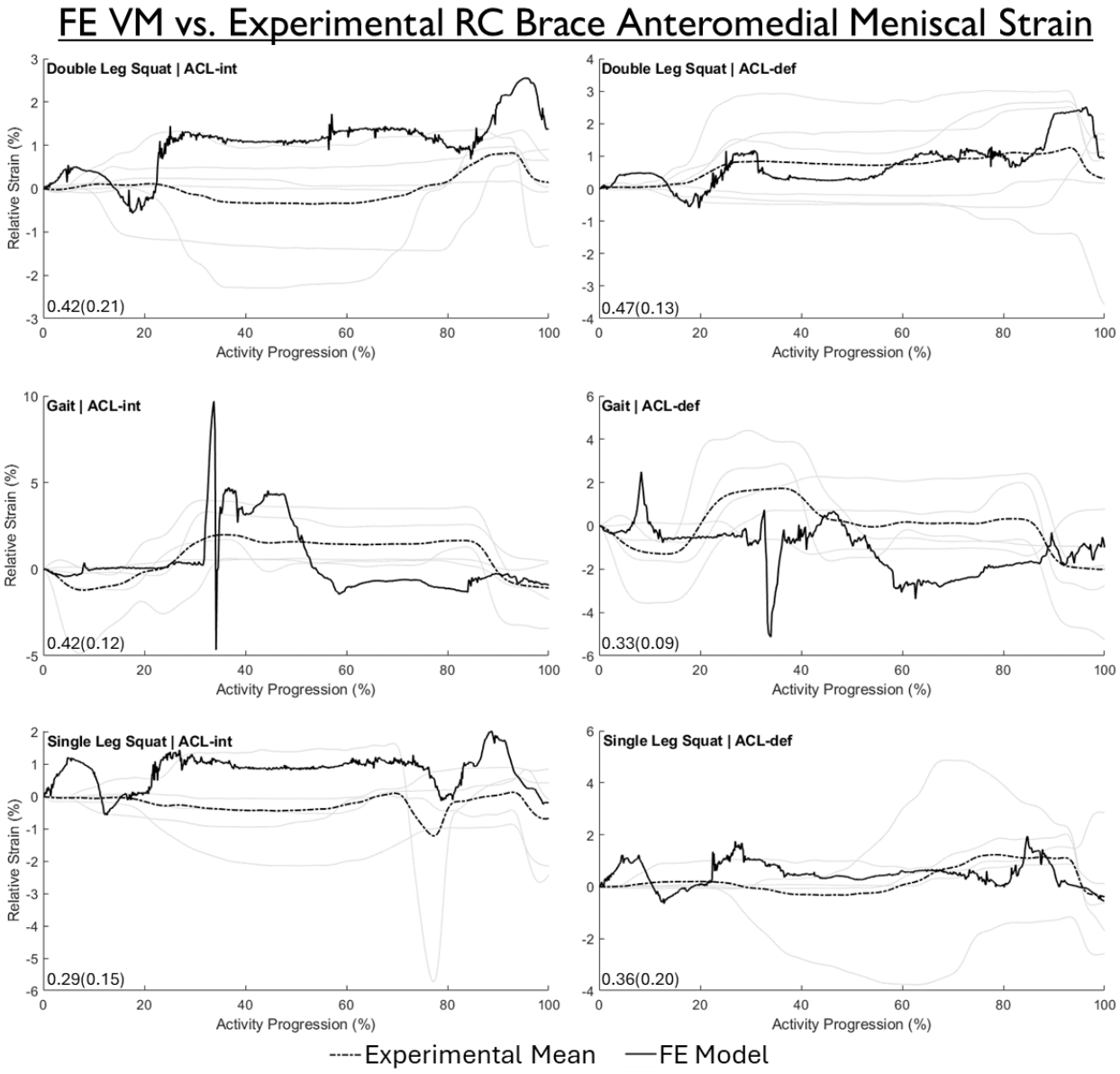


Figure 6.17: FE valgus moment (VM) anterolateral meniscus strain compared with Rebound Cartilage (RC) braced experimental strain mean and corridors.

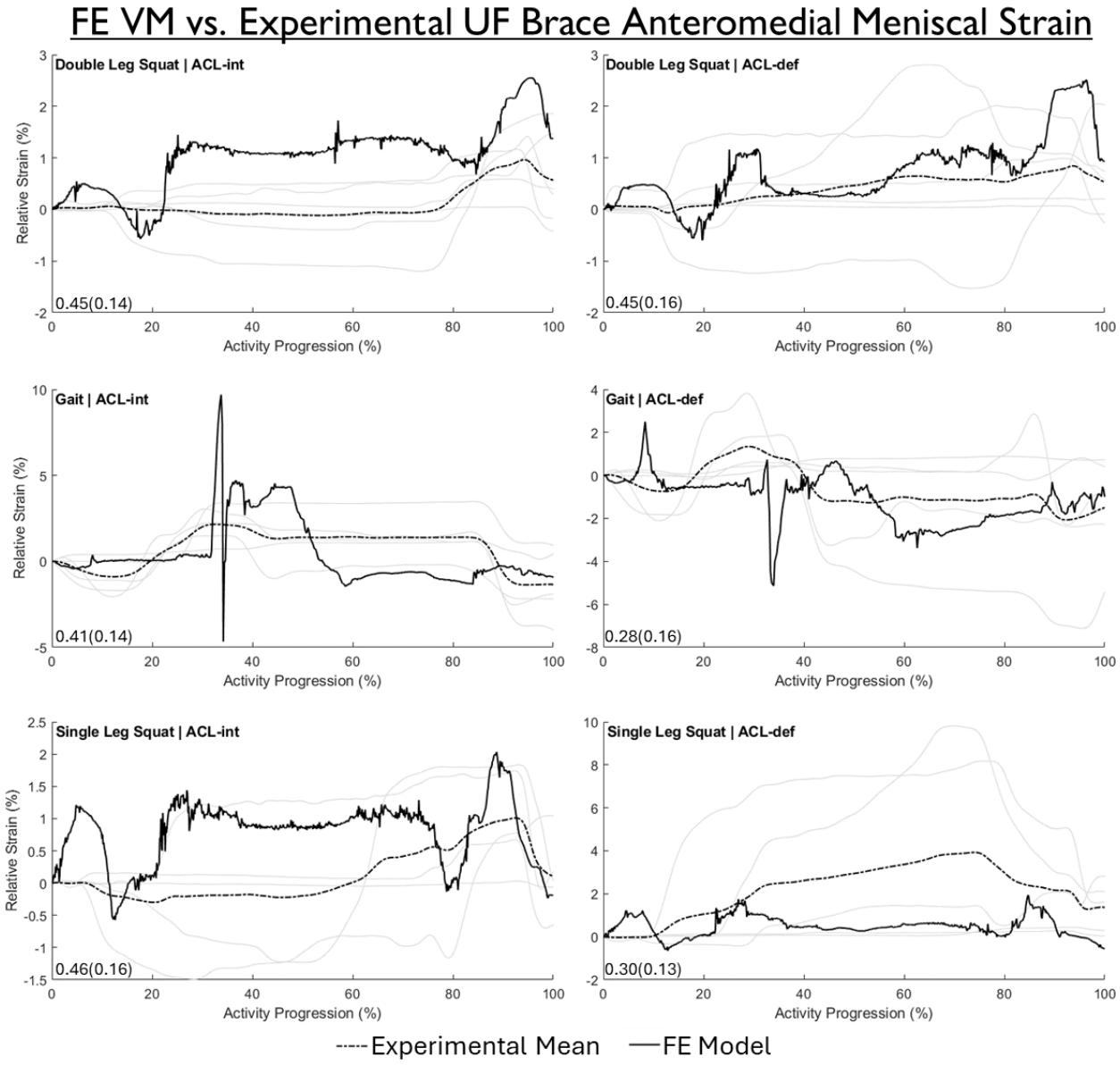


Figure 6.18: FE valgus moment (VM) anterolateral meniscus strain compared with Unloader Fit (UF) braced experimental strain mean and corridors.

### 6.4.6 *Tibial Cartilage Pressure*

Mean medial and lateral pressure outcomes revealed nearly identical results between the NB-VM simulations for DLS and SLS during the ACL-intact (Table 6.14) and ACL-deficient (Table 6.15) states. In the ACL-intact scenario the FE pressures with the VM were almost congruent with the unbraced simulations during the squat simulations and more noticeably different during gait simulations (Fig. 3). Gait resulted in decrease

medial compartment pressure during the initial 32% of the simulation and increased pressure between 48–100% of the simulation. The lateral compartment pressure was always elevated with the VM compared to the unbraced scenario (Fig. 6.19). This trend was somewhat similar in the experimental gait simulations where gait resulted in decreased medial pressure during the initial third of the gait followed by elevated medial pressures in the latter half of the activity (Fig. 5.5). The ACL-deficient state showed similar trends in gait simulations compared to the ACL-intact state as well as greater differences between the unbraced and VM during squat simulations, especially during single leg squats (Fig. 6.20). Further analysis of the ACL-deficient single leg simulations revealed that the total force on both cartilage parts differed by 1-3% and the pressure differences were due to changes in area. The ACL-deficiency coupled with greater muscle force magnitudes in single leg squats resulted in a larger force distribution that did not occur during double leg squats.

Table 6.14: FE tibiofemoral pressure for the unbraced (NB) and valgus moment (VM) simulations in the ACL-intact state.

| | DLS | | Gait | | SLS | |
|---|---|---|---|---|---|---|
| | NB | VM | NB | VM | NB | VM |
| Med. Mean P (MPa) | 1.7 | 1.7 | 0.7 | 0.7 | 2.3 | 2.3 |
| Lat. Mean P (MPa) | 2.4 | 2.4 | 1.0 | 1.2 | 2.7 | 2.6 |
| Med. Mean P (MPa) | 2.5 | 2.5 | 1.2 | 1.2 | 4.0 | 3.8 |
| Lat. Mean P (MPa) | 4.1 | 4.1 | 1.6 | 1.9 | 3.8 | 3.8 |

Med: Medial, Lat: Lateral, DLS: double leg squat; SLS: single leg squat, NB: Unbraced, VM: Valgus moment

Table 6.15: FE tibiofemoral pressure for the unbraced (NB) and valgus moment (VM) simulations in the ACL-deficient state.

| | DLS | | Gait | | SLS | |
|---|---|---|---|---|---|---|
| | NB | VM | NB | VM | NB | VM |
| Med. Mean P (MPa) | 2.0 | 1.9 | 0.8 | 0.7 | 2.8 | 3.0 |
| Lat. Mean P (MPa) | 2.4 | 2.5 | 1.1 | 1.3 | 1.7 | 2.6 |
| Med. Mean P (MPa) | 3.1 | 2.5 | 1.7 | 1.5 | 4.4 | 3.7 |
| Lat. Mean P (MPa) | 4.1 | 4.2 | 1.9 | 2.4 | 4.4 | 4.1 |

Med: Medial, Lat: Lateral, DLS: double leg squat; SLS: single leg squat, NB: Unbraced, VM: Valgus moment

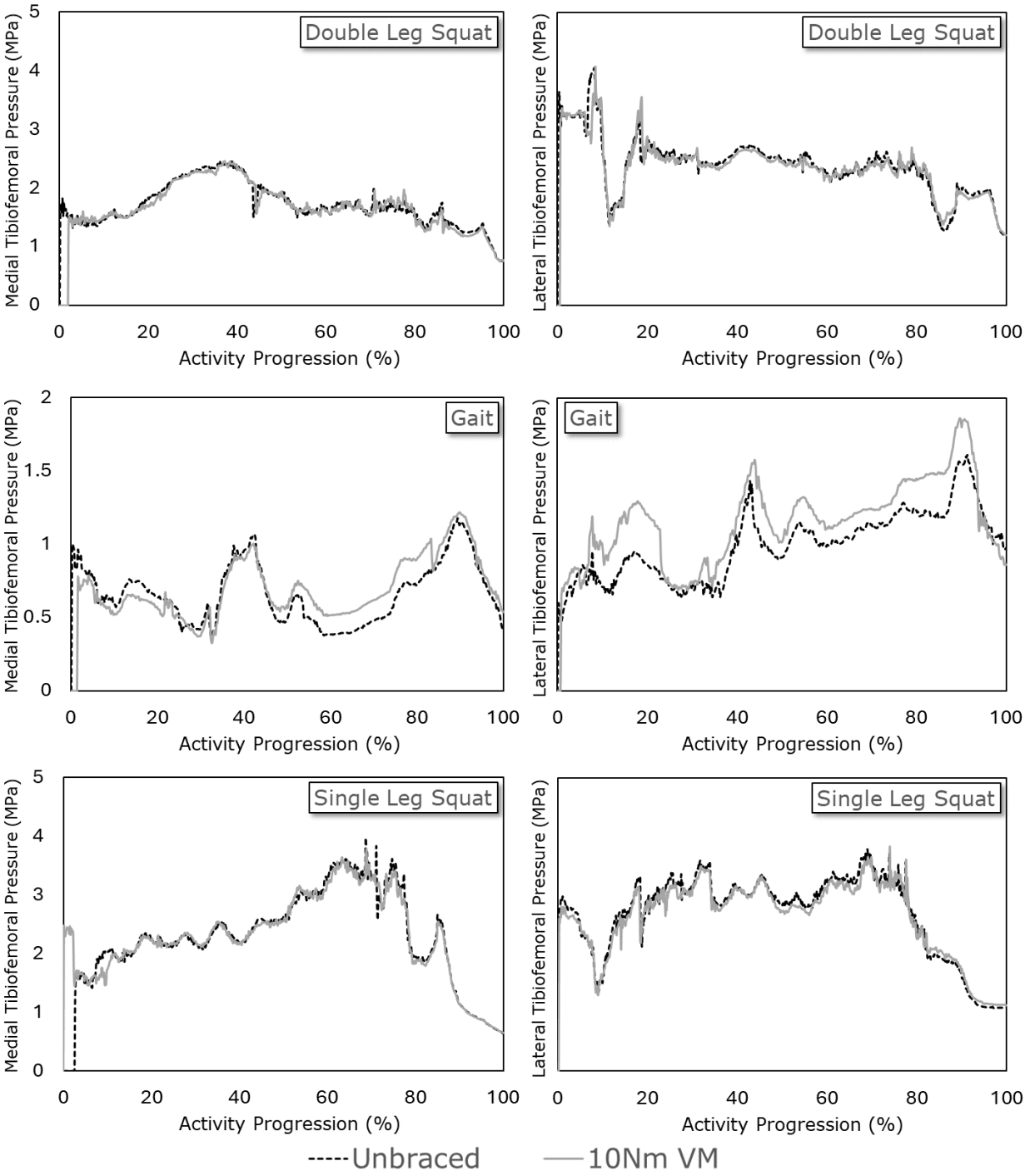


Figure 6.19: ACL-intact medial (left) and lateral (right) FE tibiofemoral joint pressures where VM is valgus moment.

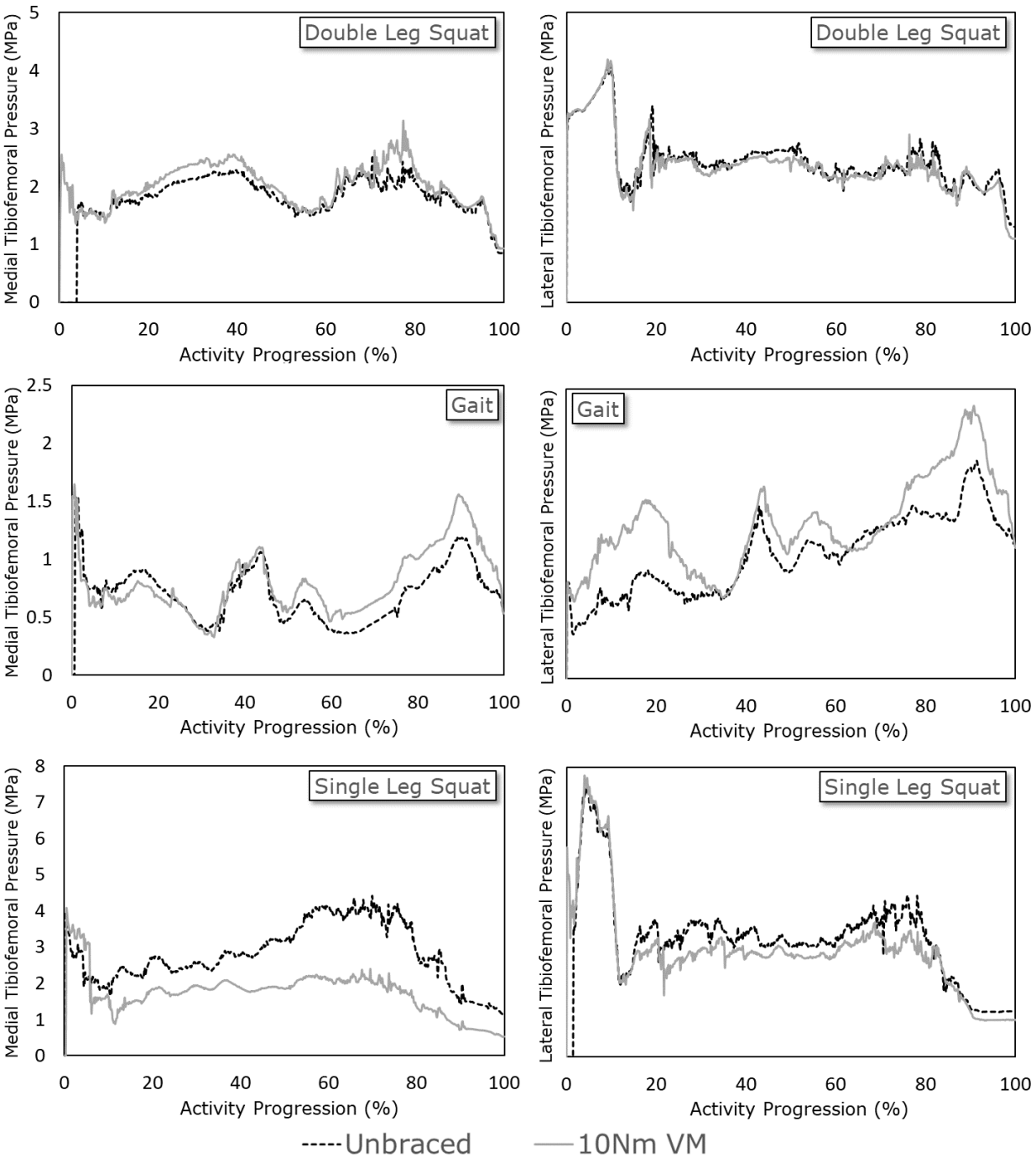


Figure 6.20: ACL-deficient medial (left) and lateral (right) FE tibiofemoral joint pressures where VM is valgus moment.

Similar to the experimental results, the relative change in medial pressure was compared between VM and NB scenarios and every ADL had mean and peak reductions in medial compartment pressure with the application of the VM (Fig. 6.21). There were

increases in the lateral mean pressures during the DLS and gait simulations in both ACL states and during SLS, ACL-deficient as evidenced by ΔP>0 (Fig. 6.22) indicating an intended valgus contact pressure shift. The VM in SLS, ACL-intact reduced medial compartment pressure, though there was a negligible decrease in mean ΔP indicating that the VM had an overall slightly unintended effect. Moreover, both ACL-intact squat activities had the least noticeable effect of the VM due to the negligible changes in mean medial pressure and contact pressure shift (i.e., ΔP) (Figs. 6.21a–6.22a). Peak pressure outcomes demonstrated an intended VM effect due to the reductions in medial pressure and lateral contact pressure shifts in every test condition (Figs. 6.21b–6.22b). The VM had a greater effect in the ACL-deficient state since there were more substantive reductions in medial pressure and greater contact pressure shifts.

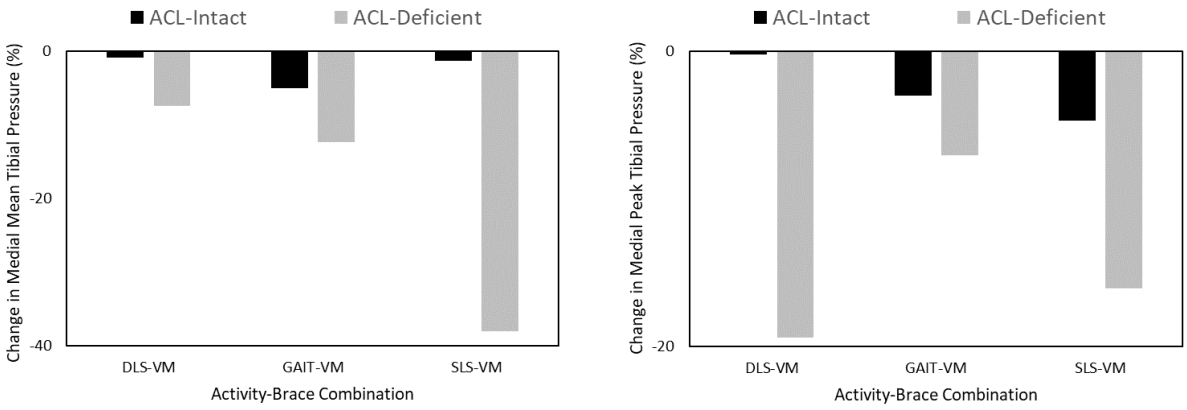


(a) (b)

Figure 6.21: Percent difference in (a) mean and (b) peak medial tibial cartilage pressure between braced and unbraced test conditions.

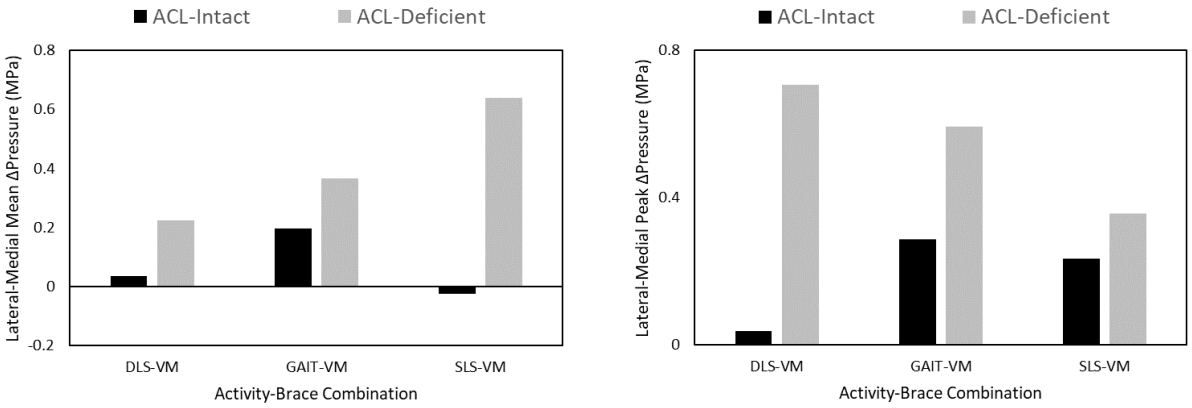


(a) (b)

Figure 6.22: Lateral and medial tibial cartilage (a) mean and (b) peak pressure differences for each activity-brace combination relative to unbraced-activity combinations.

# VII. Discussion

There is copious research that has investigated unloader braces on outcomes related to pain, comfort, quality of life, muscle activation, functional performance, gait, and posture. The nuances of this study include measuring less commonly reported outcome measures (i.e., tissue strain and pressure) with multiple unloader braces, ADLs, and ACL-states, adapting the in-vitro testing conditions to a finite element model, and assessing the model's feasibility to measure strain and pressure while simulating a braced scenario.

## 7.1 Experimental Strain and Pressure Analyses with Unloader Knee Braces

Previous studies have investigated identical (or nearly identical) off the shelf knee braces investigated in this study. The RC brace has been tested as a rehabilitative brace or preventative brace in patients with meniscectomies or OA symptoms and demonstrated clinical significance related to pain reduction and comfort (Ebert et al., 2014; Hershman et al., 2020; Thorning, 2016; Yeargan, 2021). Thorning et al. (2016) investigated biomechanical outcomes and reported no significant differences in KAM or knee flexion moment during gait while wearing the brace ($p>.05$). The UF brace has not been extensively researched; although a newer Ossür brace with a similar unloading mechanism, the Unloader One, was reported as the brace with the most published evidence amongst unloader braces (Mistry et al., 2018). The Unloader One has been investigated in sample populations with a wide range of ages, osteoarthritic symptoms, and testing conditions; the brace demonstrated varying amounts of improvements in KOOS, cartilage thickness and volume regeneration, comfort, external KAM, and media tibial compartment forces (Dessery et al., 2017a; Dessery et al., 2017b; Ebert et al., 2014; Hall et al., 2019; Hall et al., 2021; Konopka et al., 2021; Peterson et al., 2019; Ylinen et al., 2021; Yu et al., 2016). The Unloader One is more suitable for moderate to severe OA,

whereas the UF brace is recommended for mild to moderate OA. This study selected the RC and UF braces because investigating frequently researched knee braces would be more relevant to the research community, the design and support differences seemed to indicate that the RC and UF braces were the furthest from each other on the OA relief spectrum, and these differences warranted investigating two braces that are used in a wide range of patient injuries with varying degrees of OA or tibiofemoral joint symptoms.

### 7.1.1 *Posteromedial and Anteromedial Meniscus Strain Analysis*

Strain in the meniscus has been correlated to injury and the posteromedial meniscus is a common site when investigating strain due to its injury susceptibility (Allaire et al., 2008; LaPrade et al., 2014; Pearsall & Hollis, 2004). It was originally conceived that the unloading moment in the RC and UF braces would result in a posteromedial meniscal strain decrease and posterolateral meniscus strain increase. Posterolateral meniscus strain was an intended study metric, though it could not be measured due to DVRT interference with the lateral straps on both braces. Anteromedial meniscus strain was substituted as an experimental outcome measure since it has also been measured by other studies and is reported as a less frequent albeit equally complex injury site (LaPrade et al., 2014, Seitz et al., 2021).

Several of the posteromedial meniscus and anteromedial meniscus strain outcomes during braced scenarios were negative (Figs. 5.1–5.2). This study considered the zero strain reference as the initial length in each NB scenario during every activity-ACL test condition, which resulted in some braced strain outcomes commencing at nonzero values. Thus, the strain measured in the present study is relative and a negative value does not indicate tissue compression. Based on the orientation of the DVRT and radial meniscus deformation due to hoop stresses, a negative DVRT strain indicates relatively less tension compared to the reference state.

Former studies used DVRTs to obtain the true reference length in the ACL and a procedure to determine the ACL's tension-compression inflection point has been reported

(Zhang et al., 2021). Studies that used DVRTs to measure meniscus strain did not report an inflection point and considered an arbitrary zero strain reference based on a state, condition, or desired outcome based on their study objectives (Fleming et al., 2004). Determining reference lengths are a limitation of DVRTs and lengths can therefore be inconsistent between studies, for example Pearsall & Hollis (2004) used a different reference length prior to loads applied at each flexion angle, whereas Seitz et al. (2012) applied a 50 N axial load at an unreported flexion angle when considering the zero reference strain states. A similar study used the DKS to investigate brace outcomes on meniscus strain and considered the initial state in the NB scenario as the reference length (Tomescu et al., 2018). The present study opted to use the NB state as the zero strain reference since objective one was to compare brace outcomes to the NB scenario. It is not relevant to this study that the absolute zero strain is indeterminate since the braced strains would be relative to the NB strain regardless of the initial NB value.

Both unloader knee braces tested in this study significantly lowered mean and peak posteromedial meniscus strains compared to the NB scenario while the ACL was intact ($p<.05$). In the ACL-deficient state neither brace had a significant effect on posteromedial meniscus strain ($p>.05$). Furthermore, there was no significant interaction between the bracing scenario and activity ($p>.05$), which is affirmative since braces are expected to provide the same quality of treatment irrespective of the activity performed. None of the ANOVA interactions for mean and peak anteromedial meniscus strains were significant ($p>.05$), and strain with a brace was only significant ($p<.05$) for mean strain between the NB-UF combination and peak strains between the NB-RC and NB-UF combinations.

There is a pragmatic benefit with investigating brace performance during gait and double and single leg squats since they reflect typical ADLs such as ambulating, stair ascension/descension, chair sit to stand, chair stand to sit, and lifting objects (Edemekong et al., 2022; Laubenthal et al., 1972; Mündermann et al., 2008). Unloader brace performance has been widely reported during gait or squat activities (Arazpour et al., 2014; Christine et al., 2020; Choi et al., 2011; Dessery et al., 2014, Duivenvoorden et al.,

2015; Ebert et al., 2014; Goodwin et al., 2019; Haladik et al., 2014; Hall et al., 2021; McGibbon et al., 2021; Pfeiffer et al., 2019; Thorning et al., 2016; Yu et al., 2016), although, a direct comparison of the brace outcomes with this study was not possible since none of these prior studies investigated meniscus strain. When considering studies that have investigated posteromedial meniscus or anteromedial meniscus strains the state of the ACL has seen minimal investigation (Hollis & Pearsall, 2000; Seitz et al., 2021; Tomescu et al., 2018; Tomescu et al., 2020) and none of these studies incorporated unloader braces. Therefore, it is only feasible to compare NB posteromedial meniscus and anteromedial meniscus strain outcomes with prior research.

Previous studies reported ACL-intact mean posteromedial meniscus strains of -2.0–3.0% depending on the flexion angle and loading condition (Hollis & Pearsall, 2000; Pearsall & Hollis, 2004, Kolaczek et al., 2016; Tomescu et al., 2018), while mean posteromedial meniscus strain in an ACL-deficient state was between -0.92–3.5% (Hollis & Pearsall, 2000, Tomescu et al., 2018). The mean posteromedial meniscus strains during an NB state reported in the present study for the ACL-intact (-0.83–1.4%) and ACL-deficient (-2.1–2.2%) states are similar to the previous studies. Mean anteromedial meniscus strains from former studies were between 0.48–1.5% during the ACL-intact state and 0.96–2.4% during the ACL-deficient state (Hollis & Pearsall, 2000; Pearsall & Hollis, 2004, Seitz et al., 2012), which have slightly higher maximum values compared with the anteromedial meniscus strain in the present study (-0.68–0.67%). Anteromedial meniscus strain was previously measured during a squat with simulated muscle forces and resulted in a mean of 1.2% (range: 0.2–1.9%) (Seitz et al., 2021), which is higher than the mean of -0.2% during the present ACL-intact squats. The higher mean anteromedial meniscus strains reported by Seitz et al. (2021) were potentially attributed to higher axial loads and a high dynamic flexion speed of 90 °/s during squats. It is not possible to compare peak muscle forces during squats since they were not reported. The knee flexion speed was lower in the current study and the squat simulation was 0.4 s slower, which could have resulted in the lower mean strain.

### 7.1.2 *Medial and Lateral Tibiofemoral Contact Pressure Analysis*

Tibiofemoral joint pressure has been positively correlated with meniscus injury severity and clinical recommendations have been made to reduce joint pressure during meniscus rehabilitation (Cottrell et al., 2008; Lee et al., 2006). Tekscan model 4000 resistive pressure sensors have been used in previous studies to investigate tibiofemoral pressure under different meniscus health, allograft, transplant, or fixation conditions and demonstrated a reduction in joint pressure with different surgical interventions; however, there is presently a gap for experimentally measured tibiofemoral pressure under different unloader brace and/or ACL state conditions (Agneskirchner et al., 2007; Becher et al., 2008; Becker et al., 2005; Drewniak et al., 2007; Harris et al., 1999; Padalecki et al., 2014; Saeidi et al., 2021; Seitz et al., 2012; Thambyah et al., 2005, Van Thiel et al., 2011).

The mean and peak ACL-intact NB pressures measured in this study are directly comparable to previous literature (Fig. 7.1). This study measured joint pressure outcomes with different brace and ACL-state conditions; however, only joint force differences with a brace in an ACL-intact state can be compared to previous literature that has experimentally measured the load reduction capabilities of unloader or osteoarthritic braces. Anderson et al. (2003) reported nonsignificant relative medial intercondylar mean (SD) joint force ratios of 0.8 (0.3) and 0.7 (0.4) during braced double and single leg stances, respectively; and Kutzner et al. (2011) reported significant and nonsignificant mean medial force reductions of 7-10% (during gait), 6-26% (during stair ascension), and 6-17% (during stair descension) depending on the brace. The present study reported reductions in medial compartment loads for the RC brace, while the UF brace resulted in greater overall joint contact forces. The RC brace resulted in 1-13% reduced mean medial compartment force compared to the NB scenario and 18% lower to 7% higher peak medial compartment force depending on ACL-activity combination. Medial (mean and peak) compartment force with the UF brace were 3–7% greater than the NB scenarios.

Although prior research reported a reduction in medial compartment loads with unloader braces, their findings have limitations since pressure is a more commonly used outcome measure of meniscus or joint injuries (Thambyah et al., 2005). Across all ACL-activity combinations for the RC brace, the medial tibiofemoral contact forces with the brace were 3% lower compared to the NB scenarios, whereas the contact pressure was 6% lower than the NB scenario. Overall, changes in force were not as indicative of brace efficacy as changes in pressure. For example, there were certain ACL-activity combinations which resulted in negligible force differences (e.g., -2% for ACL-intact, SLS) and greater pressure differences due to the effect of the brace on contact area (e.g., -9% for ACL-intact, SLS). Moreover, the UF brace yielded increases in medial compartment forces, which would indicate an unfavourable outcome based on previous studies; However, this brace had decreases in medial compartment pressures during DLS and gait, thus indicating favourability in those activities. Similarly, the RC brace had force decreases in most test conditions, which would indicate an effective brace based on former studies; however, based on the increases in medial compartment pressure during SLS the RC brace did not unload the joint as expected. Therefore, when investigating the unloading capacity of unloader braces it is advisable to measure contact area in conjunction with force.

The minimum damage threshold for articular cartilage has been reported as approximately 18 MPa (Repo & Finlay, 1977) and mean pressure resulting in fracture was found to be 25 MPa (Haut, 1989). The peak pressures in this study were less than 4 MPa, which implies the BCs were not severe enough to cause cartilage injury. Therefore, it is difficult to assess whether the mean 0.07–0.51 MPa medial to lateral pressure shifts observed in healthy cadaveric specimens are clinically significant shifts that may occur in injured knee joints equipped with these unloader knee braces.

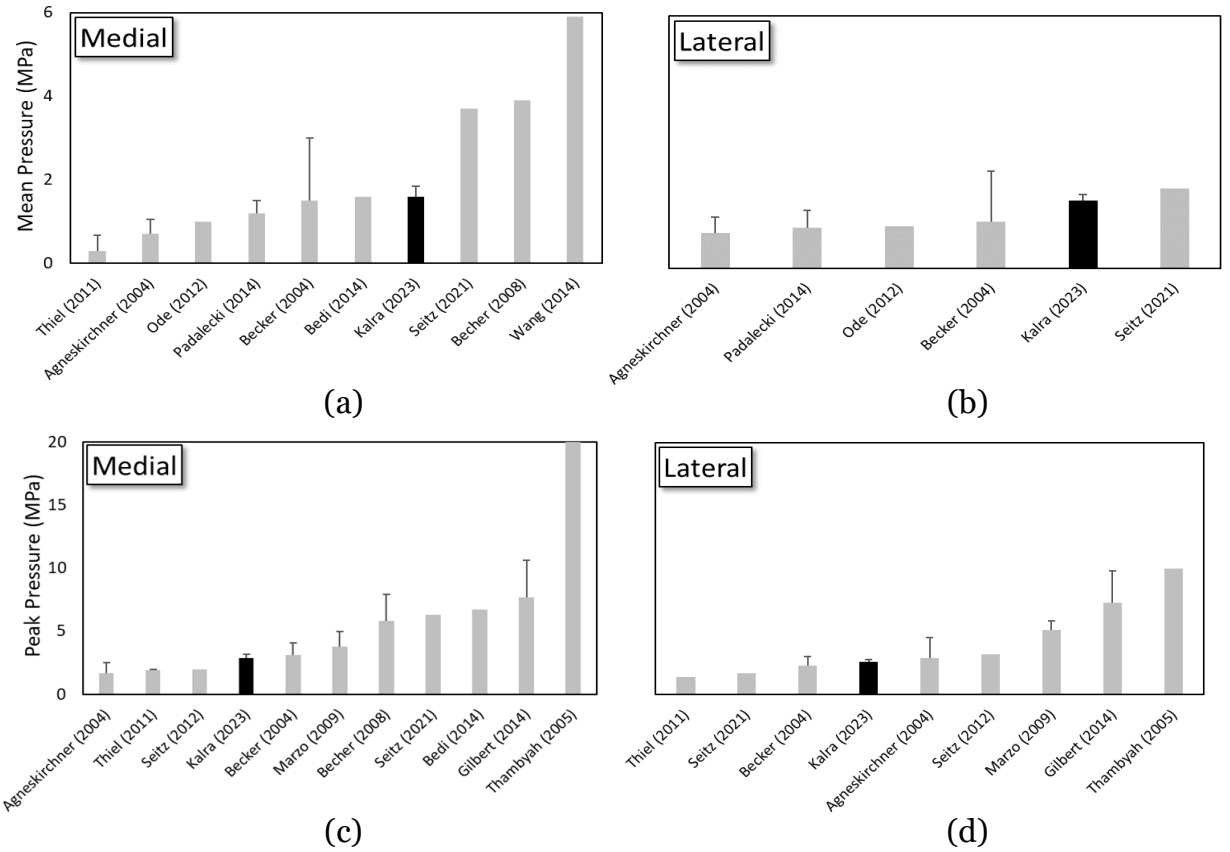


Figure 7.1: Comparison of (a) mean medial, (b) mean lateral, (c) peak medial, and (d) peak lateral pressures from this study with previous literature.

### 7.1.3 *Brace Efficacy Related to Strain, Medial Unloading, and Pressure Shift*

The strain outcomes indicated both braces had an intended effect on the posteromedial meniscus in the ACL-intact state since lower strain means less stretch in the meniscus, which is postulated to decrease the likelihood of injury. Moreover, the clinical significance of both braces being efficacious in each activity favours brace adherence rates since it would be cumbersome for patients to change a brace when transitioning between ADLs. The lack of efficacy in the ACL-deficient state shows the increased instability in the knee is perhaps too great for these braces to overcome since they were not designed to resist excessive AP translation. There is an observable reduction in anteromedial meniscus strain with the RC brace during DLS and gait and with the UF brace during each activity while the ACL is intact (Fig. 5.2), though future studies with a

larger sample size are needed to identify significant reductions. Therefore, is it only reasonable to conclude these braces can be recommended for clinical trials in patients with isolated meniscus tears based on posteromedial meniscus strain outcomes.

Both braces unloaded the medial compartment as hypothesized resulting in lower medial compartment pressures and a medial to lateral compartment pressure shift for all DLS and gait test combinations (see §5.3). In SLS, both braces increased the medial pressure while also shifting contact pressure to the lateral compartment. A reason for the elevated medial compartment pressure alongside an effective brace unloading during SLS could have been the elevated muscle forces acting upon the knee joints or the excess strap tension that were necessary to secure the braces during the SLS trials. As previously stated, there were increases in measured tibial cartilage force in some of the braced test conditions, these increases were the highest in the SLS trials. The elevated muscle forces in SLS resulted in greater medial and lateral joint compression, though the lateral compartment was compressed more than the medial compartment. Theoretically medial unloader braces would decrease medial compartment pressure and increase lateral pressure. Both braces had unintended pressure increases in both compartments; although, the larger increase in the lateral compartment indicated an intended contribution from the unloading moment in shifting the majority of the increase to the lateral compartment. It is important to reiterate the pressure increase in the medial compartment only happened in SLS and despite a medial to lateral contact pressure shift it is difficult to assert whether the braces were efficacious during SLS due to the increase in medial compartment pressure. Future studies are necessary to characterize whether the elevated muscle forces in SLS exceeded the joint unloading or brace moment thresholds to definitively determine brace efficacy in SLS.

Unloader braces have been theorized to help meniscus injuries due to their ability to unload the affected joint compartment and this study theorized an unloading characteristic would result in a strain reduction (Bhatia et al., 2014; Cavanaugh & Killian, 2012; Kovacs et al., 2002; Rao et al., 2015). This study demonstrated that this theory

depends on ACL state and may be conditional based on the activity. Posteromedial meniscus strain was reduced for every braced ACL-intact activity while the valgus moment unloaded the joint in DLS and gait. Furthermore, posteromedial meniscus strain was higher in braced ACL-deficient activities despite a noticeable medial unloading effect in DLS and gait activities. Generally, as the medial compartment was unloaded there was a decrease in posteromedial meniscus strain during the ACL-intact state with DLS and gait; and the effective brace unloading in the ACL-deficient state for DLS and gait was unable to reduce posteromedial meniscus strain. During SLS changes in strain and pressure were mutually exclusive likely due to the change in valgus-varus angulation when shifting to a single leg stance. Shifting to a single leg stance shifts the leg medially, increases the frontal plane projection angle, and can increase knee valgus resulting in a load shift to the lateral compartment (Munro et al., 2017). Since pressure was localized in the centre regions of the joint compartment and increases in pressure likely did not affect the posterior section of the meniscus tissue where strain was measured, the pressure increases during SLS had no influence on strain.

Strain outcomes caution against using the braces tested in this study during ACL-deficient states when the focus is on meniscus health, whereas pressure outcomes caution against performing single leg squats with these braces when the focus is on medial cartilage health. While posteromedial meniscus strain was lower in ACL-intact braced SLS activities, the elevated medial tibial pressures warrant further investigation to definitively determine efficacy in SLS. Overall, both braces were conditionally efficacious since they reduced posteromedial meniscus strain in each ACL-intact activity, decreased medial compartment pressure in DLS and gait, and caused a medial to lateral contact pressure shift in all activities. Future in-vivo or clinical studies can investigate joint pain or function and the pertinence of these braces or 3-point unloader braces in future clinical trials should depend on the health of the knee joint and ADLs or loading conditions.

The relationship between the unloader brace moment and meniscus strain or joint pressure is a current literature gap. This study investigated braces intended for different

injury severities that were designed to apply differing levels of unloading moments. The UF brace is advertised as the lightest functional OA brace intended to provide pain relief for mild to moderate unicompartmental OA and is ideal for normal daily activities and low to moderate intensity sports and hobbies. Whereas the RC brace is designed to provide unicompartmental load reduction during knee rehabilitation following tibial plateau fractures, cartilage damage, or meniscus repair. While the brace moment for each brace was not quantified the manufacturer indicated that the RC brace was more supportive and capable of generating a larger moment arm about the knee center, thus implying it would generate a larger brace moment. There was no difference in the posteromedial meniscus strain outcomes between the two braces during the ACL-intact state or in the anteromedial meniscus strain outcomes in either ACL state. During the ACL-deficient state the mean and peak posteromedial meniscus strains were significantly lower in the RC brace than the UF brace ($p<.05$). It is conceivable that the increased support, stability, load reduction, and brace moment capabilities of the RC brace led to a reduction in strain because the RC brace was designed for rehabilitation during the healing process rather than pain relief. The knee joint is more unstable during the ACL-deficient state and the RC brace appeared to be more capable of restoring stability, therefore the strain reduction between braces was more pronounced in the ACL-deficient state.

Interestingly the UF brace had a higher reduction in mean medial tibial pressure and contact pressure shift in both ACL states, whereas the RC brace resulted in higher peak medial pressure reductions and pressure shifts. The RC brace resulted in a greater magnitude of medial unloading as well as a greater magnitude of medial to lateral contact pressure shift than the UF brace implying that it exhibited a greater valgus moment due to its rehabilitative intent, extra strap, and added support.

### 7.1.4 *Sources of Experimental Error and Sensitivity Analysis*

A source of instrument error in this study was the effect that the simulator's positional changes had on the DVRT sensor in between activity trials. Any negligible positional change in the meniscal tissue at the end of each trial affected the initial gauge length of the DVRT, and this was an unavoidable error since manually attempting to reposition the DVRT in between trials would have caused greater damage to the tissue and produced larger strain differences in between trials. Furthermore, transecting the ACL required a fully flexed knee joint that also altered DVRT gauge lengths when transitioning from ACL-intact to -deficient trials. This operational error was again unavoidable since it was mandatory to flex the knee joint and removing the DVRT while transecting the ACL would have altered the gauge length to a greater degree than leaving the sensor attached. A source of methodological error was the absence of a baseline meniscus strain measurement pre and post the dynamic squat and gait tests. It is impossible to discern whether there was permanent tissue deformation or quantify the degree of viscoelastic effects over the course of the testing sequence. It is advisable to refine this methodology to conduct a baseline static or dynamic strain measurement prior to the first trial, following all ACL-intact trials, prior to the first ACL-deficient trial, and at the end of all trials. There were human and instrument errors associated with the measurement of tibiofemoral pressure. The pressure sensor was not synchronised the with simulator and was manually triggered well in advance to the start of each test. Thus, the pressure trials had varying durations and had to be time synchronized based on the initial presence of a noticeable increase in pressure. Finally, there was a methodological error due to the exclusion of strap tension in this study. Ideally, this study would have applied these braces to in-vivo participants and measured the strap tension in order to apply the braces to the cadaveric specimens with similar tensions. Strap tension has been shown to affect the maximum net knee moment in certain valgus configurations (Pollo et al., 2002) and would have been a feasible parameter for a sensitivity analysis in an in-vitro design. Varying strap tension and the ensuing valgus moment would have been

informative because it could provide more context regarding differences between the RC and UF braces, could be used to correlate the valgus unloading moment with strain or pressure, and could yield variable valgus moment BC for a similar sensitivity analysis in the FE model.

## 7.2 Computational Strain and Pressure Analyses with Valgus Unloading Effect

Finite element models overcome many of the experimental testing challenges when investigating human tissue responses and a selection of studies have utilized FE models to investigate meniscus strain (Aspden, 1985; Bendjaballah et al., 1995; Halonen et al., 2013; Mononen et al., 2013; Peña et al., 2005; Spilker et al., 1992; Yao et al., 2006; Zielinska et al., 2006), tibiofemoral cartilage contact pressure (Guo et al., 2009; Kiapour et al., 2014; Kwon et al., 2013; Li et al., 2001; Pena et al., 2005; Park et al., 2019; Wang et al., 2014), or unloader/osteoarthritic knee braces (Haris & Beng Chye Tan, 2021; Shriram et al., 2019; Stamenović et al., 2008; Stamenović et al., 2009). This study investigated posteromedial meniscus strain and contact pressure while simulating a valgus unloading effect during gait and squat ADLs.

While many FE studies created custom models, the right lower extremity of the 50$^{th}$ percentile male has been used to investigate a jump landing simulation using the BCs of the DKS (Polak, 2019). This former study simulated the ACL strain response of the model and reported similar peak strains and time to peak strains in comparison with experimental outcomes and previous literature. The former study enhanced the model to simulate a jump landing, however there were additional necessary enhancements to replicate gait and squat ADLs in the model from its original seated occupant position. The majority of the enhancements were done congruently with leg extension or ADL simulations in response to challenges and model performance. The targets during leg extension were based on the initial ~10° experimental flexion angles and the joint separation distance targets were relative to the original distances in the seated model. The

original minimum joint space distances were 1.9 mm and 3.0mm in the medial and lateral compartments, respectively, and a +0.5 mm threshold was established to minimize the tibiofemoral joint separation and ensure continuous contact.

### 7.2.1 *Analysing Knee Ligament Enhancements*

The model included 3D solid parts for the ACL, LCL, MCL, and PCL and this study applied a hyperelastic isotropic material model with ligament specific stress-strain curves based on ligament geometry and experimental data, which is reflective of other FE studies (Ramaniraka et al., 2005; Vairis et al., 2013; Wan et al., 2011). Ligament force-elongation curves were obtained from previous literature and converted to stress-strain curves based on the FE ligament cross-sectional areas and original lengths. Preliminary uniaxial tensile test outcomes revealed the force-elongation ligament response in the model did not match experimental inputs. Thus, the literature experimental force-elongation curves were calibrated using the ratio between FE and literature cross-sectional areas until the model output closely matched the experimental inputs. This calibration ensured the FE ligaments produced nearly identical force-elongation responses as the prior experimentally measured responses.

It was conceived that the original ligament material models were overly compliant and resulted in excessive tibiofemoral joint separate during extension simulations. Uniaxial tests determined that the ACL was more compliant than experimental studies and calibrating the ACL response to the experimental force-elongation response greatly reduced joint separation and improved leg extension performance; although it did not achieve the target flexion angle, nor did it adequately reduce the separation distance. The remaining ligament material models were enhanced in a similar fashion and while each enhancement resulted in improved performance, the outcomes did not achieve the targets and enhancements were made to the menisci.

### 7.2.2 *Analysing Meniscus Enhancements*

The majority of model enhancements were made to the menisci and menisci cartilage interactions. The menisci material model was modified from an elastic-plastic to an elastic material model. Prior studies investigating the isolated meniscus employed material models to reflect the tissue's viscoelastic, anisotropic nature; however, a linear elastic, isotropic model has been used in previous studies (Table 3.1). Moreover, it has been stated that a linear model is reasonable for strains between 2–8% and an elastic model can be utilized due to the large viscoelastic time constant of the meniscus (Haut Donahue et al., 2003; Spilker et al., 1992).

The separation of the meniscus parts from the tibial cartilage parts, the inclusion of meniscus horn attachments, and a meniscus mesh refinement were the geometric enhancements made to the surrounding knee joint structures. The shared nodes in the original model prevented independent motion between the menisci and tibial cartilage and severely restricted the joint in initial extension simulations. It was necessary to separate the menisci from the cartilage for model biofidelity, function, and performance. Enhancing the menisci-cartilage geometry and the material model resulted in a nearly extended knee joint with excessive radial translation to the menisci tissues and joint. One-dimensional springs were included to model the meniscus horns at each attachment site based on a combined horn stiffness from a separate study to address the excess radial translations (Hauch et al., 2010). Hauch et al. (2010) reported a mean meniscus horn stiffness value of 180.5 N/mm and further reported differences in horn stiffnesses depending on the attachment site (i.e., medial vs. lateral and anterior vs. posterior). This study initially implemented equal horn stiffnesses at each attachment site. Subsequent simulations of a DLS with site specific horn stiffnesses found negligible differences (i.e., <1%) on relative posteromedial meniscus strain, thus 180 N/mm was retained for all four attachment sites. It is recommended to separate the menisci from the tibial cartilage and add horn attachments in all future versions of the M50 and other GHBMC FE models for

a more biofidelic, anatomically correct geometry and applications involving an extended range of motion.

### 7.2.3 *Verification and Validation of the Experimental BCs Applied to the FE Model*

The enhancements to the ligaments and menisci yielded an acceptable flexion angle for the squat simulations, though the joint separation distances were above the target values. The singular, aggressive force or displacement BC that was initially used to extend the joint was absolved and a combination of kinetic and kinematic BCs were instituted for a more natural joint extension. A manual optimization based the mean experimental quadriceps, hamstrings, and gastrocnemius force values and the experimental hip velocity was repeated until each joint compartment achieved the target minimum flexion angle and separation distance.

A successful FE extension allowed for the calculation of muscle moment arms, which were used to obtain model specific quadriceps, hamstrings, and gastrocnemius muscle force-time histories for each ADL. Previous FE studies investigating gait or squat activities have applied kinematic BCs based on experimental measurements or former literature with differing muscle force implementation. Examples of muscle force BC implementations include a femur force in the axial direction (Guo et al., 2009; Mononen et al., 2013), resultant knee joint reaction force (Halonen et al., 2013), or individual quadriceps and hamstrings muscle force contributions (Kiapour et al., 2014). The process in this study has been extensively validated in previous studies on the DKS and it was similarly applied to the model as if it were an in-vitro specimen (Cassidy et al., 2013; Hangalur et al., 2016; Bakker et al., 2016; Tomescu et al., 2018). Measuring the FE moment arms and applying the formulations developed in these previous studies does not require experimental data. Experimental moment arms depend on the location of the muscle force cable placement, in the model they depend on the muscle force vector placement. Modifying the placements would alter the moment arm values and ensuing

muscle force computations that are based on the muscle moments taken from Tomescu et al. (2018). The experimental muscle moment arms from different cadavers resulted in different muscle force-time histories and identical muscle moments. Likewise in the model, the calculated moment arms were used to create a unique set of muscle force time-histories that resulted in identical muscle moments and rotations about the knee and hip joints. Therefore, the ligament extrusion method used to calculate FE muscle moment arms and the prior method to scale muscle moments based on moment arms provide a theoretical framework that can be used in other FE models to compute model specific muscle forces. The framework requires simulating a passive flexion and/or extension and obtaining flexion angle and nodal displacement at the muscle attachment site.

The FE global kinematics were validated using previously reported squat and gait flexion angle data (Tomescu et al., 2018). The FE DLS, SLS, and gait simulations had higher initial flexion angles than the reference data by 5.0°, 6.3°, and 7.1° respectively. The larger angles were intentionally selected to approximate the initial experimental flexion angle, which was ~5–15° greater than the reference data to avoid specimen hyperextension. The FE kinematics for DLS and SLS activities were nearly identical to the reference in-vivo data with CORA values ≥ 0.97. The congruent squat flexion outcomes were expected since knee flexion is manipulated by identical hip and ankle velocity BCs between the experiment and model, the hip velocity was the prime contributor, and the hip joint had larger displacements than the ankle joint. Effectively, the squat simulations required one BC to achieve knee flexion as opposed to two BCs during gait. The FE gait had a CORA rating of 0.74 when compared to the reference. The model closely resembled the reference data until 345 ms where the in-vivo participant reached full extension during gait at 345 ms and recorded a minimum flexion angle of 0.5°, while the model reached a minimum flexion angle of 20.7° at 380 ms. Additionally, following minimum flexion there was a local maximum at 550 ms in the in-vivo data that was less pronounced in the FE gait simulation. The differences between FE and in-vivo gait are likely due to the increase in ankle displacement, the unmodified initial geometry, or possible

differences between the in-vivo data and the experimental tests. The extension simulation conducted prior to the squat simulations resulted in slightly greater knee joint laxity that reduced penetrations and resulted in a nearly extended knee joint with a minimum flexion angle of 2.6º. The gait simulation did not have initial extension BCs to distract the joint. Another plausible reason for gait differences between the model and in-vivo data is due to the assumption that the in-vivo flexion angle is identical to the experimental flexion angle. Cadaveric flexion angle was not measured since these were taken from previously validated ADLs using the DKS (Tomescu et al., 2018). Moreover, measures were taken to protect the specimens against hyperextension or full extension on the DKS to avoid specimen damage; thus, it is possible the specimens on the DKS also did not achieve flexion angles as low as the in-vivo participant. Future experimental studies on the DKS are recommended to include goniometer measurements.

### 7.2.4 *FE vs. Experimental Posteromedial Meniscus Strain Analysis*

Initial simulations of the ADLs revealed the need for an enhancement to the menisci mesh. The original mesh element size was approximately 5 mm, which was also the approximate pin distance of the DVRT used to measure meniscus deformation. Measuring FE meniscus tissue deformations with a 5 mm element length resulted in strain calculations across a single element. Reducing the mesh element size to 2.5 mm reduced the mean and peak strains and reflected a more distributed strain outcome across the posterior regions of the menisci. Further mesh reductions resulted in minimal strain differences. The posteromedial meniscus strains in the model were contained within the experimental sample set for the DLS and gait activities, whereas the FE strains during SLS are higher than the experimental strains. It was expected that the FE strains would differ from the mean experimental sample strains since the specimens were not chosen to match the biological characteristics of the model. To overcome the biological inequality a single specimen comparison that most closely resembled the model was augmented and the FE posteromedial strain outcomes showed greater size, shape, and progression trends

and greater CORA ratings compared with specimen #3 rather than compared to the overall experimental sample means. Overall, CORA values for gait and DLS were higher than SLS (Figs. 7.2-7.4). The lower SLS CORA ratings are attributed to the elevated FE strains compared to the experiment for all brace scenarios and ACL states. These higher FE strains and consequently lower CORA ratings can be attributed to postural modifications between a double vs. single leg squat that were not captured in the model. Shifting to a single leg stance shifts the leg medially, increases the frontal plane projection angle, and can increase knee valgus resulting in a load shift to the lateral compartment (Munro et al., 2017). The increase in valgus is the plausible cause of negative strains in the experiment. In the model there was no change in valgus during SLS.

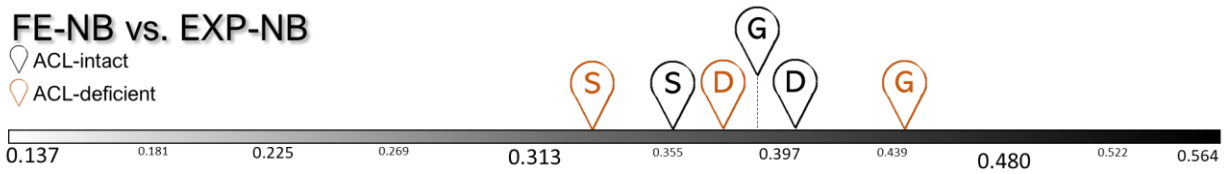

Figure 7.2: CORA ratings comparing FE-NB to experiment-NB where D: DLS, G: Gait, S: SLS.

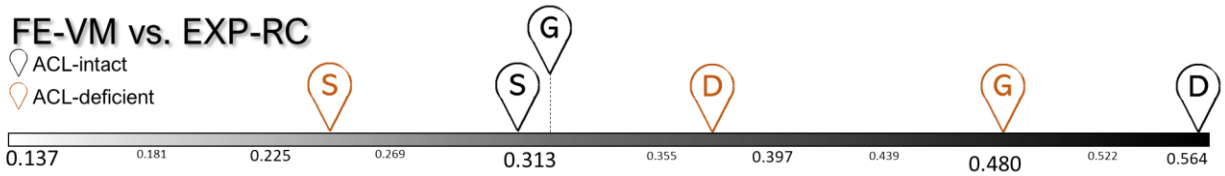

Figure 7.3: CORA ratings comparing FE-VM to experiment-RC where D: DLS, G: Gait, S: SLS.

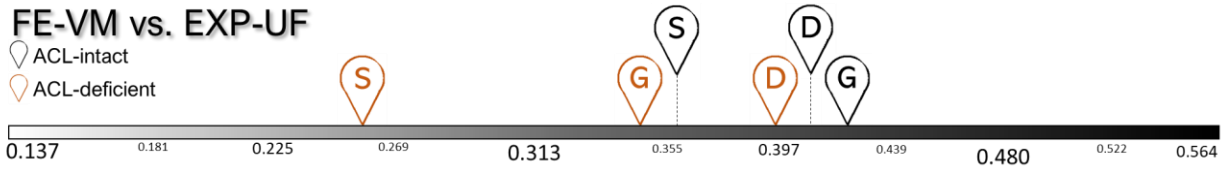

Figure 7.4: CORA ratings comparing FE-VM to experiment-UF where D: DLS, G: Gait, S: SLS.

The SLS valgus shift was captured during the in-vivo measurement and is mimicked naturally on the DKS since the unconstrained ML DOF in the ankle joint permits variable valgus-varus angulation, and the coupling effect with the SLS BCs resulted in a valgus shift which produced the lowest posteromedial meniscus strains amongst all ADL. Furthermore, the mean unbraced SLS strains are negative while the

DLS and gait strains are positive, which affirms a valgus shift during the SLS trials. Similar to the experiment, the FE ankle joint was unconstrained in AP translation, ML translation, flexion-extension, and internal-external rotation. Unlike a cadaveric knee, the model has limitless ROM when applying BCs and unperturbed parts can be nonreactive to BCs on adjacent parts. For example, initial joint positioning and muscle cable preloads in an experimental SLS occur prior to the activity; due to the knee's limited valgus-varus ROM one or both pre-activity actions can cause a ML shift in the ankle joint. In the model the initial positioning simulations and muscle force preloads did not have to adhere to anatomical valgus-varus limitations, and thus would not result in ML ankle shifts. The FE DLS and SLS simulations utilized different initial leg positions, joint kinematics, and magnitudes of muscle forces, as in the experiment. However, the model used identical knee joint angles in the coronal plane, whereas the experiment likely resulted in differences between the DLS and SLS activities due the muscle force preloads and anatomical limits of a knee joint. Essentially, in the experiments the cadaver transition to a pseudo single leg stance and SLS is a slower, more forceful version of a DLS. Whereas, in the model a SLS is a slower, more forceful version of a DLS without a medial shift in ankle position or transition to a single leg stance.

### 7.2.5 *FE vs. Experimental Tibial Cartilage Pressure Analyses*

There was a large range of differences in the pressure outcomes between the model and experiment depending on the activity-brace-ACL combination and the joint compartment. It was not expected for the two methods to produce similar pressures since the model was treated like a unique 'specimen' and model specific muscle forces were computed similar to every specimen. It was anticipated that the pressure trends between certain ADLs and VM states would resemble the experimental outcomes. In the experimental and computational methods the pressures were the lowest during gait and the highest during SLS. The experimental SLS resulted in greater mean and peak pressures compared with DLS and gait, while gait was marginally higher than DLS despite

lower muscle forces during gait. The experimental gait was likely more similar to the DLS than expected due to the muscle force cable preloads and initial loads incurred by the initial flexed position of the knee joint. The model commenced from a true zero load state and the proportional relationship between muscle force magnitude and tibiofemoral pressure was as expected.

Most simulations resulted in higher FE pressures compared to the experiment due to larger forces in the model. The mean contact areas were 376 $mm^2$ (experiment) vs. 411 $mm^2$ (model) for the medial compartment and 388 $mm^2$ (experiment) vs. 377 $mm^2$ (model) for the lateral compartment. The FE medial and lateral compartment forces had percent differences of 7-14% and 6-46%, respectively when compared to the experimental means for DLS and gait activities. Additionally, SLS in the model resulted in larger tibial force increases by 55–59% (medial) and 61–69% (lateral) compared to the experimental means. The model reported the highest tibial compartment forces in SLS and the lowest in gait, which is expected since the SLS had the highest magnitude of muscle forces. Accordingly, the FE SLS tibial pressures were the highest amongst all ADLs and gait pressures were the lowest. Additionally, mean and peak lateral cartilage pressures in the model were consistently greater than medial pressures, which was not observed in the experimental. Most of the FE simulations reported relatively higher lateral condyle force than the experiment (DLS, ACL-intact did not) leading to higher lateral pressures, which can possibly be attributed to the FE valgus-varus angulation discussed earlier.

### 7.2.6 *Validation of the ACL-deficient State*

This study simulated an ACL-deficient state similar to one of the experimental conditions. A FE study modeled an ACL-deficient state by transecting the ACL prior to MRI and model creation (Yao et al., 2006), whereas other works included the ACL in the complete model and excluded the part when simulating the deficient state, which was the approach undertaken in the present study (Ali et al., 2017; Moglo et al., 2003; Vairis et al., 2016). Removing the ACL resulted in a modified geometry that retained squat and

gait function with similar kinematic changes as reported in previous studies. A squatting action in ACL-deficient patients resulted in 3-4 mm of increased ATT and 1º greater mean internal tibial rotation (Yamaguchi et al., 2009), while gait resulted in slightly greater internal tibial rotation (by 1.2º) during 26-34% of the gait cycle, non significant differences in mean ATT, and a greater range of ATT amongst participants (Shabani et al., 2015). Relative to the ACL-intact simulations, the ACL-deficient FE outcomes demonstrated 2.0 mm more ATT with 1.0º higher internal tibial rotation during the squat simulations and no ATT with 1.4º of increased internal tibial rotation during the initial 40% of gait. The i) increased ATT during squats, ii) absence of ATT during gait, iii) identical internal tibial rotations during squats, and iv) almost identical tibial rotation during similar period of the gait cycle are affirmative model responses of an ACL deficiency. Furthermore, mean and peak strains decreased during the squat simulations and increased during gait simulations when the ACL was deficient in the experiment and the model. The magnitude of change was also similar between the experiment and model for each ADL, though mean strain differences were more similar than peak strain (Table 7.1). Thus, removing the ACL resulted in identical behaviour and similar overall strain differences between the experimental and computational approaches. It has been previously reported that an ACL deficiency can cause 3-4 times greater ATT compared with healthy individuals, though the loading conditions were dissimilar to squats or gait (Beynnon et al., 2002; Torzilli et al., 1994). The BCs in this study resulted in similar ACL-deficient outcomes compared with previous works, future studies are necessary to investigate additional loading conditions in an ACL-deficient state on joint stability, function, and performance in the model.

Table 7.1: Differences in posteromedial meniscus strain (%) between ACL-deficient and ACL-intact states where (-) implies a decrease.

| | Mean Strain (%) | | Peak Strain (%) | |
|---|---|---|---|---|
| | Experiment | Model | Experiment | Model |
| DLS | -0.8 | -0.9 | -0.2 | -1.9 |
| Gait | 0.8 | 0.2 | 1.3 | 0.8 |
| SLS | -1.3 | -1.3 | -0.5 | -3.3 |

### 7.2.7 *Validation of the Valgus Moment Effect*

Posterolateral meniscus strain in the model was higher than posteromedial meniscus strain which is not reflective of previous cadaveric studies (Hollis et al., 2000; Seitz et al., 2012). These studies applied an axial load to cadaveric specimens at static flexion angles and measured medial and lateral meniscus strains. One in-vitro study reported that the medial and lateral tibial plateaus each experience peak contact stresses during different stances of gait (Wang et al., 2014). FE studies have reported higher pressure in the medial (Mohamed Nor & Osman, 2012) or lateral (Haut Donahue et al., 2003) tibial condyles depending on the loading scenario and model formulation. It is plausible that if lateral tibial pressure is higher than medial pressure in some situations, then posterolateral meniscus strain could also be higher than posteromedial meniscus strain especially since the lateral meniscus encompasses a greater area of the total lateral plateau than the medial. The model experienced greater lateral contact pressures, thus the higher posterolateral meniscus strains were as expected. Experimentally measured posterolateral meniscus strain responses during ADL remains a literature gap, and this study utilized FE posterolateral meniscus strains as a relative comparator between NB and VM simulation conditions.

The VM was applied to simulate the effect of a medial unloader brace by applying equal magnitude, opposite direction moments to the distal femur and distal tibial according to Self et al. (2000). The VM stressed the lateral tibiofemoral condyle leading to an unloading effect in the medial tibiofemoral condyle as expected (Fig. 6.4). In many simulations posterolateral meniscus strain increased with the VM while posteromedial meniscus strain did not change. This trend was not theorized, though it does not indicate an absence of the VM effect because the increase in posterolateral meniscus strain indicates (i) that the VM performed the intended medial to lateral load shift, and (ii) that the model is responsive to a VM implementation.

The implementation of the VM in the present study is similar to past FE analyses of an osteoarthritic brace by Stamenović et al. (2008, 2009). These studies modeled a

brace using three parts composed of shell elements consisting of a sock, strap, and inflatable bladders. Importantly, these former studies applied pressure over a surface, which is analogous to the distributed moment applied over a series of nodes in the present study.

This method differs from other studies that measured different in-vivo BCs for unbraced and braced scenarios (Shriram et al., 2017), or modeled a knee-brace structure using aluminum linkages, hinges, and springs (Haris et al., 2021). There are advantages to simulating braced and unbraced BCs since unloader knee braces have been shown to affect kinematics and muscle co-contraction ratios during certain gait stances (Arazpour et al., 2014; Fantini Pagani, 2013). The present study utilized experimental BCs from a previous study that investigated squat and gait activities in an unbraced participant and chose to apply these BCs to the VM simulations to isolate the effect of the VM. Moreover, the chosen methodology allows future research to conveniently modify the VM magnitude, loading curve, or application; whereas a braced in-vivo approach would require acquiring new data to simulate alternate brace scenarios. There are advantages in modeling a knee brace to simulate the kinematic influence of the brace. The study by Haris et al. (2021) investigated the effects of strap tension, pre-tension, and torsion springs using a modeled unloader brace under axial loading at static flexion angles. The study reported decreases in tibiofemoral contact pressure and von Mises stress on the cartilage and menisci at certain flexion angles with the brace, though it did not simulate ADLs. Thus, it remains unclear how a modeled unloader brace will perform under a multitude of high-rate dynamic BCs and is a consideration for future work.

### 7.2.8 *The VM Effect Related to Strain, Medial Unloading, and Pressure Shift*

The VM produced similar posteromedial meniscus strains and higher posterolateral meniscus strains compared to the NB simulations in the ACL-intact state. Posteromedial meniscus strain was at most 0.1% different for the VM simulations compared to the NB simulations. The posterolateral meniscus strain differences between

NB vs. VM were more apparent for gait than the DLS and SLS activities (Fig. 6.9). The mean posterolateral meniscus strain was at most 0.2% higher between the NB and VM scenarios for both squat ADLs and up to 0.9% higher during gait. Peak posterolateral meniscus strain demonstrated higher strain outcomes during all three activities by up to 2.4% with the VM. The increase in VM posterolateral meniscus strain reflects higher loading on the lateral tibiofemoral compartment, which is indicative of an effective valgus unloading outcome. The extended position of the model for the squat simulations is a plausible cause of lower mean strain differences with the VM scenario because extending the joint resulted in a subtle amount of greater joint separation. During the ACL-deficient state the VM was similar to the NB scenario for posteromedial meniscus strain and resulted in lower posterolateral meniscus strain for the majority of simulations, which is indicative of an ineffective valgus unload. Interestingly, both knee braces were also efficacious during the ACL-intact state and inefficacious during the ACL-deficient state based on posteromedial meniscus strains measured experimentally.

The VM showed comparable trends in the anteromedial meniscus and anterolateral meniscus strains to their respective posterior regions for both ACL states. The VM had a greater impact on mean and peak anterior strains during the gait simulations than the squat simulations. Both squat simulations indicated strain differences of at most 0.1% between the NB and VM simulations, while gait consistently increased anterolateral meniscus mean and peak strains during both ACL states by up to 1.2% and 2.9%, respectively, once again indicating a lateral load shift due to the VM.

As previously stated, a medial or valgus unloader mechanism should theoretically unload the medial compartment and cause a medial to lateral pressure shift, or alternatively the lateral pressure should be greater than the medial pressure. In each of the ADLs there was a reduction in the medial compartment pressure with the VM, which was observed in the experimental DLS and gait. The FE SLS simulations did not experience greater levels of joint compression with the VM in the same manner as the specimens did with the braces and the SLS activities in the model reflected medial

pressure reductions as expected. The VM lateral and medial pressure differences (i.e., ΔP) indicated that the model mostly resulted in a contact pressure shift (Figs. 6.22). The mean positive ΔP values indicate an affirmative VM effect in every simulation except for SLS,ACL-int, and peak ΔP>0 affirms an intended VM effect in all ADLs. In spite of absolute pressure differences between the model and experiment the simulated VM effect emanated the outcomes of the experimental braces and demonstrated the feasibility of the model to investigate unloader brace characteristics on tibiofemoral compartment pressures.

### 7.2.9 *Novel Contributions from the FE Model*

This study demonstrated that high rate dynamic ADLs can be simulated in a FE environment without extensive modifications to the original seated 50$^{th}$ percentile male model to obtain tissue strain and cartilage pressure responses. The implementation of the model was to develop a framework to adapt the right leg of the seated occupant to a standing position and verify and validate a previously developed experimental approach while simulating squat and gait ADLs. There are interesting applications with the model beyond the scope of this study including the response in strain or pressure based on different brace loading curves, investigating brace efficacy with varying valgus-varus angulations, brace efficacy in osteoarthritic or meniscus injury scenarios, the influence of ACL injury or ATT severity coupled with OA or meniscus injuries, and region specific meniscus strain responses. This study focused on experimental strain measurements at anterior and posterior regions of the tissue. It is feasible to expand on these measures to include additional tissue regions. A former study experimentally measured strain in these regions and the model demonstrated similar strains when with preliminary strain computations in the central section of the tissue (Jones et al., 1996) (Fig. 7.5).

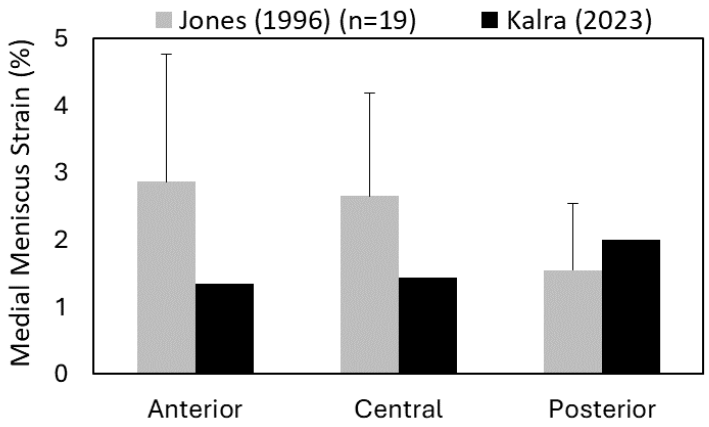

Figure 7.5: Sample measurement of region specific medial meniscus strains in the model compared with literature.

Posterolateral meniscus strains were not an objective within this study due to experimental limitations, yet posterolateral meniscus strain was a novel and relevant outcome measure that proved useful for several reasons. It was originally theorized that posterolateral meniscus strain would increase with a valgus unloading moment. This theory could not be tested experimentally and was confirmed in the model. The posterolateral meniscus strains increased and showed greater changes than the posteromedial meniscus strains with the VM and demonstrated the efficacy of the VM as well as the model's capacity to simulate an unloading response on tissue strain. In the context of this study posterolateral meniscus strain changes with the VM were more pertinent than absolute strain magnitudes. To contextualize posterolateral meniscus strain magnitudes, future studies are necessary to validate posterolateral meniscus strain by simulating identical BCs from the former experimental studies in the model. By validating posterolateral meniscus strain against an independent set of data it would be feasible for future simulation studies to understand the effect of a VM on the strain response in both menisci, which remains a research gap.

In experimental tests there was a counterintuitive increase in medial compartment pressure with both unloader braces during SLS and SLS with these braces was cautioned until future studies can investigate the pressure increase. The VM in the model resulted in an anticipated decrease in medial pressure during SLS indicating that a valgus

unloading moment can unload the medial compartment irrespective of the activity performed. In addition to higher muscle forces during SLS, there is likely a combination of factors why the unloader braces did not reduce medial compartment pressure in experimental testing such as muscle cable preloads applied during the initial stance, the unknown valgus moment magnitudes provided by the braces, and variable strap tensions when securing the brace. These factors do not exist in the model and sequentially implementing these conditions in future modeling studies could help confirm whether unloader braces or valgus moments are not suitable to reduce medial compartment pressures in SLS, or whether the present experimental conditions resulted in isolated increases in medial compartment pressures in SLS with the considered unloader braces.

## 7.3 Limitations

The experimental tests were limited to sagittal plane motions and did not capture any forces in the coronal or transverse planes. The input BCs for the experiment (and model) were taken from a previous study that obtained data from one healthy in-vivo participant that used identical BCs for the ACL-intact and -deficient states. Specimen specific muscle forces accounted for some inter-specimen kinetic variability, though the kinematic BCs were identical across specimens and ACL states. Tomescu et al. (2018) measured ADLs in multiple participants and opted to use a single participant due to large sample variabilities in the mean outcomes when compared to a typical population. Investigating the effect of different kinematic and kinetic profiles from multiple healthy and ACL compromised participants would not be feasible on a single specimen given that each specimen was presently tested for 36 trials. Supplementing additional experimental participant BCs would require removing some of the brace or ACL test conditions and modify the scope of this study. Moreover, testing ADLs in additional healthy or ACL-deficient participants would result in different kinematic and kinetic responses, and the ensuing effects of the unloader braces could be obscured by the BC variations. Nevertheless, individuals with an ACL deficiency may have different meniscus strain

responses than the ones reported in this study, and the reported ACL-deficient strains should be viewed relative to the ACL-intact strains.

The foam stiffness used to envelope the specimens and support the brace was based on the previously measured stiffness of contracted muscle. Realistically muscle stiffness varies based on sex, age, BMI, activity level, and level of exertion. Stiffened muscle was mandatory to properly secure the brace during the high rate ADLs. Future studies with variable foam stiffnesses are necessary to determine the influence of stiffened muscle on strain and pressure outcomes.

The comprehensive experimental procedure required multiple freeze-thaw cycles for each specimen, which affect biological tissue responses. A saline solution was consistently applied and specimens retained their texture and tissue consistency on deep tissues despite some desquamation on superficial tissues. Since this study was interested in differences between bracing scenarios and ACL states the freeze-thaw cycles would not likely have affected the relative comparators between the conditions.

The calibration for the pressure sensors was conducted on a flat surface that was not representative of a knee joint. Seitz et al. (2012) calibrated the same sensors used in this study under the same environmental conditions as their in-vitro tests; though, it is unclear what these conditions were. This study utilized one sensor for each specimen and conducted a 10-point calibration recommended rather than the manufacturer's recommended 2-point method that has been shown to be more erroneous at extreme pressure values (Brimacombe et al., 2009; Wilharm et al., 2013). The calibration outcomes demonstrated high correlation ($r \geq 0.98$), though additional research is required to determine if calibrating within the same in-vitro environment affects the correlation and pressure outcomes.

Some FE studies have created models based on cadaveric scans and are able to compare in-vitro and in-silico outcomes. A limitation with this study is the lack of an identical cadaveric comparator to the model. There were no cadaveric specimens identical or similar to the model in terms of physical characteristics and the model was within one

SD of the experimental mean height, mass, and BMI (Table 7.2). Potentially testing at least one cadaveric specimen to physically match the model could have enabled a direct comparison for moment arm, strain, and pressure outcomes. To mitigate this limitation the model was compared to a single closest matching specimen and demonstrated comparable size, phase, and progression trends with CORA ratings in the order of 0.50. Overall, the model outcomes demonstrated good conformance with the experimental ones since they were within the experimental corridors and one SD of the means.

The material model for the menisci and tibial cartilage was approximated as isotropic linear elastic. Enhancing the material formulations to better represent the nonlinear behaviour of these tissues may have provided more representative strain and pressure outcomes, though a linear elastic model resulted in good conformance with experimental outcomes due to the low range of strain values during the experimental and computational ADLs.

Table 7.2: Specimen donor information including the FE participant characteristics ranked by BMI.

| ID (#) | Sex (F/M) | Foot Orientation | Age (years) | Height (cm) | Mass (kg) | BMI (kg/m$^2$) |
|---|---|---|---|---|---|---|
| 6 | F | R | 47 | 157 | 34 | 14 |
| 2 | M | R | 50 | 188 | 61 | 17 |
| 3 | F | R | 50 | 165 | 50 | 18 |
| 7 | M | L | 60 | 165 | 50 | 18 |
| 5 | M | R | 54 | 165 | 54 | 20 |
| 8 | F | R | 55 | 173 | 59 | 20 |
| 4 | M | R | 44 | 180 | 73 | 22 |
| 10 | F | L | 50 | 173 | 68 | 23 |
| FE | M | R | 26 | 175 ± 3 | 77 ± 4 | 25 ± 2 |
| 9 | M | R | 57 | 183 | 98 | 29 |
| 1 | F | L | 30 | 178 | 107 | 34 |
| Experimental Mean (n=10) | | | 49.7 | 173 | 65.3 | 21.5 |
| Experimental SD (n=10) | | | 8.4 | 9.6 | 22.3 | 5.9 |

F: Female, M: Male, L: Left, R: Right, BMI: body mass index, SD: standard deviation

An unloader brace was represented by a valgus moment, which did not incorporate brace kinematics or strap tensions. The VM implementation simulated the fundamental response of an unloading moment during ADLs indicating that the model is responsive to

a simplified brace implementation and was selected based on the study objectives to understand the effect of an isolated VM on strain and pressure.

# VIII. Conclusion

This study used an existing in-vitro approach to investigate the efficacy of two commercially available unloader knee braces on the medial meniscus and tibiofemoral joint, and further implemented this approach in a pre-existing 50$^{th}$ percentile male FE model. The purpose and all four study objectives were accomplished and demonstrated the efficacy and extent of unloader braces on the medial meniscus using experimental and computational approaches. The novel strengths of this study are (i) its quantification of meniscus tissue strain response under the influence of unloader knee braces, (ii) the discovery that unloader braces have differing effects on posteromedial meniscus strain depending on the state of the ACL, (iii) the framework presented for the successful implementation of experimental ADLs to the model, (iv) the verified VM and the validated ACL deficiency simulating an unloader brace and ACL injury in the model, (v) the ability of the model to simulate comparable meniscus strains and tibiofemoral pressures to the experimental outcomes, and (vi) an overall congruence between the medial unloading moment with the FE VM and the experimental braces.

## 8.1 Revisiting the Hypotheses

Hypothesis 1, unloader braces reduce in-vitro posteromedial meniscus strain and shift ML pressure (not proven): It was hypothesized that there would be strain differences between the ACL-intact and -deficient states; however, there was a preconceived notion that the unloader braces would have similar outcomes during both ACL states. The original hypothesis was proven for both knee braces during the ACL-intact state based on the significant reduction in posteromedial meniscus strain and proven for both braces based on ML pressure shifts in all test conditions, though it was not proven due to nonsignificant reductions in posteromedial strain during the ACL-deficient state.

Hypothesis 2, lateral compartment stresses exceed medial with the FE-VM (proven): An isolated FE VM simulation demonstrated greater stresses in the lateral tibiofemoral compartment compared to the medial with the application of the VM and further caused a reduction in medial compartment pressures in every test condition. The latter was a unique finding that demonstrated that the VM in the model can unload the medial compartment irrespective of the ADL whereas the experimental conditions were unable to. The FE VM provides an effective theoretical simulation of an unloader brace effect in alternate ADLs that may not be experimentally feasible.

Hypothesis 3, the VM reduces FE posteromedial meniscus strain and shifts ML pressure (proven): This was a replica of Hypothesis 1 adapted to the model. Mean posteromedial meniscus strain had negligible differences between the NB and VM scenarios in the model while posterolateral meniscus strain increased, which induced that posterolateral meniscus strain could also serve as a representative metric of VM effect for the same reason that lateral compartment stress was increased with the VM. Therefore, the strain component of this hypothesis was proven due to the increase in posterolateral meniscus strain that is analogous with the same VM outcomes leading to a decrease in posteromedial meniscus strain. Finally, the effect of the VM was proven based on the observed medial to lateral tibiofemoral pressure shifts in 11 of the 12 unique simulation conditions in both ACL states.

Hypothesis 4, FE strains and pressure will resemble experimental outcomes and trends (not proven): Due to unique FE specific muscle forces and unmatched cadaveric specimens the model was treated as a unique 'specimen' and differences were expected between the two methods. The FE posteromedial meniscus mean and peak strains were within 1–2 SD of experimental means for all ADLs. FE strains were within the experimental corridors during DLS and gait. Strains for the FE-SLS simulations were higher than the experimental corridors and observed an inverse sense that was postulated due to different valgus-varus angulations. The FE mean tibiofemoral pressures were within ±1 SD and peak pressures were within ±2 SD of the experimental outcomes. The

experimental and model strain differences during single leg squats in all ADLs disproved this hypothesis. Medial compartment pressures were more comparable between the computational and experimental approaches than the lateral pressures, which again suggests valgus-varus differences. Importantly, the pressure trends between the experiment and model were identical with SLS resulting in the highest pressure and gait resulting in the lowest pressures.

This objective demonstrated additional successes between the model and experiments that could not be anticipated when formulating the hypothesis. There was no explicit objective to validate the ACL-deficient state in the model, rather the removal of the ACL part was meant to compare between ACL-intact and -deficient states within the model. The deficient ACL in the model produced comparable knee joint kinematics with previous literature and the strain differences without the ACL in the model reflected the patterns observed with the experiment. Furthermore, both the experimental and FE bracing scenarios were not efficacious in the ACL-deficient state. Finally, the magnitude of the pressure difference ($\Delta P$) between the lateral and medial compartments were highly similar between the experimental and computational approaches indicating that the simulated VM was reflective of an unloader brace moment.

## 8.2 Recommendations for Future Work

Future studies are recommended to investigate lateral meniscus strains under the effect of an unloading moment. If this is not possible in a high rate dynamic experimental ADL then it is recommended during a static condition at discrete flexion angles or a quasistatic condition under passive flexion. Additionally, the strains in the lateral meniscus can be validated against prior experimental studies that have measured posterolateral meniscus strain using identical BCs. Following posterolateral meniscus strain validation the framework presented in this study can be used to study the effect of VM in both meniscus tissues. Quantifying the unloading brace moment could be done with an experimental three-point bending test. Furthermore, conducting in-vivo squat

and gait ADLs with an instrumented brace would provide a variable brace moment BC input for future ADL modeling studies. This study demonstrated an increase in FE posterolateral meniscus strain with the VM, and additional data to match these outcomes and compare posterolateral meniscus strain magnitudes would be invaluable. Similarly, measuring unloader brace moment during the investigated ADLs would yield a more representative VM for the model and apply a variable VM throughout knee flexion. Finally, experimental researchers are encouraged to investigate the differences in calibration outcomes when pressure sensors and calibrated within the knee's anatomical environment vs. a flat indenter approach used in the present study. A selection of computational recommendations are further enhancements to the menisci and cartilage material models, reducing/eliminating part penetrations, modifying the initial BC for the SLS simulation, and modeling an unloader brace to simulate brace kinematics. A nonlinear material model representing the biphasic nature of the menisci and cartilage would be more biofidelic and permit more aggressive ADL simulations that exceed the low linear recommended strain range. Improving part penetrations within the knee joint would further enhance the model's ability to simulate gait and fully extend the knee in other simulations or applications. Applying an initial BC to create a SLS specific valgus-varus position would more naturally simulate a SLS during a single leg stance. Incorporating brace kinematics into the model with a brace model would be a useful supplement to the VM unloading presented in this study. A final recommendation for future studies undertaking dual in-vitro and in-silico approaches is to obtain cadaveric specimens that are nearly identical or identical to the physical characteristics of the model.

# References


Abrams, G. D., Frank, R. M., Gupta, A. K., Harris, J. D., Mccormick, F. M., & Cole, B. J. (2013). *Trends in Meniscus Repair and Meniscectomy in the United States , 2005–2011*. *The American journal of sports medicine*, *41*(10), 2333-2339. https://doi.org/10.1177/0363546513495641

Agneskirchner, J. D., Hurschler, C., Wrann, C. D., & Lobenhoffer, P. (2007). The Effects of Valgus Medial Opening Wedge High Tibial Osteotomy on Articular Cartilage Pressure of the Knee: A Biomechanical Study. *Arthroscopy – Journal of Arthroscopic and Related Surgery*, *23*(8), 852–861. https://doi.org/10.1016/j.arthro.2007.05.018

Alentorn-Geli, E., Myer, G. D., Silvers, H. J., Samitier, G., Romero, D., Lázaro-Haro, C., & Cugat, R. (2009). Prevention of non-contact anterior cruciate ligament injuries in soccer players. Part 1: Mechanisms of injury and underlying risk factors. *Knee Surgery, Sports Traumatology, Arthroscopy*, *17*(7), 705–729. https://doi.org/10.1007/s00167-009-0813-1

Ali, A. A., Harris, M. D., Shalhoub, S., Maletsky, L. P., Rullkoetter, P. J., & Shelburne, K. B. (2017). Combined measurement and modeling of specimen-specific knee mechanics for healthy and ACL-deficient conditions. *Journal of Biomechanics*, *57*, 117–124. https://doi.org/10.1016/j.jbiomech.2017.04.008

Ali, A. A., Shalhoub, S. S., Cyr, A. J., Fitzpatrick, C. K., Maletsky, L. P., Rullkoetter, P. J., & Shelburne, K. B. (2016). Validation of predicted patellofemoral mechanics in a finite element model of the healthy and cruciate-deficient knee. *Journal of biomechanics*, *49*(2), 302-309.

Allaire, R., Muriuki, M., Gilbertson, L., & Harner, C. D. (2008). Biomechanical consequences of a tear of the posterior root of the medial meniscus: Similar to total meniscectomy. *Journal of Bone and Joint Surgery*, *90*(9), 1922–1931. https://doi.org/10.2106/JBJS.G.00748

Allen, A. A., Caldwell Jr, G. L., & Fu, F. H. (1995). Anatomy and biomechanics of the meniscus. *Operative techniques in orthopaedics*, *5*(1), 2-9.

Allen, C. R., Wong, E. K., Livesay, G. A., Sakane, M., Fu, F. H., & Woo, S. L.-Y. (2000). Importance of the medial meniscus in the anterior cruciate ligament-deficient knee. *Journal of Orthopaedic Research*, *18*(1), 109–115. https://doi.org/10.1002/jor.1100180116

Altman, R., Asch, E., Bloch, D., Bole, G., Borenstein, D., Brandt, K., Christy, W., Cooke, T. D., Greenwald, R., Hochberg, M., Howell, D., Kaplan, D., Koopman, W., Longley, S., Mankin, H., McShane, D. J., Medsger, T., Meenan, R., Mikkelsen, W., … Wolfe, F. (1986). Development of criteria for the classification and reporting of osteoarthritis: Classification of osteoarthritis of the knee. *Arthritis & Rheumatism*, *29*(8), 1039–1049. https://doi.org/10.1002/art.1780290816

An, K. N., Takahashi, K., Harrigan, T. P., & Chao, E. Y. (1984). Determination of muscle orientations and moment arms. *Journal of biomechanical engineering*, *106*(3), 280-282.

Anderson, I. A., MacDiarmid, A. A., Harris, M. L., Gillies, R. M., Phelps, R., & Walsh, W. R. (2003). A novel method for measuring medial compartment pressures within the knee joint in-vivo. *Journal of Biomechanics*, *36*(9), 1391–1395. https://doi.org/10.1016/S0021-9290(03)00158-1

Andrews, K., Lu, A., Mckean, L., & Ebraheim, N. (2017). Review: Medial collateral ligament injuries. *Journal of Orthopaedics*, *14*(4), 550–554. https://doi.org/10.1016/j.jor.2017.07.017

Arazpour, M., Hutchins, S. W., Bani, M. A., Curran, S., & Aksenov, A. (2014). The influence of a bespoke unloader knee brace on gait in medial compartment osteoarthritis: A pilot study. *Prosthetics and Orthotics International*, *38*(5), 379–386. https://doi.org/10.1177/0309364613504780

Asano, T., Akagi, M., & Nakamura, T. (2005). The functional flexion-extension axis of the knee corresponds to the surgical epicondylar axis: In vivo analysis using a biplanar image-matching technique. *Journal of Arthroplasty*, *20*(8), 1060–1067. https://doi.org/10.1016/j.arth.2004.08.005

Aspden, R. M. (1985). A model for the function and failure of the meniscus. *Engineering in Medicine*, *14*(3), 119–122. https://doi.org/10.1243/EMED_JOUR_1985_014_028_02

Astur, D. C., Oliveira, S. G., Badra, R., Arliani, G. G., Kaleka, C. C., Jalikjian, W., ... & Cohen, M. (2011). Updating of the anatomy of the extensor mechanism of the knee using a three-dimensional viewing technique. *Revista Brasileira de Ortopedia*, *46*, 490-494.

Augat, P., Hast, M. W., Schemitsch, G., Heyland, M., Trepczynski, A., Borgiani, E., Russow, G., Märdian, S., Duda, G. N., Hollensteiner, M., Bottlang, M., & Schemitsch, E. H. (2021). Biomechanical models: key considerations in study design. *OTA International: The Open Access Journal of Orthopaedic Trauma*, *4*(2S), 1–6. https://doi.org/10.1097/oi9.0000000000000099

Bakker, R. (2014). *The Effect of Sagittal Plane Mechanics on Anterior Cruciate Ligament Strain During Jump Landing* [Master's thesis, University of Waterloo]. UWSpace. http://hdl.handle.net/10012/9048

Bakker, R., Tomescu, S., Brenneman, E., Hangalur, G., Laing, A., & Chandrashekar, N. (2016). Effect of sagittal plane mechanics on ACL strain during jump landing. *Journal of Orthopaedic Research*, *34*(9), 1636-1644.

Baldwin, M. A., Clary, C. W., Fitzpatrick, C. K., Deacy, J. S., Maletsky, L. P., & Rullkoetter, P. J. (2012). Dynamic finite element knee simulation for evaluation of knee replacement mechanics. *Journal of Biomechanics*, *45*(3), 474–483. https://doi.org/10.1016/j.jbiomech.2011.11.052

Barnes, C. L., Cawley, P. W., & Hederman, B. (2002). Effect of CounterForce brace on symptomatic relief in a group of patients with symptomatic unicompartmental osteoarthritis: a prospective 2-year investigation. *American journal of orthopedics*, *31*(7), 396-401.

Beaufils, P., & Pujol, N. (2017). Management of traumatic meniscal tear and degenerative meniscal lesions. Save the meniscus. *Orthopaedics and Traumatology: Surgery and Research*, *103*(8), S237–S244. https://doi.org/10.1016/j.otsr.2017.08.003

Becher, C., Huber, R., Thermann, H., Paessler, H. H., & Skrbensky, G. (2008). Effects of a contoured articular prosthetic device on tibiofemoral peak contact pressure: a biomechanical study. *Knee Surgery, Sports Traumatology, Arthroscopy : Official Journal of the ESSKA*, *16*(1), 56–63. https://doi.org/10.1007/s00167-007-0416-7

Becker, R., Wirz, D., Wolf, C., Göpfert, B., Nebelung, W., & Friederich, N. (2005). Measurement of meniscofemoral contact pressure after repair of bucket-handle tears with biodegradable implants. *Archives of Orthopaedic and Trauma Surgery*, *125*(4), 254–260. https://doi.org/10.1007/s00402-004-0739-5

Beillas, P., Papaioannou, G., Tashman, S., & Yang, K. H. (2004). A new method to investigate in vivo knee behavior using a finite element model of the lower limb. *Journal of biomechanics*, *37*(7), 1019-1030.

Beillas, P., Begeman, P. C., Yang, K. H., King, A. I., Arnoux, P. J., Kang, H. S., Kayvantash, K., Brunet, C., Cavallero, C., & Prasad, P. (2001). Lower Limb: Advanced FE Model and New Experimental Data. *SAE Technical Papers*, *45*, 1–25. https://doi.org/10.4271/2001-22-0022

Bendjaballah, M. Z., Shirazi-Adl, A., & Zukor, D. J. (1995). Biomechanics of the human knee joint in compression: reconstruction, mesh generation and finite element analysis. *The Knee*, *2*(2), 69–79. https://doi.org/10.1016/0968-0160(95)00018-K

Berns, G. S., Hull, M. L., & Patterson, H. A. (1990). Implementation of a five degree of freedom automated system to determine knee flexibility in vitro. *Journal of Biomechanical Engineering*, *112*, 392–400.

Betts, J. G., Young, K. A., Wise, J. A., Johnson, E., Poe, B., Kruse, D. H., ... & DeSaix, P. (2022). Anatomy and Physiology 2e. OpenStax. https://openstax.org/books/anatomy-and-physiology-2e/pages/8-4-bones-of-the-lower-limb

Beynnon, B. D., & Fleming, B. C. (1998). Anterior cruciate ligament strain in-vivo: a review of previous work. *Journal of biomechanics*, *31*(6), 519–525.

Beynnon, B. D., Fleming, B. C., Labovitch, R., & Parsons, B. (2002). Chronic anterior cruciate ligament deficiency is associated with increased anterior translation of the tibia during the transition from non-weightbearing to weightbearing. *Journal of Orthopaedic Research*, *20*(2), 332–337. https://doi.org/10.1016/S0736-0266(01)00115-2

Beynnon, B., Howe, J. G., Pope, M. H., Johnson, R. J., & Fleming, B. C. (1992). The measurement of anterior cruciate ligament strain in vivo. *International Orthopaedics*, *16*, 1–12.

Bhatia, S., Laprade, C. M., Ellman, M. B., & Laprade, R. F. (2014). Meniscal root tears: Significance, diagnosis, and treatment. *American Journal of Sports Medicine*, *42*(12), 3016–3030. https://doi.org/10.1177/0363546514524162/FORMAT/EPUB

Boden, B. P., Sheehan, F. T., Torg, J. S., & Hewett, T. E. (2010). Non-contact ACL Injuries: Mechanisms and Risk Factors. *American Academy of Orthopaedic Surgeons*, *18*(9), 520–527.

Boyd, K. T., & Myers, P. T. (2003). Meniscus preservation; rationale, repair techniques and results. *The Knee*, *10*(1), 1–11. https://doi.org/10.1016/S0968-0160(02)00147-3

Briggs, K. K., Matheny, L. M., & Steadman, J. R. (2012). Improvement in Quality of Life with Use of an Unloader Knee Brace in Active Patients with OA: A Prospective Cohort Study. *J Knee Surg*, *25*(05), 417–422.

Brimacombe, J. M., Wilson, D. R., Hodgson, A. J., Ho, K. C. T., & Anglin, C. (2009). Effect of Calibration Method on Tekscan Sensor Accuracy. *Journal of Biomechanical Engineering*, *131*(3), 034503. https://doi.org/10.1115/1.3005165

Brouwer, R. W., Van Raaij, T. M., Verhaar, J. A. N., Coene, L. N. J. E. M., & Bierma-Zeinstra, S. M. A. (2006). Brace treatment for osteoarthritis of the knee: a prospective randomized multi-centre trial. *Osteoarthritis and cartilage*, *14*(8), 777-783.

Browner, B. D. (2003). *Skeletal trauma: basic science, management, and reconstruction (Vol. 1)*.

Burgin, L. V., Edelsten, L., & Aspden, R. M. (2014). The mechanical and material properties of elderly human articular cartilage subject to impact and slow loading. *Medical engineering & physics*, *36*(2), 226-232.

Butler, D. L., Kay, M. D., & Stouffer, D. C. (1986). Comparison of material properties in fascicle-bone units from human patellar tendon and knee ligaments. *Journal of biomechanics*, *19*(6), 425-432.

Butz, K. D., Chan, D. D., Nauman, E. A., & Neu, C. P. (2011). Stress distributions and material properties determined in articular cartilage from MRI-based finite strains. Journal of biomechanics, *44*(15), 2667-2672.

Cassidy, K., Hangalur, G., Sabharwal, P., & Chandrashekar, N. (2013). Combined in vivo/in vitro method to study anteriomedial bundle strain in the anterior cruciate ligament using a dynamic knee simulator. *Journal of Biomechanical Engineering*, *135*(3), 35001.

Cavanaugh, J. T., & Killian, S. E. (2012). Rehabilitation following meniscal repair. *Current Reviews in Musculoskeletal Medicine*, *105*(1), 46–58. https://doi.org/10.1007/s12178-011-9110-y

Cerulli, G., Benoit, D. L., Lamontagne, M., Caraffa, A., & Liti, A. (2003). In vivo anterior cruciate ligament strain behaviour during a rapid deceleration movement: case report. *Knee Surgery, Sports Traumatology, Arthroscopy*, *11*, 307–311. https://doi.org/10.1007/s00167-003-0403-6

Chandrashekar, N., Mansouri, H., Slauterbeck, J., & Hashemi, J. (2006). Sex-based differences in the tensile properties of the human anterior cruciate ligament. *Journal of Biomechanics*, *39*(16), 2943–2950. https://doi.org/10.1016/j.jbiomech.2005.10.031

Chia, H. N., & Hull, M. L. (2008). Compressive moduli of the human medial meniscus in the axial and radial directions at equilibrium and at a physiological strain rate. *Journal of Orthopaedic Research*, *26*(7), 951-956.

Choi, E. H., Kim, K. K., Jun, A. Y., Choi, E. H., Choi, S. W., & Shin, K. Y. (2011). Effects of the off-loading brace on the activation of femoral muscles-A preliminary study. *Annals of Rehabilitation Medicine*, *35*(6), 887.

Christine, W., Victor, H., Daryl, O., Todd, F., & Tyler, F. (2020). A patient-specific lower extremity biomechanical analysis of a knee orthotic during a deep squat movement. *Medical Engineering & Physics*, *80*, 1-7.

Ciccone, W. J., Bratton, D. R., Weinstein, D. M., Walden, D. L., & Elias, J. J. (2006). Structural properties of lateral collateral ligament reconstruction at the fibular head. *The American Journal of Sports Medicine*, *34*(1), 24–29.

Clayton, R. A. E., & Court-Brown, C. M. (2008). The epidemiology of musculoskeletal tendinous and ligamentous injuries. *Injury*, *39*(12), 1338–1344. https://doi.org/10.1016/j.injury.2008.06.021

Collier, S., & Ghosh, P. (1995). Effects of transforming growth factor beta on proteoglycan synthesis by cell and explant cultures derived from the knee joint meniscus. *Osteoarthritis and Cartilage*, 3*(*2), 127-138.

Cottrell, J. M., Scholten, P., Wanich, T., Warren, R. F., Wright, T. M., & Maher, S. A. (2008). A new technique to measure the dynamic contact pressures on the Tibial Plateau. *Journal of Biomechanics*, *41*(10), 2324–2329. https://doi.org/10.1016/j.jbiomech.2008.04.024

Daniel, D. M., Stone, M. Lou, Dobson, B. E., Fithian, D. C., Rossman, D. J., & Kaufman, K. R. (1994). Fate of the ACL-injured Patient: A Prospective Outcome Study. *The American Journal of Sports Medicine*, *22*(5), 632–644. https://doi.org/10.1177/036354659402200511

Delp, S. L., Loan, J. P., Hoy, M. G., Zajac, F. E., Topp, E. L., & Rosen, J. M. (1990). An Interactive Graphics-Based Model of the Lower Extremity to Study Orthopaedic Surgical Procedures. *IEEE Transactions on Biomedical Engineering*, *37*(8), 757–767. https://doi.org/10.1109/10.102791

Dessery, Y., Belzile, É. L., Turmel, S., & Corbeil, P. (2014). Comparison of three knee braces in the treatment of medial knee osteoarthritis. *Knee*, *21*(6), 1107–1114. https://doi.org/10.1016/j.knee.2014.07.024

Dessery, Y., Steultjens, M., Mannisi, M., Eskandari, B., Woodburn, J., & Pallari, J. (2017a). Clinical and biomechanical effects of a bespoke 3D printed knee brace for knee osteoarthritis. *Osteoarthritis and Cartilage*, *25*, S414-S415.

Dessery, Y., Steultjens, M., Mannisi, M., Eskandari, B., Woodburn, J., & Pallari, J. (2017b). Knee adduction moment during stair descent with a Bespoke 3d printed knee brace for knee osteoarthritis. *Osteoarthritis and Cartilage*, *25*, S139.

Dessinger, G. M., LaCour, M. T., Dennis, D. A., Kleeman-Forsthuber, L. T., & Komistek, R. D. (2021). Can an OA Knee Brace Effectively Offload the Medial Condyle? An In Vivo Fluoroscopic Study. *Journal of Arthroplasty*, *36*(4), 1455–1461. https://doi.org/10.1016/j.arth.2020.10.044

Divine, J. G., & Hewett, T. E. (2005). Valgus bracing for degenerative knee osteoarthritis: relieving pain, improving gait, and increasing activity. *The Physician and Sportsmedicine*, *33*(2), 40-46.

Dong, Y., Hu, G., Dong, Y., Hu, Y., & Xu, Q. (2012). The effect of meniscal tears and resultant partial meniscectomies on the knee contact stresses: A finite element analysis. *Computer Methods in Biomechanics and Biomedical Engineering*, *17*(13), 1452–1463.

Doral, M. N., Bilge, O., Huri, G., Turhan, E., & Verdonk, R. (2018). Modern treatment of meniscal tears. *EFORT Open Reviews*, *3*(5), 260. https://doi.org/10.1302/2058-5241.3.170067

Drewniak, E. I., Crisco, J. J., Spenciner, D. B., & Fleming, B. C. (2007). Accuracy of circular contact area measurements with thin-film pressure sensors. *Journal of Biomechanics*, *40*(11), 2569–2572. https://doi.org/10.1016/j.jbiomech.2006.12.002

Drosos, G. I., & Pozo, J. L. (2004). The causes and mechanisms of meniscal injuries in the sporting and non-sporting environment in an unselected population. *Knee*, *11*(2), 143–149. https://doi.org/10.1016/S0968-0160(03)00105-4

Duivenvoorden, T., van Raaij, T. M., Horemans, H. L. D., Brouwer, R. W., Bos, P. K., Bierma-Zeinstra, S. M. A., Verhaar, J. A. N., & Reijman, M. (2015). Do Laterally Wedged Insoles or Valgus Braces Unload the Medial Compartment of the Knee in Patients With Osteoarthritis? *Clinical Orthopaedics and Related Research*, *473*(1), 265–274. https://doi.org/10.1007/s11999-014-3947-5

Ebert, J. R., Hambly, K., Joss, B., Ackland, T. R., & Donnelly, C. J. (2014). Does an unloader brace reduce knee loading in normally aligned knees?. *Clinical Orthopaedics and Related Research*, *472*, 915-922.

Edemekong, P. F., Bomgaars, D. L., Sukumaran, S., & Schoo, C. (2022). Activities of Daily Living. 2022 Jul 3. StatPearls [Internet]. Treasure Island (FL): StatPearls Publishing. https://www.ncbi.nlm.nih.gov/books/NBK470404/#_NBK470404_pubdet_

Elkin, L. A., Kay, M., Higgins, J. J., & Wobbrock, J. O. (2021). An aligned rank transform procedure for multifactor contrast tests. *The 34th annual ACM symposium on user interface software and technology,* 754-768.

Elson, E. L., & Genin, G. M. (2016). Tissue constructs: platforms for basic research and drug discovery. *Interface focus*, *6*(1), 20150095.

Englund, M. (2008). The Role of the Meniscus in Osteoarthritis Genesis. *Rheumatic Disease Clinics of North America, 34*(3), 573–579. https://doi.org/10.1016/j.rdc.2008.05.009

Englund, M., Guermazi, A., & Lohmander, S. L. (2009). The Role of the Meniscus in Knee Osteoarthritis: a Cause or Consequence? *Radiologic Clinics of North America, 47*(4), 703–712. https://doi.org/10.1016/j.rcl.2009.03.003

Englund, M., Haugen, I. K., Guermazi, A., Roemer, F. W., Niu, J., Neogi, T., Aliabadi, P., & Felson, D. T. (2016). Evidence that meniscus damage may be a component of osteoarthritis: The Framingham study. *Osteoarthritis and Cartilage*, *24*(2), 270–273. https://doi.org/10.1016/j.joca.2015.08.005

Erbagci, H., Gumusburun, E., Bayram, M., Karakurum, G., & Sirikci, A. (2004). The normal menisci: In vivo MRI measurements. *Surgical and Radiologic Anatomy*, *26*(1), 28–32. https://doi.org/10.1007/s00276-003-0182-2

Fantini Pagani, C. H., Potthast, W., & Brüggemann, G. P. (2010). The effect of valgus bracing on the knee adduction moment during gait and running in male subjects with varus alignment. *Clinical Biomechanics*, *25*(1), 70–76. https://doi.org/10.1016/j.clinbiomech.2009.08.010

Fantini Pagani, C. H., Willwacher, S., Kleis, B., & Brüggemann, G. P. (2013). Influence of a valgus knee brace on muscle activation and co-contraction in patients with medial knee osteoarthritis. *Journal of Electromyography and Kinesiology*, *23*(2), 490–500. https://doi.org/10.1016/j.jelekin.2012.10.007

Felson, D. T. (2006). Osteoarthritis of the knee. *The New England Journal of Medicine, 345*(8), 841–848. http://www.farm.ucl.ac.be/FARM2129/2008-2009/Tulkens/AINS/Felson-et-al-osteoarthritis-of-the-knee.pdf

Felson, D. T., Couropmitree, N. N., Chaisson, C. E., Hannan, M. T., Zhang, Y., Mcalindon, T. E., Lavalley, M., Levy, D., & Myers, R. H. (1998). Evidence for a Mendelian gene in a segregation analysis of generalized radiographic osteoarthritis: The Framingham Study. *Arthritis and Rheumatism*, *41*(6), 1064–1071. https://doi.org/10.1002/1529-0131(199806)41:6<1064::AID-ART13>3.0.CO;2-K

Ferrer-Roca, O., & Vilalta, C. (1980). Lesions of the meniscus. I: Macroscopic and histologic findings. *Clinical Orthopaedics and Related Research*, *146*, 289–300.

Finger, S., & Paulos, L. E. (2002). Clinical and biomechanical evaluation of the unloading brace. *The journal of knee surgery*, *15*(3), 155–158.

Fleming, B. C., & Beynnon, B. D. (2004). In vivo measurement of ligament/tendon strains and forces: A review. *Annals of Biomedical Engineering*, *32*(3), 318–328. https://doi.org/10.1023/B:ABME.0000017542.75080.86/METRICS

Fleming, B. C., Beynnon, B. D., Nichols, C. E., Johnson, R. J., & Pope, M. H. (1993). An in vivo comparison of anterior tibial translation and strain in the anteromedial band of the anterior cruciate ligament. *Journal of Biomechanics*, *26*(1), 51–58. https://doi.org/10.1016/0021-9290(93)90612-I

Fok, A. W. M., & Yau, W. P. (2013). Delay in ACL reconstruction is associated with more severe and painful meniscal and chondral injuries. *Knee Surgery, Sports Traumatology, Arthroscopy*, *21*(4), 928–933. https://doi.org/10.1007/s00167-012-2027-1

Fox, A. J. S., Bedi, A., & Rodeo, S. A. (2012). The Basic Science of Human Knee Menisci: Structure, Composition, and Function. *Sports Health*, *4*(4), 340–351. https://doi.org/10.1177/1941738111429419

Fox, A. J. S., Wanivenhaus, F., Burge, A. J., Warren, R. F., & Rodeo, S. A. (2015). The human meniscus: A review of anatomy, function, injury, and advances in treatment. *Clinical Anatomy*, *28*(2), 269–287. https://doi.org/10.1002/ca.22456

Franz, T., Hasler, E. M., Hagg, R., Weiler, C., Jakob, R. P., & Mainil-Varlet, P. (2001). In situ compressive stiffness, biochemical composition, and structural integrity of articular cartilage of the human knee joint. *Osteoarthritis and Cartilage*, *9*(6), 582-592.

Frizziero, A., Ferrari, R., Giannotti, E., Ferroni, C., Poli, P., & Masiero, S. (2012). The meniscus tear: State of the art of rehabilitation protocols related to surgical procedures. *Muscles, Ligaments and Tendons Journal, 2*(4), 295–301).

Frobell, R. B., Lohmander, L. S., & Roos, H. P. (2007). Acute rotational trauma to the knee: Poor agreement between clinical assessment and magnetic resonance imaging findings. *Scandinavian Journal of Medicine and Science in Sports*, *17*(2), 109–114. https://doi.org/10.1111/j.1600-0838.2006.00559.x

Fu, H. C. H., Lie, C. W. H., Ng, T. P., Chen, K. W., Tse, C. Y., & Wong, W. H. (2015). Prospective study on the effects of orthotic treatment for medial knee osteoarthritis in chinese patients: Clinical outcome and gait analysis. *Hong Kong Medical Journal*, *21*(2), 98–106. https://doi.org/10.12809/hkmj144311

Fukubayashi, T., & Kurosawa, H. (1980). the contact area and pressure distribution pattern of the knee: A study of normal and osteoarthrotic knee joints. *Acta Orthopaedica*, *51*(1–6), 871–879. https://doi.org/10.3109/17453678008990887

Funk, J. R., Rudd, R. W., Kerrigan, J. R., & Crandall, J. R. (2004). The effect of tibial curvature and fibular loading on the tibia index. *Traffic injury prevention*, *5*(2), 164-172.

Gantoi, F. M., Brown, M. A., & Shabana, A. A. (2013). Finite element modeling of the contact geometry and deformation in biomechanics applications. *Journal of Computational and Nonlinear Dynamics*, *8*(4), 041013.

Gayzik, F. S., Moreno, D. P., Geer, C. P., Wuertzer, S. D., Martin, R. S., & Stitzel, J. D. (2011). Development of a full body CAD dataset for computational modeling: A multi-modality approach. *Annals of Biomedical Engineering*, *39*(10), 2568–2583. https://doi.org/10.1007/s10439-011-0359-5

Gee, S. M., Tennent, D. J., Cameron, K. L., & Posner, M. A. (2020). The Burden of Meniscus Injury in Young and Physically Active Populations. *Clinics in Sports Medicine, 39*(1), 13–27). https://doi.org/10.1016/j.csm.2019.08.008

Gehre, C., Gades, H., & Wernicke, P. (2009). Objective rating of signals using test and simulation responses. *Processding of 21st International Technical Conference on the Enhanced Safety of Vehicles Conference (ESV)*, 15–18.

Goodwin, J. S., Creighton, R. A., Pietrosimone, B. G., Spang, J. T., & Blackburn, J. T. (2019). Medial unloader braces and lateral heel wedges do not alter gait biomechanics in healthy young adults. *Journal of sport rehabilitation*, *28*(4), 354-359.

Granan, L. P., Bahr, R., Lie, S. A., & Engebretsen, L. (2009). Timing of anterior cruciate ligament reconstructive surgery and risk of cartilage lesions and meniscal tears: A cohort study based on the norwegian national knee ligament registry. *American Journal of Sports Medicine*, *37*(5), 955–961. https://doi.org/10.1177/0363546508330136

Gravlee, J. R., & Van Durme, D. J. (2007). Braces and splints for musculoskeletal conditions. *American family physician*, *75*(3), 342-348.

Greis, P. E., Bardana, D. D., Holmstrom, M. C., & Burks, R. T. (2002). Meniscal injury: I. Basic science and evaluation. *The Journal of the American Academy of Orthopaedic Surgeons, 10*(3), 168–176. https://doi.org/10.5435/00124635-200205000-00003

Greis, P. E., Johnson, D. L., & Fu, F. H. (1993). Revision anterior cruciate ligament surgery: causes of graft failure and technical considerations of revision surgery. *Clinics in Sports Medicine*, *12*(4), 839–852. http://www.ncbi.nlm.nih.gov/pubmed/8261529

Grood, E. S., & Noyes, F. R. (1976). Cruciate ligament prosthesis: strength, creep, and fatigue properties. *JBJS*, *58*(8), 1083-1088.

Guess, T. M., Razu, S., Jahandar, H., & Stylianou, A. (2015). Predicted loading on the menisci during gait: The effect of horn laxity. *Journal of biomechanics*, *48*(8), 1490-1498.

Guess, T. M., Thiagarajan, G., Kia, M., & Mishra, M. (2010). A subject specific multibody model of the knee with menisci. *Medical Engineering & Physics*, *32*, 505–515.

Guo, Y., Zhang, X., & Chen, W. (2009). Three-Dimensional Finite Element Simulation of Total Knee Joint in Gait Cycle. *Acta Mechanica Solida Sinica*, *22*(4), 347–351. https://doi.org/10.1016/S0894-9166(09)60283-4

Hajek, P. C., Gylys-Morin, V. M., Baker, L. L., Sartoris, D. J., Haghighi, P., & Resnick, D. (1987). The high signal intensity meniscus of the knee magnetic resonance evaluation and in vivo correlation. *Investigative radiology*, *22*(11), 883-890.

Haladik, J. A., Vasileff, W. K., Peltz, C. D., Lock, T. R., & Bey, M. J. (2014). Bracing improves clinical outcomes but does not affect the medial knee joint space in osteoarthritic patients during gait. *Knee Surgery, Sports Traumatology, Arthroscopy*, *22*, 2715-2720.

Halawi, M. J., & Barsoum, W. K. (2017). Unicondylar knee arthroplasty: Key concepts. *Journal of Clinical Orthopaedics and Trauma*, *8*(1), 11–13. https://doi.org/10.1016/j.jcot.2016.08.010

Hall, M., Diamond, L. E., Lenton, G. K., Pizzolato, C., & Saxby, D. J. (2019). Immediate effects of valgus knee bracing on tibiofemoral contact forces and knee muscle forces. *Gait & Posture*, *68*, 55-62.

Hall, M., Starkey, S., Hinman, R. S., Diamond, L. E., Lenton, G. K., Knox, G., … Saxby, D. J. (2021). Valgus knee bracing for medial knee osteoarthritis and varus malalignment: a pilot study. *Osteoarthritis and Cartilage*, *29*, S173-S174.

Halonen, K. S., Mononen, M. E., Jurvelin, J. S., Töyräs, J., & Korhonen, R. K. (2013). Importance of depth-wise distribution of collagen and proteoglycans in articular cartilage-A 3D finite element study of stresses and strains in human knee joint. *Journal of Biomechanics*, *46*(6), 1184–1192. https://doi.org/10.1016/j.jbiomech.2012.12.025

Han, S. K., Colarusso, P., & Herzog, W. (2009). Confocal microscopy indentation system for studying in situ chondrocyte mechanics. *Medical engineering & physics*, *31*(8), 1038-1042.

Hangalur, G., Brenneman, E., Nicholls, M., Bakker, R., Laing, A., & Chandrashekar, N. (2016). Can a knee brace reduce the strain in the anterior cruciate ligament? A study using combined in vivo/in vitro method. *Prosthetics and Orthotics International*, *40*(3), 394-399.

Haris, A., & Beng Chye Tan, V. (2021). Effectiveness of bilateral single-hinged knee bracing in osteoarthritis: A finite element study. *Proceedings of the Institution of Mechanical Engineers, Part H: Journal of Engineering in Medicine*, *235*(8), 873–882. https://doi.org/10.1177/09544119211012493

Harris, M. D., Cyr, A. J., Ali, A. A., Fitzpatrick, C. K., Rullkoetter, P. J., Maletsky, L. P., & Shelburne, K. B. (2016). A combined experimental and computational approach to subject-specific analysis of knee joint laxity. *Journal of biomechanical engineering*, *138*(8), 081004.

Harris, M. L., Morberg, P., Bruce, W. J., & Walsh, W. R. (1999). An improved method for measuring tibiofemoral contact areas in total knee arthroplasty: a comparison of K-scan sensor and Fuji film. *Journal of Biomechanics*, *32*(9), 951–958. https://doi.org/DOI: 10.1016/S0021-9290(99)00072-X

Harner, C. D., Höher, J., Vogrin, T. M., Carlin, G. J., & Woo, S. L. (1998). The effects of a popliteus muscle load on in situ forces in the posterior cruciate ligament and on knee kinematics. *The American journal of sports medicine*, *26*(5), 669-673.

Harner, C. D., Livesay, G. A., Kashiwaguchi, S., Fujie, H., Choi, N. Y., & Woo, S. L. -. (1995). Comparative study of the size and shape of human anterior and posterior cruciate ligaments. *Journal of Orthopaedic Research*, *13*(3), 429–434. https://doi.org/10.1002/jor.1100130317

Hart, H. F., Crossley, K. M., Ackland, D. C., Cowan, S. M., & Collins, N. J. (2016). Effects of an unloader knee brace on knee-related symptoms and function in people with post-traumatic knee osteoarthritis after anterior cruciate ligament reconstruction. *Knee*, *23*(1), 85–90. https://doi.org/10.1016/j.knee.2015.05.006

Hashemi, J., Chandrashekar, N., Jang, T., Karpat, F., Oseto, M., & Ekwaro-Osire, S. (2007). An alternative mechanism of non-contact anterior cruciate ligament injury during jump-landing: In-vitro simulation. *Experimental Mechanics*, *47*(3), 347–354. https://doi.org/10.1007/s11340-007-9043-y

Hauch, K. N., Villegas, D. F., & Haut Donahue, T. L. (2010). Geometry, time-dependent and failure properties of human meniscal attachments. *Journal of Biomechanics*, *43*(3), 463–468. https://doi.org/10.1016/j.jbiomech.2009.09.043

Haut, R. C. (1989). Contact pressures in the patellofemoral joint during impact loading on the human flexed knee. *Journal of Orthopaedic Research*, *7*(2), 272–280. https://doi.org/10.1002/jor.1100070216

Haut Donahue, T. L., Hull, M. L., Rashid, M. M., & Jacobs, C. R. (2003). How the stiffness of meniscal attachments and meniscal material properties affect tibio-femoral contact pressure computed using a validated finite element model of the human knee joint. *Journal of Biomechanics*, *36*(1), 19–34. https://doi.org/10.1016/S0021-9290(02)00305-6

Heckmann, T. P., Barber-Westin, S. D., & Noyes, F. R. (2006). Meniscal repair and transplantation: Indications, techniques, rehabilitation, and clinical outcome. *Journal of Orthopaedic and Sports Physical Therapy, 36*(10), 795–814. https://doi.org/10.2519/jospt.2006.2177

Hede, A., Jensen, D. B., Blyme, P., Sonne-Holm, S., & Sonne, S. (1990). Epidemiology of meniscal lesions in the knee: 1,215 open operations in copenhagen 1982-84. *Acta Orthopaedica Scandinavica*, *61*(5), 435–437. https://doi.org/10.3109/17453679008993557

Hergan, D., Thut, D., Sherman, O., & Day, M. S. (2011). Meniscal allograft transplantation. *Arthroscopy - Journal of Arthroscopic and Related Surgery*, *27*(1), 101–112. https://doi.org/10.1016/j.arthro.2010.05.019

Hershman, E. B., Jarvis, J. L., Mick, T., Dushaj, K., & Elsner, J. J. (2020). Direct treatment cost outcomes among patients with medial meniscus deficiency: results from a 24-month surveillance study. *Current Medical Research and Opinion*, *36*(3), 427-437.

Hirokawa, S., & Tsuruno, R. (1997). Hyper-elastic model analysis of anterior cruciate ligament. *Medical Engineering Physics, 19*(7), 637-651.

Hjartarson, H. F., & Toksvig-Larsen, S. (2018). The clinical effect of an unloader brace on patients with osteoarthritis of the knee, a randomized placebo controlled trial with one year follow up. *BMC Musculoskeletal Disorders*, *19*(1). https://doi.org/10.1186/s12891-018-2256-7

Hochberg, M. C., Lawrence, R. C., Everett, D. F., & Cornoni-Huntley, J. (1989). Epidemiologic associations of pain in osteoarthritis of the knee: Data from the national health and nutrition examination survey and the national health and nutrition examination-i epidemiologic follow-up survey. *Seminars in Arthritis and Rheumatism*, *18*(4), 4–9. https://doi.org/10.1016/0049-0172(89)90008-5

Hollis, J. M., Pearsall IV, A. W., & Niciforos, P. G. (2000). Change in meniscal strain with anterior cruciate ligament injury and after reconstruction. *American Journal of Sports Medicine*, *28*(5), 700–704. https://doi.org/10.1177/03635465000280051401

Hori, R. Y., & Mockros, L. F. (1976). Indentation tests of human articular cartilage. *Journal of Biomechanics*, *9*(4), 259-268.

Horlick, S. G., & Loomer, R. L. (1993). Valgus knee bracing for medial gonarthrosis.pdf. *Clinical Journal of Sport Medicine*, *3*(4), 251–255.

Irwin, A. L., Mertz, H. J., Elhagediab, A. M., & Moss, S. (2002). Guidelines for assessing the biofidelity of side impact dummies of various sizes and ages. *46th Stapp Car Crash Conference (2002), 2002-22-0016*.

Ivarsson, B. J., Genovese, D., Crandall, J. R., Bolton, J. R., Untaroiu, C. D., & Bose, D. (2009). The tolerance of the femoral shaft in combined axial compression and bending loading. *Stapp Car Crash Journal, 53*, 251–290.

Jeffcote, B., Nicholls, R., Schirm, A., & Kuster, M. S. (2007). The variation in medial and lateral collateral ligament strain and tibiofemoral forces following changes in the flexion and extension gaps in total knee replacement: a laboratory experiment using cadaver knees. *The Journal of Bone & Joint Surgery British Volume*, *89*(11), 1528–1533.

Johnson, J. E., Fischer, K. J., & McIff, T. E. (2008). Peripheral Nerve Strain: A Comparison of Strain Measuring Techniques. *Summer Bioengineering Conference, 43215*, 627-628.

Jones, J. C., Burks, R., Owens, B. D., Sturdivant, R. X., Svoboda, S. J., & Cameron, K. L. (2012). Incidence and risk factors associated with meniscal injuries among active-duty US Military service members. *Journal of Athletic Training*, *47*(1), 67–73. https://doi.org/10.4085/1062-6050-47.1.67

Jones, R. K., Nester, C. J., Richards, J. D., Kim, W. Y., Johnson, D. S., Jari, S., Laxton, P., & Tyson, S. F. (2013). A comparison of the biomechanical effects of valgus knee braces and lateral wedged insoles in patients with knee osteoarthritis. *Gait and Posture*, *37*(3), 368–372. https://doi.org/10.1016/j.gaitpost.2012.08.002

Jones, R. S., Keene, G. C. R., Learmonth, D. J. A., Bickerstaff, D., Nawana, N. S., Costi, J. J., & Pearcy, M. J. (1996). Direct measurement of hoop strains in the intact and torn human medial meniscus. *Clinical Biomechanics*, *11*(5), 295–300. https://doi.org/10.1016/0268-0033(96)00003-4

Kang, K. T., Koh, Y. G., Son, J., Kim, S. J., Choi, S., Jung, M., & Kim, S. H. (2017). Finite element analysis of the biomechanical effects of 3 posterolateral corner reconstruction techniques for the knee joint. *Arthroscopy: The Journal of Arthroscopic & Related Surgery*, *33*(8), 1537-1550.

Kennedy, J. C., Hawkins, R. J., Willis, R., & Danylchuck, K. D. (1976). Tension studies of human knee ligaments. Yield point, ultimate failure, and disruption of the cruciate and tibial collateral ligaments. JBJS, *58*(3), 350-355.

Kerrigan, J. R., Bhalla, K. S., Madeley, N. J., Funk, J. R., Bose, D., & Crandall, J. R. (2003). Experiments for establishing pedestrian-impact lower limb injury criteria. *SAE 2003 World Congress & Exhibition, 2003-01-0895*.

Kerrigan, J. R., Drinkwater, D. C., Kam, C. Y., Murphy, D. B., Ivarsson, B. J., Crandall, J. R., & Patrie, J. (2004). Tolerance of the human leg and thigh in dynamic latero-medial bending. *International Journal of Crashworthiness*, *9*(6), 607-623.

Keyak, J. H., Rossi, S. A., Jones, K. A., & Skinner, H. B. (1997). Prediction of femoral fracture load using automated finite element modeling. *Journal of biomechanics*, *31*(2), 125-133.

Khor, F., Cronin, D. S., Watson, B., Gierczycka, D., & Malcolm, S. (2018). Importance of asymmetry and anisotropy in predicting cortical bone response and fracture using human body model femur in three-point bending and axial rotation. *Journal of the mechanical behavior of biomedical materials*, *87*, 213-229.

Kiapour, A., Kiapour, A. M., Kaul, V., Quatman, C. E., Wordeman, S. C., & Hewett, T. E. (2014). Finite element model of the knee for investigation of injury mechanisms: Development and validation. *Journal of Biomechanical Engineering*, *136*(1), 011002. https://doi.org/10.1115/1.4025692

Kilcoyne, K. G., Dickens, J. F., Haniuk, E., Cameron, K. L., & Owens, B. D. (2012). Epidemiology of meniscal injury associated with ACL tears in young athletes. *Orthopedics*, *35*(3), 208–212. https://doi.org/10.3928/01477447-20120222-07

Kim, H.-Y. (2013). Statistical notes for clinical researchers: assessing normal distribution (2) using skewness and kurtosis. *Restorative Dentistry & Endodontics*, *38*(1), 52–54.

Kirkley, A., Webster-Bogaert, S., Litchfield, R., Amendola, A., MacDonald, S., McCalden, R., & Fowler, P. (1999). The effect of bracing on varus gonarthrosis. *Journal of Bone and Joint Surgery*, *81*(4), 539–548. https://doi.org/10.2106/00004623-199904000-00012

Kolaczek, S., Hewison, C., Caterine, S., Ragbar, M. X., Getgood, A., & Gordon, K. D. (2016). Analysis of 3D strain in the human medial meniscus. *Journal of the Mechanical Behavior of Biomedical Materials*, *63*, 470–475. https://doi.org/10.1016/j.jmbbm.2016.06.001

Komdeur, P., Pollo, F. E., & Jackson, R. W. (2002, July). Dynamic knee motion in anterior cruciate impairment: a report and case study. *Baylor University Medical Center Proceedings, 15*(3), 257-259.

Konopka, J. A., Finlay, A. K., Eckstein, F., & Dragoo, J. L. (2021). Effects of unloader bracing on clinical outcomes and articular cartilage regeneration following microfracture of isolated chondral defects: a randomized trial. *Knee Surgery, Sports Traumatology, Arthroscopy*, *29*, 2889-2898.

Kovacs, E., Birmingham, T., & Kirkley, A. (2002). Nonsurgical Options for the Post-Meniscectomy Knee. *Sports Medicine and Arthroscopy Review*, *10*(4), 244–252.

Kozak, M., & Piepho, H. P. (2018). What's normal anyway? Residual plots are more telling than significance tests when checking ANOVA assumptions. *Journal of Agronomy and Crop Science*, *204*(1), 86–98.

Kutzner, I., Küther, S., Heinlein, B., Dymke, J., Bender, A., Halder, A. M., & Bergmann, G. (2011). The effect of valgus braces on medial compartment load of the knee joint - in vivo load measurements in three subjects. *Journal of Biomechanics*, *44*(7), 1354–1360. https://doi.org/10.1016/j.jbiomech.2011.01.014

Kwon, O. R., Kang, K. T., Son, J., Kwon, S. K., Jo, S. B., Suh, D. S., Choi, Y. J., Kim, H. J., & Koh, Y. G. (2014). Biomechanical comparison of fixed- and mobile-bearing for unicomparmental knee arthroplasty using finite element analysis. *Journal of Orthopaedic Research*, *32*(2), 338–345. https://doi.org/10.1002/jor.22499

Lai, J. H., & Levenston, M. E. (2010). Meniscus and cartilage exhibit distinct intra-tissue strain distributions under unconfined compression. *Osteoarthritis and cartilage*, *18*(10), 1291-1299.

Laible, C., Stein, D. A., & Kiridly, D. N. (2013). Meniscal repair. *Journal of the American Academy of Orthopaedic Surgeons,* *21*(4), 204–213. https://doi.org/10.5435/JAAOS-21-04-204

Lamberg, E. M., Streb, R., Werner, M., Kremenic, I., & Penna, J. (2016). The 2-and 8-week effects of decompressive brace use in people with medial compartment knee osteoarthritis. *Prosthetics and Orthotics International*, *40*(4), 447-453.

LaPrade, C. M., James, E. W., Cram, T. R., Feagin, J. A., Engebretsen, L., & Laprade, R. F. (2014). Meniscal Root Tears: A Classification System Based on Tear Morphology. *The American Journal of Sports Medicine*, *43*(2), 363–369. https://doi.org/10.1177/0363546514559684

LaPrade, C. M., Jansson, K. S., Dornan, G., Smith, S. D., Wijdicks, C. A., & LaPrade, R. F. (2014). Altered tibiofemoral contact mechanics due to lateral meniscus posterior horn root avulsions and radial tears can be restored with in situ pull-out suture repairs. *JBJS*, *96*(6), 471-479.

Laroche, D., Morisset, C., Fortunet, C., Gremeaux, V., Maillefert, J. F., & Ornetti, P. (2014). Biomechanical effectiveness of a distraction-rotation knee brace in medial knee osteoarthritis: Preliminary results. *Knee*, *21*(3), 710–716. https://doi.org/10.1016/j.knee.2014.02.015

Laubenthal, K. N., Smidt, G. L., & Kettelkamp, D. B. (1972). A Quantatitive Analysis of Knee Motion Dring Activities of Daily Liviing. *Physical Therapy*, *52*(1), 34–43. https://academic.oup.com/ptj/article/52/1/34/4589163

Lechner, K., Hull, M. L., & Howell, S. M. (2000). Is the circumferential tensile modulus within a human medial meniscus affected by the test sample location and cross-sectional area?. *Journal of orthopaedic research*, *18*(6), 945-951.

Lee, G.-C. (2016). What's new in adult reconstructive knee surgery. *Journal of Bone and Joint Surgery – American Volume,* *98*(2), 156–165. https://doi.org/10.2106/JBJS.17.01148

LeRoux, M. A., & Setton, L. A. (2002). Experimental and biphasic FEM determinations of the material properties and hydraulic permeability of the meniscus in tension. *Journal of Biomechanical Engineering*, *124*(3), 315–321. https://doi.org/10.1115/1.1468868

Levin, S. D., Wellman, D. S., Liu, C., Li, Y., Ren, Y., Shah, N. A., & Zhang, L. Q. (2013). Biomechanical strain characteristics of soft tissue biceps tenodesis and bony tenodesis. *Journal of Orthopaedic Science*, *18*, 699-704.

Levine, J. W., Kiapour, A. M., Quatman, C. E., Wordeman, S. C., Goel, V. K., Hewett, T. E., & Demetropoulos, C. K. (2013). Clinically relevant injury patterns after an anterior cruciate ligament injury provide insight into injury mechanisms. *American Journal of Sports Medicine*, *41*(2), 385–395. https://doi.org/10.1177/0363546512465167

Li, G., Lopez, O., & Rubash, H. (2001). Variability of a Three-Dimensional Finite Element Model Constructed Using Magnetic Resonance Images of a Knee for Joint Contact Stress Analysis. *Journal of Biomechanical Engineering*, *123*(4), 341–346. https://doi.org/10.1115/1.1385841

Lin, C.-H., Hortin, M., & Irwin, A. (2018). Using Human Body Models to Assess Knee Ligament Injury in Knee Hyperextension. *SAE Technical Paper Series*, *1*, 15–17. https://doi.org/10.4271/sc18-22-0005

Lindenfeld, T. N., Hewett, T. E., & Andriacchi, T. P. (1997). Joint Loading With Valgus Bracing in Patientgs With Varus Gonarthrosis. *Clinical Orthopaedics and Related Research*, *344*, 290–297.

Lohmander, L. S., Englund, P. M., Dahl, L. L., & Roos, E. M. (2007). The long-term consequence of anterior cruciate ligament and meniscus injuries: Osteoarthritis. *American Journal of Sports Medicine,* *35*(10), 1756–1769. https://doi.org/10.1177/0363546507307396

Lu, X. L., & Mow, V. C. (2008). Biomechanics of articular cartilage and determination of material properties. *Medicine & Science in Sports & Exercise*, *40*(2), 193-199.

Łuczkiewicz, P., Daszkiewicz, K., Chróścielewski, J., Witkowski, W., & Winklewski, P. J. (2016). The influence of articular cartilage thickness reduction on meniscus biomechanics. *PloS One*, *11*(12), e0167733.

Majewski, M., Susanne, H., & Klaus, S. (2006). Epidemiology of athletic knee injuries: A 10-year study. *The Knee*, *13*(3), 184–188. https://doi.org/10.1016/j.knee.2006.01.005

Maletis, G. B., Granan, L. P., Inacio, M. C. S., Funahashi, T. T., & Engebretsen, L. (2011). Comparison of community-based ACL reconstruction registries in the U.S. and Norway. *The Journal of Bone and Joint Surgery. American Volume*, *93*(Supplement 3), 31–36. https://doi.org/10.2106/JBJS.K.00905

Maletsky, L. P., & Hillberry, B. M. (2005). Simulating dynamic activities using a five-axis knee simulator. *Journal of Biomechanical Engineering*, *127*(1), 123-133.

Markolf, K. L., O'Neill, G., Jackson, S. R., & McAllister, D. R. (2004). Effects of applied quadriceps and hamstrings muscle loads on forces in the anterior and posterior cruciate ligaments. *American Journal of Sports Medicine*, *32*(5), 1144–1149. https://doi.org/10.1177/0363546503262198

Marshall, S. W., Hamstra-Wright, K. L., Dick, R., Grove, K. A., & Agel, J. (2007). Descriptive Epidemiology of Collegiate Women's Softball Injuries: National Collegiate Athletic Association Injury Surveillance System, 1988–1989 Through 2003–2004. *Journal of Athletic Training*, *42*(2), 286. https://doi.org/10.1016/s0276-1092(08)79204-6

Martens, T. A., Hull, M. L., & Howell, S. M. (1997). An in vitro osteotomy method to expose the medial compartment of the human knee. *Journal of Biomechanical Engineering, 119,* 379–385.

Mather, R. C., Koenig, L., Kocher, M. S., Dall, T. M., Gallo, P., Scott, D. J., Bach, B. R., & Spindler, K. P. (2013). Societal and economic impact of anterior cruciate ligament tears. *Journal of Bone and Joint Surgery*, *95*(19), 1751–1759. https://doi.org/10.2106/JBJS.L.01705

Matsuda, S., White, S. E., Williams, V. G., McCarthy, D. S., & Whiteside, L. A. (1998). Contact stress analysis in meniscal bearing total knee arthroplasty. *Journal of Arthroplasty*, *13*(6), 699–706. https://doi.org/10.1016/S0883-5403(98)80016-8

Matsuno, H., Kadowaki, K. M., & Tsuji, H. (1997). Generation II knee bracing for severe medial compartment osteoarthritis of the knee. *Archives of Physical Medicine and Rehabilitation*, *78*(7), 745–749. https://doi.org/10.1016/S0003-9993(97)90083-6

Maynard, M. J., Deng, X., Wickiewicz, T. L., & Warren, R. F. (1996). The popliteofibular ligament: Rediscovery of a key element in posterolateral stability. *American Journal of Sports Medicine*, *24*(3), 311–316. https://doi.org/10.1177/036354659602400311

McGibbon, C. A., Brandon, S., Bishop, E. L., Cowper-Smith, C., & Biden, E. N. (2021). Biomechanical study of a tricompartmental unloader brace for patellofemoral or multicompartment knee osteoarthritis. *Frontiers in Bioengineering and Biotechnology*, *8*, 1-15.

McLean, C. A., & Ahmed, A. M. (1993). Design and development of an unconstrained dynamic knee simulator. *Journal of Biomechanical Engineering*, *115*(2), 144-148.

Mistry, D. A., Chandratreya, A., & Lee, P. Y. (2018). An update on unloading knee braces in the treatment of unicompartmental knee osteoarthritis from the last 10 years: a literature review. *The Surgery Journal*, *4*(03), e110-e118.

Moglo, K. E., & Shirazi-Adl, A. (2003). Biomechanics of passive knee joint in drawer: load transmission in intact and ACL-deficient joints. *The Knee*, *10*(3), 265–276. https://doi.org/10.1016/S0968-0160(02)00135-7

Mohamad Nor, N. M., Osman, N. A. A., & Atalullah Oshkour. (2012). Numerical measurement of contact pressure in the tibiofemoral joint during gait. *2012 International Conference on Biomedical Engineering, IcoBE 2012*, 38–43. https://doi.org/10.1109/IcoBE.2012.6178951

Mononen, M. E., Jurvelin, J. S., & Korhonen, R. K. (2013). Effects of radial tears and partial meniscectomy of lateral meniscus on the knee joint mechanics during the stance phase of the gait cycle—A 3D finite element study. *Journal of Orthopaedic Research*, *31*(8), 1208–1217. https://doi.org/10.1002/JOR.22358

Mordecai, S. C., Al-Hadithy, N., Ware, H. E., & Gupte, C. M. (2014). Treatment of meniscal tears: An evidence based approach. *World Journal of Orthopedics*, *5*(3), 233–241. https://doi.org/10.5312/wjo.v5.i3.233

Moyer, R. F., Birmingham, T. B., Bryant, D. M., Giffin, J. R., Marriott, K. A., & Leitch, K. M. (2015). Biomechanical effects of valgus knee bracing: A systematic review and meta-analysis. *Osteoarthritis and Cartilage, 23*(2), 178–188. https://doi.org/10.1016/j.joca.2014.11.018

Mündermann, A., Dyrby, C. O., D'Lima, D. D., Colwell, C. W., & Andriacchi, T. P. (2008). In vivo knee loading characteristics during activities of daily living as measured by an instrumented total knee replacement. *Journal of Orthopaedic Research*, *26*(9), 1167–1172. https://doi.org/10.1002/JOR.20655

Munro, A., Herrington, L., & Comfort, P. (2017). The relationship between 2-dimensional knee-valgus angles during single-leg squat, single-leg-land, and drop-jump screening tests. *Journal of Sport Rehabilitation*, *26*(1), 72–77. https://doi.org/10.1123/jsr.2015-0102

Naga, V., Karnati, P., Mohammed, A., Mohammed, A., & Maddirala, R. (2015). A review on positive effects of exercise in osteoarthritis. *European International Journal of Science and Technology*, *4*(6), 124–139. www.eijst.org.uk

Nagai, K., Yang, S., Fu, F. H., & Anderst, W. (2019). Unloader knee brace increases medial compartment joint space during gait in knee osteoarthritis patients. *Knee Surgery, Sports Traumatology, Arthroscopy*, *27*, 2354-2360.

Neville, S. R., Brandon, S. C., Brown, M. J., & Deluzio, K. J. (2018). Validation of method for analysing mechanics of unloader brace for medial knee osteoarthritis. *Journal of Biomechanics*, *76*, 253-258.

Nielsen, A. B., & Yde, J. (1991). Nielsen 1991 – Epidemiology of acute knee injuries a prospective hospital investigation.pdf. *The Journal of Trauma*, *31*(12), 1644–1648.

Orishimo, K. F., Kremenic, I. J., Lee, S. J., McHugh, M. P., & Nicholas, S. J. (2013). Is valgus unloader bracing effective in normally aligned individuals: implications for post-surgical protocols following cartilage restoration procedures. *Knee Surgery, Sports Traumatology, Arthroscopy*, *21*, 2661-2666.

Ostermeier, S., Holst, M., Hurschler, C., Windhagen, H., & Stukenborg-Colsman, C. (2007). Dynamic measurement of patellofemoral kinematics and contact pressure after lateral retinacular release: an in vitro study. *Knee Surgery, Sports Traumatology, Arthroscopy*, *15*, 547-554.

Ostrander, R. V, Leddon, C. E., Hackel, J. G., O'Grady, C. P., & Roth, C. A. (2016). Efficacy of Unloader Bracing in Reducing Symptoms of Knee Osteoarthritis. *American Journal of Orthopedics (Belle Mead, N.J.)*, *45*(5), 306–311.

Padalecki, J. R., Jansson, K. S., Smith, S. D., Dornan, G. J., Pierce, C. M., Wijdicks, C. A., & Laprade, R. F. (2014). Biomechanical consequences of a complete radial tear adjacent to the medial meniscus posterior root attachment site: In situ pull-out repair restores derangement of joint mechanics. *American Journal of Sports Medicine*, *42*(3), 699–707. https://doi.org/10.1177/0363546513499314

Park, S., Lee, S., Yoon, J., & Chae, S. W. (2019). Finite element analysis of knee and ankle joint during gait based on motion analysis. *Medical Engineering and Physics*, *63*, 33–41. https://doi.org/10.1016/j.medengphy.2018.11.003

Parween, R., Shriram, D., Mohan, R. E., Lee, Y. H. D., & Subburaj, K. (2019). Methods for evaluating effects of unloader knee braces on joint health: a review. *Biomedical Engineering Letters, 9*(2), 153–168. https://doi.org/10.1007/s13534-019-00094-z

Paterno, M. V, Rauh, M. J., Schmitt, L. C., Ford, K. R., & Hewett, T. E. (2014). Incidence of second ACL injuries 2 years after primary ACL reconstruction and return to sport. *American Journal of Sports Medicine*, *42*(7), 1567–1573. https://doi.org/10.1177/0363546514530088

Paulos, L., Noyes, F. R., Grood, E., & Butler, D. L. (1991). Knee rehabilitation after anterior cruciate ligament reconstruction and repair. *The Journal of Orthopaedic and Sports Physical Therapy*, *13*(2), 60–70. https://doi.org/10.1177/036354658100900303

Pearsall IV, A. W., & Hollis, J. M. (2004). The effect of posterior cruciate ligament injury and reconstruction on meniscal strain. *American Journal of Sports Medicine*, *32*(7), 1675–1680. https://doi.org/10.1177/0363546504265937

Peña, E., Calvo, B., Martínez, M. A., & Doblaré, M. (2006). A three-dimensional finite element analysis of the combined behavior of ligaments and menisci in the healthy human knee joint. *Journal of Biomechanics*, *39*(9), 1686–1701. https://doi.org/10.1016/j.jbiomech.2005.04.030

Peña, E., Calvo, B., Martínez, M. A., & Doblaré, M. (2007). Effect of the size and location of osteochondral defects in degenerative arthritis. A finite element simulation. *Computers in Biology and Medicine*, *37*(3), 376–387. https://doi.org/10.1016/j.compbiomed.2006.04.004

Peña, E., Calvo, B., Martínez, M. A., Palanca, D., & Doblaré, M. (2005). Finite element analysis of the effect of meniscal tears and meniscectomies on human knee biomechanics. *Clinical Biomechanics*, *20*(5), 498–507. https://doi.org/10.1016/j.clinbiomech.2005.01.009

Petersen, W., Ellermann, A., Henning, J., Nehrer, S., Rembitzki, I. V., Fritz, J., ... & Liebau, C. (2019). Non-operative treatment of unicompartmental osteoarthritis of the knee: a prospective randomized trial with two different braces—ankle–foot orthosis versus knee unloader brace. *Archives of orthopaedic and trauma surgery*, *139*(2), 155-166.

Pfeiffer, S. J., Valentine, J. A., Goodwin, J. S., Nissman, D. B., Blackburn, T., & Pietrosimone, B. (2019). Effects of a knee valgus unloader brace on medial femoral articular cartilage deformation following walking in varus-aligned individuals. *The Knee*, *26*(5), 1067-1072.

Polak, A. (2019). *ACL Strain During Single-Leg Jump Landing: An Experimental and Computational Investigation* [Master's thesis, University of Waterloo]. UWSpace. http://hdl.handle.net/10012/14339

Pollo, F. E., & Jackson, R. W. (2006). Knee bracing for unicompartmental osteoarthritis. *Journal of the American Academy of Orthopaedic Surgeons*, *14*(1), 5–11. https://doi.org/10.5435/00124635-200601000-00003

Pollo, F. E., Otis, J. C., Backus, S. I., Warren, R. F., & Wickiewicz, T. L. (2002). The American Journal of Sports Medicine Reduction of Medial Compartment Loads with Valgus Bracing of the Osteoarthritic Knee. *American Orthopaedic Society for Sports Medicine*, *30*(3), 414–421. https://journals.sagepub.com/doi/pdf/10.1177/03635465020300031801

Prodromos, C. C., Han, Y., Rogowski, J., Joyce, B., & Shi, K. (2007). A Meta-analysis of the Incidence of Anterior Cruciate Ligament Tears as a Function of Gender, Sport, and a Knee Injury-Reduction Regimen. *Arthroscopy - Journal of Arthroscopic and Related Surgery*, *23*(12), 1320–1325. https://doi.org/10.1016/j.arthro.2007.07.003

Race, A., & Amis, A. A. (1994). The mechanical properties of the two bundles of the human posterior cruciate ligament. *Journal of Biomechanics*, *27*(1), 13–24. https://doi.org/10.1016/0021-9290(94)90028-0

Ramaniraka, N. A., Terrier, A., Theumann, N., & Siegrist, O. (2005). Effects of the posterior cruciate ligament reconstruction on the biomechanics of the knee joint: A finite element analysis. *Clinical Biomechanics*, *20*(4), 434–442. https://doi.org/10.1016/j.clinbiomech.2004.11.014

Ramsey, D. K., Briem, K., Axe, M. J., & Snyder-Mackler, L. (2007). A mechanical theory for the effectiveness of bracing for medial compartment osteoarthritis of the knee. *Journal of Bone and Joint Surgery*, *89*(11), 2398–2407. https://doi.org/10.2106/JBJS.F.01136

Ramsey, D. K., & Russell, M. E. (2009). Unloader braces for medial compartment knee osteoarthritis: Implications on mediating progression. *Sports Health, 1*(5), 416–426. https://doi.org/10.1177/1941738109343157

Rannou, F., Poiraudeau, S., & Beaudreuil, J. (2010). Role of bracing in the management of knee osteoarthritis. *Current Opinion in Rheumatology*, *22*(2), 218–222. https://doi.org/10.1097/BOR.0b013e32833619c4

Rao, A. J., Erickson, B. J., Cvetanovich, G. L., Yanke, A. B., Bach, B. R., & Cole, B. J. (2015). The Meniscus-Deficient Knee: Biomechanics, Evaluation, and Treatment Options. *Orthopaedic Journal of Sports Medicine, 3*(10), 1–14. https://doi.org/10.1177/2325967115611386

Repo, R. U., & Finlay, J. B. (1977). Survival of articular cartilage after controlled impact. *Journal of Bone and Joint Surgery - Series A*, *59*(8), 1068–1076. https://doi.org/10.2106/00004623-197759080-00012

Richard, F., Villars, M., & Thibaud, S. (2013). Viscoelastic modeling and quantitative experimental characterization of normal and osteoarthritic human articular cartilage using indentation. *Journal of the mechanical behavior of biomedical materials*, *24*, 41-52.

Richard Steadman, J., Briggs, K. K., Pomeroy, S. M., & Wijdicks, C. A. (2016). Current state of unloading braces for knee osteoarthritis. *Knee Surgery, Sports Traumatology, Arthroscopy, 24*, 42–50. https://doi.org/10.1007/s00167-014-3305-x

Robinson, J. R., Bull, A. M. J., & Amis, A. A. (2005). Structural properties of the medial collateral ligament complex of the human knee. *Journal of Biomechanics*, *38*(5), 1067–1074. https://doi.org/10.1016/j.jbiomech.2004.05.034

Roos, E. M., Roos, H. P., Lohmander, L. S., Ekdahl, C., & Beynnon, B. D. (1998). Knee Injury and Osteoarthritis Outcome Score (KOOS)—development of a self-administered outcome measure. *Journal of Orthopaedic & Sports Physical Therapy*, *28*(2), 88-96.

Røtterud, J. H., Sivertsen, E. A., Forssblad, M., Engebretsen, L., & Årøen, A. (2013). Effect of meniscal and focal cartilage lesions on patient-reported outcome after anterior cruciate ligament reconstruction: A nationwide cohort study from norway and sweden of 8476 patients with 2-year follow-up. *American Journal of Sports Medicine*, *41*(3), 535–543. https://doi.org/10.1177/0363546512473571

Rupp, J. D., Reed, M. P., Madura, N. H., Kuppa, S., & Schneider, L. W. (2003, May). Comparison of knee/femur force-deflection response of the THOR, hybrid III, and human cadaver to dynamic frontal impact knee loading. *Proceedings of the 18th Internationals Conference of Experimental Safety Vehicles. National Highway Traffic Safety Administration, Washington DC*, 1–9.

Rupp, J. D., Reed, M. P., Van Ee, C. A., Kuppa, S., Wang, S. C., Goulet, J. A., & Schneider, L. W. (2002). The tolerance of the human hip to dynamic knee loading. *Stapp Car Crash Journal, 46,* 211–228.

Saeidi, M., Kelly, P. A., Netzel, C., Scadeng, M., Kumar, P., Prendergast, D., Neitzert, T., & Ramezani, M. (2021). Preliminary biomechanical cadaver study investigating a new load-sharing knee implant. *Journal of Experimental Orthopaedics*, *8*(1), 1–13. https://doi.org/10.1186/s40634-021-00379-2

Samson, D. J., Grant, M. D., Ratko, T. A., Bonnell, C. J., Ziegler, K. M., & Aronson, N. (2007). Treatment of primary and secondary osteoarthritis of the knee. *Evidence report/technology assessment, 157*, 1–157. http://europepmc.org/books/NBK38385

Sanders, T. L., Pareek, A., Kremers, H. M., Bryan, A. J., Levy, B. A., Stuart, M. J., Dahm, D. L., & Krych, A. J. (2017). Long-term follow-up of isolated ACL tears treated without ligament reconstruction. *Knee Surgery, Sports Traumatology, Arthroscopy*, *25*(2), 493–500. https://doi.org/10.1007/s00167-016-4172-4

Sarraj, M., Coughlin, R. P., Solow, M., Ekhtiari, S., Simunovic, N., Krych, A. J., MacDonald, P., & Ayeni, O. R. (2019). Anterior cruciate ligament reconstruction with concomitant meniscal surgery: a systematic review and meta-analysis of outcomes. *Knee Surgery, Sports Traumatology, Arthroscopy*, *27*(11), 3441–3452. https://doi.org/10.1007/s00167-019-05389-3

Schillhammer, C. K., Werner, F. W., Scuderi, M. G., & Cannizzaro, J. P. (2012). Repair of lateral meniscus posterior horn detachment lesions: A biomechanical evaluation. *American Journal of Sports Medicine*, *40*(11), 2604–2609. https://doi.org/10.1177/0363546512458574

Schmalz, T., Knopf, E., Drewitz, H., & Blumentritt, S. (2010). Analysis of biomechanical effectiveness of valgus-inducing knee brace for osteoarthritis of knee. *Journal of Rehabilitation Research and Development*, *47*(5), 419–430. https://doi.org/10.1682/JRRD.2009.05.0067

Schmitt, L. C., Fitzgerald, G. K., Reisman, A. S., & Rudolph, K. S. (2008). Instability, Laxity, and Physical Function in Patients With Medial Knee Osteoarthritis. *Physical Therapy*, *88*(12), 1506–1516. https://doi.org/10.2522/ptj.20060223

Schmitt, K. U., Niederer, P. F., Cronin, D. S., Morrison III, B., Muser, M. H., & Walz, F. (2019). Trauma biomechanics: an introduction to injury biomechanics. Springer.

Seil, R., & Becker, R. (2016). Time for a paradigm change in meniscal repair: save the meniscus! *Knee Surgery, Sports Traumatology, Arthroscopy, 24*(5), 1421–1423. https://doi.org/10.1007/s00167-016-4127-9

Seitz, A. M., Lubomierski, A., Friemert, B., Ignatius, A., & Dürselen, L. (2012). Effect of partial meniscectomy at the medial posterior horn on tibiofemoral contact mechanics and meniscal hoop strains in human knees. *Journal of Orthopaedic Research*, *30*(6), 934–942. https://doi.org/10.1002/jor.22010

Seitz, A. M., Schall, F., Hacker, S. P., van Drongelen, S., Wolf, S., & Dürselen, L. (2021). Forces at the Anterior Meniscus Attachments Strongly Increase Under Dynamic Knee Joint Loading. *American Journal of Sports Medicine*, *49*(4), 994–1004. https://doi.org/10.1177/0363546520988039

Self, B. P., Greenwald, R. M., & Pflaste, D. S. (2000). A biomechanical analysis of a medial unloading brace for osteoarthritis in the knee. *Arthritis Care and Research*, *13*(4), 191–197. https://doi.org/10.1002/1529-0131(200008)13:4<191::aid-anr3>3.0.co;2-c

Shabani, B., Bytyqi, D., Lustig, S., Cheze, L., Bytyqi, C., & Neyret, P. (2015). Gait changes of the ACL-deficient knee 3D kinematic assessment. *Knee Surgery, Sports Traumatology, Arthroscopy*, *23*(11), 3259–3265. https://doi.org/10.1007/S00167-014-3169-0/FIGURES/1

Shea, K. G., Pfeiffer, R., Wang, J. H., Curtin, M., & Apel, P. J. (2004). Anterior Cruciate Ligament Injury in Pediatric and Adolescent Soccer Players: An Analysis of Insurance Data. *Journal of Pediatric Orthopaedics*, *24*(6), 623–628. https://doi.org/10.1097/00004694-200411000-00005

Shefelbine, S. J., Ma, C. B., Lee, K. Y., Schrumpf, M. A., Patel, P., Safran, M. R., ... & Majumdar, S. (2006). MRI analysis of in vivo meniscal and tibiofemoral kinematics in ACL-deficient and normal knees. *Journal of orthopaedic research*, *24*(6), 1208-1217.

Shepherd, D. E., & Seedhom, B. B. (1999). The 'instantaneous' compressive modulus of human articular cartilage in joints of the lower limb. *Rheumatology*, *38*(2), 124-132.

Sherman, M. A., Seth, A., & Delp, S. L. (2013). What is a moment arm? Calculating muscle effectiveness in biomechanical models using generalized coordinates. *International design engineering technical conferences and computers and information in engineering conference, 55973,* 1–18.

Shriram, D., Praveen Kumar, G., Cui, F., Lee, Y. H. D., & Subburaj, K. (2017). Evaluating the effects of material properties of artificial meniscal implant in the human knee joint using finite element analysis. *Scientific Reports 2017*, *7*(6011), 1–11.

Shriram, D., Yamako, G., Chosa, E., Lee, Y. H. D., & Subburaj, K. (2019). Effects of a valgus unloader brace in the medial meniscectomized knee joint: A biomechanical study. *Journal of Orthopaedic Surgery and Research*, *14*(1), 1–13. https://doi.org/10.1186/s13018-019-1085-1

Slauterbeck, J. R., Kousa, P., Clifton, B. C., Naud, S., Tourville, T. W., Johnson, R. J., & Beynnon, B. D. (2009). Geographic mapping of meniscus and cartilage lesions associated with anterior cruciate ligament injuries. *Journal of Bone and Joint Surgery*, *91*(9), 2094–2103. https://doi.org/10.2106/JBJS.H.00888

Śmigielski, R., Becker, R., Zdanowicz, U., & Ciszek, B. (2015). Medial meniscus anatomy—from basic science to treatment. *Knee Surgery, Sports Traumatology, Arthroscopy*, *23*, 8-14.

Stamenović, D., Kojić, M., Stojanović, B., & Hunter, D. (2008). A finite element analysis of an osteoarthritis knee brace. *Journal of the Serbian Society for Computational Mechanics*, *2*(2), 29–41. https://www.researchgate.net/publication/234015993

Stamenović, D., Kojić, M., Stojanović, B., & Hunter, D. (2009). Pneumatic osteoarthritis knee brace. *Journal of Biomechanical Engineering*, *131*(4), 045001-1–6. https://doi.org/10.1115/1.3072890

Stephen, J. M., Halewood, C., Kittl, C., Bollen, S. R., Williams, A., & Amis, A. A. (2016). Posteromedial meniscocapsular lesions increase tibiofemoral joint laxity with anterior cruciate ligament deficiency, and their repair reduces laxity. *The American journal of sports medicine*, *44*(2), 400-408.

Spilker, R. L., Donzelli, P. S., & Mow, V. C. (1992). A transversely isotropic biphasic finite element model of the meniscus. *Journal of Biomechanics*, *25*(9), 1027–1045. https://doi.org/10.1016/0021-9290(92)90038-3

Stukenborg-Colsman, C., Ostermeier, S., Hurschler, C., & Wirth, C. J. (2002). Tibiofemoral contact stress after total knee arthroplasty Comparison of fixed and mobile-bearing inlay designs. *Acta Orthop*, *73*(6), 638–646.

Sugita, T., & Amis, A. A. (2001). Anatomic and biomechanical study of the lateral collateral and popliteofibular ligaments. *American Journal of Sports Medicine*, *29*(4), 466–472. https://doi.org/10.1177/03635465010290041501

Szivek, J. A., Anderson, P. L., & Benjamin, J. B. (1996). Average and peak contact stress distribution evaluation of total knee arthroplasties. *Journal of Arthroplasty*, *11*(8), 952–963. https://doi.org/10.1016/S0883-5403(96)80137-9

Szivek, J. A., Cutignola, L., & Volz, R. G. (1995). Tibiofemoral contact stress and stress distribution evaluation of total knee arthroplasties. *The Journal of Arthroplasty*, *10*(4), 480–491. https://doi.org/10.1016/S0883-5403(05)80150-0

Szklar, O., & Ahmed, A. M. (1987). A simple unconstrained dynamic knee simulator. *J of Biomech Eng., 109*(3), 247-251.

Taylor, K. A., Cutcliffe, H. C., Queen, R. M., Utturkar, G. M., Spritzer, C. E., Garrett, W. E., & DeFrate, L. E. (2013). In vivo measurement of ACL length and relative strain during walking. *Journal of Biomechanics*, *46*(3), 478–483. https://doi.org/10.1016/j.jbiomech.2012.10.031

Taylor, M. E., Tanner, K. E., Freeman, M. A. R., & Yettram, A. L. (1996). Stress and strain distribution within the intact femur: compression or bending?. *Medical engineering & physics*, *18*(2), 122-131.

Taylor, K. A., Terry, M. E., Utturkar, G. M., Spritzer, C. E., Queen, R. M., Irribarra, L. A., Garrett, W. E., & DeFrate, L. E. (2011). Measurement of in vivo anterior cruciate ligament strain during dynamic jump landing. *Journal of Biomechanics*, *44*(3), 365–371. https://doi.org/10.1016/j.jbiomech.2010.10.028

Thambyah, A., Goh, J. C. H., & Das De, S. (2005). Contact stresses in the knee joint in deep flexion. *Medical Engineering and Physics*, *27*(4), 329–335. https://doi.org/10.1016/j.medengphy.2004.09.002

Thorning, M., Thorlund, J. B., Roos, E. M., Wrigley, T. V, & Hall, M. (2016). Immediate effect of valgus bracing on knee joint moments in meniscectomised patients: An exploratory study. *Journal of Science and Medicine in Sport*, *19*(12), 964–969. https://doi.org/10.1016/j.jsams.2016.03.005

Tissakht, M., & Ahmed, A. M. (1995). Tensile stress-strain characteristics of the human meniscal material. *Journal of Biomechanics*, *28*(4), 411–422. https://doi.org/10.1016/0021-9290(94)00081-E

Tomescu, S. S. (2017). Knee Tissue Strains and Effectiveness of a Novel Functional ACL Knee Brace during Dynamic In-Vitro Loading [Master's thesis, University of Toronto]. TSpace Repository. https://hdl.handle.net/1807/79380

Tomescu, S., Bakker, R., Wasserstein, D., Kalra, M., Nicholls, M., Whyne, C., & Chandrashekar, N. (2018). Dynamically tensioned ACL functional knee braces reduce ACL and meniscal strain. *Knee Surgery, Sports Traumatology, Arthroscopy*, *26*(2), 526–533. https://doi.org/10.1007/s00167-017-4794-1

Tomescu, S., Bakker, R., Wasserstein, D., Kalra, M., Nicholls, M., Whyne, C., & Chandrashekar, N. (2020). Posteromedial meniscal and anterior cruciate ligament strains during dynamic activities following anterior cruciate ligament reconstruction. *Journal of Musculoskeletal Research*, *23*(02), 2050010.

Torzilli, P. A., Deng, X., & Warren, R. F. (1994). The effect of joint-compressive load and quadriceps muscle force on knee motion in the intact and anterior cruciate ligament-sectioned knee. *The American journal of sports medicine*, *22*(1), 105-112.

Untaroiu, C., Darvish, K., Crandall, J., Deng, B., & Wang, J. T. (2005). A finite element model of the lower limb for simulating pedestrian impacts. *Stapp Car Crash Journal, 49*, 157–181.

Untaroiu, C. D., Ivarsson, J., Genovese, D. R., Bose, D., & Crandall, J. R. (2008). Biomechanical injury response of leg subjected to combined axial compressive and bending loading. *Biomedical sciences instrumentation*, *44*, 141-6.

Untaroiu, C. D., Yue, N., & Shin, J. (2013). A finite element model of the lower limb for simulating automotive impacts. *Annals of Biomedical Engineering*, *41*(3), 513–526. https://doi.org/10.1007/s10439-012-0687-0

Vairis, A., Petousis, M., Stefanoudakis, G., Vidakis, N., Kandyla, B., & Tsainis, A. M. (2013). Studying the intact, ACL-deficient and reconstructed human knee joint using a finite element model. *Proceedings of the ASME International Mechanical Engineering Congress and Exposition (IMECE)*, *3A*, 1–7. https://doi.org/10.1115/IMECE2013-63795

Van Thiel, G. S., Frank, R. M., Gupta, A., Ghodadra, N., Shewman, E. F., Wang, V. M., Bach, B. R., Verma, N. N., Cole, B. J., & Provencher, M. T. (2011). Biomechanical evaluation of a high tibial osteotomy with a meniscal transplant. *The Journal of Knee Surgery*, *24*(1), 45–53. https://doi.org/10.1055/s-0031-1275401

Vavalle, N. A., Jelen, B. C., Moreno, D. P., Stitzel, J. D., & Gayzik, F. S. (2013). An Evaluation of Objective Rating Methods for Full-Body Finite Element Model Comparison to PMHS Tests. *Traffic Injury Prevention*, *14*(SUPPL1), S87–S94.

Vedi, V., Spouse, E., Williams, A., Tennant, S. J., Hunt, D. M., & Gedroyc, W. M. W. (1999). Meniscal movement: an in-vivo study using dynamic MRI. *The Journal of bone and joint surgery. British volume*, *81*(1), 37-41.

Verdonk, R., Volpi, P., Verdonk, P., Bracht, H. Van Der, Laer, M. Van, Almqvist, K. F., Eecken, S. Vander, Prospero, E., & Quaglia, A. (2013). Indications and limits of meniscal allografts. *Injury*, *44*(S1), S21–S27. https://doi.org/10.1016/S0020-1383(13)70006-8

Von Lewinski, G., Stukenborg-Colsman, C., Ostermeier, S., & Hurschler, C. (2006). Experimental measurement of tibiofemoral contact area in a meniscectomized ovine model using a resistive pressure measuring sensor. *Annals of biomedical engineering*, *34*, 1607-1614.

Wan, C., Hao, Z., & Wen, S. (2011). The finite element analysis of three grafts in the anterior cruciate ligament reconstruction. *Proceedings - 2011 4th International Conference on Biomedical Engineering and Informatics, BMEI 2011*, *3*, 1338–1342. https://doi.org/10.1109/BMEI.2011.6098519

Wang, H., Chen, T., Torzilli, P., Warren, R., Maher, S., Corresponding, §, & Maher, S. A. (2014). Dynamic Contact Stress Patterns on the Tibial Plateaus during Simulated Gait: A Novel Application of Normalized Cross Correlation. *J Biomech*, *47*(2), 568–574. https://doi.org/10.1016/j.jbiomech.2013.11.042

Wang, Y., Fan, Y., & Zhang, M. (2014). Comparison of stress on knee cartilage during kneeling and standing using finite element models. *Medical Engineering and Physics*, *36*(4), 439–447. https://doi.org/10.1016/j.medengphy.2014.01.004

Westermann, R. W., Wolf, B. R., & Elkins, J. M. (2013). Effect of ACL reconstruction graft size on simulated Lachman testing: a finite element analysis. *The Iowa Orthopaedic Journal*, *33*, 70–77.

Wijdicks, C. A., Ewart, D. T., Nuckley, D. J., Johansen, S., Engebretsen, L., & Laprade, R. F. (2010). Structural properties of the primary medial knee ligaments. *American Journal of Sports Medicine*, *38*(8), 1638–1646. https://doi.org/10.1177/0363546510363465

Wilharm, A., Hurschler, C., Dermitas, T., & Bohnsack, M. (2013). Use of Tekscan K-scan sensors for retropatellar pressure measurement avoiding errors during implantation and the effects of shear forces on the measurement precision. *BioMed Research International*, *2013*, 1–7.

Wilson, W. T., Deakin, M. A. H., Payne, A. P., Picard, F., & Wearing, S. C. (2012). Comparative analysis of the structural properties of the collateral ligaments of the human knee. *Journal of Orthopaedic & Sports Physical Therapy.*, *42*(4), 345–351.

Withrow, T. J., Huston, L. J., Wojtys, E. M., & Ashton-Miller, J. A. (2008). Effect of Varying Hamstring Tension on Anterior Cruciate Ligament Strain During in Vitro Impulsive Knee Flexion and Compression Loading. *The Journal of Bone and Joint Surgery (American)*, *90*(4), 815. https://doi.org/10.2106/JBJS.F.01352

Woo, S. L., Hollis, J. M., Adams, D. J., Lyon, R. M., & Takai, S. (1991). Tensile properties of the human femur-anterior cruciate ligament-tibia complex. The effects of specimen age and orientation. *The American Journal of Sports Medicine*, *19*(July), 217–225. https://doi.org/10.1177/036354659101900303

Wu, J. Z., Herzog, W., & Epstein, M. (1998). Effects of inserting a pressensor film into articular joints on the actual contact mechanics. *Journal of Biomechanical Engineering*, *120*(5), 655–659.

Yamaguchi, S., Gamada, K., Sasho, T., Kato, H., Sonoda, M., & Banks, S. A. (2009). In vivo kinematics of anterior cruciate ligament deficient knees during pivot and squat activities. *Clinical Biomechanics*, *24*(1), 71–76. https://doi.org/10.1016/J.CLINBIOMECH.2008.08.007

Yang, K. H. (2017). Basic finite element method as applied to injury biomechanics. Academic Press.

Yao, J., Snibbe, J., Maloney, M., & Lerner, A. L. (2006). Stresses and strains in the medial meniscus of an ACL deficient knee under anterior loading: A finite element analysis with image-based experipmental validation. *Journal of Biomechanical Engineering*, *128*(1), 135–141. https://doi.org/10.1115/1.2132373

Yao, J., Wen, C., Cheung, J. T. M., Zhang, M., Hu, Y., Yan, C., ... & Fan, Y. (2012). Deterioration of stress distribution due to tunnel creation in single-bundle and double-bundle anterior cruciate ligament reconstructions. *Annals of biomedical engineering*, *40*, 1554-1567.

Yeargan, A., Thomas, M. L., Thomas, C., & Evans, T. (2021). Safety, Efficacy and Short-Term Results with Intra-Articular Bone Marrow Concentrate for Arthritic Knee Pain. *J Regen Med* 11: 1. of, 4, 2.

Yeh, P. C., Starkey, C., Lombardo, S., Vitti, G., & Kharrazi, F. D. (2012). Epidemiology of isolated meniscal injury and its effect on performance in athletes from the National Basketball Association. *American Journal of Sports Medicine*, *40*(3), 589–594. https://doi.org/10.1177/0363546511428601

Ylinen, J., Pennanen, A., Weir, A., Häkkinen, A., & Multanen, J. (2021). Effect of biomechanical footwear on upper and lower leg muscle activity in comparison with knee brace and normal walking. *Journal of Electromyography and Kinesiology*, *57*, 102528.

Yu, B., McClure, S. B., Onate, J. A., Guskiewicz, K. M., Kirkendall, D. T., & Garrett, W. E. (2005). Age and gender effects on lower extremity kinematics of youth soccer players in a stop-jump task. *American Journal of Sports Medicine*, *33*(9), 1356–1364. https://doi.org/10.1177/0363546504273049

Yu, S. P., Williams, M., Eyles, J. P., Chen, J. S., Makovey, J., & Hunter, D. J. (2016). Effectiveness of knee bracing in osteoarthritis: pragmatic trial in a multidisciplinary clinic. International *Journal of Rheumatic Diseases*, *19*(3), 279-286.

Zielinska, B., & Haut Donahue, T. L. (2006). 3D finite element model of meniscectomy: Changes in joint contact behavior. *Journal of Biomechanical Engineering*, *128*(1), 115–123. https://doi.org/10.1115/1.2132370

Zhang, Q., Adam, N. C., Hosseini Nasab, S. H., Taylor, W. R., & Smith, C. R. (2021). Techniques for in vivo measurement of ligament and tendon strain: a review. *Annals of biomedical engineering*, *49*, 7-28.

# Appendix A: Experimental Reliability

Experimental repeatability was assessed by computing and root mean square error (RMSE) (Eq. A.1) and normalised RMSE (nRMSE) (Eq. A.2) of the posteromedial meniscus strains between two trials for each of the 18 unique experimental conditions. Overall, the experimental sample had a mean (SD) RMSE of 2.4(3.2) % (n=10) and nRMSE of 0.41(0.45) (Table 9.1). The RMSE is strongly influenced by specimens #2, 4, and 6 due to greater intertrial variability. However, this variability is accentuated due to the sensitive nature of the DVRT. For example, the unbraced ACL-deficient gait trials in specimen #4 were the two least comparable trials with a strain RMSE of 120%. When further analysing the changes in DVRT deformation between these trials there was a 0.7 mm difference in the initial DVRT value and mean difference of 0.125 mm over the trial durations. The normalised strain RMSE compares the strain RMSE relative to the mean strain for each test condition and demonstrates a mean percent difference of 0.41 between any two trials across all specimens (n=10). Thus, it can be stated that while there are high inter-specimen strain variabilities, there is low intra-specimen strain variability due to the low nRMSE.

$$\mathrm{RMSE} = \sqrt{\frac{1}{n}\sum_{i=1}^{n} |T_1 - T_2|_i^2} \tag{A.1}$$

$$\mathrm{nRMSE} = \frac{\mathrm{RMSE}}{\mu} \tag{A.2}$$

where:
$T_1$ and $T_2$ are trials 1 and 2
$\mu$ is the overall mean of both trials

Table A.1: Mean root mean square and normalised root mean square errors for experimental posteromedial meniscus strain.

| Specimen ID# | RMSE | nRMSE |
|---|---|---|
| 1 | 0.2(0.3) | 0.05(0.07) |
| 2 | 2.8(5.6) | 0.55(1.09) |
| 3 | 1.7(3.3) | 0.3(0.59) |
| 4 | 11.1(26.4) | 1.53(3.64) |
| 5 | 1.4(2.2) | 0.29(0.44) |
| 6 | 3.7(10.1) | 0.78(2.14) |
| 7 | 1.0(1.1) | 0.18(0.2) |
| 8 | 0.9(1.4) | 0.20(0.32) |
| 9 | 0.5(1.1) | 0.11(0.23) |
| 10 | 0.6(1.4) | 0.11(0.26) |
| Mean(SD) (n=10) | 2.4(3.2) | 0.41(0.45) |